THE IMPACT OF MALNUTRITION ON HOST-MICROBE INTERACTIONS IN THE INTESTINE

by

Eric Brown

B.Sc University of Guelph 2010

A THESIS SUBMITTED IN PARTIAL FULFILLMENT OF

THE REQUIREMENTS FOR THE DEGREE OF

DOCTOR OF PHILOSOPHY

in

THE FACULTY OF GRADUATE AND POSTDOCTORAL STUDIES

(MICROBIOLOGY AND IMMUNOLOGY)

THE UNIVERSITY OF BRITISH COLUMBIA

(VANCOUVER)

April 2017

Abstract

Early-life malnutrition results in childhood growth stunting, increased intestinal permeability, along with significant changes in the intestinal microbiota and metabolite composition. Here, we aim to characterize and further understand how malnutrition results in these intestinal consequences, and use this knowledge to develop a model to study environmental enteropathy (EE), a chronic inflammatory disease of the small intestine. Three-week-old C57BL/6 mice administered a protein and fat malnourished diet where compared with mice fed an isocaloric standard diet and found to be moderately growth stunted, with barrier dysfunction as observed decreased abundance of tight-junction proteins and increase in intestinal permeability to dextran. Mice given the malnourished diet were also found to have an altered small intestinal microbiota and metabolome, notably including profound changes in the Bacteroidetes and Proteobacteria species able to colonize the upper small intestine, correlated with large differences in the bile acid composition. The colon of malnourished mice had an altered mucosal microbiota composition, a thinner mucus layer and a greater number of microbes able to cross the mucus barrier was visualized by microscopy. We used these data to inform our development of a model for EE in mice. Features of EE include growth stunting, intestinal permeability, villous blunting and chronic intestinal inflammation. After screening a number of microbial cocktails, we demonstrate that early life consumption of a malnourished diet, in combination with exposure to a cocktail of *Bacteroidales* and *E. coli* species, remodels the small intestine to resemble the major features of EE observed in humans. Furthermore, this *Bacteroidales* and *E. coli* exposure induces an influx of pro-inflammatory intraepithelial lymphocytes in the small intestine, along with increased prevalence of bacterial species adhering to the epithelium, each of which could be initiating the onset of EE features. Further, we infected

the malnourished mice with the enteric pathogens *H. polygyrus,* and *S.* Typhimurium, and observed striking differences in number of microbes able to colonize the small intestine. These findings provide new evidence of the intestinal impacts of malnutrition, and describe a novel murine model that can be used to elucidate the pathophysiology of this understudied disease.

Preface

Select data from Chapter 2 has already been published in a peer-reviewed journal. Data from Fig 2.1, 2.2, 2.4, 2.5, 2.7, 2.8, 2.9 and Tables 2.2 and 2.3 are published.

Eric M. Brown, Marta Wlodarska, Benjamin P. Willing, Pascale Vonaesch, Jun Han, Lisa A. Reynolds, Marie-Claire Arrieta, Marco Uhrig, Roland Scholz, Oswaldo Partida, Christoph Borchers, Philippe J. Sansonetti, B. Brett Finlay. (2015). Diet and specific microbial exposure trigger features of environmental enteropathy in a novel murine model. *Nature Communications* 6:7806 doi:10.1038/ncomms8806.

Dr. Marta Wlodarska helped with the mucus studies and histology. Dr. Ben Willing did the pyrosequencing data analysis. Dr. Jun Han and Dr. Cristoph Borchers performed the bile acid and untargeted metabolomics analysis. Dr. Lisa Reynolds, Dr. Marie-Claire Arrieta, Oswaldo Partida, Roland Scholz and Marco Uhrig assisted me with various mouse experiments.

Dr. Brett Finlay helped conceive the project, write the manuscript, mentored and supervised its participants. I conceived of the project, wrote the manuscript and either performed, analyzed or designed all experiments in this manuscript.

A version of Chapter 3 has already been published in a peer-reviewed journal.

Eric M. Brown, Marta Wlodarska, Benjamin P. Willing, Pascale Vonaesch, Jun Han, Lisa A. Reynolds, Marie-Claire Arrieta, Marco Uhrig, Roland Scholz, Oswaldo Partida, Christoph Borchers, Philippe J. Sansonetti, B. Brett Finlay. (2015). Diet and specific microbial exposure trigger features of environmental enteropathy in a novel murine model. *Nature Communications* 6:7806 doi:10.1038/ncomms8806.

Dr. Marta Wlodarska helped with FACS experiments and assisted in performing the mouse experiments. Dr. Jun Han and Dr. Cristoph Borchers performed the bile acid and untargeted metabolomics analysis. Dr. Lisa Reynolds assisted in carrying out the mouse experiments and FACS data analysis. Dr. Marie-Claire Arrieta assisted in the qPCR microbiome analysis. Pascale Vonaesch performed the FISH analysis on jejunal tissues. Oswaldo Partida, Roland Scholz and Marco Uhrig assisted me with various mouse experiments. Dr. Brett Finlay helped conceive the project, write the manuscript, mentored and supervised its participants. I conceived of the project, wrote the manuscript and either performed, analyzed or designed all experiments in this manuscript.

A version of Chapter 4 is currently being prepared for submission. Dr. Lisa Reynolds performed the FACS analysis and worm infections of mice. Tara Brosschot performed the ELISAs on mouse serum for immunoglobins. Dr. Marta Wlodarska assisted in the mouse experiments for the *Salmonella* and *Citrobacter* infections. Dr. Courtney Heim generated data used in Fig. 4.12, Fig. 4.14 and aided in designing sphingolipid related experiments. Dr. Daniel O'Connell performed the TF-seq data analysis and created the method used to generate Fig. 4.15. Dr. Xiaobo Ke created the *SPT* knockout in *Bacteroides thetaiotaomicron.* Dr. Alex Kostic analyzed the RNA-seq data used in Fig. 4.17. Dr. Ramnik Xavier supervised and partially funded the work from sub-chapter 4.6. Dr. Brett Finlay both supervised and funded the rest of the work, and provided guidance on experiments. For the remainder of this manuscript I designed and performed all experiments, analyzed all remaining data not mentioned above.

Versions of figures and some text have been published in Chapter 1. Figure 1.2, 1.3 and 1.4 have been previously published in a peer reviewed journal.

Eric M. Brown, Manish Sadarangani, B Brett Finlay. (2013). The role of the immune system in governing host-microbe interactions in the intestine. *Nature Immunology* 14(7): 660-667. I conceived of, and edited this manuscript, and wrote approximately 80% of the manuscript. The remaining 20% was written by Dr. Manish Sadarangani. Dr. Brett Finlay edited the manuscript and oversaw its acceptance.

List of publications arising from my thesis work:

1. Marie-Claire Arrieta, Manish Sadarangani, **Eric M Brown**, Shannon L Russell, Michael Nimmo, John Dean, Stuart E Turvey, Edmond S Chan, B. Brett Finlay. (2016). A humanized microbiota mouse model of ovalbumin-induced lung inflammation. Gut Microbes doi:10.1080/19490976.2016.1182293

2. Rosana BR Ferreira, Yanet Valdez, Brian K Coombes, Subash Sad, Joost W Gouw, **Eric M Brown**, Yuling Li, Guntram A Grassl, L Caetano M Antunes, Navkiran Gill, Mimi Truong, Roland Scholz, Lisa A Reynolds, Laskshmi Krishnan, Ahmed A Zafer, Neta Sal-Man, Michael J Lowden, Sigrid D Auweter, Leonard J Foster, B Brett Finlay. (2015). A highly effective component vaccine against non-typhoidal Salmonella enterica infections. mBio 6:5 doi:e01421-15

3. **Eric M. Brown**, Marta Wlodarska, Benjamin P. Willing, Pascale Vonaesch, Jun Han, Lisa A. Reynolds, Marie-Claire Arrieta, Marco Uhrig, Roland Scholz, Oswaldo Partida, Christoph Borchers, Philippe J. Sansonetti, B. Brett Finlay. (2015). Diet and specific microbial exposure trigger features of environmental enteropathy in a novel murine model. *Nature Communications* 6:7806 doi:10.1038/ncomms8806
4. **Special Research Highlight** Katrina Ray. (2015) New mouse model of EE. *Nature Reviews Gastroenterology and Hepatology12*, 489 doi:10.1038/nrgastro.2015.144

5. Marie-Claire Arrieta, Leah T. Stiemsma, Nelly Amenyogbe, **Eric M. Brown**, B. Brett Finlay. (2014). The intestinal microbiome in early life: health and disease. *Frontiers in Immunology.* 5: 427.

6. Yanet Valdez, **Eric M. Brown**, B. Brett Finlay. (2014). Influence of the microbiota on vaccine effectiveness. *Trends in Immunology.* 35(11): 526-537.

7. Curtis Huttenhower, Rob Knight, C Titus Brown, J Gregory Caporaso, Jose C Clemente, Dirk Gevers, Eric A Franzosa, Scott T Kelley, Dan Knights, Ruth E Ley, Anup Mahurkar, Jacques Ravel, **The Scientists for the Advancement of Microbiome Research**, Owen White. (2014). Advancing the microbiome research community. *Cell.* 159(2): 227-230.

8. Jacques Ravel, Martin J. Blaser, Jonathan Braun, **Eric M. Brown**, Frederic D. Bushman, Eugene B. Chang, Julian Davies, Kathryn G. Dewey, *et al.* (2014). Human Microbiome Science: Vision for the Future, Bethesda, Md., July 24-26 2013. *Microbiome.* 2 (1):1-11

9. Gregor Reid, Nicholas Nduti, Wilbert Sybesma, Remco Kort, Tobias R Kollmann, Rod Adam, Hamadi Boga, **Eric M. Brown**, *et al.* (2014). Harnessing microbiome and probiotic research in sub-Saharan Africa: recommendations from an African workshop. *Microbiome.* 2(1):12.

10. Marta Wlodarska, Christoph A Thaiss, Roni Nowarski, Jorge Henao-Mejia, Jian-Ping Zhang, **Eric M Brown,** Gad Frankel, Maayan Levy, Meirav N Katz, William M Philbrick, Eran Elinav, B Brett Finlay, Richard A Flavell. (2014). NLRP6 inflammasome regulates the intestinal host-microbial interface by orchestrating goblet cell mucus secretion. *Cell*. 156:1045-1059.

11. **Eric M. Brown,** Claire Arrieta, B Brett Finlay. (2013). A fresh look at the hygiene hypothesis: how intestinal microbial exposure drives immune effector responses in atopic disease. *Seminars in Immunology* 25(4): 378-387.

12. **Eric M. Brown,** Manish Sadarangani, B Brett Finlay. (2013). The role of the immune system in governing host-microbe interactions in the intestine. *Nature Immunology* 14(7): 660-667.

The mouse work presented in this thesis was approved by the UBC Animal Care Committee, certificate numbers: A14-0164 and A12-0169

Table of Contents

List of Tables

List of Figures

List of Symbols

α alpha

ß beta

γ gamma

μ micron

∂ delta

% percent

$Gene^{-/-}$ genetic deletion of a gene

List of Abbreviations

AB/PAS	alcian blue/ periodic acid-Schiff
AMP	antimicrobial peptide
ATP	adenosine triphosphate
BG	*Bacteroides-E. coli* mix
BHI	brain heart infusion
BMDM	bone-marrow derived macrophage
BMDC	bone-marrow derived dendritic cell
B. ovatus	*Bacteroides ovatus*
B. fragilis	*Bacteroides fragilis*
B. vulgatus	*Bacteroides vulgatus*
B. dorei	*Bacteroides dorei*
B. theta	*Bacteroides thetaiotaomicron*
CBA	cytokine bead array
CCL	C-C motif chemokine
CD	cluster of differentiation
CerPE	ceramide phosphoethanolamine
CFU	colony forming units
CLDN	claudin
CO_2	carbon dioxide
CON	control
DAPI	4',6-diamidino-2-phenylindole
DC	dendritic cell
DNA	deoxyribonucleic acid
E. coli	*Escherichia coli*
EDTA	ethylenediaminetetraacetic acid
EE	Environmental enteropathy
EHEC	Enterohaemorrhagic Escherichia coli
ELISA	enzyme-linked immunosorbent assay
EPEC	Enteropathogenic Escherichia coli

FAA	fastidious anaerobe agar
FACS	fluorescence-activated cell sorting
FBS	fetal bovine serum
FITC	fluorescein isothiocyanate
GALT	gut-associated lymphoid tissue
GAPDH	glyceraldehyde 3-phosphate dehydrogenase
GF	germ free
GFP	green fluorescent protein
H&E	hematoxylin and eosin
H. polygyrus	*Heligmosomoides polygyrus bakerei*
HRP	horseradish peroxidase
IBD	inflammatory bowel disease
IEC	intestinal epithelial cell
IEL	intestinal epithelial lymphocyte
Ig	immunoglobulin
IL	interleukin
ILC	innate lymphoid cell
IL-1R	interleukin-1 receptor
IFN	interferon
JAX	Jackson Laboratory
KO	knockout
LB	luria broth
LP	lamina propria
LPL	lamina propria lymphocyte
LPS	lipopolysaccharide
M cell	microfold cell
MAL	malnourished
MALDI	matrix-assisted laser desorption/ionization
MAMP	microbe-associated molecular pattern
MCP-1	monocyte chemotactic protein-1
MLN	mesenteric lymph node

MS	mass spectrometry
mRNA	messenger ribonucleic acid
MyD88	myeloid differentiation primary response gene 88
MZ	mass-charge ratio
NaCl	sodium chloride
NADPH	nicotinamide adenine dinucleotide phosphate
NK	natural killer
NLR	nucleotide-binding oligomerization domain-like receptor
NOD	nucleotide-binding oligomerization domain
OTU	operational taxonomic unit
PBS	phosphate-buffered saline
PCR	polymerase chain reaction
P. distasonis	*Parabacteroides distasonis*
PRR	pattern recognition receptor
Reg3	regenerating islet-derived protein 3
Relm	resistin-like molecule
Rf	retardation factor
ROS	reactive oxygen species
RNA	ribonucleic acid
rRNA	ribosomal ribonucleic acid
RT-PCR	real-time polymerase chain reaction
RUTF	ready-to-use therapeutic foods
SAM	severe acute malnutrition
SCFA	short-chain fatty acid
SILAC	stable-isotope labelling with amino acids in cell culture
Th	T-helper
Treg	T-regulatory cell
TGF	transforming growth factor
TJP	tight-junction protein
TLC	thin-layer chromatography
TLR	toll-like receptor

TNF	tumor necrosis factor
TSLP	thymic stromal lymphopoietin
UBC	University of British Columbia
UC	ulcerative colitis
vs.	versus
WT	wild-type

Acknowledgements

Reflecting on this journey towards the completion of this thesis, I couldn't have done it without the help and support of colleagues, friends and family in the UBC community and back home in Ontario. First of all, it has been an honour to work in the Finlay laboratory and be supervised by Dr. Brett Finlay. I have appreciated Brett's enthusiasm for science, and all of his support and guidance which has made my PhD experience an enjoyable and productive one. Brett is the ultimate enabler which has given me a unique grad school experience, full of many opportunities which have had such a positive impact on by scientific career. He has also enabled me to become an independent thinker in the lab and given me the confidence I need to continue to pursue academia.

To all members of the Finlay lab, thank you for making these past six years such a rewarding and memorable time, while providing unwavering support especially during all the difficult moments. I think the lab environment and culture here is truly special and one I am going to miss. The culture of the lab is one that fosters collaboration, healthy critiques, friendship and a number of mentors and role models to look up to. In my mind, this all begins with Deng, Lisa Thorson and Theresa who all manage to keep the lab running smoothly. Despite all the turnover in the lab in the past six years, the essence of what it means to be in the Finlay lab has stayed constant and you three are a big reason for that! I need to specifically thank some people who have helped me the most in my lab journey:

Deng- for always being down to chat science and especially sports over the years, not many people around here are real sports fans like us and I'm going to miss all the daily chats and lunches.

Lisa Reynolds- for being the best baymate ever, I couldn't ask to have sat beside a better scientist and a better person, aside from all the late lab nights, FACS help, long mouse experiments, and general help you've giving me over the years, I think I need to thank you most for being a great friend. Also for putting up with all my non-tube labelling and crazy far out science theories. I still think IgD is important!

Marta Wlodarska- looking back, you definitely helped me the most out of anyone in the lab, and many of these experiments here were down with your help, guidance and amazing lab hands to which I am super grateful. The time we spent together in the lab made me not only a better scientist but a better person and I am truly thankful.

Joris van der Heijden- I still remember crossing paths with you in the hall, seeing you and your crazy hair, goofy smile and general friendliness and I knew right away we'd be great friends. I wasn't wrong, and I am appreciative of all the coffee room times, science chats over beers, dinners, trips and being my #1 lab co-prankster.

Roland Scholz- for just being an awesome guy to have around, keeping my spirits up on those long lab days, all the parties, trips and dry ice bombs. Wouldn't have been the same without you man.

Shannon Russell- for being a great friend and so helpful to me in the beginning feeling welcome in the lab. Teaching me the ways of grad school and all the pointers along the way, and for being my microbiota co-collaborator along the way.

Outside of the lab, I want to acknowledge Pascale Vonaesch, who has been an incredible collaborator for this whole project and one of the first people I met who was working on malnutrition and EE. Working together with you has had a big impact on this project and can't stress how important all those skype chats were when I was the only person working in this area in the lab. Erik Nielson, Scott Lambie and Ray Socha, thanks for making up what was a great morning coffee room crew, friends and coffee is the best way to start the day. Later on, during my PhD I learned that collaborating with friends in and outside the lab is not only fun but can make things quite productive. Thanks to Craig Kerr for providing proteomics help, Else Bosman for helping me get all those knockout mice, Nelly for helping with the germ-free mouse work, Claire and Ben for the bioinformatics help, Lisa for teaching me everything about worms and Oswaldo for teaching me everything about protozoa.

My four-month visit to the Broad Institute at the end of my 4th year had an enormous scientific impact on me professionally and personally. I need to thank Dr. Ramnik Xavier for letting me come into the lab and work on my sphingolipid project, supporting me throughout and also taking me on later as a post doc! I also need to thank the microbiome crew at the Broad, Hera Vlamakis, Doug Kenny, Tim Arthur, Alex Kostic, Moran Yassour, Melanie Shirmer and Daniel O'Connell for making me feel so welcome during my visit and helping me get my project

off the ground. Will always remember what a fomite is. Look forward to working with all of you in the future!

I was very lucky during my PhD to have a helpful supportive and engaging committee, who pushed me to do better science and shaped many of my ideas in the development of my project. First of all, Tobi your early feedback to me was part of my inspiration in creating the EE mouse model, and I need to thank you for being a great collaborator over the years. Also for inviting me to the Kenya microbiome conference, a life experience I will never forget. Kelly, you helped me on my journey to becoming an "card-carrying" mucosal immunologist, need to thank you for all those chats in your office early on and general enthusiasm about my project which helped me through some of the tougher times early on. Bill, I want to thank you for also giving me so much help and support through the years, the fun time at the Paris conference, and being a great person to talk to about science and life.

To me, a PhD learning and life experience is not only found in the lab but the large concentration of smart, funny, engaging and amazing people who you happen to be surrounded by on campus and in the department. My PhD wouldn't have been the same without our Microballology dodgeball/karaoke team, the most tremendous departmental team, just tremendous. To everyone who was part of that team, including Keith Mewis, Mike Jones, Craig Kerr, Erik Nielson, Sean Workman, and Jan Burian, gonna miss you guys. Chatting science and life over drinks, and the comradery of the team was something special. My time at UBC was also enriched by my five years playing hockey with the Eulers/Breadwings teams, as well as all those people who came along for my wilderness, mountain adventures through the years.

I need to thank my funding sources, who paid my salary and provided money to my project. Funding from CIHR provided me my salary for four years and before that I had a 4-year fellowship provided by UBC. Thanks to the Michael Smith Foundation for providing me my scholarship to visit Boston for four months. Brett, thank you again for being very flexible with lab funds to let me do the experiments I wanted to do and paying me in the early years. UBC is a fantastic school to work for everyday and is full of great people. I need to thank the Department of Microbiology and Immunology staff and administrators for running things so well, especially Darlene Birkenhead.

Lastly, I need to thank my family, especially my mom and dad for always being there for me no matter what, helping me financially getting through being a poor graduate student, giving me two amazing role models and always remembering to ask how my mice are. You guys raised me to have a love of science, and always supported me in my pursuits in life. I certainly wouldn't be where I am today if it wasn't for you. Graeme, thank you for the brotherly encouragement and the yearly football trips I always look forward to. Will always remember that trip you came to visit! Laura and Evan, thanks for being just awesome siblings through this whole thing and making me look forward to every family trip. Looking forward to living closer and all our future fun.

To my mom and dad who have always supported me through thick and thin during this journey

Chapter 1: Introduction

1.1 The global burden of malnutrition and enteric disease

1.1.1 The vicious cycle of early-life malnutrition and enteric disease

In 2016, the World Health Organization (WHO) published a study, which showed of all deaths in children under 5 years old, approximately 45% are attributable to malnutrition (World Health Organization and Nutrition for Health and Development, 2013). Nutritional defects early in life also lead to a significant growth impairment, as 146 million children are growth stunted which predisposes them to poor health outcomes and decreased cognitive function (Guerrant et al., 2013; Bourke et al., 2016). Growth stunting is often apparent at birth and in many cases weight-for-age and length-for-age *Z* scores (standard deviation changes from normal) continue to decline over the first 2 years of life, with little recovery thereafter (Victora et al., 2008). Maternal height and infant birthweight are consistent predictors of infant growth (Prendergast and Humphrey, 2014). Stunted children are shorter than healthy reference populations, and this is quantified by having a height-for-age *Z* score less than 2. Despite the known predisposition for early-life stunting to result in immunodeficiency, metabolic imbalance and cognitive defects, in many cases, stunting does not present with any clinical symptoms (Dewey and Begum, 2011).

In contrast, severe acute malnutrition (SAM), quantified by having a height-for-age *Z* score less than 3, affects approximately 52 million children and those children with SAM show more clinical symptoms than those with stunting (Kerac and Seal, 2014). SAM, also

referred to as wasting, is characterized by loss of fat and muscle across the body, especially evident in the thighs, upper arms, and ribs, and some cases where children lose all their abdominal muscles resulting in protruding bellies (Collins et al., 2006). A disease called Kwashiorkor is seen in children with SAM, which is also known as "edematous malnutrition" and is clinically diagnosed mainly by the presence of symmetrical edema, and a fatty liver (Collins, 2007). Managing the effects of SAM can be done using protein, micronutrient and energy dense foods, yet in many cases these children are still at high risk of dying due to impaired organ function, co-infections and refusal of re-feeding treatments (Mengesha et al., 2016). When we discuss stunting and malnutrition henceforth, we will be discussing it in terms of those children without diagnosed SAM, but with a more subclinical presentation of protein malnutrition.

Reversing global trends of childhood stunting and malnutrition is a priority, with the WHO officially recommending re-feeding of malnourished children with ready to use therapeutic foods (RUTF) as the main intervention. So far, clinical trials have shown that currently available therapeutic food interventions, such as RUTF, fail to fully restore health in over half of all malnourished children (Bhutta et al., 2008). Reasons for the lack of 100% efficacy in nutritional interventions for malnutrition are yet to be fully understood. However, a recent study showed that antibiotic treatment preceding the nutritional intervention leads to an improvement of the health defects caused by malnutrition, indicating the importance of understanding the microbial-driven disease pathologies and underlying defects in intestinal function contributing to malnutrition (Trehan et al., 2013). The intestinal tract is where a vast majority of nutrients are absorbed and is the single largest interface of humans with their external

environment, making its normal functioning central to be able to resist diseases caused by malnutrition. Apart from dietary intake, studies of malnourished individuals are beginning to highlight the fact that environmental exposures early in life, resulting from poor sanitation and hygiene, correlates with stunting and malnutrition rates worldwide (Humphrey, 2009).

One of these early life environmental exposures than impact malnutrition are enteric pathogens. Chronic, recurrent infections are a defining feature of populations in the developing world living in areas of poor sanitation and hygiene. For example, in Bangladesh, approximately two-thirds of children will have a diarrhea episode in their first 6 months of life (Ahmed et al., 2014a). When enteric infections result in diarrhea, they can cause a high mortality rate in malnourished children, ~5 deaths per 1,000 children less than 5 years of age, a number which has improved significantly due to oral rehydration therapy (Guerrant et al., 2013). As mortality rates decline, there is a significant and persistent impact on morbidity later in life after these early life enteric infections and malnutrition (Schaible and Kaufmann, 2007). It is well documented that malnutrition can cause a secondary risk of immunodeficiency and a greater susceptibility to infection in humans (Katona and Katona-Apte, 2008). However, infection itself can also contribute to malnutrition, and this sets up a vicious cycle; an inadequate diet impacts the immune system, increasing the incidence and severity of infection, which leads to an altered metabolism and nutrient loss, exacerbating malnutrition of the host (Kau et al., 2011; Guerrant et al., 2008) (Fig. 1.1).

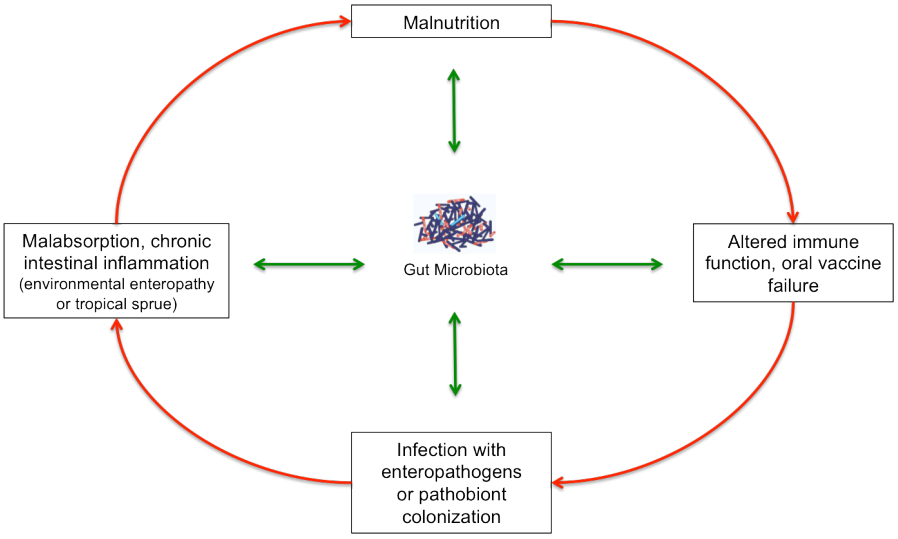

Figure 1.1 The vicious cycle of malnutrition and enteric disease

A secondary impact of this vicious cycle between malnutrition and infection is that nutrition can impact the function of the mammalian adaptive immune system, and thus the responses to vaccines (Savy et al., 2009). Protein intake and micronutrients are important for immune function, including vitamin A, zinc, copper and iron (Kaufman et al., 2011; Ibs and Rink, 2003; Muñoz et al., 2007). A number of studies reported altered systemic and mucosal immunity in malnourished subjects, including reduced sIgA in the intestine, atrophy of lymphatic tissues, fewer circulating B cells, and a shift in the balance of Th1 and Th2-associated cytokines (Bourke et al., 2016). During vitamin A deficiency, for example, lack of retinoic acid results in altered functions of DCs, Th2 responses and ILC2 populations in gut presenting antigens

(Spencer et al., 2014). Given the significant impact of malnutrition on the host immune system, it not surprising that many studies report a link between malnutrition and worldwide vaccine efficacy, however this is particularly evident in oral vaccines which have decreased efficacy in regions with poor sanitation and a high incidence of stunting (Serazin et al., 2010; Levine, 2010). Oral vaccines with decreased efficacy include rotavirus, ETEC, *Cholera, Shigella,* and polio vaccines (Levine, 2010). By the age of 6 months, before many vaccines aim to be administered, a large percentage of children who live in poor sanitary conditions and developing countries, such as India, Bangladesh, and Malawi have already had at least one diarrheal episode (Guerrant et al., 2008b; DeBoer et al., 2012; Scharf et al., 2014). A recent study in mice demonstrates that post-infectious oral vaccination efficacy is ablated, due to re-arrangement of secondary lymphoid tissues, such as Peyer's Patches, after infection with *Yersinia pseudotuberculosis* and this phenotype was partially due to the altered composition of the intestinal microbiota post-infection (Fonseca et al., 2015). Whether this finding is relevant in humans and can be extrapolated to include other intestinal pathogens is unknown, but it certainly should be followed up on given the understudied effect of early life pathogen exposure on adaptive and mucosal immunity. Injectable vaccines show greater efficacy in malnourished and developing country populations. However, vaccine development for enteric infections from gut pathogens such as *Salmonella, Campylobacter, E. coli, Shigella,* and *Cryptosporidium,* will require a potent stimulation of memory B and T-cells in mucosal lymphoid organs; an outcome that can only be achieved by oral vaccination (Serazin et al., 2010). Discoveries in how to raise the efficacy of oral vaccines will be required to break the vicious cycle and decrease the incidence of stunting worldwide.

1.1.2 Environmental enteropathy

Individuals living in areas of poor sanitation are also susceptible to developing chronic intestinal inflammation independently of any known infectious etiology. Biopsies from the small intestine of these individuals reveal many distinct characteristics of a subclinical disorder called environmental enteropathy (EE) (Korpe and Petri, 2012; Owino et al., 2016). This condition, also known as tropical enteropathy or more recently environmental enteric dysfunction (EED), is a poorly characterized chronic inflammatory disease that primarily affects the small intestine (Keusch et al., 2014). EE afflicts individuals who are born in or reside for relatively long periods of time in areas with poor sanitation and who have a high exposure to fecal-contaminated water and food (Korpe and Petri, 2012; Humphrey, 2009). The hallmarks of EE are growth stunting, malabsorption, increased gut permeability, villous blunting, and chronic intestinal inflammation and inflammatory cell infiltrate independent of any known infectious etiology (Keusch et al., 2014; Kosek et al., 2014). The most striking feature of EE is the flattened villi, increased crypt depth and inflammatory cell infiltrate, only viewed in the rare occurrences when small intestinal specimens where attained from children with EE-features (Prendergast and Kelly, 2012). This phenotype is similar to what is seen in celiac disease, and results in decreased surface area for the absorption of nutrients; a crucial function of the small intestine in humans. As a majority of the nutrient absorption occurs in this area of the digestive tract, EE can lead to malabsorption of essential fats, vitamins and micronutrients (Kau et al., 2011). Recent studies have shown that gross histopathologic changes like this can be observed in children who present with no other clinical infection or symptoms and are otherwise “healthy” aside from their stunted growth and, in many cases, increased gut permeability (Ngure et al., 2014). These findings of compromised

small intestinal integrity, certainly puts the subject with EE at risk for increased immune exposure and translocation of microbes and their MAMPs into the systemic circulation. The villous blunting viewed in EE is primarily in the upper small intestine (duodenum and jejunum), and these regions of the intestine are not well adapted to iteratively experience chronic microbial assault (El Aidy et al., 2015). This is evidenced by the link between EE and small intestinal bacterial overgrowth (SIBO), as well as the presence of highly activated CD4+ and CD8+ γ∂ T-cells found in histological specimens from children with EE (Campbell et al., 2003).

Despite these striking morphological findings of villous blunting in the limited studies of children with EE, we lack a clear clinical definition of EE (Petri et al., 2014). Due to the unethical nature and invasiveness of obtaining small intestinal biopsies of children with EE, especially difficult given the subclinical nature of its symptoms, we must rely on biomarkers to better define EE. There are a number of biomarkers that have been utilized to assess the intestinal integrity, inflammation and permeability seen in EE, including serum CRP, LPS, I-FABP, zonulin, citrulline, fecal calprotectin and alpha-antitrypsin (Korpe and Petri, 2012; Guerrant et al., 2016). The most commonly used biomarker to define EE is the lactulose-mannitol ratio, which is determined using an assay where, after 12 hours of fasting, a set ratio of lactulose and mannitol is ingested and the resulting ratio of these sugars is assessed in the urine. Lactulose should not be metabolized once absorbed from the gut and increased lactulose crossing the intestinal barrier compared to mannitol indicates a barrier dysfunction and thus increased intestinal permeability (Lee et al., 2014). In theory, the test is well regarded as an accurate measure of intestinal permeability, however the practicalities in the field of performing this test are limited (Sequeira et al., 2014). It is extremely time-consuming and labour intensive, and

mistakes are commonly made which skew the results. It should be the research goal of the field studying EE to agree upon easily assayable, accurate and EE-specific biomarkers to better characterize this disease.

The study of EE as a bona-fide intestinal disease that leads to malabsorption and growth stunting is still in its infancy. We've known for a while that the cause of early life growth stunting is multifactorial (Owino et al., 2016). Historically, the two main factors resulting in early-life growth stunting have been cited as insufficient and inadequate dietary intake early in life, and chronic, repeated infections causing diarrhea and inflammation. While these two factors are most certainly pertinent, we have recently begun to accept and realize EE, a chronic inflammatory condition, may be as or more important to the worldwide prevalence of growth stunting and there are large trials underway to understand the link between sanitation, chronic inflammation and stunting (Prendergast et al., 2015). To ameliorate growth stunting, we have been developing interventions by addressing the first two factors (nutrition and diagnosed diarrheal infections), and absence or presence of diarrhea was once the primary endpoint in many clinical studies aimed to reverse growth stunting. These studies, on the whole, have been largely unsuccessful in reversing the trend of growth stunting (Humphrey, 2009). We have now come to appreciate that much of worldwide growth stunting happens independently of the constant presence of diarrhea or any known infectious etiology (Humphrey, 2009). Rather, the presence or absence of EE-features (such as intestinal permeability, villous blunting, malabsorption and inflammation) correlates closely with early-life growth rates (Ngure et al., 2014). Developing interventions which are targeted against the features of EE have gained importance as a way to improve healthy growth of children throughout the developing world and in regions of poor

sanitation (Petri et al., 2014). These interventions also include those to improve oral vaccine efficacy and break the vicious cycle of malnutrition (Fig. 1.1).

Immunologically, individuals with EE show the skewing to a Th1 response in the gut environment, and an increase in activated intraepithelial CD8+ lymphocytes (Campbell et al., 2003). Inflammatory cytokines secreted by polarized Th1 cells, such as IFN-γ and TNF-α, can lead to intestinal tissue damage and greater epithelial cell turnover (Veitch et al., 2001). Studies on adults in Zambia with EE show evidence of increased T-cell activation as measured by CD69 and HLA-DR expression (Bickler, 2006). It is therefore a possibility that histopathological changes observed in EE could be mediated by T-cell induced inflammatory damage. A study in mice showed that constant, early-life exposure to pathogenic *E. coli* generates a population of memory CD8+ T-cells with a broader, "leaky" response that can extend to commensal *E. coli* (Hand et al., 2012). Thus, the presence of these cells could, by mistake, be responding to the *E. coli* present in the intestine, triggering chronic intestinal inflammation. Whether this is taking place in humans with EE-features is unknown, but remains a plausible hypothesis for the induction of EE and subclinical inflammation. While many immunological characteristics of this disease remain poorly characterized, it seems reasonable to postulate that individuals living in regions with high oral exposures to water and food contaminated with microbes will have an altered intestinal immune system than those without these exposures (Bourke et al., 2016). This altered immune system seen in individuals with EE could be behind the poor vaccine efficacy in developing countries. Oral vaccination involves the introduction of an immunogenic antigen or attenuated-organism, and as mentioned previously, there is significant heterogeneity in the responses to oral vaccination in children living in industrialized societies compared to children

raised in areas of poor sanitation in developing countries (Levine, 2010). For example, it was demonstrated that excessive bacterial growth in the small intestine of children in less developed countries may contribute to the low antibody response to an oral cholera vaccine (Lagos et al., 1999). SIBO is commonly observed in children with EE (Mello et al., 2012).

Increased intestinal permeability, a key feature of EE, could also yield a possible explanation for the dampened responses to vaccines in developing countries. Many patients with EE show increased intestinal permeability or a "leaky" gut barrier (Ahmed et al., 2014b). This leaky barrier exposes the systemic immune system to a greater variety of potentially harmful and immunogenic antigens translocating the mucosal barrier. This constant exposure of microbial and external antigens to the systemic immune system could lead to systems of tolerance, rather than the immune system eliciting an effector response to attempt to clear the antigen (Biswas and Lopez-Collazo, 2009). Thus, in children with EE-features, there could be the differing tolerance capabilities due to alterations in the mucosal immune system imparted by distinctive environmental exposures in regions of poor sanitation. It is well known that immune tolerance is correlated with increased exposure to an antigen, even one that is typically immunogenic. A good example of this is seen in endotoxin tolerance. Exposure of the immune system to small amounts of endotoxin over a period of time leads to mechanisms down regulating the NF-κB responses to LPS, as these signals are damaging to the host in the face of constant exposure (Blackwell et al., 1997). It's recently been demonstrated that circulating immune cells isolated from the blood of South African and Ecuadorian children display a significantly ablated cytokine response against a wide-variety of TLR agonists (Smolen et al., 2014). This represents a plausible mechanism of how increased systemic exposure to MAMPs can alter immune

mechanisms and possibly alter the immune response to extraneous antigenic exposure. In situations, like children being raised in poor sanitary environments, where the host is constantly exposed systemically to small levels of external antigens, the threshold of this damaging response could be raised and more tolerogenic mechanisms promoted.

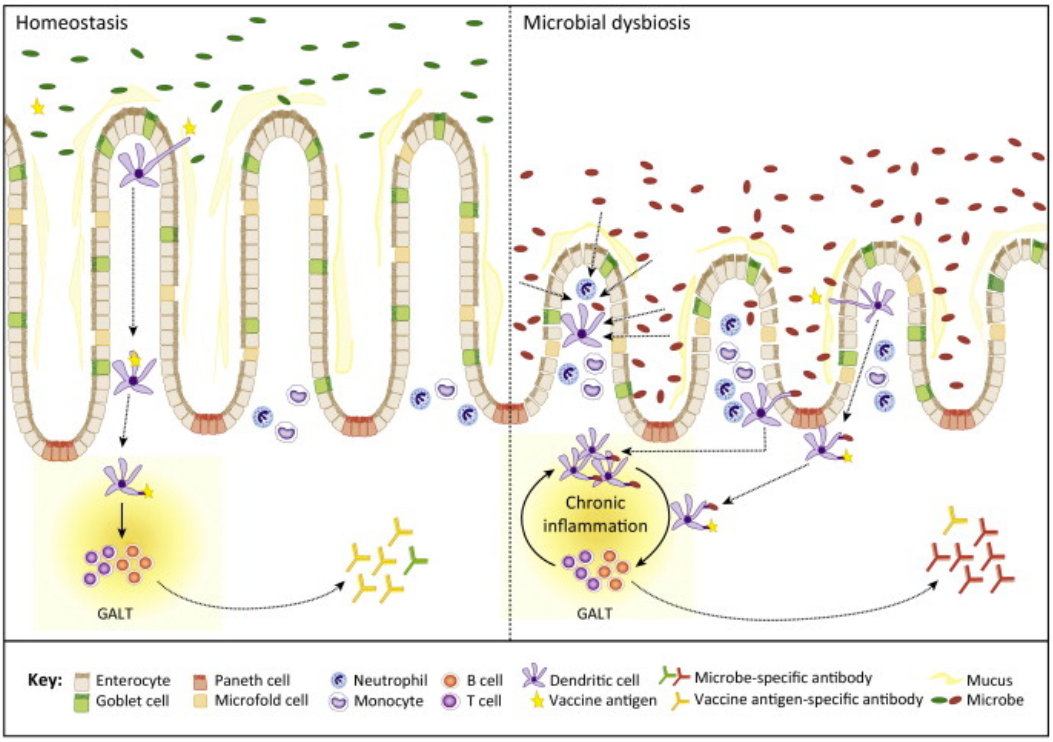

Figure 1.2 Representation of how early-life microbial dysbiosis and EE-features could impact vaccine responses

There is still much to learn regarding EE, including its pathophysiology, prevalence, and a thorough assessment of potential therapeutics to reverse it. However, taken together, much has been learned about EE in the last decade, since the Gates Foundation and others have begun funding this research. Recent developments in technology, including endoscopy and genomic techniques, promise to provide a roadmap to a greater understanding of this complex condition. The push to define EE using more robust and practical biomarkers is underway, as well as the aim to identify whether specific subsets of the disease occur in different geographical regions of the world (Korpe and Petri, 2012). Gut-on-a-chip technology and the development of preclinical animal models will be crucial for generating preclinical data to use in the field as therapeutic interventions. To achieve a greater understanding of the pathophysiology of EE, future studies should focus more on the small intestine as a region to sample for correlates of the disease, rather than fecal samples. The intestinal microbiome and immune system function and role in the disease should be addressed with focused, specific, testable hypothesis to unravel the complexities of all possible interactions which could result in development of EE. As it turns out, EE and malnutrition may also play a large role in not only growth stunting but the cognitive impairment seen in children in developing countries (Guerrant et al., 2013). The role of the gut-brain connection in this cognitive decline and should be assessed, as well as if the presence of EE-features early in life play a role in brain function. Given that EE is now regarded as the main factor behind the persistence and irreversibility of malnutrition, answering these questions and addressing these problems will be of utmost importance to improve childhood health and ameliorate stunting worldwide.

1.2 Interactions between the microbiome, immunity and metabolism in the intestine

1.2.1 Diet-induced microbiota shifts shape immunity and metabolism in the intestine

The double-burden of obesity and malnutrition has had a substantial impact on human health globally. Obesity and diabetes rates have almost doubled since 1980 worldwide, more than 40 million children under 5 were overweight in 2011(Riley et al., 2013) and 170 million children are malnourished (Lutter et al., 2011). Diet and nutrition early in life play an important role in these metabolic disorders. However, the prevalence and severity of obesity and malnutrition cannot be attributed to over-eating or food insecurity alone (Gordon et al., 2012b). Early-life dietary intake is a strong driver of one's composition of intestinal microbes (David et al., 2014). In turn, diet driven alteration of the intestinal microbiota can feed back into host metabolism and immunity, with differing consequences dependent on the composition and metabolic potential of the colonizing microbes (Sommer and Backhed, 2013). Early in life, weight gain and height are important measures of human health, and are surrogate markers for nutritional status. Human populations across differing geographical regions face two separate problems relating to nutritional status; malnutrition and obesity. In each condition, the interrelationship between the microbiota, metabolism and immunity in life plays an important role in determining outcomes of severity of diseases seen in malnourished and obese humans, such as EE in malnourished children and early onset of type 2 diabetes in obese children (Kau et al., 2011). Interestingly, studies show early-life malnutrition also confers an increased risk of obesity in adulthood (Bourke et al., 2016). Some features of obesity overlap with those of malnutrition, including a fatty liver, microbial dysbiosis, increased intestinal permeability,

increased in systemic inflammation, high-blood pressure, and increased risk of chronic infections (Bourke et al., 2016).

In obesity, seminal research early on implicated the composition of the intestinal microbiota as mediators of weight gain, as the ratio between Bacteroidetes and Firmicutes in the gut correlated with the ability of the host to extract energy from their diet (Turnbaugh et al., 2009). Furthermore, in twins discordant for obesity, transfer of their microbiota into germ-free mice was sufficient to account for their variations in weight, independent of genetics (Ridaura et al., 2013). The mechanisms that the microbiota use to signal a shift in host metabolism include signaling through TLR5 (Vijay-Kumar et al., 2010), GLP-1/2 (Cani et al., 2009) and mediating systemic LPS levels (Cani et al., 2007), indicating both altered microbiota and immune function are linked to the pathophysiology of obesity. Obesity has an inflammatory component that can account for the development of metabolic disease, reflected by higher levels of circulating inflammatory proteins, increased adipokine secretion by tissues and dysregulated activation of leukocytes across various tissue sites, including the liver and brain (Gregor and Hotamisligil, 2011). This immune dysregulation is characterized by inflammatory infiltrate of adipose tissue by M2 macrophages, and CD8+/CD4+ T cells which express increased levels of inflammatory cytokines including IL-17A, TNF-α and IFN-γ (Gregor and Hotamisligil, 2011). The importance of inflammation was also exemplified in a study which showed the blockade of TNF-α signaling in mice leads to protection from insulin resistance in a mouse model of obesity (Uysal et al., 1997).

It is now clear that early life changes in our microbiota composition can alter susceptibility to developing obesity later in life. As discussed previous, mode of delivery at birth can alter the early-life microbial community, where C-section born microbiota is more similar to that of the skin microbiota, rather than vaginal. In a study of Brazilian children with obesity, subjects born by C-section had a significantly higher risk to be obese as young adults compared to those born by vaginal delivery (Mesquita et al., 2013). Similarly, children fed infant formula rather than breast-milk for the first 6 months of life were more than twice as likely to be obese later in life compared to children who were bottle-fed (Gibbs and Forste, 2014). Aside from the nutritional intake early in life, many children are exposed to antibiotics throughout their childhood. Sub-therapeutic doses of several classes of antibiotics have widely been used as early life growth-promoters in the agriculture industry for decades. Mechanisms of this effect were unclear until recently, where a study showed these sub-therapeutic doses are sufficient to alter the intestinal microbiota, which resulted in enrichment of key microbial genes involved in carbohydrate metabolism to create SCFAs, as well as systemic changes to hepatic lipid and cholesterol metabolism, leading to increased adiposity in young mice (Cho et al., 2012). Thus, low levels or exposure to antibiotic can induce subtle shifts in the microbial ecosystem, selecting for an environment more conducive for weight gain and energy harvest. Epidemiological studies show early-life antibiotic use and obesity is correlated, as states in the U.S. with the highest obesity rates also have the highest rates of antibiotic use (Riley et al., 2013). Numerous studies have shown presence/absence of specific microbes can modulate and program life-long changes in immunity (Hooper et al., 2012), yet future studies must assess in greater detail how these changes could impact metabolic disease progression. The early life microbiota is less stable and resilient, and more sensitive to alterations that can lead to life-long programmed changes in

immunity or metabolism, resulting in increased risk of obesity, along with its disease associations (Yatsunenko et al., 2012). By understanding the differing energy harvest and metabolic capabilities of each child's microbiota, we may be able to create microbiota-based interventions to reverse susceptibility to obesity early in life. Two recent studies demonstrated that treatment of obese mice with *Akkermansia muciniphila* ameliorated symptoms of high-fat diet-induced metabolic disorders, including fat-mass gain, metabolic endotoxemia, adipose tissue inflammation, and insulin resistance (Shin et al., 2014; Everard et al., 2013). Colonization with *A. muciniphila* increased intestinal endocannaboid levels, controlling inflammation, and also increased the thickness of the inner mucus layer (Everard et al., 2013). These treatments required viable *A. muciniphila,* highlighting the importance of the metabolic output of the bacterium, and hinted that its mechanism of impact on immunity and metabolism was not mediated by innate immune recognition. These studies and future efforts hold hope that susceptibility to obesity could be controlled early in life through the microbiota and disease outcomes of obesity could also be improved by probiotics.

Similar to obesity, the composition of the gut microbiota also plays a role in the etiology and symptoms of malnutrition (Tilg and Moschen, 2013) and this relationship is also bi-directional (Kane et al., 2015). During the first two years of life in malnourished children, there is an immature development of the intestinal microbiota compared to healthy, case-controlled, children (Subramanian et al., 2014), and a comprehensive study across multiple geographical regions concluded children consistently harbor a significantly more diverse early-life microbiota composition in low socioeconomic regions of the world (Yatsunenko et al., 2012). Function and composition of the intestinal microbiota also plays a role in the development and severity of

malnutrition. Utilizing a similar strategy as mentioned previously, transferring the feces from Malawian twins discordant for severe protein malnutrition into germ-free mice, Smith *et al* were able to show a more direct role for the microbiota in mediating symptoms of malnutrition (Smith et al., 2013). Furthermore, germ-free mice fed a Malawian diet and Malawian microbes lost weight quickly, and this effect could not be fully reversed after feeding with a diet of therapeutic food, implying changes in the microbiota can persistently alter host immunity and metabolism. Which microbes were driving this effect were discovered using a IgA sorting and sequencing method called IgA-SEQ which aims to sequence the microbes which are targeted by IgA and compare those to the sequences that were untargeted. Using this method, a approximately 13 strains of Bacteroidetes and Proteobacteria were found to be highly-targeted by IgA and alone could transfer the growth stunting effect (Kau et al., 2015). IgA targeting implies the host has recognized this bacterial species, and studies show they will target beneficial microbes such as *Akkermansia* and *Lactobacillus* during homeostasis and pathobionts during inflammation and dysbiosis (Palm et al., 2014). These studies indicate microbes can play a role in causing malnutrition however the role of microbes in exacerbating malnutrition is complex and multifaceted, and only beginning to be understood. Studies in humans have uncovered enzymatic functions for the microbiota early in life that could also be altered and lead to malnutrition. Breast milk provides an important source of nutrients for children during their first six months of life, and it is an important dietary factor which promotes the growth and development of health-associated species in the microbiota (Walker and Iyengar, 2015). Breast milk is composed of many complex glycosylated proteins, and many members of gut bacteria have enzymes to release these sugars from breast milk, unlocking them for use of both the bacteria and the host (Zivkovic et al., 2011). For example, humans do not make sialic acid for the first three months of life,

instead relying on the microbiota to release it from dietary sources such as breast milk, and recent studies suggest malnourished mothers have less sialylated breast milk which contributes to developmental problems for their children including growth stunting and susceptibility to pathogens (Charbonneau et al., 2016a). Regional differences in the fucosylation of breast milk also exists, these people are labelled as "secretors" and "non-secretors," and the secretor status of breast milk also influences the resistance to pathogens, as fucose as a number of positive benefits to intestinal health (Charbonneau et al., 2016b; Lewis et al., 2015).

It is the goal moving forward to reverse malnutrition by leveraging what we now know is a dysbiotic microbiota which develops during poor dietary intake. Symptoms of malnutrition could be reversible early in life using a probiotic approach, as studies in mice have shown *Clostridium scindens* (Blanton et al., 2016), and *Lactobacillus plantarum* (Schwarzer et al., 2016) result in growth promotion only when given early in life during this 'critical window.' The success of these studies relies upon genetically identical mice with dietary and environmental exposures that are carefully controlled. Translating this success to humans who are malnourished will be a challenge, with field studies showing microbial-based therapies based upon a single microbial strain unsuccessful (Galpin et al., 2005). We will likely need to identify personalized or regionalized strategies to address malnutrition and use dietary treatment along with any probiotic to allow the best chance for colonization of the microbe.

Of note for both obesity and malnutrition, evidence is accumulating that diet-induced effects on body physiology can be passed on through epigenetic re-programming of maternal and paternal DNA. Further, a critical early window exists in a child's life, where its environmental

exposures (including diet and microbes) can shift the immune-metabolism-microbiota interactions to pathophysiological states which also lead to alterations in host growth rates, metabolism and immunity, ultimately resulting in diseases relating to obesity and malnutrition (such as type 2 diabetes and EE, respectively). A new study suggests the impact of diet and environmental change stresses on the host can be passed on maternally to children, through epigenetic modulation of the DNA by methylation (Dominguez-Salas et al., 2014). Maternal transfer of genes resulting in children being more susceptible to obesity and malnutrition has also been documented (Victora et al., 2008). For example, community-based studies of obesity show prior dietary practices and exposure to a social "meta-community" of microbes within social groups can effect responses to dietary interventions and obesity rates (Griffin et al., 2017). Thus, maternal dietary and microbial exposures are also crucial to the development of the microbiota early in life, as children may inherit genes with differing potential for predisposition for malnutrition or obesity, based on the diet of their mother. For malnutrition, maternal health is of particular importance for early-life seeding of the intestinal microbiome, and immune development through breast-milk (Gordon et al., 2012a). Future studies thus must focus not only on early-life therapeutic interventions to promote improved intestinal health to combat obesity and malnutrition, but also focus on maternal health to achieve a holistic approach to quelling the impact malnutrition and obesity have on society today.

1.2.2 The role of the mucosal immune system in maintaining intestinal homeostasis

To understand how diet-induced changes to immunity and the microbiota can result in chronic inflammatory diseases, such as EE, it's first important to grasp the complexity of the

interaction between the microbiome and the intestinal immune system. The intestinal immune system in germ-free mammals is underdeveloped, deficient in many immune components including circulating antibodies, mucus production, AMP production and mucosal T cells (Cebra, 1999). This indicates that the presence of intestinal microbiota induces immune maturation. Simultaneously the immune system must be able to sense what microbes are present and respond appropriately. A variety of proteins called pattern recognition receptors (PRRs) are expressed by IECs and many hematopoietic cells and mediate interactions between the immune system and the microbiota. Expression of these PRRs is crucial for maintaining homeostasis with the intestinal microbiota (Abreu, 2010). PRRs include Toll-like receptors (TLRs) and nuclear oligomerization domain like receptors (NLRs), which recognize microbe-associated molecular patterns (MAMPs), including lipopolysaccharide (LPS), lipid A, peptidoglycan, flagella and microbial RNA/DNA, leading to a variety of downstream signaling pathways (Takeuchi and Akira, 2010). PRR-MAMP interactions are crucial in promoting mucosal barrier function, regulating the production of mucins, AMPs, IgA and IL-22(Carvalho et al., 2012a). Accumulating evidence suggests a loss of specific PRRs can lead to an altered microbial composition and intestinal barrier defects leading to microbial invasion of systemic organs. The composition of the ileal microbiota in TLR2-, TLR4-, TLR5- and TLR9-deficient mice was shown to remain stable in the short term, however TLR deficiency led to longer-term familial shifts in microbial composition (Ubeda et al., 2012). Specifically, deficiency of TLR5, which recognizes bacterial flagellin, leads to an increased translocation of commensals to the liver and spleen, increased susceptibility to colitis and metabolic abnormalities (Vijay-Kumar et al., 2010; Vijay-Kumar et al., 2007). These observations suggest that the abnormalities seen in short-term TLR-deficiencies may result from a barrier defect in the containment of commensals, rather than

compositional shifts in the microbiota. Mice lacking the adaptor protein MyD88 have increased colonization of the liver and spleen by commensal microbiota (Slack et al., 2009) and reconstitution of MyD88 in Paneth cells limited the microbial penetration into these tissues (Vaishnava et al., 2008). Aside from the well-described role as a TLR adaptor protein, MyD88-deficiency also leads to a loss of signaling events downstream of the IL-1 receptor, including production of IL-1, IL-18 and IL-33 (Salcedo et al., 2010). Recently the inflammasome has garnered increased attention as an important regulator of intestinal homeostasis. NLRP6-deficiency in mice leads to a decreased production of IL-18 from the inflammasome, increased susceptibility to DSS-colitis and an altered colonic microbiota enriched in the *Prevotellaceae* and TM7 (Elinav et al., 2011). NLRP6 expression in the epithelium can also positively regulate autophagy cell processes and goblet cell mucus secretion in the colon (Wlodarska et al., 2014).

Pattern recognition of MAMPs is particularly important in the small intestine, which lacks a thick mucus layer segregating the microbiota (Santaolalla and Abreu, 2012). Here, recognition of luminal antigens by intestinal dendritic cells (DCs) is an important mode of sensing and controlling the immune response to the microbiota (Coombes and Powrie, 2008). Recent evidence has shown $CD103^+$ DCs, a subset of DCs crucial to intestinal homeostasis, can sample luminal antigens in the small intestine through direct luminal sampling (Farache et al., 2013), goblet cell-mediated delivery (McDole et al., 2012) or through M-cell transcytosis in Peyer's Patches (Coombes and Powrie, 2008). More experimental data is needed to explore the impact and prevalence of each these mechanisms. It is hypothesized different modes of antigen sampling could lead to alternate outcomes (Knoop et al., 2013), and future studies in this area will be important to understand how the immune system responds to the intestinal microbial

composition. Though innate barriers segregate the microbiota from the IECs, it is clear that controlled sensory mechanisms exist to sample the microbiota composition, and this is a key regulator of homeostasis.

While the innate immune system provides protection via the mucus layer, AMPs and ILCs to indiscriminately control microbial composition and penetration of the epithelium, the adaptive immune system provides a further layer of protection. This is mediated by the production of IgA, acting as a link between these two arms of the immune system. While non-specific IgA binds to microbial surface glycans causing bacterial agglutination (Mestecky and Russell, 2009), microbe-specific IgA is the main adaptive immune response controlling the microbiota. IgA production results from stimulation of B cells in Peyer's Patches by DCs, which sample the small number of bacteria penetrating through the mucus layer (Bemark et al., 2012). The cytokine milieu found in this environment, and in particular the presence of TGF-β, results in B cell class switching to produce IgA, which is then transcytosed back into the intestinal lumen (Macpherson and Uhr, 2004). Secreted IgA is preferentially utilized to recognize the microbiota and it possesses a variety of unique properties, tuning it to respond effectively to an environment filled with microbial antigens. Host repertoires of IgA coat a majority of the intestinal microbiota without eliciting potent and potentially damaging responses, and seem to be specific for distinct bacterial epitopes of commensals (Palm et al., 2014). The repertoire of secreted IgA is constantly shifting to respond to the changing intestinal microbial environment and might be dynamically shaped to mirror the composition of the microbiota (Hapfelmeier et al., 2010). How microbiota-specific IgA mediates epithelial protection is unclear, although a number of functions have been described. The action of IgA may include trapping of organisms

in the mucus, prevention of epithelial cell invasion and alteration of bound bacteria, including abrogation of bacterial resistance to the oxidative burst response (Peterson et al., 2007). The importance of IgA in keeping the systemic immune system ignorant of the microbiota is evident by the fact that IgA-deficient mice show priming of IgG responses against organisms which would be expected to form part of the microbiota (Macpherson et al., 2000). In addition, IgA may also have a role in shaping microbiota composition. Mice lacking genes for IgA class switching have an expansion of Firmicutes, notably epithelial-associated segmented-filamentous bacteria, and *Rag2*$^{-/-}$ mice have an altered microbiota, which can be restored after bone marrow reconstitution (Suzuki et al., 2004). Furthermore, mice deficient in somatic hypermutation genes have an expansion of microbiota in the small intestine and impaired mucosal defense (Wei et al., 2011). The current literature, based on mouse models, suggests that IgA adds an immunological buffer to host–microbiota interactions in the intestine and the affinity of microbe-IgA interaction required to achieve this buffering appears to be bacterial species-specific (Slack et al., 2012). Yet the mechanisms and signaling pathways of how IgA functions in humans remain poorly understood and more studies are needed to examine how IgA interacts with human commensals.

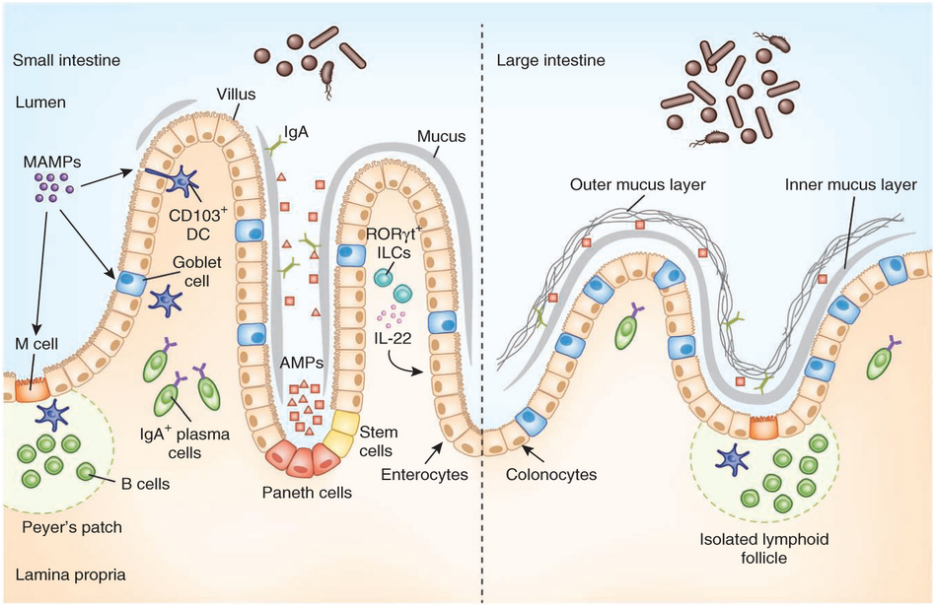

Figure 1.3 Anatomical and chemical barriers to the microbiota provided by the intestinal immune system

T-cell mediated responses and also important in maintaining intestinal homeostasis. A number of T-cell subsets are involved in containment of the microbiota, including $CD4^+$ $CD25^+$ $FoxP3^+$ regulatory T-cells (Tregs), and Th17 cells. Their functions range from providing help for B cells in production of IgA to avoiding autoimmunity and chronic inflammation. IgA production results from both T-cell dependent and independent pathways (Bemark et al., 2012), however the degree of interaction between IgA and T-cells within the intestinal submucosa is unclear. Aside from their suppressor function, Treg cells can differentiate to act as helper cells to induce microbiota specific IgA responses. In one study, depletion of Treg cells resulted in a decrease in IgA^+ B cells and subsequent adoptive transfer of Tregs cells into $Tcr\beta^{-/-}$ x $Tcr\delta^{-/-}$ mice was able to reverse this process (Cong et al., 2009). Whether this interaction occurred in Peyer's patches, isolated lymphoid follicles or in the lamina propria was not examined. *In vitro* studies suggested that this was dependent on TGF-β activity (Borsutzky et al., 2004), but further investigation is required to fully understand the precise nature and location of this interaction. In

healthy hosts, Treg cells prevent excessive cell-mediated immune responses, which would cause harmful inflammation, allowing tolerance of the microbiota. The importance of Treg cells is highlighted in the *Helicobacter hepaticus* colitis model in *Rag2*$^{-/-}$ mice, where adoptive transfer of Treg cells is sufficient to inhibit inflammation. This is via suppression of Th1 responses and T cell-independent innate immune-induced inflammation, with the latter mechanism being via IL-10 and TGF-β dependent pathways (Maloy et al., 2003; Read et al., 2000). TGF-β also has a key role in maintaining homeostasis of the intestinal microbiota, being required for T cell dependent regulation of IgA production and suppression of innate immune-induced inflammation. TGF-β also stimulates differentiation of Th17 cells (Li et al., 2007), and a number of Th17-derived cytokines, including IL-17 and IL-22 have key roles in regulation of the normal intestinal microbiota (Basu et al., 2012). The balance between differentiation of Th17 and Treg cell subsets is reciprocally regulated in the intestine, mediated by STAT3-mediated cytokines such as IL-6 and IL-23 (Ahern et al., 2010; Littman and Rudensky, 2010). The significance of the differing locations of these two cell types is not completely clear, however, as both are able to suppress colitis in adoptive transfer studies of mice (Foussat et al., 2003).

Over millions of years of host-microbe co-evolution, the intestinal immune system has used various strategies to respond to the microbial environment in a way that benefits host health. These strategies are multilayered, multifunctional and interconnected, and function in a tissue-specific manner to avert immune-mediated epithelial damage. Constant feedback from multiple layers of immunity, including specialized IECs and innate and adaptive immune cells, is required to contain and tolerate the microbial load. As the inherent complexities of the system

become clearer, a number of open questions remain. For example, the human gut is colonized with stable communities of eukaryotic microorganisms and a broad diversity of viruses. Being the dominant members of the community, bacteria have been the subject of much of the focus, but how the intestinal immune system interacts with eukaryotic microorganisms is unclear, especially in the context of malnutrition and diet-induced microbial changes.

As techniques for system-wide analysis improve, it will be important to understand the bi-directional relationship of the host-microbial system if new therapeutics are to be developed to combat inflammatory diseases such as EE. It is unknown to what level the microbial composition of an individual is driven by host immunity and genetics or by inherent dynamics of the microbial system. For example, it is unclear whether microbial dysbiosis seen after deletions of specific immune genes is due to resulting inflammation from proximity of microbiota to IECs or is due to the loss of function of immune effectors themselves. Constant feedback between host and microbe is required to find and maintain a homeostatic balance. In unbalanced situations, such as in chronic inflammatory diseases like EE, a working knowledge of how these systems interact will further the potential for targeted system-wide interventions that best improve health and prevent disease.

1.3 Conclusion

Current literature outlined here suggests that, given all we know about nutrition-immune-microbiota interactions, there is still much to learn about how these interactions play a role, if any, in the pathophysiology of EE and exacerbation of malnutrition. **We hypothesize that malnutrition alters the small intestinal microbiota, metabolism and immune system which,**

in combination the with specific microbial exposure, could be the trigger for EE-features and these features can be reproduced in a murine model system. In this study, we aim to determine: (1) the microbiota, immune and metabolic changes in the small intestine after early-life malnutrition; (2) whether we can utilize these data to reproduce the defining features of human EE reproducibly in mice; (3) how early-life malnutrition impacts enteric infection and discover novel mechanisms which could potentially trigger EE-features.

In spite of its broad impact on worldwide malnutrition and mortality, the pathogenic mechanisms of EE have received little attention and the underlying etiology is unknown. The lack of an animal model is a major limitation in understanding the basic mechanisms leading to EE and development of a model would be fundamental for generating therapeutic interventions in the clinic. An aberrant inflammatory response to the intestinal microbiota is now known as a major component in the etiology of inflammatory bowel diseases, however changes in the microbial, immune and metabolic architecture of the intestine during malnutrition are mostly unknown. This work will collectively increase our understanding of the interplay between the microbiota, metabolism and immunity during malnutrition and hopefully provide a working murine model to aid in the understanding of EE, such as how it is triggered and how it could be reversed. Work from this study may lead to the development of new and much needed diagnostic and therapeutic tools for the study of EE in humans.

Chapter 2: Characterizing the impact of malnutrition on the intestinal microbiome, metabolism and epithelial barrier function

2.1 Introduction

Early-life malnutrition results in childhood growth stunting, increased intestinal permeability, along with significant changes in intestinal microbiota composition and metabolite abundance (Kau et al., 2011). Here, we aim to characterize and further comprehend how malnutrition results in these intestinal consequences in the mammalian intestine, and the understanding of this will aid in the goal of reversing the impact of malnutrition worldwide.

Both function and composition of the intestinal microbiota also plays a role in the development and severity of malnutrition. This has been documented through GF transfer studies of microbiome communities from malnourished twins discordant for symptoms of malnutrition, and revealed the microbiota composition played a role in these differing malnutrition symptoms, even in humans with the same genetic background (Smith et al., 2013). IgA-SEQ has identified a subset of microbes, mainly Bacteroidetes and Enterobacteriaceae, which drive this phenotype of increased inflammation and growth stunting (Kau et al., 2015). However, the intestinal impact of malnutrition and vice versa goes beyond the composition of the microbiota, and we now understand microbes in our gut are responsible for synthesizing and bio-transforming a number of metabolites in the intestine such as bile acids, SCFAs, vitamins, lipids, lignans, and polyphenols (Donia and Fischbach, 2015). Malnutrition can be thought of as a form of metabolic syndrome, understanding how the immature and dysbiotic microbial community impacts host metabolism will be critical for targeting which nodes of this system to treat with therapeutics.

Urine and serum metabolites have been analyzed in malnourished children in Brazil (Mayneris-Perxachs et al., 2016), revealing broad changes in metabolites present that link to liver function, such as urobilinogen or indicate the presence of low grade systemic inflammation. In many of these cases, microbes play a role in their metabolism and synthesis. The best studied metabolite that can be bio-transformed by gut microbes are bile acids (Donia and Fischbach, 2015). Studies in humans have analyzed if these metabolites are changed during malnutrition, mostly sampling the serum of malnourished children and funding correlations between growth stunting, inflammation and which bile acids are present in serum (Semba et al., 2016). Some functions of bile acids include aiding the absorption of nutrients such as vitamins and lipids in the intestine, and providing antimicrobial and anti-inflammatory signaling benefits to the host (Monte, 2009). Which bile acids that are present in different areas of the intestine can influence the absorptive potential of the gut and lead to or be the result of microbial changes (Sayin et al., 2013). As we become closer to understanding which bile acids play critical roles in intestinal health, screening for bile acids correlating to health and disease is proposed to be an important read-out for improvement of intestinal health. Vitamins and SCFAs play significant roles in the intestine as well, interacting with the immune system and metabolic pathways to provide energy to cells, maintain tolerance to intestinal antigens and promote mucus barrier function (Krajmalnik-Brown et al., 2012).

Barrier function in particular is altered during malnutrition early in life. The intestinal tract is the only organ of the body aside from the skin that is constantly exposed to our external environment, much of which is potentially harmful to the host if allowed to reach other organs in our bodies. We have a variety of mechanisms to control what is permitted to be absorbed in the

intestine. As mentioned previously, the intestinal barrier is made up of a number of chemical and anatomical barriers including the mucus layer, tight junction proteins, antibodies, antimicrobial peptides and epithelial cells themselves (Brown et al., 2013). A number of these barriers break down during malnutrition and best studied is both moderate and severe protein malnutrition. In severe protein malnutrition there is a decreased amount of IgA that crosses into the intestine and decreased expression of antimicrobial peptides (Hashimoto et al., 2012). Further, in many cases severe malnutrition results in increased serum endotoxin levels and circulating bacterial products (Kelly et al., 2004). These observations are also indicative of systemic inflammation, which can be analyzed by increased C-reactive protein (CRP), and cytokines such as IL-6 and TNF-α (Guerrant et al., 2016). Improper functioning or destruction of tight junction proteins in the intestine are thought to be the main culprit for this barrier breach. Zonulin and fatty-acid binding protein (FABP) are common serum biomarkers for intestinal epithelial cell health and tight junction function that are changed during malnutrition, providing non-invasive measures of barrier function, much needed due to the challenge of obtaining intestinal biopsies (Guerrant et al., 2016). The lactulose-mannitol duel sugar testing remains the gold standard for identifying increased intestinal permeability and barrier dysfunction in humans, and a number of studies have linked increased lactulose in the urine to nutritional status in humans (Lee et al., 2014). As mentioned previously, there are a number of problems with this assay for practical use in the field, including degradation of sugars and stability of the urine over time. There is a need to develop alternate strategies which aim to correct this issue and provide a more accurate and practical non-invasive strategy for assessment of permeability and barrier function.

Our understanding of how malnutrition impacts the intestinal environment is limited not only by the practicality and accuracy of the assays but there is also a sampling problem. Our most practical method of analyzing the intestine is taking a fecal sample, however that only is representative the colonic environment and is not representative of the small intestine which is approximately two-thirds of the intestine. Obtaining samples from the small intestine is invasive and, in many cases, unethical (Ngure et al., 2014). We then must rely on studies of other mammalian model systems to fully grasp and characterize how malnutrition impacts the gut. To date, these studies have been lacking in the field. A few use germ-free transfers of malnourished microbiota from humans (Smith et al., 2013), and others have studied the intestinal consequences of severe malnutrition and fasting (Gordon et al., 2012a), but we have very little data on how moderate malnutrition will change the microbiome and metabolite composition in the gut and how this relates to barrier function. Before we can develop a new murine model to study diseases such as EE and other chronic intestinal inflammatory maladies of the developing world (areas with poor sanitation), we must first study the baseline of how diet alone effects these markers of intestinal health.

Here we use a murine model system to describe the impact of early-life malnutrition on epithelial barrier function, metabolome, and relate these changes to the composition of the intestinal microbiome. Three-week-old C57BL/6 mice administered a protein and fat malnourished diet (7% and 5% respectively) gained significantly less weight than isocaloric control-fed mice, and this phenotype was observed alongside decreased abundance of tight-junction proteins and increase in intestinal permeability to dextran. Mice given the malnourished diet were also found to have an altered intestinal microbiota and metabolome, notably including

profound changes in the bile-acid profile, where there were large differences between conjugated and unconjugated bile acids and vitamins A, B, D and E abundance. In each case, we aim to see these changes in host physiology in the context of which microbes are present and attempt to connect these observations to provide a holistic view on how the dietary shift to lower protein and fat alters the intestinal environment.

2.2 Materials and methods

2.2.1 Animal studies

All animal work was done according to the Canadian Council on Animal Care guidelines, utilizing protocols that were approved for use by the Animal Care Committee at the University of British Columbia. Three-week-old, female C57BL/6 mice were ordered for each experiment (Jackson Laboratory, Bar Harbor, ME) and housed in a barrier animal facility at the University of British Columbia (UBC) with a 12 hr light-dark cycle. Upon arrival, mice were randomized and housed into separate groups (4-5 per cage) which were either fed a malnourished diet moderately low in protein (7%) and fat (5%) or an isocaloric control diet with 20% protein and 15% fat, similar to one used in previous studies to induce protein malnutrition[56] (Research Diets, New Brunswick, NJ, Table 2.1). The chow was irradiated before use and mice were given the diet *ad libitum* throughout experiments.

2.2.2 RNA isolation and cDNA synthesis

Approximately 1 cm of the jejunum was excised and immediately submerged in RNA*later*™ (Qiagen, Valencia, CA) and stored at 4ºC overnight and then at -80ºC for subsequent RNA extraction. The RNA of the tissue was extracted using RNeasy Mini kit (Qiagen, Valencia, CA)

according to the manufacturer's instructions. RNA concentration and purity were determined using a NanoDrop ND-1000 (NanoDrop Technologies, Wilmington, DE, USA) and reverse transcription was completed with the Quantitect RT kit (Qiagen, Valencia, CA) utilizing a total of 1 μg RNA as template for the reaction.

2.2.3 Real-time qPCR for host gene expression

Real-time qPCR analysis for host gene expression was performed utilizing Quantitect SYBR-Green Mastermix (Qiagen, Valencia, CA), using primers listed in Table 3.1. PCR was performed in 10 μL reaction volumes on an Applied Biosystems 7500 machine and cycles consisted of 95°C for 15 min and 40 cycles of 95°C for 15 s, 60°C for 30s and 72°C for 30s. Glyceraldehyde-phosphate-dehydrogenase (GAPDH) was found to be an appropriate endogenous control and was used for normalization. Relative expression was calculated using the ΔΔC(t) method relative to the control mice.

2.2.4 FITC-dextran uptake assay

In order to directly assess intestinal permeability *in vivo*, mice were gavaged with 80 mg/mL of 4 kDa FITC-dextran (Sigma-Aldrich) at a volume of 150 μL, after food deprivation for 4 hours. Four-hours post inoculation, serum was collected from mice post-mortem and measured for FITC concentration using a plate reader (Tecan, Maennedorf, Switzerland). FITC was measured against a standard curve of serially diluted FITC-dextran, and the plate was read with the excitation of 485 nm and emission of 530 nm.

2.2.5 Histology

Intestinal sections 2 cm in length from the duodenum, jejunum, ileum and colon of mice were collected and immediately placed in 10% buffered formalin overnight at room temperature. Paraffin-embedded tissues were cut into 5 μm slices and stained with hematoxylin and eosin (H&E) using standard techniques. H&E stained tissues were visualized under a light microscope and villous length, and crypt depth of each crypt and villous of the tissue were enumerated using Axiovision version 4.6 software. Livers were excised, cut and stained with H&E in a similar manner as stated above and visualized under a light microscope for signs of pathology. For visualizing the mucus layer, 1 cm sections of the jejunum or colon were excised from mice, immediately submerged into methanol-Carnoy's fixative for 2 hrs at 4°C and then transferred to 100% ethanol. Paraffin-embedded tissues were cut into 5 μm slices and stained with Alcan blue-periodic acid (AB-PAS) using standard techniques.

2.2.6 DNA extraction and microbiome analysis

In order to assess the composition of the microbiota, sections from the small intestine and colon or fecal pellets of malnourished or control-fed mice were homogenized using a bead-beating method (FastPrep instrument, MP Biomedicals, Solon, OH), and total DNA was extracted using a Stool DNA Extraction Kit (Qiagen, Valencia, CA). 16S rRNA gene fragments were PCR amplified with nucleotide-bar-coded primer pairs 27F: 5′-AGAGTTTGATCMTGGCTCAG-3′and 510R: 5′-GWATTACCGCGGCKGCTG-3′ for pyrosequencing and 341F: 5'-CCTACGGGAGGCAGCAG-3' and 518R: 5'-ATTACCGCGGCTGCTGG for Ilumina. Each 50 μL of PCR contained 22 μL of water, 25 μL of TopTaq Master Mix, 0.5 μL of each forward and reverse barcoded primer, and 2 μL of template DNA. The PCR program consisted of an initial

DNA denaturation step at 95°C for (5 min), 25 cycles of DNA denaturation at 95°C (1 min), an annealing step at 50°C (1 min), an elongation step at 72°C (1 min), and a final elongation step at 72°C (7 min). Controls without template DNA were included to ensure that no contamination occurred. Amplicons were run on a 2% agarose gel to ensure adequate amplification. PCR products were gel-purified (QIAquick gel extraction kit, Qiagen, Valencia, CA). Purified samples were diluted 1:50 and quantified using PicoGreen (Invitrogen) in the TECAN M200 (excitation at 480 nm and emission at 520 nm). Each amplicon (100 ng) was pooled and sequenced using either a 454 Titanium platform (Roche, Branford, CT) or a Hi-Seq 2000 bidirectional Illumina sequencing and Cluster Kit v4 (Macrogen Inc.). For Illumina, library preparation was done using TruSeq DNA Sample Prep v2 Kit (Illumina) with 100 ng of DNA sample and QC library by Bioanalyzer DNA 1000 Chip (Agilent).

2.2.7 Bioinformatics

Sequences were preprocessed, de-noised, and quality-filtered by size using Mothur (Schloss et al., 2009). Representative sequences were clustered into OTUs using CrunchClust and classified against the Greengenes Database according to 97% similarity. Any OTUs present less than five times among all samples were removed from the analysis. Quality sequences were obtained by removing sequences with ambiguous bases, a quality read length less than 200 bases and/or chimeras identified using chimera.uchime. Quality sequences were aligned to the Silva bacterial reference alignment and operational taxonomic units (OTU) were generated using a dissimilarity cutoff of 0.03. Differences in microbial communities between groups and intestinal sites were investigated using the phylogeny-based weighted UniFrac distance metric (PCA plot) or plot using a non-metric distribution system (NMDS). The Bray Curtis index was used as a measure of

similarity in microbial composition. Diversity, similarity and abundance of bacterial OTUs and families were compared using the Mann-Whitney *U*-test or Student's *t*-test, and the Bonferroni correction was applied in cases of multiple comparisons.

2.2.8 Metabolite extraction

Mouse small intestine digesta samples (luminal contents) were collected, weighed and homogenized in water followed by addition of acetonitrile for metabolite extraction. After vortex mixing, 30 second sonication, and centrifugation, the clear supernatants were collected and dried under a gentle nitrogen gas flow. The dried metabolite residues were dissolved in 40% acetonitrile containing 0.01% formic acid, 4 μL per mg of the raw material. After 15 sec vortex and 30 sec sonication, each sample was further diluted 1:2 with water. Twelve-μL aliquots were injected for untargeted metabolic fingerprinting by ultrahigh-performance liquid chromatography – electrospray ionization/mass spectrometry (UPLC-ESI/MS).

2.2.9 UPLC-FTMS.

A Waters Acquity UPLC system coupled to a Thermo LTQ-Orbitrap Velos Pro mass spectrometer was used for metabolomic analysis. The mass spectrometer was equipped with a heated ESI source and was operated in the Fourier transform (FT) MS scan mode with mass resolution of 60,000 FWHM at m/z 400. The m/z detection range was 80 to 1200. A Waters BEH C_{18} UPLC column (2.1 mm x 50 mm, 1.7 μm) was used for chromatographic separation with the mobile phases being water-0.01%formic acid (solvent A) and acetonitrile-0.01% formic acid (solvent B). The binary solvent elution gradient was 5% to 40% B in 6 min and 40% to 100% B in 15 min. The mobile phase was kept at 100% B for 2 min before column equilibration with 5%

B for 4 min between injections. The column temperature was 50 ^{o}C and the flow rate was 0.3 mL/min. Two LC-MS runs per sample were performed in the (+) and (-) ion detection modes, respectively. Lock mass calibration was applied to ensure mass accuracy throughout LC-MS runs.

2.2.10 Data processing

The positive and negative ion UPLC-FTMS datasets were converted to the mzXML files using the MSCovert tool (ProteoWizard) and processed using the XCMS package (http://metlin.scripps.edu/xcms/) in the R platform (http://www.r-project.org/). For each dataset, peak detection and integration was performed using the centWave algorithm (Tautenhahn et al., 2008). Retention time (RT) shift correction was achieved considering at least 200 peak groups. After two iterations of peak grouping, imputation of missing data was performed by returning to the raw spectral data and integrating the areas of the missing peaks using the 'fillPeaks' algorithm. Finally, a data matrix was generated from each UPLC-MS dataset and imported into Microsoft Excel. After peak de-isotoping and removal of the significant background noise signals observed in each UPLCMS blank run the data was saved as two-dimensional (m/z-RT vs. peak area) matrices amenable to subsequent statistics and further data analysis.

2.2.11 Metabolic pathway analysis

The resulting m/z values after data processing were searched against the METLIN database (http://metlin.scripps.edu/metabo_batch.php?&return=yes) for metabolite identification. The metabolic pathways that the identified metabolites were involved in were matched using the Kyoto Encyclopedia of Genes and Genomes (KEGG) pathway tool, permitting the

overrepresentation analysis to determine overrepresented pathways in each treatment group. Multivariate statistical analysis (random forest, PCA) and overrepresentation analysis was carried out using the Metaboanalyst version 2.5 software (http://www.metaboanalyst.ca/MetaboAnalyst/), based upon recommendations from previous published protocols (Xia et al., 2012). The data from the positive and negative ion mode detection were treated separately in the statistical analysis. In the analysis, missing values were assumed to have been below the level of detection in the parameters. Each dataset was normalized to the median of each of the observed peaks, following a log transformation of the data. The Welch's two-sample *t*-test was used to determine significant changes between groups ($p<0.05$; fold-change >2).

2.2.12 Vitamin-targeted metabolomics

The samples were analyzed by UPLC-MRM/MS on a Dionex UltiMate 3400 RSLC system coupled to an AB Sciex 4000 QTRAP triple-quadrupole mass spectrometer equipped with an electrospray ionization source. The standard substances of vitamin A (retinal, retinol, retinoic acid), B1 (thiamine), B2 (riboflavin), B3 (niacinamide), B6 (pydidoximine, pyridoxine, pyridoxal, pyridoxal-mono-phosphate), B7 (biotin), B9 (folic acid), D2, D3, E (α-tocopherol, δ-tocopherol, and δ-tocotrienol), K1 and K2, were purchased either from Sigma-Aldrich or from Cayman Chemicals Inc. The MRM transitions of individual analytes were optimized by direct infusion of a standard solution of each compound into the MS instrument. Each sample was added with a methanolic BHT (2 mg/mL) solution at a ratio of 15 μL per mg of the small intestine digesta. Vitamins were extracted by homogenizing the samples at a shaking frequency of 30 Hz for 1 min twice using a Retsch MM400 mixer mill and with the aid of two 3-mm

stainless steel metal balls, followed by 5-min sonication in an icy water bath. The samples were then centrifuged in a micro-centrifuge at 12,500 rpm and 4^{o}C for 10 min. A 300-μL aliquot of the supernatant was transferred into a 3-mL borosilicate glass test tube and mixed with 300 μL of water and 900 μL of hexane. After 1 min vortex mixing, the tubes were centrifuged at 4000 rpm and 10 ^{o}C in a Beckman R22 centrifuge to separate the supernatant organic phase from the lower aqueous phase. The supernatants were carefully pipetted out to another sets of 3-mL test tubes. The fat-soluble vitamins were further extracted from the aqueous phase with 900 μL of hexane two more times. After liquid-liquid extraction, the pooled organic phase for each sample was dried down in a speed-vacuum concentrator at room temperature. The dried residue was reconstituted in 100 μL of ethanol. A 20-μL aliquot was injected for quantitation of the fat-soluble vitamins by LC-(+)ESI-MRM/MS on Waters BEH C18 (2.1 x 50 mm, 1.7 μm) UPLC column and with 0.1% formic acid in water and acetonitrile as the mobile phase for binary solvent gradient elution. An efficient elution gradient was 50% to 100% B in 10 min. The column temperature was 50^{o}C and the flow rate was 300 μL/min. The aqueous phases were loaded onto reversed-phase polymeric HLB cartridges (60 mg/1mL, Waters Inc.), which have been activated with 1 mL of methanol and equilibrated with 1 mL of 50% methanol before use. Under a 5-inch Hg vacuum, the flow-throw fractions were collected and the resins were washed with 1 mL of 50% methanol with the flow-through fractions collected. The pooled flow-through fractions were dried in a nitrogen evaporator at 30 ^{o}C. The residue from each sample was reconstituted in 100 μL of 2% methanol. A 20-μL aliquot was injected for quantitation of the water-soluble vitamins by UPLC-MRM/MS with (+) or (-) ESI and on a Waters BEH C18 (2.1 x 150 mm, 1.7 μm) UPLC column and using 0.01% formic acid in water and methanol as the mobile phase for binary solvent gradient elution. The efficient elution gradient was 2% B for 0.5

min and 2% to 50% B in 8 min. The column temperature was 30 ^{o}C and the flow rate was 250 μL/min. The concentrations of all the detected vitamins were calculated from the standard calibration curves of individual vitamins, which were prepared with the use of their authentic compounds.

2.2.13 Bile-acid targeted metabolomics

Each sample was homogenized in LC-MS grade water at a ratio of 150 μL per 10 mg raw material and with the aid of 5-mm stainless steel metal balls. Bile acids were extracted by addition of acetonitrile at a ratio of 350 μL per 10 mg raw material followed by vortexing and sonication (1 min) in an ice-water ultrasonic bath. The samples were centrifuged. 20 μL of the supernatants were precisely taken out and mixed with a predefined mix of 14 deuterium-labeled bile acids as the internal standards. The mixtures were subjected to phospholipid-depletion solid-phase extraction according to a validated protocol for sample cleanup and bile acid enrichment. The flow-through fractions were collected and then dried under a gentle nitrogen flow. The dried residues were dissolved in 200 μL of 50% methanol. 10 μL were injected for quantitation by UPLC-MRM/MS. A Dionex UPLC system was connected to an AB Sciex 4000 QTRAP mass spectrometer which was operated in the negative ion multiple-reaction monitoring (MRM) mode and with electrospray ionization. UPLC separation was carried out on a 15 cm long C-18 UPLC column with water-acetonitrile-formic acid as the mobile phase for binary gradient elution using a developed and validated protocol for comprehensive analysis of bile acids in biological samples (Han et al., 2015). The column temperature was 45 ^{o}C and the flow rate was 0.35 mL/min. 45 bile acids (including the 19 targeted bile acids) were involved in the quantitation by UPLC/scheduled MRM/MS. Concentrations of the detected bile acids were

calculated with internal standard calibration from the linearly regressed standard calibration curves of individual bile acids. The lower limits of quantitation were 0.08 n moles/mg for all the bile acids.

2.2.14 Short-chain fatty acid analysis

Small intestinal samples were weighed and combined with 25% phosphoric acid, vortexed and centrifuged until a clear supernatant was obtained. Supernatants were submitted for GC analysis to the Department of Agricultural, Food and Nutritional Science of the University of Alberta. Samples were analyzed as previously described (Campbell et al., 1997), with modifications. Briefly, samples were combined with 4-methyl-valeric acid as an internal standard and 0.2 ml was injected into the Bruker Scion 456 gas chromatograph, using a Stabilwax-DA 30m x 0.53mm x 0.5um column (Restek, Bellefonte, PA). A standard solution containing acetic acid, propionic acid, isobutyric acid, butyric acid, isovaleric acid, valeric acid and caproic acid, combined with internal standard was injected in every run. The PTV injector and FID detector temperatures were held at 250°C for the entire run. The oven was started at 80°C and immediately ramped to 210°C at 45°C/min, where it was held for 5.11 mins. Total run time was 8.00 mins. Helium was used at a constant flow of 20.00ml/min.

2.2.15 Total IgA Determination

Total IgA concentrations were measured in the feces and small intestinal luminal content using a commercially available ELISA kit (eBioscience). Fecal and small intestinal homogenates were weighed and diluted to 1:1000 for the assay. Sample concentrations were determined by

assessing the OD 450nm using a plate reader (Tecan, Maennedorf, Switzerland), compared to a standard curve, and normalized to weight of the fecal content.

2.2.16 Fluorescent *in-situ* hybridization

A 1 cm section of the colon was excised from mice, immediately submerged into methanol-Carnoy's fixative for 2 hrs at 4°C and then transferred to 100% ethanol. Fixed tissues were paraffin-embedded, cut with a microtome to a thickness of 6-10 μm and transferred to glass slides. The slides were let dry overnight, the tissues then fixed with 4% paraformaldehyde for 10 min at room temperature prior to permeabilization with a solution of 1 mg/ml lysozyme from Eggwhite at 37°C for 1hr. The tissues where then pre-incubated for 1hr at 42°C in hybridization buffer (20mM Tris-HCl, pH 8.0, 0.9M NaCl, 0.01% SDS, formamide, depending on the probe) (Sigma-Aldrich) and then the slides were let dry at 37°C and incubated overnight at 42°C with the respective probe linked to Alexa 555 (Invitrogen, Carlsbad, CA) in the corresponding hybridization buffer at a probe concentration of 50 nM. The following probes were used; all-Bacterial probe (Eub338), Firmicutes (equimolar mixture of LGC354A, B and C), Bacteroidetes (Bac303) and Gamma-Proteobacteria (Gam42a). Details on the probes can be found at ProbeBase (Loy et al., 2007) and the sequences of the probes used is listed in Table 3.3. The tissues were then incubated for 20 min with Alexafluor488-Phalloidin (130 nM) and DAPI at a concentration of 1 μg/ml prior to mounting with Prolong reagent. The slides were imaged on a Cell Voyager CV100 using a 40x oil immersion objective and stitched (90% overlap) and analyzed using Fidji.

2.2.17 Statistical analysis

Statistical significance for the difference between two treatment groups was calculated by using a two-tailed Student's *t*-test or the Mann-Whitney *U*-test (for non-parametric data) unless otherwise stated. For assessing statistical significance among three or more groups, a one-way ANOVA with post hoc Tukey's test was utilized. Statistical analysis was performed with assistance from GraphPad Prism Software Version 6.00 (GraphPad Software, San Diego California USA, www.graphpad.com). Statistical significance was given as *** p-value < 0.001; ** p-value < 0.01; * p-value < 0.05; ns (not significant) p-value > 0.05. The results are expressed as the mean value with standard error of the mean (SEM), unless otherwise indicated.

2.3 Moderate protein and fat malnutrition leads to growth stunting and barrier dysfunction

We first sought to characterize the impact of a moderately malnourished diet on the growth rate, intestinal architecture and barrier function of the small intestine in young mice. Post-weaning, mice were randomized into receiving either a malnourished diet (7% protein, 5% fat) or isocaloric control diet (20% protein, 15% fat) (Fig. 2.1a, Table 1). Both groups consumed equivalent weights per day of the chow (Fig. 2.2a). Mice fed the malnourished diet gained significantly less weight over time, in comparison to mice fed the isocaloric control diet (Fig. 2.1b). Growth stunting of the malnourished mice was evident as they gained an average of 30% less weight after 21 days (Fig. 2.1c). At this time point, malnourished mice also had considerably shorter tails, a surrogate marker for length of the mouse (Fig. 2.1d). There was a decreased expression of *insulin-like growth factor 1* (*IGF1*), which encodes a growth factor hormone, and

angiotensin-converting enzyme 2 (*ACE2*), which is necessary for protein uptake (Hashimoto et al., 2012), in the jejunum of malnourished mice (Fig. 2.2b,c). Next, the barrier function of the jejunum was assessed by analyzing mRNA expression levels of *tight-junction protein 1* (*TJP1)*, *claudin-2 (CLDN2)*, *claudin-4 (CLDN4)*, and *claudin-15 (CLDN15)*. *TJP1*, the product of which is ZO-1, a major component of tight-junction assembly and function (Fasano, 2011), was expressed at lower levels in malnourished mice (Fig. 2.1e). In contrast, the expression of *CLDN2* was up-regulated in the jejunum of malnourished mice, which is also indicative of increased permeability based on previous reports (Ulluwishewa et al., 2011) (Fig. 2.1e). However, the expression of other claudin transcripts (*CLDN4/15*) was similar between the groups of mice (Fig. 2.1e).

Table 2.1 A breakdown of the ingredients and calorie content in the malnourished and control diet.

	Control Diet		**Malnourished Diet**	
Ingredients	**Grams (%)**	**Kcal (%)**	**Grams (%)**	**Kcal (%)**
Casein	200	800	71	284
L-Cysteine	3	12	1.07	4
Corn Starch	346	1384	557	2228
Maltodextrin 10	45	180	70	280
Dextrose	250	1000	250	1000
Sucrose	0	0	2.41	10
Cellulose BW200	75	0	75	0
Inulin	25	25	25	25
Soybean Oil	70	630	23.3	210
Mineral Mix S10026	10	0	10	0
Dicalcium Phosphate	13	0	13	0
Calcium Carbonate	5.5	0	5.5	0
Potassium Citrate, 1 H2O	16.5	0	16.5	0
Vitamin Mix V10001	10	40	10	40
Choline Bitartrate	2	0	2	0
Total	**1071.05**	**4071**	**1131.83**	**4081**
Protein	19.0	20	6.4	7
Carbohydrates	63.1	65	80.6	88
Fat	6.5	15	2.1	5
Total		**100**		**100**
kcal/gm	**3.77**		**3.77**	

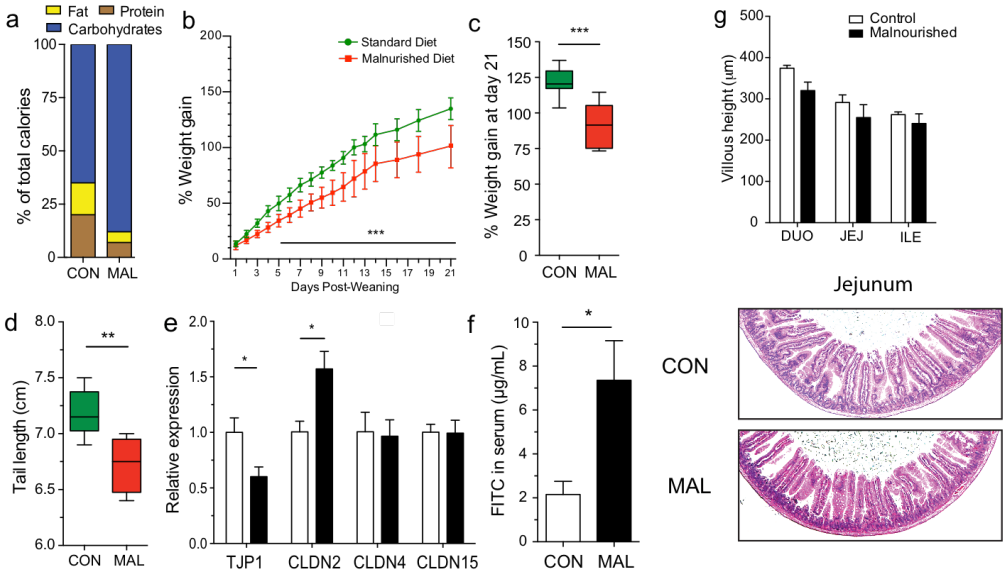

Figure 2.1 Assessment of the growth rate and intestinal barrier function in C57BL/6 mice fed a malnourished or isocaloric control diet.
(a) A schematic of the components of each diet, expressed as a percent of total calories. (b) Mice were given each diet post-weaning, and daily weight change was assessed daily over a period of 21 days. The data is representative of the 3 independent experiments, n=8 mice per group. Data points represent the mean and error bars the S.D. (***p<0.001, repeated measures ANOVA). After 3 weeks of being fed each diet, the total amount of (c) weight gained and (d) final tail lengths were calculated. In the box and whisker plots shown, the middle bar represents the mean, the bottom and top of the box are the first and third quartiles, and whiskers indicate the range of the data. Data are representative of 3 independent experiments, n=8 mice per group (***p<0.001, Student's *t*-test). (e) The jejunal mRNA expression of *TJP1, CLDN2, CLDN4* and *CLDN15* are expressed as fold-change relative to the control-fed mice. Bars indicate the mean with S.E., and are representative of 2 independent experiments, 8 mice per group (*p<0.05, Student's *t*-test). (f) Concentration of FITC in the serum was assessed 4 hours post-administration orally, after mice were fed each diet for 3 weeks. Bars indicate the mean with S.E., and are representative of 2 independent experiments, n=8 per group (*p<0.05, Student's *t*-test). (g) The average measured villous height in the duodenum, jejunum and ileum with representative H&E stained images of jejunum sections from mice exposed to each diet. Bar graph indicates the mean with S.E., and is representative of 3 independent experiments, 8 mice per group.

In order to measure whether these gene expression changes also had a functional impact on barrier function, mice were fed FITC-labeled dextran and subsequent FITC levels were measured in the serum. There was a 3.5-fold increase in the serum concentration of FITC in malnourished mice compared to controls, indicating an increase in intestinal permeability (Fig. 2.1f). Barrier dysfunction did not significantly impact total secretory IgA levels in the jejunum, an important antibody for host epithelial defense (Fig. 2.2d). Additionally, sections of the small intestine (duodenum, jejunum and ileum) were visualized microscopically and no significant signs of inflammation, goblet cell depletion, histopathology or villous blunting were observed in the mice fed the malnourished diet (Fig. 2.1g, Fig. 2.2e). These data suggest the malnourished diet led to a moderate growth stunting, and increased intestinal permeability relative to the isocaloric control diet independent of small intestinal histopathology.

(**a**) The average daily intake of chow was determined by weighing the food each day and

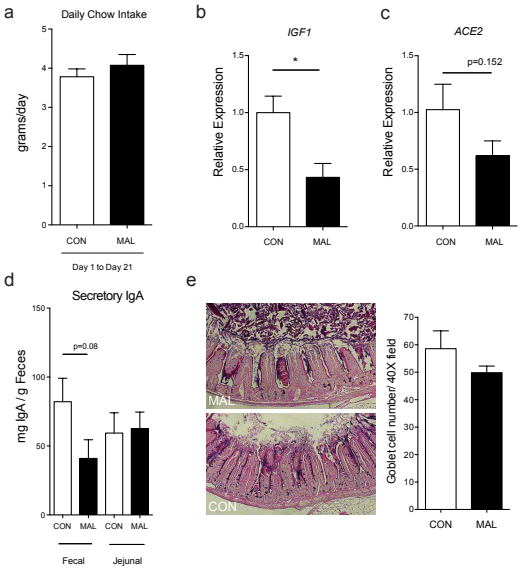

Figure 2.2 Assessing gene expression, food intake and barrier function in malnourished and control mice.
averaging difference in weight of the food over 3 weeks of mice on each of the diet. The mRNA expression of (**b**) *IGF1* and (**c**) *ACE2* in the jejunum was determined by real-time qPCR analysis. (**d**) The concentration of secretory IgA in the fecal content and jejunal content was assessed using an ELISA. (**e**) Representative images and histological assessment of AB-PAS stained jejunal tissues from malnourished and control mice. Mucins stain a blue or dark purple on the outer edge of each tissue, and mucus-secreting goblet cells stain dark purple in the epithelium. The number of goblet cells was enumerated and graphed for each tissue. Bars indicate the mean with S.E, and all data are representative of 2 independent experiments, 8 mice per group (*$p<0.05$, Student's *t*-test).

We next sought to understand the impact of early life malnutrition on colonic barrier function in young mice. The mucus layer in the colon, an important chemical, immunological and anatomical barrier critical for maintaining intestinal homeostasis (Johansson et al., 2011), was significantly thinner in malnourished mice (13.79um +/- 0.5765) compared to mice fed an isocaloric control diet (17.49um +/- 1.147) for three weeks (Fig. 2.3a). The number of goblet cells were enumerated, with no observed changes in expression or abundance, nor any changes in colonic histopathology were observed such as ulceration or any tissue inflammation (Fig. 2.3).

The function of the mucus layer is primarily to protect epithelial cells from direct exposure to the gut microbiome, thus to determine the functional impact of the thinner mucus layer in malnourished mice we stained Carnoy's fixed colonic tissues with a Fluorescent *in-situ* hybridization (FISH) probe which anneals to universally to all bacterial 16S rDNA. Upon analysis of the fluorescent probes under a microscope, we observed an increase in the number of bacteria (stained in red) able to cross the mucus layer and bind to the epithelium (Fig 2.3b). There were bacteria observed crossing the mucus barrier in 20% of control-fed mice and 60% in malnourished mice, three-weeks after being fed each diet.

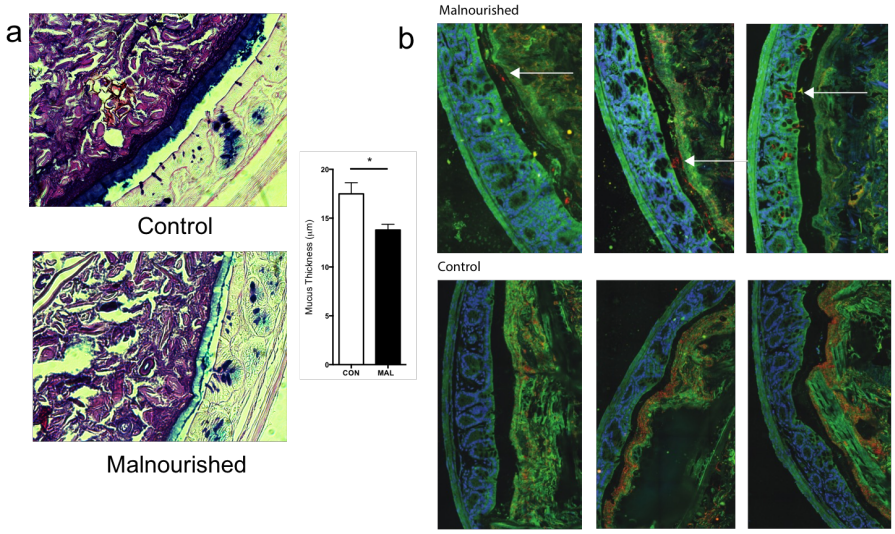

Figure 2.3 Malnutrition causes a thinning of the colonic mucus layer and increased number of bacteria in crossing the inner mucus layer.
(**a**) Quantification of inner mucus layer thickness on colon tissues which were fixed in Carnoy's fixative, embedded in paraffin and stained with AB/PAS to visualize and measure the width of the mucus layer (blue). Inner mucus layer width was determined by an average of 5 measurements per 40x field, with 5 fields counted per tissue section. A bar graph to the right show the relative difference in mucus layer thickness, which is found to be different when analyzed using the Student's *t*-test (*$p<0.05$). Results are representative of 2 independent experiments, n=5 mice per group. (**b**) Carnoy's-fixed distal colon tissues were probed for total 16S rDNA (Eub338) and γ-Proteobacteria-specific 16S rDNA (Gam42a) abundance using Fluorescent *in-situ* hybridization (FISH). Images are representative of 2 independent experiments from malnourished and control mice. Actin is stained in green (488PHalloidin), cell nuclei in blue (DAPI) and bacteria are stained in red (Eub338 and Gam42a). White arrows point towards the presence of tissue-associated bacteria or bacteria within the villi (100x resolution).

2.4 Malnutrition results in shifts in composition and localization of the intestinal microbiota

To test whether malnutrition alters the small intestinal microbiota in mice, we performed 454 pyrosequencing of the 16S rRNA genes from the microbiota in the duodenum and ileum of the mice 3 weeks after being fed the malnourished or isocaloric control diet. We found dramatic shifts in the bacterial species composition of both the ileum and duodenum in the malnourished mice, compared to those on the control diet (Fig. 2.4a). The ileum of malnourished mice showed both an expansion of species from the Bacteroidetes and Proteobacteria phyla, and decrease in the *Lachnospiraceae* and *Clostridiales* families compared to control mice (Fig. 2.4a, Fig. 2.5). The duodenum of malnourished mice also had an abnormal and significant expansion in the proportion of bacteria belonging to the phyla Bacteroidetes and Proteobacteria (largely the *Enterobacteriaceae* family) (Fig. 2.4a,b, Fig. 2.5), which are normally found at high abundance in the lower intestinal tract nearer the colon in C57BL/6 mice (Gu et al., 2013). Normal residents of the duodenum, the Gram-positive bacteria from *Lactobacillaceae* and *Erysipelotrichaceae* families were decreased in abundance in the malnourished duodenum with a striking 45% reduction in the abundance of *Lactobacillaceae* (Fig. 2.4b). This decrease coincided with an increase in abundance of a more diverse set of OTUs from the *Bacteroidales, Prevotella, Lachnospiraceae, Clostidiales, Pseudomonas, Escherichia, Peptostreptococcaceae* and *Ruminococcaceae* groups (Table 2.2). As visualized on the PCA plot, the dietary changes cause the microbial community of the duodenum to have greater similarity with the ileum microbial community and this can be quantified by assessing the UniFrac distance, a measure of community similarity (Fig. 2.4c). Using this measure, we found the resident microbiota in the

malnourished duodenum was significantly more similar ($p<0.01$, Student's *t*-test) to the ileal community than the community in the control duodenum samples (Fig. 2.4c). There was also a marked increase in bacterial diversity of the duodenum in malnourished mice compared to those in the control diet, as seen in the phylogenetic distribution at the genus level and quantified using the inverse Simpson's diversity index (Fig. 2.5b,c). Furthermore, qPCR quantification of 16S copies in the duodenal microbiota verified that the family-level microbial differences observed in the pyrosequencing data were consistent across multiple experiments (Fig. 2.4d-h). Overall, these data suggest the malnourished diet remodeled the bacterial community in the duodenum to more closely resemble the ileum, where Gram-negative species (Bacteroidetes and Proteobacteria) were more abundant, displacing the indigenous Gram-positive Firmicutes, such as *Lactobacillaceae* (Fig. 2.5d).

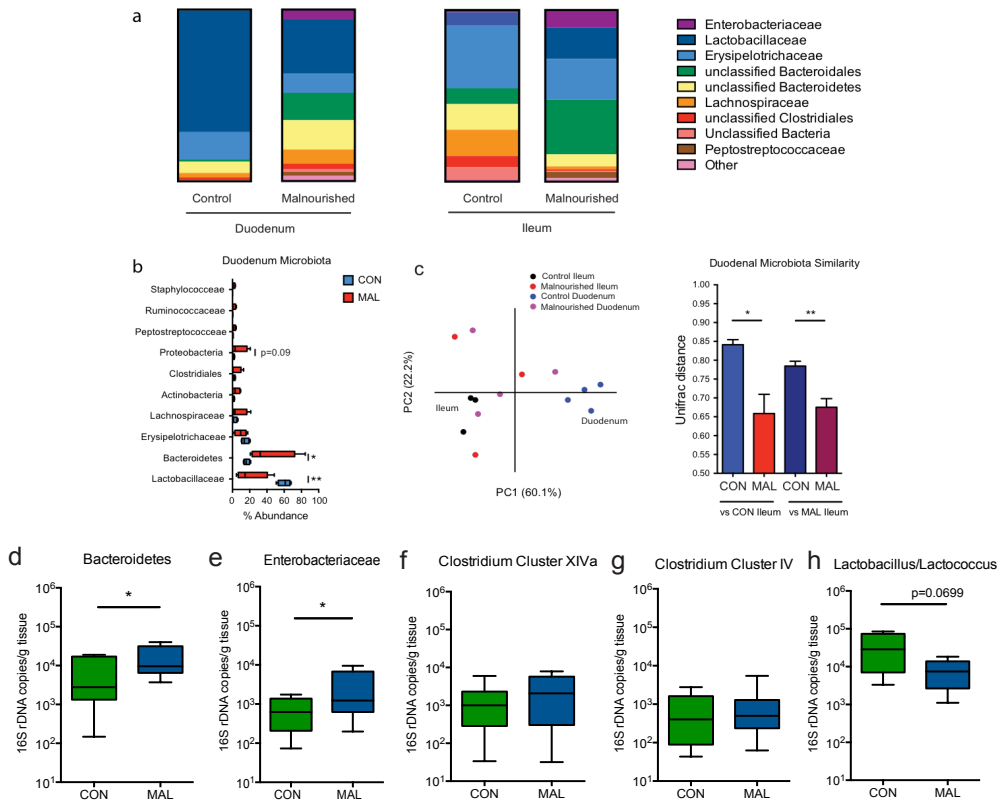

Figure 2.4 Relative abundance of the small intestinal microbiota in malnourished and control mice.

(**a**) A chart summarizing the pooled percent abundance of the duodenal (n=4) and ileal (n=3) microbiota by family classification using the 16S rRNA gene. (**b**) A PCA plot of the microbial communities in the duodenum (n=4) and ileum (n=3) of mice on each diet. Communities were plotted based on a measure of UniFrac distance between the communities. This UniFrac distance measure was used to quantify the similarity between the microbiota in the duodenum of malnourished and control mice to the control ileum (left two bars) and the malnourished ileum (right two bars). A lower value indicates greater community similarity. Bars indicate the means with S.E. (**c**) OTUs at the phylum and family level of taxonomy were plotted on a box and whisker graph to show changes in percent abundance relative to the total number of OTUs in the duodenum of malnourished and control mice. OTUs from the Lactobacillaceae (**p<0.01), Bacteroidetes (*p<0.05), and Proteobacteria (p=0.09) were the 3 most significantly changed between the mice (Mann-Whitney *U*-test). Real-time qPCR analysis of (**d**) mouse intestinal Bacteroidetes-specific 16S rDNA, (**e**) *Enterobacteriaceae*-specific 16S rDNA, (**f**) Clostridium cluster XIVa 16S rDNA, (**g**) Clostridium cluster IV 16S rDNA and (**h**) *Lactobacillus/Lactococcus* in each gram of duodenal tissue. Analysis was performed on DNA extracted from duodenal tissue of malnourished and control mice. Data is pooled from 3 independent experiments, 12 mice per group and bars indicate the mean with S.E. (*p<0.05, Student's *t*-test).

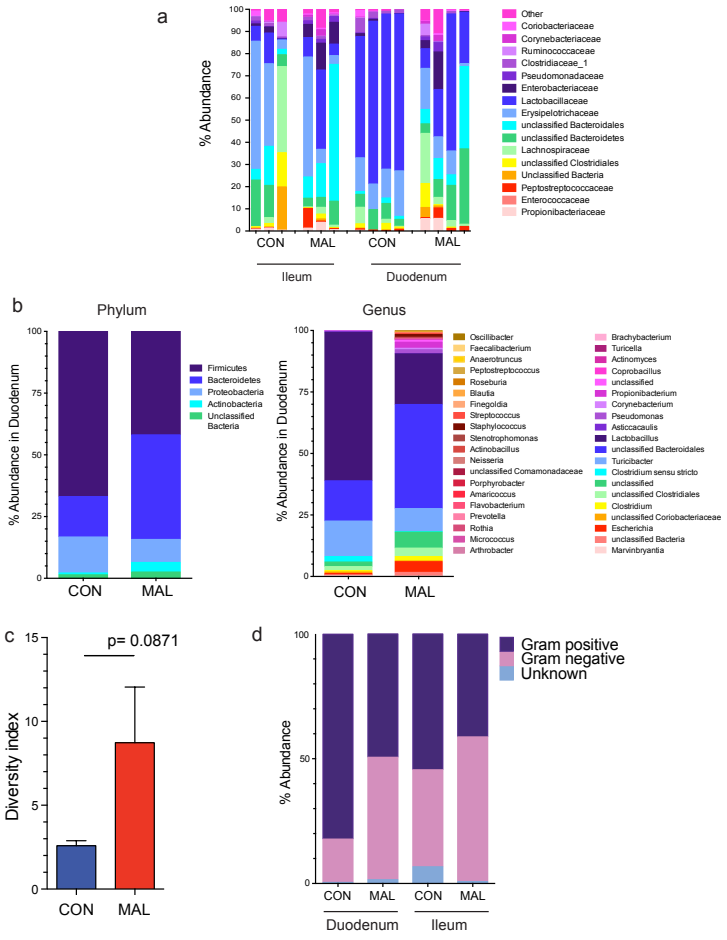

Figure 2.5 High-throughput 16S rRNA sequencing of the small intestinal microbiota in malnourished and control mice.

(**a**) A chart summarizing the percent abundance of the duodenal (n=4) and ileal (n=3) microbiota by family classification in each individual mouse, using the 16S rRNA gene. (**b**) The pooled percent abundance of the duodenal microbiota by phylum and genus taxonomic classification using the 16S rRNA gene.(**c**) A graph of the diversity in the duodenal microbiota of the malnourished and control mice (n=4) as measured by the inverse Simpson's Index method. Bars indicate the mean with S.E. (p=0.08, Student's *t*-test). (**d**) Percent abundance of OTUs that are either Gram-negative or Gram-positive in the duodenum and ileum of malnourished and control mice.

Table 2.2 A list of the most significantly changed OTUs in the duodenal microbiome in malnourished and control mice.

OTU Classification	Rank	Relative Abundance (%)		*P*-value*
		Con	Mal	
Escherichia_Shigella	Genus	0.056	5.21	0.2890
Unclassified Bacteroidales	Order	1.27	14.46	0.0286
Unclassified Bacteroidetes	Phylum	6.30	15.57	0.2000
Lachnospiraceae	Family	2.40	7.44	0.3429
Unclassified Clostridiales	Order	1.48	2.99	0.3838
Pseudomonas	Genus	0.18	1.53	0.2486
Prevotella	Genus	0.00	0.062	0.1878
Peptostreptococcaceae	Family	0.00	0.21	0.1143
Ruminococcaceae	Family	0.08	1.44	0.3297
Lactobacillus	Genus	67.22	28.82	0.0571
Turicibacter	Genus	15.09	10.09	0.2603
Clostridiaceae	Family	3.06	0.36	0.0286

Statistical analysis performed using a Mann-Whitney *U*-test, corrected for multiple comparisons.

After observing the large changes to the microbial community in the small intestine of mice fed each diet, we obtained samples from both the feces and colonic tissue of mice 3 weeks after being fed the control and malnourished diet and analyzed the microbiome using high-throughput sequencing of the 16SrRNA gene by Illumina. We hypothesized that we would also observe changes in the composition in the colon of malnourished mice, and further, the presence of a unique mucosal-associated bacterial community. The first metric we tested was the relative diversity of observed OTUs both malnourished and control mice, and found that fecal microbiota of malnourished were less diverse, as indicated by the Chao1 and Shannon indices, two different measures of α-diversity (Fig. 2.6a). As visualized on the NMDS plot, the dietary changes cause the microbial community of both the feces and mucosa to be significantly different in the control and malnourished diet, with each sample clustering together on the plot (Fig. 2.6b). This

indicates that there is a unique mucosal-associated bacterial community compared to the fecal community and this community shifts to an altered state in both the feces and mucosa of malnourished mice (Fig. 2.6b). In analyzing which bacterial taxa were most significantly altered in each sample, we found that species from *Akkermansia,* Actinobacteria and *Ruminococcus* had a greater abundance in both the mucosa and fecal samples of control-fed mice (Fig. 2.6c-e). In the malnourished mice, we found that bacteria from the Porphyromonadaceae family were more abundant in the mucosa of the colon (Fig. 2.6f). Of note, the OTUs from *Akkermansia* and Porphyromonadaceae were observed to a magnitude of 5-10 fold in the mucosal-associated samples compared to the fecal analysis (Fig. 2.6c,f), indicating these species were part of the driving factor behind the mucosal-associated vs fecal-associated changes in the NMDS plot (Fig. 2.6b).

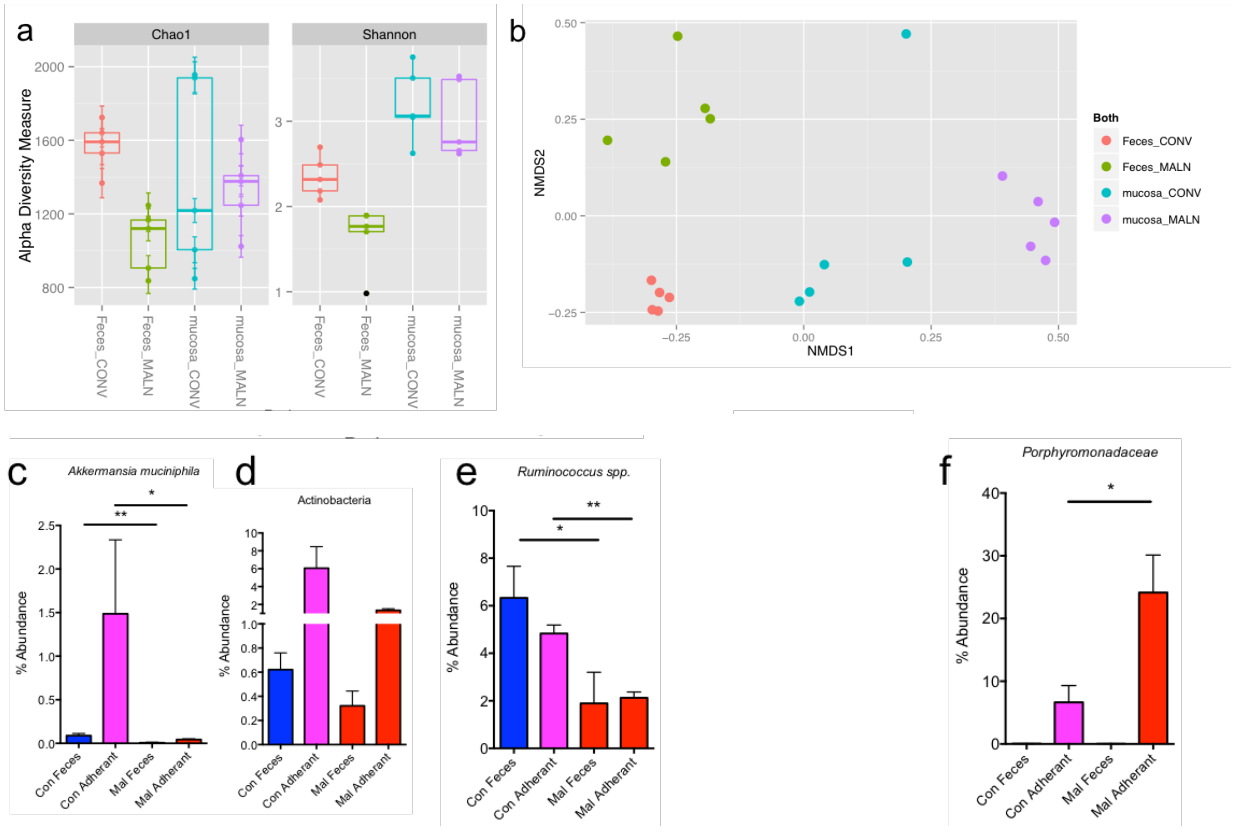

Figure 2.6 Relative abundance of the fecal and mucosal-associated intestinal microbiota in malnourished and control mice.

(**a**) Two charts showing α-diversity of the gut microbiota in the feces and mucosa of control and malnourished mice, as observed using the Chao1 and Shannon diversity index (n=5). (**b**) A NMDS plot of the microbial communities in the feces (n=5) and mucosa (n=5) of mice on each diet. Each dot on the represents the position one mouse fecal or mucosal sample, relative to the other samples, using Kruskal's NMDS algorithm. OTUs that were most significantly enriched in both the mucosa (adherent) and fecal samples of control-fed mice are visualized here using a bar graph measuring percent abundance of (**c**) Akkermansia (**p<0.01), (**d**) Actinobacteria and (**e**) Ruminococcus (*p<0.05; **p<0.01), the 3 most significantly changed between the mice (Mann-Whitney U-test). (**f**) The single OTU that was significantly enriched in both the mucosa and fecal samples of malnourished mice is shown here using a bar graph measuring percent abundance of Porphyromonadaceae (*p<0.05; Mann-Whitney U-test).

2.5 Malnutrition alters the intestinal metabolome

As malnutrition leads to drastic shifts in the intestinal microbiota, we hypothesized this would also impact the metabolic environment of the host small intestine. After 3 weeks of treatment with either diet and concurrent with our microbial analysis, contents of the small intestine in malnourished and control diet mice were assessed for abundance changes of the metabolites using untargeted metabolomic analysis by UPLC-FTMS. The method detected and relatively quantitated over 3500 unique metabolite features and approximately 420 showed differential abundances between malnourished and control mice ($p<0.05$; >2-fold change). Overall, the metabolite profile of the malnourished small intestine substantially shifted from the profile of control mice, as shown by unsupervised principal component analysis (PCA) (Fig. 2.7a). When all metabolites detected in the positive ion mode were visualized on a heat map, malnourished and control groups clustered together in the dendogram indicating the diet shifted the metabolome to an alternate state (Fig. 2.7b). Each of these observations held true for metabolites detected on the negative ion channel.

Using the metabolite matches from the positive and negative ion mode, based on mass to charge ratio (m/z) values found with the Kyoto Encyclopedia of Genes and Genomes (KEGG) database, we determined specific pathways that were enriched by the malnourished or control diet. Metabolites in the bile acid biosynthesis pathway (37% of pathway metabolites impacted; $p<0.001$), linoleic acid metabolism, and amino acid biosynthesis were all significantly over-represented in the control diet (Fig. 2.7c). The changes in the amino acid biosynthesis pathways were expected in the control mice, given the higher protein content of their diet, supporting the accuracy of our method and analysis. The most striking over-representation in malnourished mice was the greater abundance of metabolites in the steroid biosynthesis pathway (28% of

pathway impacted; $p<0.001$) (Fig. 2.7d). More specifically, many of these steroid metabolites represented those from the vitamin D biosynthesis pathway. Random forest analysis was implemented to identify discriminatory features between the two diets, and it ranked a vitamin D metabolite as the most significant feature between the samples from the malnourished mice and controls (Table 2.3). Of note, the vitamin D pathway is known to impact many aspects of intestinal homeostasis, including gut inflammation (Assa et al., 2014) and bile-acid production (Schmidt et al., 2010). Pathways for sphingolipid biosynthesis were also over-represented in the small intestine of malnourished mice, an unexpected result due to the deficiency of fat (5% vs 15%) in the malnourished diet (Fig. 2.7d). However, sphingolipid metabolism can also be influenced by other factors including epithelial cell damage, and bacteria, such as the Bacteroidetes which contain sphingolipids in their membrane which can interact with the host (An et al., 2011).

Table 2.3 Most significant metabolite features upregulated in the small intestine of malnourished (yellow) and upregulated in control mice (blue) as determined by the Random Forest algorithm.

Biochemical Name	MZ/RT	Mean Decrease Accuracy*	P-value (*t-test)*	Fold Change	Pathway
25-hydroxyvitamin D3	401.34099/13.97	0.010197	0.0126	9.261121114	Vitamin D metabolism
5,9-hexacosadienoic acid	415.36048/10.32	0.010167	0.07584	9.984408818	Fatty acid metabolism
Not determined	480.27765/4.13	0.0095	0.06038	4.81442954	N/A
Dehydroepiandrosterone 3-glucuronide	487.23114/12.14	0.0091667	0.02146	4.377919983	Steroid biosynthesis
Not determined	557.36625/7.08	0.009	0.02101	9.837171854	N/A
Not determined	308.29477/8.99	0.009	0.05241	6.7656939	N/A
D-Urobilinogen	591.31751/6.39	0.009	0.16924	51.61731217	Bilirubin metabolism
Not determined	432.32318/13.48	0.0085667	0.04659	4.991777729	N/A
L-tyrosine	182.08116/0.52	0.0085	0.05542	4.490194451	Amino acid metabolism
7-ketodeoxycholic acid	407.27953/6.07	0.0081667	0.01052	5.878640664	Bile acid metabolism
Not determined	555.42304/13.37	0.0081667	0.00057	4.958823421	N/A
Not determined	426.30034/12.46	0.0081667	0.10915	12.26049061	N/A
Not determined	484.33006/9.13	0.008	0.08897	6.034367899	N/A
Phytenoic Acid	311.29444/13.82	0.0078333	0.07204	4.807276589	Fatty acid metabolism
Not determined	574.39284/7.07	0.0076667	0.01903	7.444808495	N/A
Not determined	376.27345/13.63	0.0075667	2.67E-06	5.583238881	N/A
LysoPC(20:0)	574.38654/11.4	0.0075	0.00184	3.835402686	Lipid metabolism
N-oleoyl tyrosine	446.32632/12.64	0.0075	0.10891	7.527675391	Fatty acid metabolism
Dihydroxycholestanoic acid	435.35087/7.49	0.0075	0.12485	7.282721622	Bile acid metabolism
Not determined	479.25137/13.01	0.0075	0.00873	4.695383928	N/A
Not determined	454.33135/13.95	0.0075	0.09990	7.979301	N/A
4α-formyl-4β-methyl-5α-cholesta-8,24-dien-3β-ol	443.35179/13.94	0.0074667	0.00077	26.05893193	Cholesterol metabolism
Not determined	466.2619/3.5	0.0073333	0.03404	3.836387738	N/A
Not determined	418.34393/14.28	0.0073333	0.00970	4.915347782	N/A

*Sorted by mean decrease accuracy

We confirmed these metabolome changes with a targeted metabolomics approach to quantify the concentrations of bile acids, vitamins and microbial-produced short chain fatty acids (SCFAs) in the small intestine. These three classes of metabolites were both evidenced to be altered in malnourished mice, and produced or modified by members of the microbiota. In the small intestine, bile-acid targeted metabolomics revealed a number of significant changes in the bile acid pool between the malnourished and control, supporting the pathway analysis data from the untargeted metabolomics screen (Fig. 2.7e, f). In the malnourished small intestine, there was a shift towards lower concentrations of tauro-conjugated bile acids, and conversely, higher levels of unconjugated bile acids, with the ratio between the two being significantly altered (Fig. 2.8a-c). Each tauro-conjugated bile acid detected in this analysis was lower in the malnourished small intestine, with the concentrations of tauro-ω-muricholic acid, tauro-α-muricholic acid, tauroursodeoxycholic acid, taurohyodeoxycholic acid and taurochenodeoxycholic acid reaching statistical significance (Mann-Whitney *U*-test) (Fig. 2.7e). In the unconjugated pool, the concentrations of muricholic acid, ursodeoxycholic acid, and 7-ketodeoxycholic acid were all significantly higher in the malnourished small intestine (Mann-Whitney *U*-test) (Fig. 2.7f).

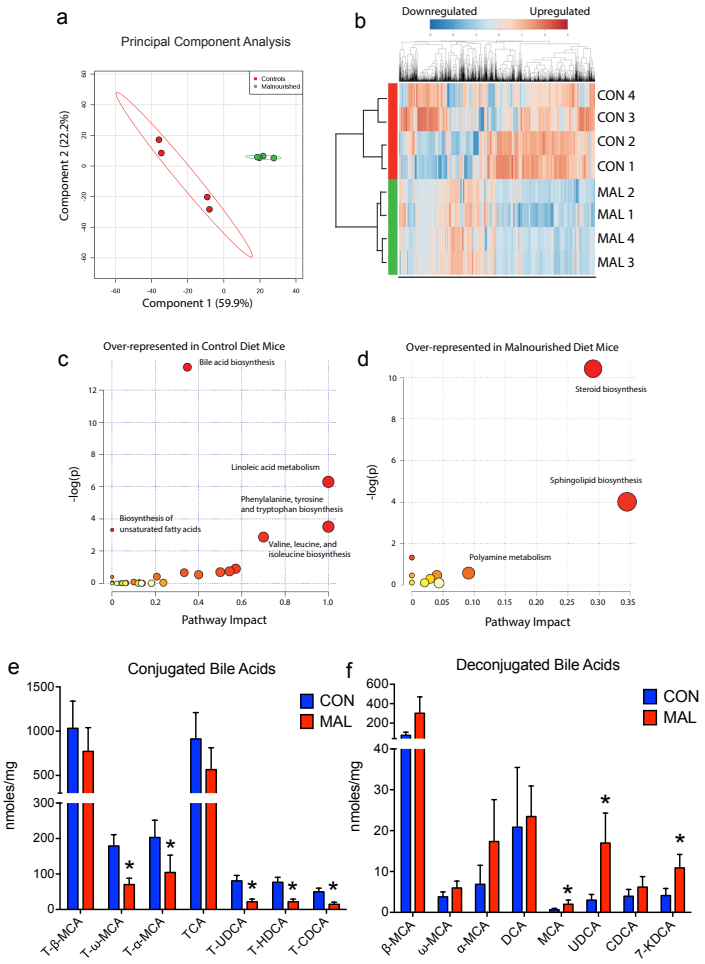

Figure 2.7 Untargeted and targeted metabolomics of the small intestinal metabolome. (**a**) A principal component analysis (PCA) plot showing separation of metabolomic data as detected by the positive ion channel from malnourished mice (green) and control mice (red). (**b**) A heat map of the relative abundance of all metabolites identified from the small intestinal metabolome as detected by the positive ion channel from malnourished and control mice (n=4). The malnourished and control samples clustered together in the dendogram based upon cluster analysis by the Ward method, with a Pearson distance measure. The heat map scale is a $\log_2$ base, from the range of -3 (blue) to +3 (red). Plots showing over-represented pathways using Metaboanalyst 2.5 software in (**c**) control mice and (**d**) malnourished mice, as identified by the Kyoto Encyclopedia of Genes and Genomes database. The plot is graphed based upon the log(p-value; Welch's *t*-test) (y-axis) and percent of pathway impacted (x-axis). The size of the circles represents the number of metabolites identified to be part of the pathway. (**e**) Tauro-conjugated bile acid and (**f**) unconjugated bile acid concentrations in the small intestine of malnourished and control as determined by targeted metabolomics. Bars represent the means +/- S.E., 4 mice per group (*p<0.05, Mann-Whitney *U*-test). T, tauro conjugation; MCA, muricholic acid; CA, cholic acid; UDCA, ursodeoxycholic acid; HDCA, hyodeoxycholic acid; CDCA, chenodeoxycholic acid; KDCA, ketodeoxycholic acid.

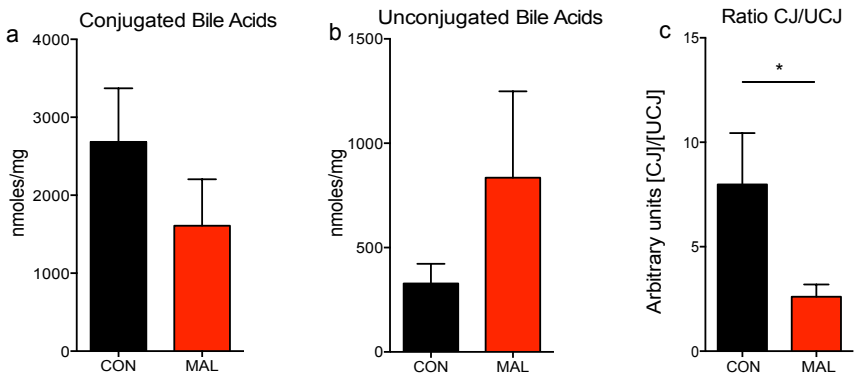

Figure 2.8 Bile acid targeted metabolomics.
Pooled data representing all bile acids found in the small intestinal content of malnourished and control mice that are either (**a**) tauro-conjugated or (**b**) unconjugated bile acids. (**c**) The ratio of the concentrations of conjugated:unconjugated bile acids in the small intestine. Bars indicate the mean with S.E, 4 mice per group (*$p<0.05$, Student's *t*-test).

In the feces, bile acid targeted metabolomics data showed many changes in the concentration of both conjugated and unconjugated bile acids, however in contrast to the small intestine, significantly lower concentrations of secondary, unconjugated bile acids were detected compared to higher concentrations of conjugated bile acids (Fig 2.9). More specifically, tauro-β-muricholic acid, taurocholic acid and taurochenodeoxycholic acid were all detected in significantly higher levels in malnourished feces (Fig 2.9). There was no change in concentrations for β-muricholic acid, ω-muricholic acid, or α-muricholic acid, indicating it was the conjugation of these bile acids that was changing rather than the base bile acid structure. The secondary bile acids lithocholic acid, hyodeoxycholic acid, and ursodeoxycholic acid, which are enzymatically produced by the microbiota (Duboc et al., 2013), were found in lower

concentrations in the feces of malnourished mice. Of the 34 bile acids analyzed, the 14 represented here (Fig 2.9) were the bile acids whose concentration we were able to detect at level >0.5 n moles/mg of feces, and considered to be acting at a biologically relevant concentration.

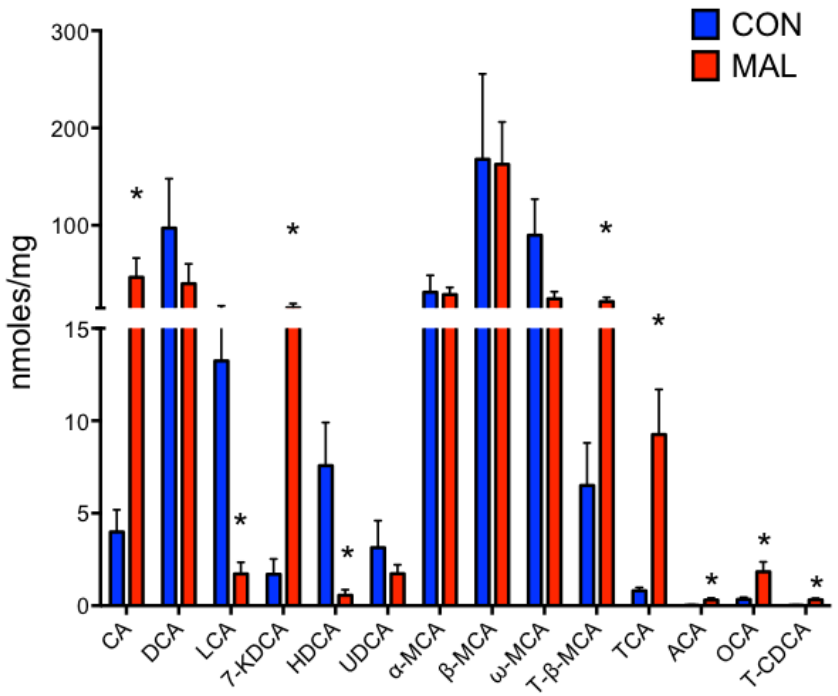

Figure 2.9 Fecal bile acid targeted metabolomics
Tauro-conjugated bile acid and unconjugated bile acid concentrations in the feces of malnourished and control as determined by targeted bile-acid metabolomics. Bars represent the means +/- S.E., 4 mice per group (*$p<0.05$, Mann-Whitney *U*-test). T, tauro conjugation; MCA, muricholic acid; CA, cholic acid; UDCA, ursodeoxycholic acid; HDCA, hyodeoxycholic acid; CDCA, chenodeoxycholic acid; KDCA, ketodeoxycholic acid.

Polar and non-polar contents from the small intestine of malnourished and control mice were also tested for the presence of vitamins predicted to be found in the intestine, including vitamin A, vitamin B1, vitamin B2, vitamin B3, vitamin B5, vitamin B6, vitamin B7, vitamin B12, vitamin D3, and vitamin E. Results from the vitamin-targeted metabolomics analysis showed the malnourished diet induced large shifts in the luminal concentrations of many vitamins in the small intestine (Fig. 2.10), which are not due to altered concentrations of vitamins in the diets as they are identical (Table 2.1). Malnutrition also induced significant reductions in vitamin A metabolites (retinol and retinal), vitamin B1, vitamin B6, vitamin B12 and vitamin E (α-tocopherol) and elevated concentrations of vitamin D3 and vitamin B7 (Fig. 2.10). The change in concentration of vitamin D3 observed is consistent with the untargeted metabolomics data which showed large changes in metabolites with a cholesterol backbone such as vitamin D derivatives (Table 2.3) and bile acids (Fig. 2.7). It is important to note these observations relate to concentrations of vitamins found in the intestine, and thus do not necessarily correlate to vitamins found systemically in the serum for example.

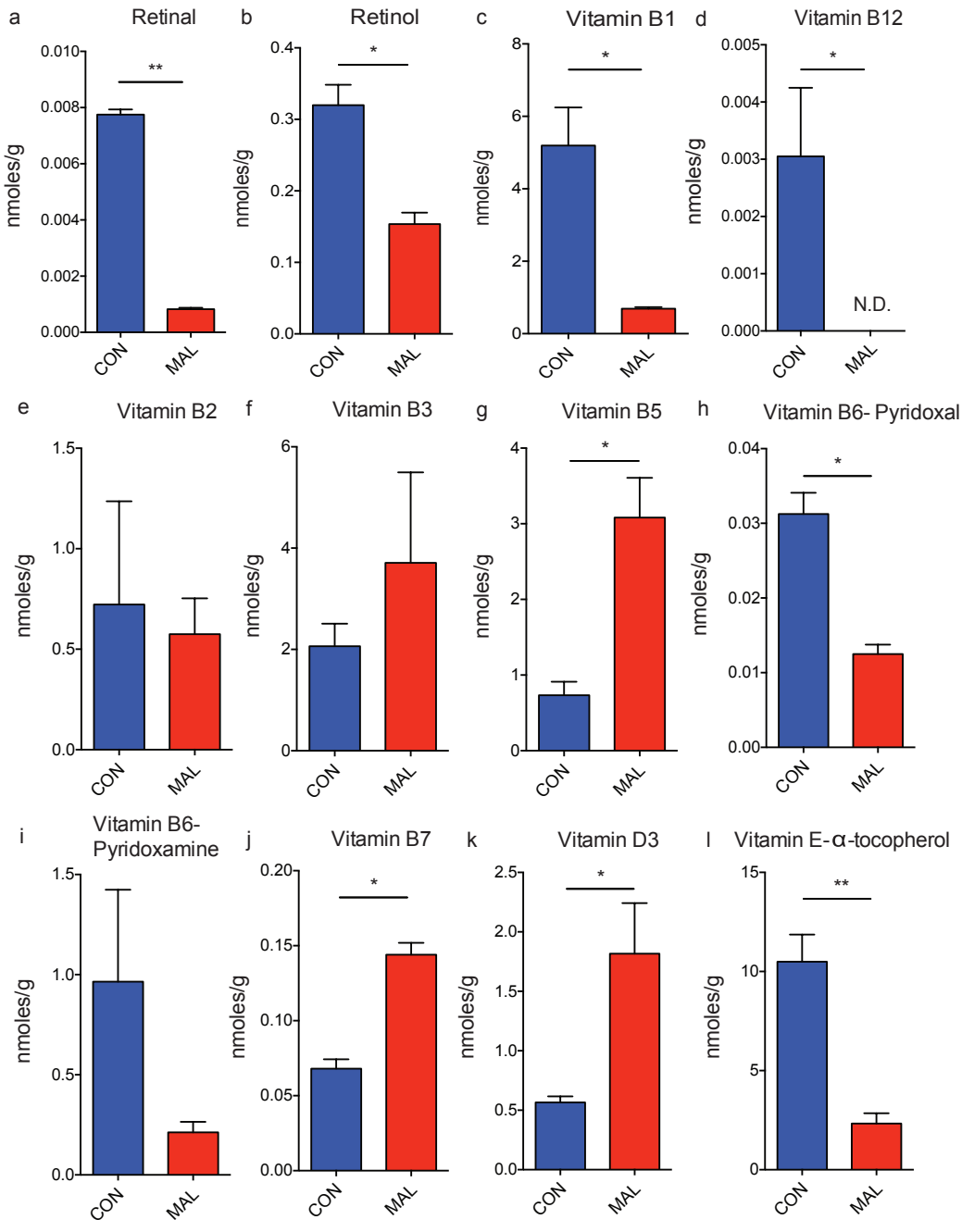

Figure 2.10 Vitamin-targeted metabolomics
The concentrations of 12 vitamins found in the small intestinal content of malnourished and control mice. Bars indicate the mean with S.E, 4 mice per group, N.D. equals not detected. Statistical analysis was performed using the Mann-Whitney *U*-test (*p<0.05,**p<0.01)

Short-chain fatty acids (SCFAs) are microbially-produced metabolites which have been shown to be sensed by the host epithelial and immune cells to promote a wide-variety of anti-inflammatory mechanisms (den Besten et al., 2013). Here, we analyzed small intestinal and fecal samples from control and malnourished mice for presence of 7 SCFAs; acetic acid, propionic acid, isobutyric acid, butyric acid, isovaleric acid, valeric acid, and caproic acid (Fig. 2.11). No significant differences in SCFAs were observed, although there was a general trend towards greater total concentrations of each SCFA in the malnourished small intestine (Fig. 2.11a). In the feces, the was also less butyric acid in malnourished mice, however this was a trend that did not meet statistical significance (Fig. 2.11b). There was a large amount of variability in the detection of butyric acid and other SCFAs observed in the mouse samples and since these SCFAs can be produced by members of the microbiota, we ran a correlation analysis between microbiota and SCFA where abundance of every detected OTU from the feces of malnourished and control mice were correlated with the amount of each SCFA detected (Fig 2.12). We did not find any correlations that reached statistical significance, however the largest differences were observed in the butyric acid samples from each mouse (Fig 2.12a). To understand which members of the microbiota could be responsible for the butyric acid production in our mice, we ran another correlation analysis comparing the most significant taxa detected from all the control-fed mouse fecal samples with butyric acid concentrations in control mice. Based on this analysis, there was a tendency for taxa from the Lachnospiraceae family to be correlated with greater levels of butyric acid in samples and samples with high levels of Bacteroidetes in the feces had a lower concentration of butyric acid on average.

These data clearly show that a malnourished diet exerts a strong, measurable impact on the metabolite content in the small intestine and colon, mainly in the biosynthesis or bioavailability of steroids, vitamins, and bile acids, and may be contributing to or a result of changes in bacterial composition.

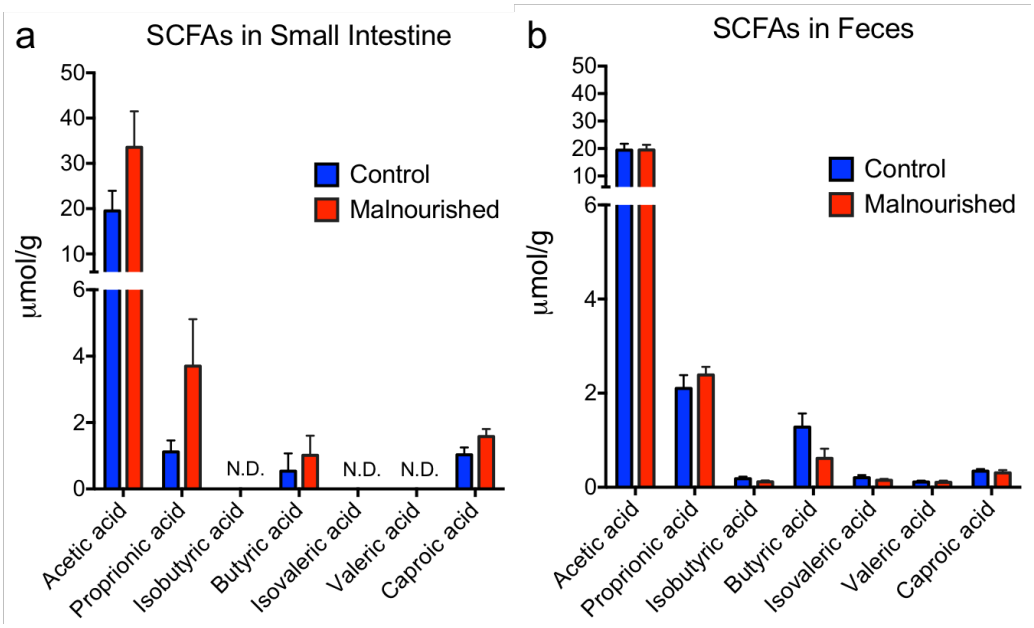

Figure 2.11 Short-chain fatty acid analysis.
(**a**) The concentration of 7 short-chain fatty acids (SCFAs) in the small intestinal content of malnourished and control mice. The concentrations of isobutyric, isovaleric and valeric acid were not detected (N.D.) in this analysis. Bars indicate the mean with S.E, 4 mice per group. (**b**) The concentration of 7 short-chain fatty acids (SCFAs) in the feces of malnourished and control mice. Bars indicate the mean with S.E, 8 mice per group.

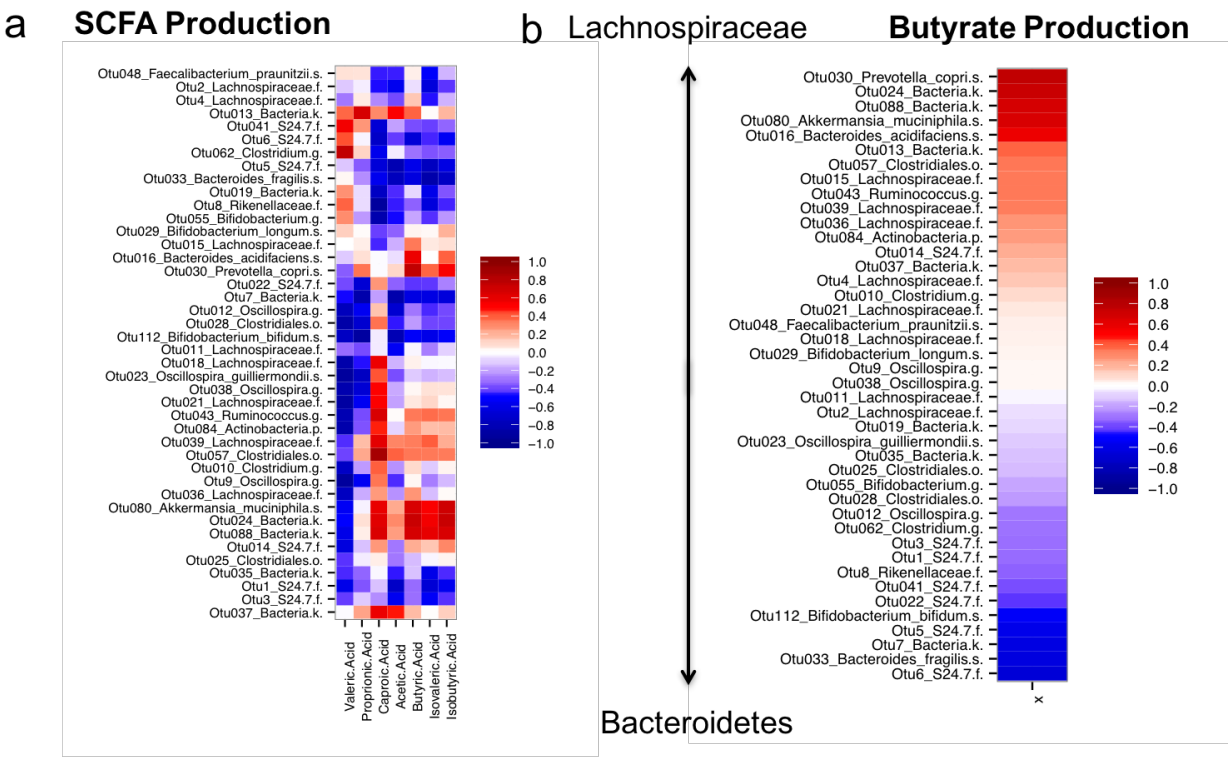

Figure 2.12 Short-chain fatty acid concentrations and correlations with intestinal microbiota

(**a**) A heat-map using Pearson correlation analysis of the concentration of 7 SCFAs in the feces of malnourished and control mice and the corresponding abundance of the most-significantly changes taxa in the mice. The legend on the right is a Pearson rank from most significantly correlated (red) to least significantly correlated (blue). (**b**) A heat-map using Pearson correlation analysis of the concentration of butyrate in the feces of malnourished and control mice and the corresponding abundance of the most-significantly changes taxa in the mice. The legend on the right is a Pearson rank from most significantly correlated (red) to least significantly correlated (blue).

2.6 Discussion

In this study, we sought to do an in-depth characterization of the effect of moderate protein and fat malnutrition early in life on growth, epithelial barrier function, composition and localization of the microbiota, and changes in the intestinal metabolome in mice. We discovered that the malnourished diet we utilized, which mimics that of moderately protein-malnourished humans in South America and Africa, causes early-life growth stunting, increased intestinal permeability, and changes in the colonic mucus layer thickness. We further characterized the changes each diet caused to the composition and localization of the intestinal microbiota and the metabolome in the small and large intestine and determined which microbial species and metabolites change during malnutrition, data which will be important as we aim to both replicate and reverse symptoms of malnutrition in humans using this murine system. The malnourished diet we utilized was similar to the regional basic diet used to induce moderate protein-energy malnutrition in mice in previous studies (Maier et al., 2013; Teodósio et al., 1990; Ueno et al., 2011). However, these studies did not characterize the impact of the diet on the microbiota, metabolism, intestinal immune cells, or mucus barrier function. In doing these analyses, we utilized a holistic approach to demonstrate novel observations in how malnutrition in mice alters the small and large intestinal microenvironment.

The first thing we wanted to assess was the level to which the malnourished diet impacted the growth rate of mice, as percent content of protein in the diet strongly correlates to weight gain. When three-week old mice were randomized on to each diet, the ones fed the malnourished diet took approximately 3-5 days to begin to show a decrease in their growth

velocity compared to the control mice and after 3 weeks the difference in weight gain between the mice was less than many studies which use 2% protein in the diet to model malnutrition. Our study fills a gap where mice were only moderately malnourished, a reflection of millions of children who are not clinically malnourished with Kwashiokor or muscle wasting, but nevertheless consume a diet with lower protein and fat than required for healthy growth (Ahmed et al., 2014b). Previous studies have shown that malnutrition results in increased intestinal permeability, and we also found increased permeability as described through lower levels of *TJP1* and increased *CLDN2* expression in small intestinal epithelial cells, also functionally more dextran able to cross the epithelium into the blood, consistent with studies using different diets inducing protein and fat malnutrition (Ueno et al., 2011). Transcript levels of tight junction proteins have been shown to correlate well with protein level and the increased expression of *CLDN2* was puzzling at first since in general, studies have correlated lower levels of many claudins and tight-junction proteins to increased permeability (Ueno et al., 2011). There is evidence for increased Claudin-2 resulting in increased permeability in the intestine from studies in mice, indicating it forms a pore that allows increased paracellular flow of water and small cations, yet a consensus on the function for this protein in epithelial cells remains elusive (Wada et al., 2013).

The mucus layer in the intestine forms a chemical and anatomical barrier to constrain the passage of microbial and metabolic products from interacting with the epithelium (Johansson et al., 2011). The small intestine lacks a continuous and structured mucus layer, thus we analyzed the mucus layer in the colon of malnourished and control mice. The thinner mucus layer observed has also been reported in mice given antibiotics (Wlodarska et al., 2011), in obesity

(Everard et al., 2013), and in mice with lack of innate-immune function (Wlodarska et al., 2014). Signals and metabolites from the microbiota, including SCFAs and NLR-agonists, have been shown to promote mucus secretion in the intestine, leading us to hypothesize that microbial species could be changing in the malnourished mice which aside from just the components of the diet, could result in the lack of a healthy mucus barrier. We are cognizant of the potential of artifacts when measuring the mucus layer in histological samples, and in staining the colon sections for the presence of bacteria crossing the mucus layer using FISH, we aimed to ask the question whether the thinner mucus layer had a functional impact of whether microbes could pass through the barrier. The result of greater numbers of bacteria observed close to the epithelium of malnourished mice compared to control mice could indicate differences in the composition and resilience of the mucus layer in malnourished mice.

As only recently has the microbiota been implicated driving phenotypes observed during malnutrition, little data existed characterizing the changes in the composition of the microbes, especially in the small intestine due to sampling issues in humans (Gordon et al., 2012a). Following up on the phenotypes in barrier function and growth, we aimed to characterize the microbiota to understand how it could relate to these observations. We found the malnourished diet resulted in changes in the composition and localization of the microbiota, as the duodenal microbial community contained more diversity of taxa, and an expansion of Gram-negative species from the Bacteroidetes and Proteobacteria which are normally restricted to the ileum or colon. The decrease in the resident Lactobacillaceae species of the upper small intestine observed is of note due to the probiotic potential of *Lactobacillus* species as anti-inflammatory and pro-digestive health agents (Deshpande et al., 2011). Changes to the ileum were subtler than in the

duodenum, yet the increase in Bacteroidetes and Proteobacteria was also evident in malnourished mice, indicating the small intestinal environment of malnourished mice is more conducive to the colonization and proliferation of genera from these phyla. In the colon, malnourished and control microbiota were found to be distinct communities as measured by the NMDS plot, however changes were more evident in the mucosal-associated microbiome. Notably *Akkermansia,* a known mucin degrader and potential marker for gut health, was more abundant in the control-fed mice and this fact is supported by other studies showing *Akkermansia* abundance is sensitive to dietary shifts (Everard et al., 2013). The changes in microbiota inhabiting the mucosa in mice fed each diet could be a function of the composition of the mucus, as changing glycosylation patterns (e.g. more fucosylation or sialyation) can change which microbes are permitted to inhabit this environment and/or which metabolic products are available for growth. In this study, we were not able to detect any changes in mucus composition or glycosylation and future studies should look into this area using specialized techniques to isolate mucins from the host. We are also not able to conclude to what impact these microbiota changes impact the growth rate or barrier dysfunction. However, associations can be made, for example *Lactobacillus* are well-documented to improve barrier function and a healthy intestinal tract normally is one which *Akkermansia* can flourish and promote anti-inflammatory systems and aid in reversing the potential for metabolic disease (Blanton et al., 2016). There was also a lack of overall diversity in the colonic microbiota, in contrast to the increased diversity found in the duodenum. This dietary shift could be resulting from decreased amount of food products that are able to be fermented, thus decreased availability of a wide variety of bacterial growth factors across many genera resulting in a lack of promotion of a robust and diverse fecal bacterial community.

To further link the microbial composition in the intestine to observed phenotypes of malnourished mice and better characterize the impact on the gut environment (which to date has been understudied), we characterized the metabolites in the gut to understand not just which taxa are present but how they could functionally be changing the metabolism of the intestine. The metabolomic analysis of the small intestine revealed for the first time that malnutrition leads to drastic shifts in small intestinal bile acid pool. Specifically, a reduction in tauro-conjugated bile acids was observed in malnourished mice, which are important for fat and nutrient uptake in the small intestine (de Aguiar Vallim et al., 2013), and based upon previous reports in patients with tauro-conjugated bile acid deficiency, also could be linked to the observed alterations the luminal bioavailability of the fat-soluble vitamins A, D and E (Setchell et al., 2013). Bile acids changes could also factor into the observed resemblance of the microbiota in the malnourished duodenum to that of the ileum. Many studies report bile acids are one of the major mechanisms to restrict bacteria proliferation in the upper small intestine (Hofmann and Eckmann, 2006) and can impact host-microbial interactions during intestinal inflammation (Duboc et al., 2013). Bile acid changes can also result in diarrhea and as mentioned previously, malabsorption of lipids and fat-soluble vitamins, an observation of some significance given the propensity of malabsorption endemic to many regions of the world with poor nutrient availability and sanitation (DiBaise and Islam, 2012).

In the large intestine, the bile acid profile resembled in some ways what is seen in patients with Inflammatory Bowel Diseases (IBDs) such as Crohn's and Ulcerative colitis, where there is a greater proportion of conjugated bile acids which are not re-absorbed in the ileum and leak into the feces (Duboc et al., 2013). Further, the low levels of secondary bile acids, enzymatically produced by many of the Firmicutes in the microbiota, is also a hallmark of the

intestine in IBD (Wlodarska et al., 2015). The decrease in butyrate in feces is an observation which could have a connection with the thinner mucus layer based on previous studies showing its beneficial effect on mucus secretion. Decreased diversity of the intestinal microbiota is also seen in IBD and particularly the Lachnospiraceae species *Ruminococcus* showed a large decrease in the malnourished mouse colon. *Ruminococcus* species from the Lachnospiraceae are important producers of not only butyrate but also enzymes such as bile-salt hydrolases which de-conjugate bile acids and produce secondary bile acids such as lithocholic acid (Wahlström et al., 2016). Another interesting observation is the fact that obesity shares some similarity with observed intestinal phenotypes in malnutrition, including barrier dysfunction, gut microbiota dysbiosis, and bile-acid changes (Kau et al., 2011). We propose that during moderate malnutrition, the intestinal microbiota are reassembled into a community that has a greater potential to adhere to the host epithelium and mucus, colonize the upper small intestine, and can amplify changes the diet imparts on host metabolism such as bile acids. Further studies need to elucidate how we can leverage these observations to promote intestinal health in malnourished individuals and which microbes are responsible to drive side-effects of malnutrition such as growth velocity and epithelial barrier function. Numerous germ-free studies are asking the question of which species are promoted by which dietary components and how they are interacting with the host to direct immune and metabolic pathways linked to growth, barrier function as well as gut motility (Charbonneau et al., 2016b). These studies, many involving germ-free transfers of human microbiota, reveal microbiota species can transfer some of these features of malnutrition like growth stunting and intestinal permeability/inflammation. However, this is an artificial system meant to amplify any observation and we need more studies looking at conventionally-raised mammals to understand what these complex associations actually mean for human health.

2.7 Summary

This is the first animal study which aimed to characterize how a moderately malnourished diet (in protein and fat) can impact the epithelial barrier function such as mucus secretion and dextran permeability and relate these changes to the composition and localization of the microbiota. Early-life malnutrition can lead to growth stunting and increased intestinal permeability independent of any histopathological changes. The microbial community shifts across the small and large intestine were characterized, notably in taxa from the Bacteroidetes, Proteobacteria and Lachnospiraceae, sampling different regions to give a global understanding of how this community changes and what it could mean to host health. There is a homeostatic imbalance in the ability of microbes to colonize different regions of the host mucus layer and upper small intestine in malnourished mice. This imbalance can lead to or can be a result of the changes in the bile acid profile of malnourished mice, which has alterations in the concentration of tauro-conjugated and microbially-produced secondary bile acid metabolites, impacting how the host intestine functions metabolically. Aside from bile acids, for the first time we performed SCFA and vitamin-targeted analysis of the malnourished intestine. Untargeted analysis showing a change in sphingolipid metabolism and steroid biosynthesis in the gut. Malnutrition early in life clearly results in a distinct signature viewed through profound alterations in the metabolite and microbiota composition. Results from this study will help us understand what drives many of the secondary impacts of malnutrition and how we can reverse them.

Chapter 3: Developing a murine model of environmental enteropathy

3.1 Introduction

As we introduced previously, our microbiota and their metabolites can mediate the impact of malnutrition on host metabolism. Many malnourished children are raised in areas of poor sanitation, which increases the incidence of exposure to potentially pathogenic organisms which can both influence and be a result of malnutrition. Early life fecal-oral microbial exposure during a critical window of growth and development in children can have a lasting impact on the host's ability to derive nutrients from the diet. There is an increasing appreciation for the strong effect these early life microbial and environmental exposures have on the susceptibility to disease and intestinal health. Diet alone cannot explain the pervasiveness and persistence of malnutrition across the globe, and healthy intestinal function is of critical importance for maintaining healthy growth, cognitive development and nutrient balance (Subramanian et al., 2014; Ngure et al., 2014).

A poorly understood disorder of small intestine called environmental enteropathy (EE), also referred to as tropical enteropathy or environmental enteric dysfunction, is now widely recognized to be a major contributor to childhood malnutrition (Korpe and Petri, 2012; Prendergast and Kelly, 2012; Keusch et al., 2014), and is thought to be the reason why current therapeutic interventions in malnourished children are efficacious less than one-third of the time (Petri et al., 2014). This disease impacts the function of the small intestine, and features include chronic intestinal inflammation, villous blunting, and increased intestinal permeability,

ultimately resulting in diminished nutrient uptake, adversely affecting growth and development (Kosek et al., 2014; Humphrey, 2009). As a subclinical disorder, EE presents without diarrhea or presence of any known infectious etiology, unlike tropical sprue (Korpe and Petri, 2012) and is mainly observed in regions of the world with poor sanitation and hygiene, suggesting microbial exposure or the microbiota play a role in its development (Ahmed et al., 2014b). Until recently, studies incorrectly assumed diarrhea was the primary driver of early life growth stunting, whereas now it is recognized that many of the sequelae of malnutrition happen independently of diarrhea (Ngure et al., 2014). The etiology of EE has not been experimentally demonstrated, but one hypothesis in the literature is that the increased ingestion of fecal-associated bacteria early in life (due to poor sanitation and hygiene) can lead to a pathological shift in microbe-host interactions in the small intestine and chronic inflammation exacerbating malnutrition (Humphrey, 2009).

Mechanisms explaining how the microbiota may impact EE and malnutrition are yet to be elucidated, however there are many studies implicating a link between early life diet and environmental exposures altering immunity and the microbiota which can drive the pathophysiology and diseases related to malnutrition in a paradoxically similar way to how the microbiota could impact obesity early in life. As the efficacy of nutritional recovery after early life malnutrition remains low, a seminal study noted a significant improvement in nutritional recovery and mortality rates post-antibiotic treatment in children with severe-acute malnutrition (Trehan et al., 2013). The authors did not sequence the microbiota in these children to correlate differences in recovery rate from severe-malnourished, however one can imagine that the antibiotic treatment (amoxicillin) shifted the microbiota into a compositional arrangement more

favorable for nutrient uptake, regulated by shifts in immune function and metabolism. Ecological theory suggests malnutrition could alter the state of the microbiota to dysbiosis and a composition and function unable to recover back to homeostatic interactions without being re-set past the tipping point (Relman, 2013).

Similar to other metabolic and inflammatory disorders, EE-afflicted individuals have increased inflammatory infiltrate in tissues (small intestine) along with presence of systemic inflammatory markers including IL-1b, IL-6, circulating LPS and CCL2 (Prendergast et al., 2015). A limited number of studies have been able to assess the populations of immune cells infiltrating the small intestine, yet those that have reveal increased numbers of intraepithelial lymphocytes (IELs), specifically CD8+ T cells, gamma-delta T-cells and activated T-cells as measured by CD25 (Campbell et al., 2003). In helminth co-infection studies, gut CD8+ memory T cells can become activated and microbiota-specific in the small intestine (Hand et al., 2012), which could implicate the products of intestinal T cells as drivers of the chronic immune activation and inflammation seen in EE. Aside from generating immune activation, microbial products and functions have been linked to increasing intestinal permeability (Fasano, 2011), and mechanisms discussed here which include zonulin release, could be mediating the intestinal permeability seen in children with malnutrition and EE. Presence of a small intestinal microbiota with more invasive potential (i.e. gram-negative coliforms) could mediate the inflammatory and permeability effects on the host. Protein malnourishment makes the host more susceptible to gut inflammation, and mechanisms for this were assessed by a study in mice lacking an important regulator in amino acid homeostasis, angiotensin-converting enzyme-2 (ACE2). Mice deficient in ACE2 were more susceptible to inflammation and cell death by exposure to DSS, and transfer

of the microbiota from ACE2 mice to germ-free mice transferred over the inflammatory phenotype, implicating the microbiota in this relationship (Hashimoto et al., 2012). Thus, early-life protein malnutrition could result in an increased inflammatory response to insult by fecal-coliforms that are normally tolerated by the host. In this way, early life malnutrition can set forth a vicious cycle where early life malnutrition alters the programming and function of the immune system, leading to increased potential for colonization of harmful pathogens or pathobionts which can colonize in the small intestine, lead to EE features (chronic inflammation, villous blunting, malabsorption and permeability) that disrupt gut homeostasis, exacerbating the effect of malnutrition (Guerrant et al., 2008a).

Unfortunately, EE is largely understudied due to the difficulty in obtaining samples directly from the small intestine in humans, which requires invasive biopsies deemed unethical due to the subclinical nature of EE. Thus, insight into the connection between metabolism, microbiota and immunity in the malnourished intestine is limited. Furthermore, many human studies take only fecal samples to assess the microbiota composition in malnutrition and EE cases, yet this does not capture the small intestinal bacterial community, an important consideration since the fecal microbiota composition is not representative of those microbes colonizing the small intestine (Simrén et al., 2013), where pathology of this disease occurs. Thus, there is a major unmet need for a preclinical animal model of EE and these models will be crucial in order to understand the pathogenesis of EE, its impact on malnutrition and to develop therapies.

Here we describe the first animal model of EE and we demonstrate that both diet and oral microbial exposure to specific bacteria are required for the induction of EE in a mammalian host.

Utilizing this model, we were able to achieve for the first time, an in-depth characterization of the impact of malnutrition on the microbiota, metabolism and immune system in the mammalian small intestine, along with assessing the impact of enteric infection. These studies provide a preclinical model to test therapeutics and will enable a greater understanding of the pathophysiological nature of EE.

3.2 Materials and methods

3.2.1 Animal studies

All animal work was done according to the Canadian Council on Animal Care guidelines, utilizing protocols that were approved for use by the Animal Care Committee at the University of British Columbia. Three-week-old, female C57BL/6 mice or TLR4-/- mice were ordered for each experiment (Jackson Laboratory, Bar Harbor, ME) and housed in a barrier animal facility at the University of British Columbia (UBC) with a 12 hr light-dark cycle. Upon arrival, mice were randomized and housed into separate groups (4-5 per cage) which were either fed a malnourished diet moderately low in protein (7%) and fat (5%) or an isocaloric control diet with 20% protein and 15% fat, similar to one used in previous studies to induce protein malnutrition[56] (Research Diets, New Brunswick, NJ, Table 2.1). The chow was irradiated before use and mice were given the diet *ad libitum* throughout experiments.

3.2.2 RNA isolation and cDNA synthesis.

Approximately 1 cm of the jejunum was excised and immediately submerged in RNA*later*™ (Qiagen, Valencia, CA) and stored at 4ºC overnight and then at -80ºC for subsequent RNA extraction. The RNA of the tissue was extracted using RNeasy Mini kit (Qiagen, Valencia, CA)

according to the manufacturer's instructions. RNA concentration and purity were determined using a NanoDrop ND-1000 (NanoDrop Technologies, Wilmington, DE, USA) and reverse transcription was completed with the Quantitect RT kit (Qiagen, Valencia, CA) utilizing a total of 1 μg RNA as template for the reaction.

3.2.3 Real-time qPCR for host gene expression.

Real-time qPCR analysis for host gene expression was performed utilizing Quantitect SYBR-Green Mastermix (Qiagen, Valencia, CA), using primers listed in Table 3.1. PCR was performed in 10 μL reaction volumes on an Applied Biosystems 7500 machine and cycles consisted of 95°C for 15 min and 40 cycles of 95°C for 15 s, 60°C for 30s and 72°C for 30s. Glyceraldehyde-phosphate-dehydrogenase (GAPDH) was found to be an appropriate endogenous control and was used for normalization. Relative expression was calculated using the ΔΔC(t) method relative to the control mice.

3.2.4 Real-time qPCR analysis for bacterial abundance.

The assessment of bacterial abundance was performed using Quantitect SYBR-Green Mastermix (Qiagen, Valencia, CA) and group-specific primers for 16S rRNA (Table 3.1). PCR was performed on an Applied Biosystems 7500 machine. The abundance of 16S rRNA in the small intestinal sample was determined by comparing the C_T values to the values generated by standard curves. The standard curves were developed from applying the group specific primers to DNA purified from cultured ATCC strains of bacteria with a known value of 16S copies per ng of DNA. Results were expressed in total 16S copies per gram of tissue extracted.

Table 3.1 A list of all qPCR primers and sequences utilized in this study for host gene expression and assessment of bacterial 16S rDNA abundance.

Host Gene Target	Sequence (5' -> 3')	Annealing Temp. (°C)
TJP1	Fwd- CCCTGAAAGAAGCGATTCAG Rev- CCCGCCTTCTGTATCTGTGT	60
CLDN2	Fwd- ATACTACCCTTTAGCCCTGACCGAGA Rev- CAGTAGGAGCACACATAACAGCTACCAC	60
CLDN4	Fwd- CGCTACTCTTGCCATTACG Rev- ACTCAGCACACCATGACTTG	60
CLDN15	Fwd- GCAGGGACCCTCCACATATTG Rev- AGTTCATACTTGGTTCCAGCATACGTG	60
IGF1	Fwd- TTCAGTTCGTGTGTGGACCGAG Rev- TCCACAATGCCTGTCTGAGGTG	60
ACE2	Fwd- TGGTCTTCTGCCATCCGATT Rev- CCATCCACCTCCACTTCTCTAA	60
CRYP	Fwd- GAGAGATCTGGTATGCTATTG Rev- AGCAGAGTGTGTACATTAAAT	60
ANG	Fwd- CTCTGGCTCAGAATGAAAGGTACGA Rev- GAAATCTTTAAAGGCTCGGTACCC	60
REG3	Fwd- AAGCTTCCTTCCTGTCCTCC Rev- TCCACCTCTGTTGGGTTCAT	60
MMP7	Fwd- CACTCTAGGTCATGCCTTCGC Rev- GGTGGCAGCAAACAGGAAGTT	60
RELMB	Fwd- GCTCTTCCCTTTCCTTCTCCAA Rev- AACACAGTGTAGGCTTCATGCTGTA	60
GAPDH	Fwd- ATTGTCAGCAATGCATCCTG Rev- ATGGACTGTGGTCATGAGCC	60

Bacterial Target	Sequence (5' -> 3')	Annealing Temp. (°C)
Eubacteria 16S rRNA (total bacteria)	Fwd- ACTCCTACGGGAGGCAGCAGT Rev- ATTACCGCGGCTGCTGGC	60
Bacteroidetes 16S rRNA	Fwd- GGTTCTGAGAGGAAGGTCCC Rev- GCTGCCTCCCGTAGGAGT	60
Clostridium cluster IV	Fwd- ACAATAAGTAATCCACCTGG Rev- CTTCCTCCGTTTTGTCAA	60
Clostridium cluster XIVa	Fwd- ACTCCTACGGGAGGCAGC Rev- GCTTCTTAGTCAGGTACCGTCAT	60
Lactobacillus/Lactococcus	Fwd- AGCAGTAGGGAATCTTCCA Rev- CACCGCTACACATGGAG	60
Enterobacteriaceae 16S rRNA	Fwd-CATTGACGTTACCCGCAGAAGAAGC Rev- CTCTACGAGACTCAAGCTTGC	56

3.2.5 FITC-dextran uptake assay

In order to directly assess intestinal permeability *in vivo*, mice were gavaged with 80 mg/mL of 4 kDa FITC-dextran (Sigma-Aldrich) at a volume of 150 µL, after food deprivation for 4 hours. Four-hours post inoculation, serum was collected from mice post-mortem and measured for FITC concentration using a plate reader (Tecan, Maennedorf, Switzerland). FITC was measured against a standard curve of serially diluted FITC-dextran, and the plate was read with the excitation of 485 nm and emission of 530 nm.

3.2.6 Histology

Intestinal sections 2 cm in length from the duodenum, jejunum and ileum of mice were collected and immediately placed in 10% buffered formalin overnight at room temperature. Paraffin-embedded tissues were cut into 5 µm slices and stained with hematoxylin and eosin (H&E) using

standard techniques. H&E stained tissues were visualized under a light microscope and villous length, and crypt depth of each crypt and villous of the tissue were enumerated using Axiovision version 4.6 software. Livers were excised, cut and stained with H&E in a similar manner as stated above and visualized under a light microscope for signs of pathology. For visualizing the mucus layer, 1 cm sections of the jejunum were excised from mice, immediately submerged into methanol-Carnoy's fixative for 2 hrs at 4°C and then transferred to 100% ethanol. Paraffin-embedded tissues were cut into 5 μm slices and stained with Alcan blue-periodic acid (AB-PAS) using standard techniques.

3.2.7 DNA extraction

In order to assess the composition of the microbiota, sections from the small intestine of malnourished or control-fed mice +/- bacterial gavage were homogenized using a bead-beating method (FastPrep instrument, MP Biomedicals, Solon, OH), and total DNA was extracted using a Stool DNA Extraction Kit (Qiagen, Valencia, CA).

3.2.8 Bacterial strains

All commensal bacterial strains that are used in our study were of human origin, and were provided to us by Emma Allen-Vercoe (University of Guelph) or ordered from the DSMZ culture collection (Leibniz Institute, Germany). Commensal bacteria strains were all grown on fastidious anaerobe agar (FAA) (LabM) in anaerobic conditions. All strains are listed below in Table 3.2

Table 3.2 A description of all bacterial strains utilized in this study. Strains provided by E.A.V are in highlighted in blue, DSMZ in yellow, VSL#3 in purple, and ATCC in green.

Cocktail	Acronym	Strains	Source
Bacteroides-E. coli	BG	*Bacteroides vulgatus* 3/1/40A *Bacteroides fragilis* 3/1/12 *Bacteroides ovatus* 3/8/47 *Bacteroides dorei* 5/1/36 (D4) *Parabacteroides distasonis* 2/1/33B *Escherichia coli* 3/2/53 *Escherichia coli* 4/1/47	Biopsies and Feces
VSL3 Probiotic Mix	VSL3	*Streptococcus thermophilus* *Bifidobacterium breve* *Bifidobacterium longum* *Bifidobacterium infantis* *Lactobacillus acidophilus* *Lactobacillus plantarum* *Lactobacillus paracasei* *Lactobacillus bulgaricus*	VSL#3® (Sigma-tau pharmaceuticals Inc., Gaithersburg, MD)
Ruminococcus Mix	RC	*Anaerotruncus colihominus* DSM 17241 *Ruminococcus gnavus* 2/1/58 *Ruminococcus torques* 3/1/46	Feces
Clostridium Mix	CLO	*Clostridium paraputrificum* *Clostridium clostridioforme* *Clostridium subterminale*	Feces and biopsies
Prevotella Mix	PV	*Prevotella oralis* CC98A *Prevotella copri* DSM 18205 *Prevotella ruminocola* ATCC 19189	Feces and biopsies
Bacteroides Mix	BAC	*Bacteroides vulgatus* 3/1/40A *Bacteroides fragilis* 3/1/12 *Bacteroides ovatus* 3/8/47 *Bacteroides dorei* 5/1/36 (D4) *Parabacteroides distasonis* 2/1/33B	Biopsies and Feces
Enterobacteriaceae Mix	EC	*E. coli* 3/2/53 *E. coli* 4/1/47	Biopsies
Peptostreptococcaceae Mix	ST	*Peptostreptococcus russellii* DSM 23041 *Filifacter villosus* DSM 1645	Feces

3.2.9 Bacterial cocktail preparation and inoculation

In an anaerobic chamber, bacterial cultures from frozen stock were first plated on FAA, and subsequently pure cultures were selected and mixed together at a 1:1 ratio in sterile, reduced PBS. Bacterial mixtures in PBS were removed from the anaerobic chamber and immediately transported to the animal facility to carry out gavage experiments. The volume of the mixture received per mouse was 100 μL, at a concentration of 10^9 cells/mL. The concentration of the mixture in cell/mL was carried out using a UV spectrometer, and gavage doses confirmed after by back-titering the inocula on FAA. In experiments using heat-inactivated bacteria, the bacterial mixture was incubated for 2 hrs at 80°C, and plated on FAA to confirm the absence of growth.

3.2.10 IEC and IEL isolation

The upper 5cm of the small intestine of mice was excised, attached fat and Peyer's Patches removed, and tissues were cut longitudinally to further remove luminal contents by washing with ice-cold PBS. Epithelial cells were isolated using a PBS buffer containing 1 mM EDTA, 1 mM DTT and 5% FBS, shaking at 37°C for 10 min. This supernatant was filtered and combined with RPMI 1640 and centrifuged at 1500 rpm to isolate the IECs. The intact intestinal tissue was re-suspended in additional PBS buffer containing 1 mM EDTA, 1 mM DTT and 5% FBS, shaking at 37°C for 20 min in order to isolate IELs. Lymphocytes were further purified using a 40% Percoll gradient, re-suspended in RPMI 1640 with 5% FBS and enumerated using a Cell Counter (BD Biosciences).

3.2.11 Flow cytometry

Purified lymphocytes were counted using an automatic cell counter (Countess, BD Biosciences). Cells were stained with fluorochrome-conjugated antibodies against CD45 (clone 30F-11), CD3ε (eBio500A2), CD4 (RM4-5), CD8 (53-6.7), NK1.1 (PK136), and γδ TCR (eBioGL3) (eBioscience), and their populations were analyzed by an LSR II flow cytometer (BD Biosciences) using software packages from CellQuest and FlowJo version 8.7.

3.2.12 Western blotting

Total IECs were lysed with MP-40 and protease inhibitor cocktail (Roche Diagnostics, Basel, Switzerland) for 10 min on ice. The resulting lysis solution was centrifuged at 13 000 rpm for 10 min, and the supernatant was collected. The protein concentration of each sample supernatant was quantified using a bicinchoninic acid assay (Sigma-Aldrich). Equal concentrations of the samples were electrophoresed through a 12% SDS polyacrylamide gel and transferred onto nitrocellulose membrane (Millipore, Darmstadt, Germany). Membranes were probed with anti-claudin-2 and anti-actin primary antibodies (Invitrogen, Carlsbad, CA) and then a secondary anti-rabbit/mouse-HRP antibody.

3.2.13 Fecal calprotectin determination

Fecal content of mice was collected, weighed, homogenized in PBS, centrifuged and the resulting supernatant was stored at -80°C. The concentration of calprotectin in feces was performed on the fecal supernatants using a S100A8/S100A calprotectin ELISA kit as per manufacturer's instructions (Hycult Biotechnology). The resulting concentration of calprotectin

was determined by assessing the OD 450 nm using a plate reader (Tecan, Maennedorf, Switzerland), comparing to a standard curve of known concentrations of calprotectin.

3.2.14 Serum zonulin determination

Serum zonulin concentrations were measured using a zonulin ELISA kit (Abcam, Cambridge, UK) as per the manufacturer's instructions. Sample concentrations were determined by assessing the OD 450nm using a plate reader (Tecan, Maennedorf, Switzerland), compared to a standard curve. This assay only identifies the active, un-cleaved form of zonulin in the sera of mice.

3.2.15 IEC and IEL cytokine quantification analysis

For *ex vivo* quantification of cytokine secretion in the small intestinal tissues, jejunal slices of tissue were washed with complete tissue culture media (RPMI, 10% FBS, 1% glutamine and 1% of 1:1 penicillin/streptomycin) and cultured in 1 mL of the same media in 24 well plates for 24 hours at 37°C, 5% carbon dioxide. The supernatants were screened for the production of inflammatory cytokines using a CBA flex set (BD Biosicences). For analysis of IEL-secreted cytokines, isolated lymphocytes were cultured in complete tissue culture media 24-well plates at a density of $1.0x10^6$ cells/mL. Cells were stimulated with 4 ng/mL of rIL-2 and 1 μg/mL of anti-CD3/CD28 and incubated for 48 hours at 37°C. The resulting supernatants were used to determine the amount of TNF-α, IFN-γ and IL-17A using murine-specific ELISA kits (BD Bioseciences), relative to a standard curve, according to the manufacturer's recommendations.

3.2.16 Fluorescent *in-situ* hybridization

A 1 cm section of the jejunum was excised from mice, immediately submerged into methanol-Carnoy's fixative for 2 hrs at 4°C and then transferred to 100% ethanol. Fixed tissues were paraffin-embedded, cut with a microtome to a thickness of 6-10 μm and transferred to glass slides. The slides were let dry overnight, the tissues then fixed with 4% paraformaldehyde for 10 min at room temperature prior to permeabilization with a solution of 1 mg/ml lysozyme from Eggwhite at 37°C for 1hr. The tissues where then pre-incubated for 1hr at 42°C in hybridization buffer (20mM Tris-HCl, pH 8.0, 0.9M NaCl, 0.01% SDS, formamide, depending on the probe) (Sigma-Aldrich) and then the slides were let dry at 37°C and incubated overnight at 42°C with the respective probe linked to Alexa 555 (Invitrogen, Carlsbad, CA) in the corresponding hybridization buffer at a probe concentration of 50 nM. The following probes were used; all-Bacterial probe (Eub338), Firmicutes (equimolar mixture of LGC354A, B and C), Bacteroidetes (Bac303) and Gamma-Proteobacteria (Gam42a). Details on the probes can be found at ProbeBase (Loy et al., 2007), and the sequences of the probes used is listed in Table 3.3. The tissues were then incubated for 20 min with Alexafluor488-Phalloidin (130 nM) and DAPI at a concentration of 1 μg/ml prior to mounting with Prolong reagent. The slides were imaged on a Cell Voyager CV100 using a 40x oil immersion objective and stitched (90% overlap) and analyzed using Fidji.

Table 3.3 A list of all FISH probes utilized in this study, along with the sequence and formamide concentrations used.

Probe Name	Target	Sequence (5' -> 3')	Formamide Concentration
Eub338	Total Bacteria (Eubacteria)	5'- GCT GCC TCC CGT AGG AGT -3'	30%
Gam42a	γ-Proteobacteria	5'- GCC TTC CCA CAT CGT TT -3'	30%
LGC354a-c	Firmicutes	a) 5'- TGG AAG ATT CCC TAC TGC -3' b) 5'- CGG AAG ATT CCC TAC TGC -3' c) 5'- CCG AAG ATT CCC TAC TGC -3'	30%
BAC303	Bacteroidetes	5'- CCA ATG TGG GGG ACC TT -3'	0%

3.2.17 Statistical analysis

Statistical significance for the difference between two treatment groups was calculated by using a two-tailed Student's *t*-test or the Mann-Whitney *U*-test (for non-parametric data) unless otherwise stated. For assessing statistical significance among three or more groups, a one-way ANOVA with post hoc Tukey's test was utilized. Statistical analysis was performed with assistance from GraphPad Prism Software Version 6.00 (GraphPad Software, San Diego California USA, www.graphpad.com). Statistical significance was given as *** p-value < 0.001; ** p-value < 0.01; * p-value < 0.05; ns (not significant) p-value > 0.05. The results are expressed as the mean value with standard error of the mean (SEM), unless otherwise indicated.

3.3 A screen of bacterial exposure reveals Bacteroidales-*E. coli* cocktail replicates features of EE

Given the malnourished induced shifts in the small intestinal microbiota and metabolome, we postulated that oral exposure to only specific species of bacteria would be necessary to induce EE features in a malnourished mouse (Fig. 3.1). We utilized the small intestinal microbial data to rationally select taxonomically grouped mixtures of species with a propensity to colonize the small intestine more readily in malnourished mice and subsequently orally exposed mice on both diets to these cocktails of cultured bacterial species (Fig. 2.4, Fig. 2.5). In this model, young mice were randomized onto either the control or malnourished diet for two weeks, then gavaged every 2 days with each bacterial cocktail for an additional 6 days, and finally the characteristic pathological features of EE were assessed one week after the last gavage. Alternatively, to measure growth rates, malnourished mice were gavaged every 3 days post-weaning for a total of 2 weeks, and EE features were assessed one week later (Fig 3.2). Remarkably, we found that in combination with the malnourished diet the oral exposure to defined mixture of *Bacteroidales* and *E. coli* (BG) was able to trigger villous blunting and exacerbate the effect of the malnourished diet on growth stunting, intestinal permeability and inflammation resulting in intestinal disease which is strikingly similar to features of human EE (Fig. 3.3a-d). Importantly, mice given a standard diet and exposed to BG did not show any pathological consequences and maintained normal growth compared to untreated, control mice (Fig. 3.3a,b).

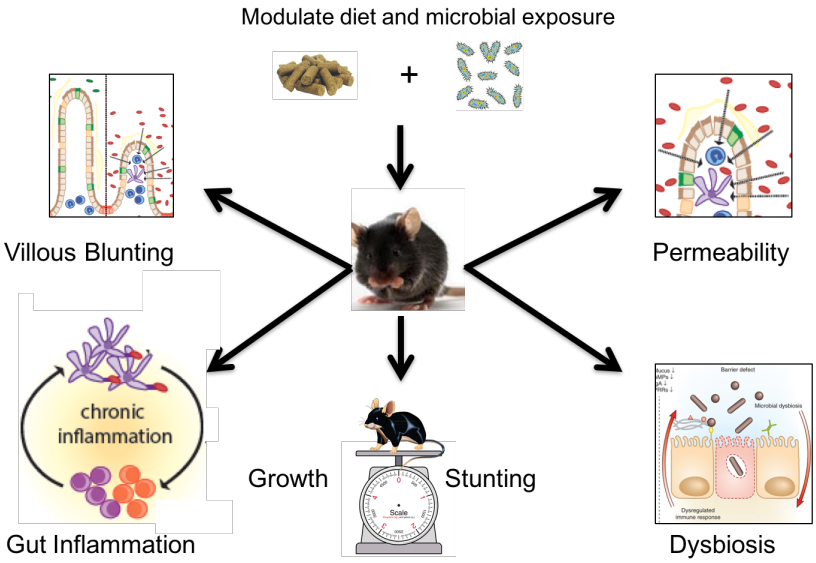

Figure 3.1 Strategy for the development of a EE mouse model

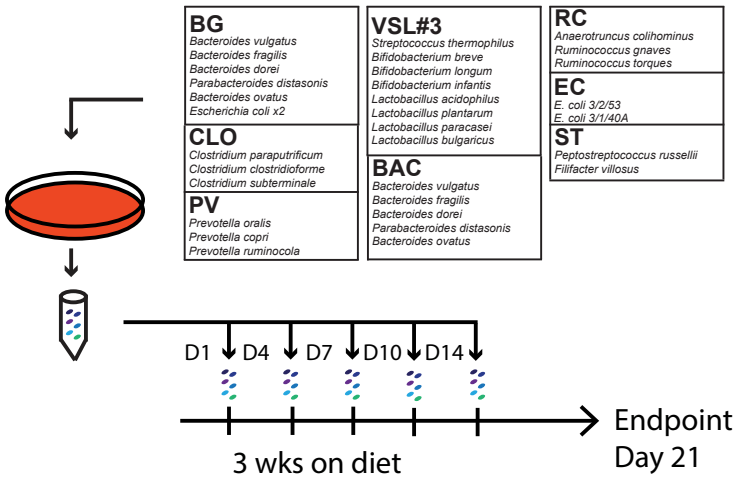

Figure 3.2 A schematic of the experimental design used to administer the various microbial cocktails to malnourished mice.
Three-week old mice were given the malnourished diet and exposed to each microbial mixture listed by oral gavage 5 times over a 2-week period. After the experimental endpoint 1 week later, mice were assessed for growth rate, tail-length, villous architecture and, in some cases, inflammation.

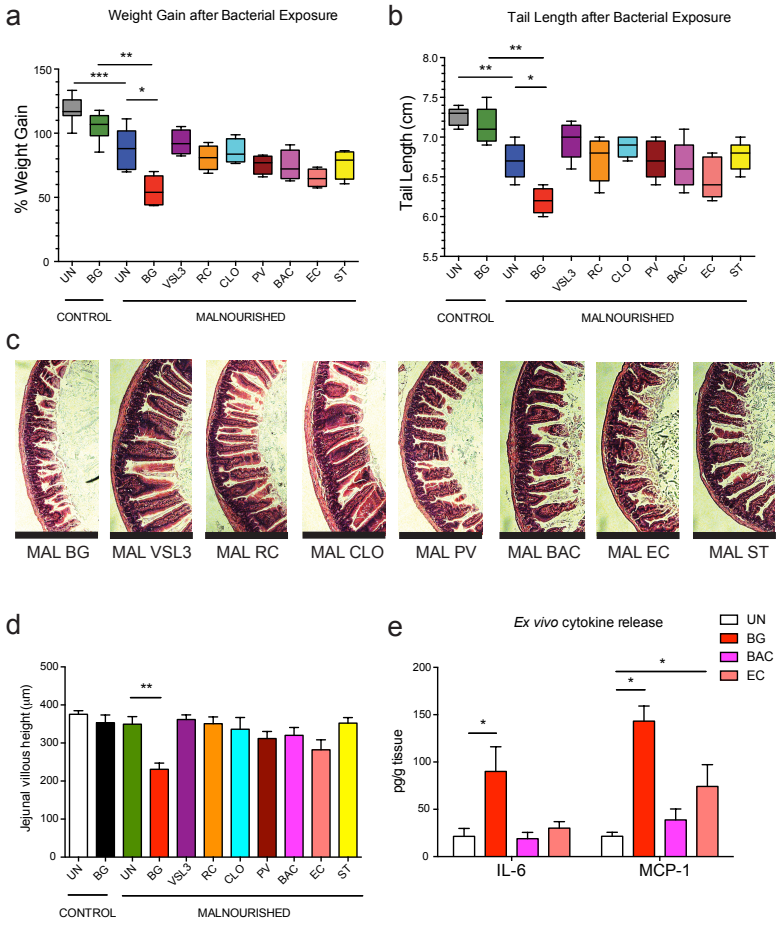

Figure 3.3 A screen of the impact of oral exposure of mice to various microbial mixtures on growth rate, villous architecture and inflammatory markers in malnourished mice.
After 3 weeks of exposure to each microbial mixture and being fed each diet, the total amount of (**a**) weight gained and (**b**) final tail lengths were calculated. Data on malnourished and control, unexposed mice (MAL-UN and CON-UN) are the same as presented in Figure 1, for comparison (n=8). The remaining data is based on 5 mice per group and is representative of 2 independent experiments (**c**) Representative images of the jejunal architecture from of H&E stained tissues from malnourished mice exposed to the microbial mixtures. (**d**) The histological assessment of villous height were measured in the malnourished and control mice exposed and unexposed to the microbial mixtures over a period of 3 weeks. Data from the images and graphs are representative of 2 independent experiments, 5 mice per group (**e**) Concentrations of IL-6 and MCP-1 released in the tissue culture media by jejunal sections of tissue from BG-exposed, EC-exposed, BAC-exposed and unexposed malnourished mice as measured by a cytokine bead array. Data is representative of 2 independent experiments, 5 mice per group. Statistical analysis was performed using a one-way ANOVA with post hoc Tukey's test (*p<0.05, **p,0.01, ***p<0.001).

Malnourished mice exposed to BG showed increased growth stunting (25% less weight) as compared to unexposed malnourished mice (Fig. 3.3a). The increased weight loss in the BG-exposed malnourished mice was accompanied with increased intestinal permeability (Fig. 3.4b-d). When comparing jejunal gene expression of tight junction proteins of the malnourished mice to the BG-exposed malnourished mice, we found that there is a further increase in *CLDN2* expression, both at the gene and protein level (Fig. 3.4b,c), and a further reduction of *CLDN4* expression in the BG-exposed malnourished mice (Fig. 3.4b), suggesting an exacerbation of intestinal permeability. The heightened intestinal permeability of the BG-exposed malnourished mice was functionally relevant as increased levels of FITC in the serum were measured after oral administration of FITC-dextran compared to unexposed malnourished mice and control mice (Fig. 3.4d). Zonulin levels in the serum have been shown previously to correlate to increased intestinal permeability in many intestinal diseases, by regulating tight junction proteins, and is a biomarker for human EE (Korpe and Petri, 2012). We observed that BG-exposed malnourished mice have a 4-fold increase of zonulin in the serum, compared to unexposed malnourished mice and control mice (Fig. 3.4e).

Villous blunting is a histological hallmark of human EE and we show that BG exposure induced villous blunting, as BG-exposed malnourished mice had significantly shorter villi in the jejunum (250μm on average) compared to the villi of unexposed malnourished mice (350μm on average) (Fig. 3.4f, Fig. 3.3c). An alternative measure of villous blunting is the ratio of the villous length to crypt depth, which decreased from 4:1 in the malnourished mice to 2.5:1 in the BG-exposed malnourished mice (Fig. 3.4f). Given the histological differences, we assessed whether BG exposure induced small intestinal inflammation in malnourished mice. We measured *ex vivo* jejunal cytokine secretion from cultured jejunal sections and found significantly elevated

interleukin (IL)-6 and monocyte chemotactic protein-1 (MCP-1) production in BG-exposed malnourished mice only (Fig. 3.4g). To further confirm the presence of chronic inflammation in this model, we tested the impact of BG-exposure on another EE biomarker, fecal calprotectin, whose levels correlate positively with intestinal inflammation (Konikoff and Denson, 2006). The concentration of calprotectin in the feces of BG-exposed malnourished mice was 2.5 greater than controls or unexposed mice, confirming the presence of significant intestinal inflammation (Fig. 3.4h). Notably, the BG exposure had no effect on TJP expression and protein levels, intestinal permeability, serum zonulin or fecal calprotectin levels in mice fed the control diet (Fig. 3.4b-d, g).

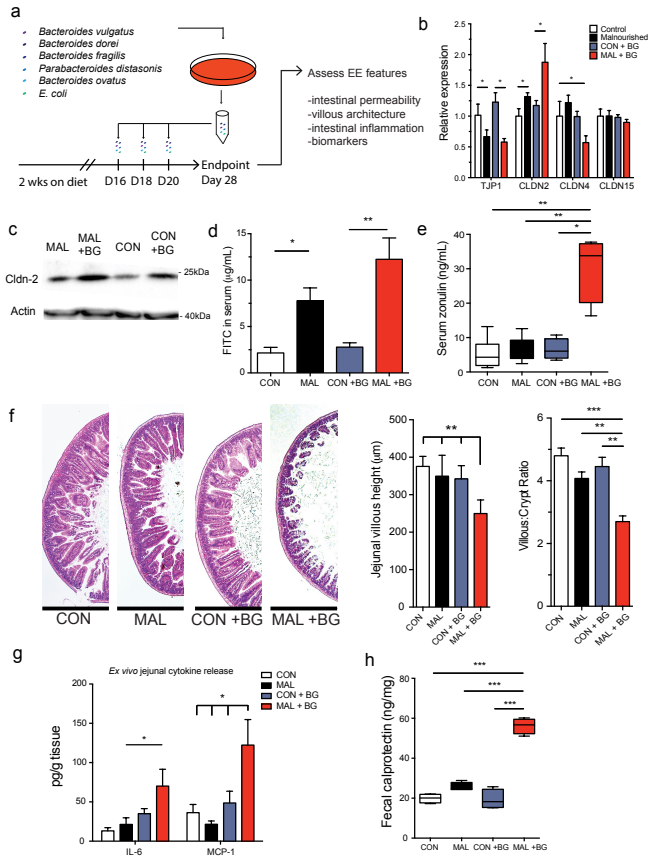

Figure 3.4 Characterizing the impact of Bacteroidales-*E. coli* oral exposure on small intestinal histopathology, inflammation and intestinal permeability in malnourished and control mice.

(**a**) A schematic of the experimental design used to administer the *Bacteroidales-E. coli* cocktail. (**b**) The jejunal mRNA levels of *TJP1, CLDN2, CLDN4* and *CLDN15* were determined on unexposed mice on each diet (white and black bars), and BG-exposed mice on each diet (blue and red bars). The values are expressed as fold-change relative to the control, unexposed mice. Representative of 3 independent experiments, n=5 per group (**c**) Levels of CLDN2 protein blotted from extracted protein from jejunal IECs relative to the actin control. Blot is representative of 3 samples, and 2 independent experiments. (**d**) Four hours after FITC-dextran administration, concentration of FITC in the serum in malnourished and control mice (n=8) and BG-exposed malnourished and control mice (n=8). Representative of 2 independent experiments (**e**) Box and whisker plot of the concentration of zonulin in the sera of malnourished and control mice (n=8) and BG-exposed malnourished and control mice (n=8). Data is pooled from 2 independent experiments. (**f**) Histological assessment of H&E stained jejunal tissues from BG-exposed and unexposed malnourished and control mice. Images and graphs are representative of 3 independent experiments, 5 mice per group (**g**) Concentrations of IL-6 and MCP-1 released in cultured jejunal tissue sections from BG-exposed and unexposed malnourished and control mice as measured by ELISA. Data is representative of 2 independent experiments, 5 mice per group (**h**) Box and whisker plot of the concentration of fecal calprotectin in BG-exposed or unexposed malnourished mice (n=4 per group). Statistical analysis was performed using the one-way ANOVA with post hoc Tukey's test (*p<0.05, **p<0.01, ***p<0.001).

Unexpectedly, neither the administration of the *Bacteroidales* species alone (BAC) nor the *E. coli* species alone (EC) were sufficient to trigger the growth stunting, inflammation or villous blunting characteristic of EE as seen with the combined BG (Fig. 3.3e). This implies the *Bacteroidales* species and *E. coli* isolates work synergistically to impart their effect on the small intestine. We also assessed 5 additional bacterial mixtures including a *Ruminococcus* mix, *Clostridium* mix, *Prevotella* mix, *Peptostreptococcaceae* mix, along with VSL#3, a commercial probiotic, and found that only exposure to BG was able to exacerbate the effects of malnourishment and result in the development of EE features (Fig. 3.3a-d).

3.4 The BG challenge alters microbial colonization patterns

We next analyzed the bacterial colonization levels in the small intestine of mice on each diet, with or without exposure to the BG. We found malnourished mice and BG-exposed malnourished mice had a significant increase in adherent, cultivable anaerobic bacteria in the jejunum compared to control mice (Fig. 3.5a). Quantification of 16S rRNA levels in jejunal tissue showed a similar trend to the culture-based analysis, as mice fed a malnourished diet had more bacteria associated with the small intestinal tissue (Fig. 3.5b). Surprisingly, BG-exposed malnourished mice did not have appreciably more bacteria adhering to the small intestine in comparison to the malnourished, unexposed group, despite the extensive villous blunting and increase in intestinal inflammation (Fig. 3.5b). Bacteroidetes 16S rRNA expression analysis showed similar levels of Bacteroidetes (MIB) in BG-exposed and unexposed malnourished mice, which was greater than the control groups (Fig. 3.5c). *Enterobacteriaceae* 16S rRNA expression analysis showed more adherent *Enterobacteriaceae* in the small intestine of BG-exposed malnourished mice compared to unexposed malnourished mice and importantly this was not seen

in BG-exposed control mice (Fig. 3.5d). These data suggest mice given a malnourished diet are more susceptible to colonization of bacteria in the small intestine, especially those from the *Enterobacteriaceae* family.

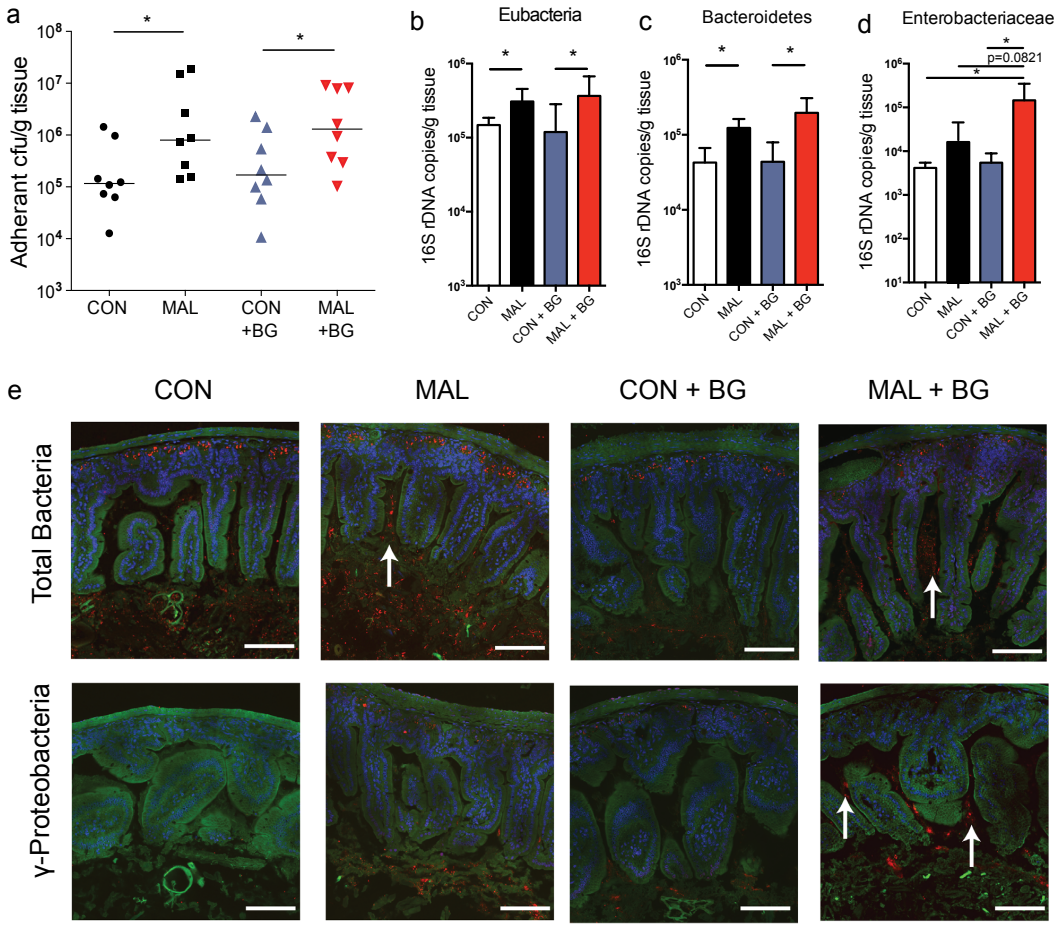

Figure 3.5 Assessing the abundance, colonization and localization of small intestinal microbiota in mice with or without Bacteroidales-E. coli oral exposure.
(**a**) The total adherent anaerobic colony forming units (CFUs) per gram of washed jejunal tissue in BG-exposed or unexposed malnourished and control mice. Data are pooled from 2 independent experiments (n=8), and bars indicate median values (*p<0.05, Mann-Whitney *U*-test). Real-time qPCR analysis of (**b**) the total Eubacteria 16S rDNA copies, (**c**) mouse intestinal Bacteroidetes-specific 16S rDNA and (**d**) *Enterobacteriaceae*-specific 16S rDNA, in each gram of jejunal tissue. Analysis was performed on DNA extracted from washed jejunum tissue of BG-exposed or unexposed malnourished and control mice. All data in (**b**)-(**d**) are pooled from 2 independent experiments (n=8), and bars indicate the mean with S.E. (*p<0.05, one-way ANOVA with post hoc Tukey's test). (**e**) Carnoy's-fixed jejunal tissues were probed for total 16S rDNA (Eub338) and γ-Proteobacteria-specific 16S rDNA (Gam42a) abundance using Fluorescent *in-situ* hybridization (FISH). Images are representative of BG-exposed or unexposed malnourished and control mice. Actin is stained in green (488PHalloidin), cell nuclei in blue (DAPI) and bacteria are stained in red (Eub338 and Gam42a). Scale bar indicates 100μm length, and white arrows point towards the presence of tissue-associated bacteria or bacteria within the villi.

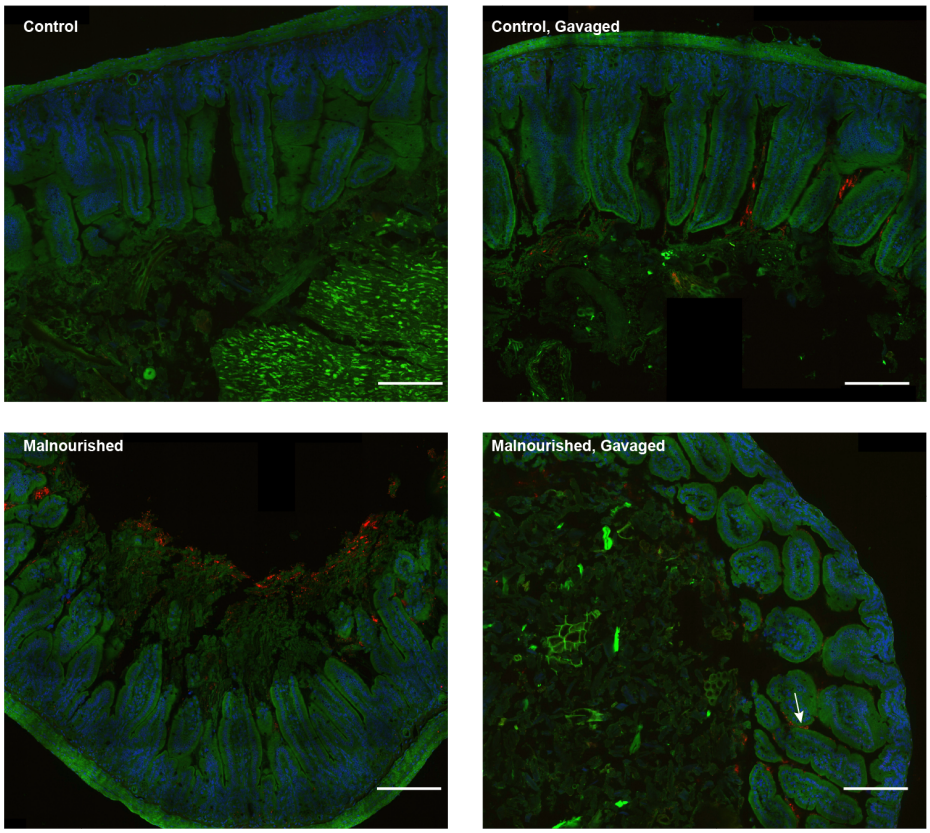

Figure 3.6 FISH analysis of the Bacteroidetes in malnourished and control mice with or without Bacteroidales-E. coli oral exposure.
Jejunal tissues preserved in Carnoy's solution were probed for Bacteroidetes-specific 16S rDNA (BAC) abundance using FISH. Images are representative of BG-exposed and unexposed malnourished and control mice. Actin is stained in green (488PHalloidin), cell nuclei in blue (DAPI) and bacteria are stained in red (Bac303). Scale bar indicates 100μm length, and arrows indicate tissue-associated Bacteroidetes.

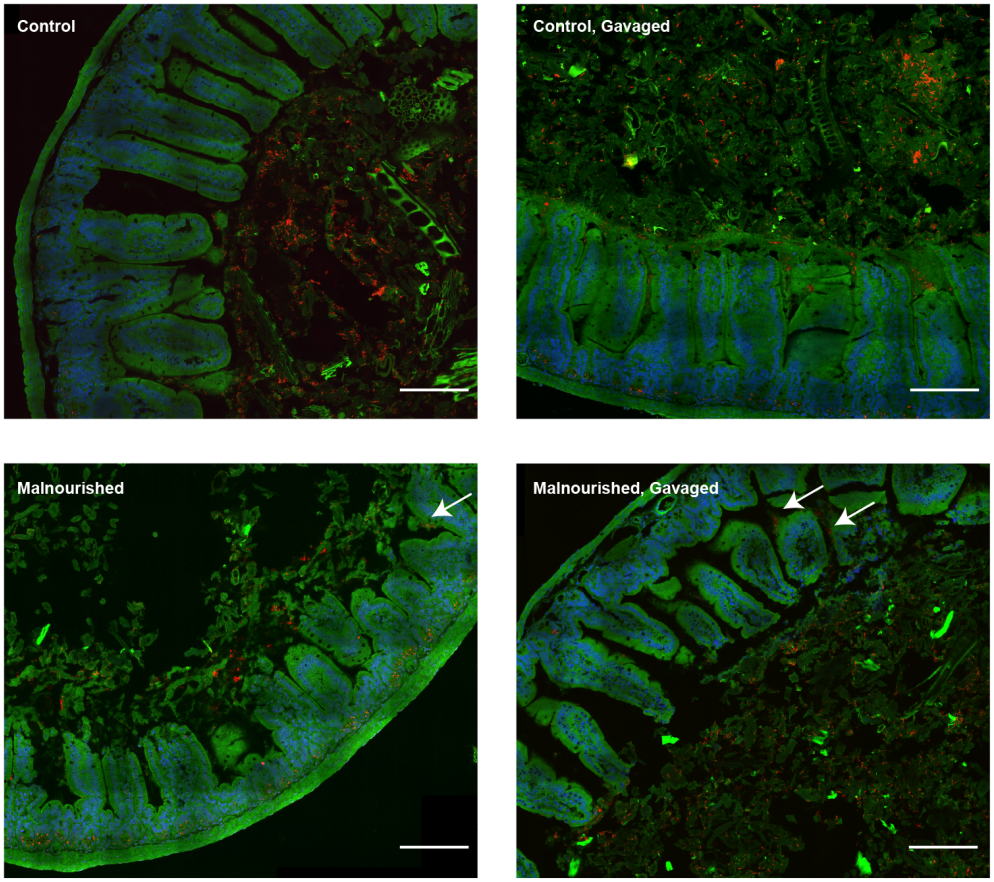

Figure 3.7 FISH analysis of the Firmicutes in malnourished and control mice with or without Bacteroidales-E. coli oral exposure.
Jejunal tissues preserved in Carnoy's solution were probed for Firmicutes-specific 16S rDNA abundance using FISH. Images are representative of BG-exposed and unexposed malnourished and control mice. Actin is stained in green (488PHalloidin), cell nuclei in blue (DAPI) and bacteria are stained in red (LGC354a-c). Scale bar indicates 100μm length, and arrows indicate tissue-associated Firmicutes.

To distinguish the localization of bacteria in the small intestine and visually confirm the increase in tissue-associated bacteria in the small intestine, histological slices of the tissues were subjected to analysis using FISH. By using a universal bacterial DNA probe, a larger number of stained bacteria could be visualized between the villi and associated with the epithelium of the jejunum of malnourished mice (Fig. 3.5e). Even more prominent was the increase of tissue-associated bacteria after the administration of BG to malnourished mice, where large numbers of bacteria were found to reside along the epithelium and deep within the villi (Fig. 3.5e). Using γ-Proteobacteria specific probes, the increase in tissue-associated bacteria in this phylum was most striking in the BG-exposed malnourished mice (Fig. 3.5e). Complementing the pyrosequencing and qPCR data, FISH analysis also revealed an expansion of Bacteroidetes in the jejunal samples, a decrease in the amount of Firmicutes, and more adherent bacteria along the epithelium in all groups (Fig. 3.6, Fig. 3.7). Overall, of the groups analyzed by FISH, γ-Proteobacteria penetrated deep into the crypts more so than species from the Firmicutes or Bacteroidetes phyla (Fig. 3.5e, Fig. 3.6, Fig. 3.7).

3.5 Potential immune mechanisms in the pathophysiology of EE-features

Due to the presence of intestinal inflammation and villous blunting observed after BG-exposure, we investigated the impact of diet and BG on the intestinal immune cell populations. We hypothesized that shifts in lymphocytes in the small intestine could be driving inflammation and consequently, the barrier defect observed in the malnourished mice. We first isolated lymphocytes from the small intestine and discovered that the malnourished diet led to increase in numbers of intraepithelial lymphocytes (IELs) in the duodenum compared to control mice and

that this difference was greater in BG-exposed malnourished mice, although not statistically significant (p=0.051) (Fig. 3.8a). Within the duodenum IEL compartment there was a 5-fold increase in the numbers of γδ T-cells in the malnourished mice and a similar 5-fold increase in BG-exposed malnourished mice, compared to controls (Fig. 3.8b). The majority of the influx of γδ T-cells consisted of CD8+γδ T-cells in both BG-exposed and unexposed malnourished mice (Fig. 3.8c, Fig. 3.9a). CD4+ and CD8+ αβT-cell numbers in the IEL compartment were not significantly different between groups, however abundance of double-positive CD4+CD8+ γδ T-cells, counter intuitively, decreased in abundance after BG was administered (Fig. 3.9b). Much of this influx of IELs in the duodenum was driven by the malnourished diet alone, however NKT-cells were significantly more abundant in BG-exposed malnourished mice compared to malnourished mice (Fig. 3.8d). Cultured IELs from the duodenum of BG-exposed malnourished mice secreted significantly greater quantities of TNF-α and IFN-γ, as well as a trend for elevated IL-17A compared to unexposed malnourished and control mice, after T-cell specific stimulation (Fig. 3.8e). These findings suggest that the malnourished diet is sufficient to induce the IEL influx, however heightened cytokine production by these cells is only triggered with exposure to the BG and this may contribute to the inflammation and villous blunting observed specifically in the BG-exposed malnourished mice.

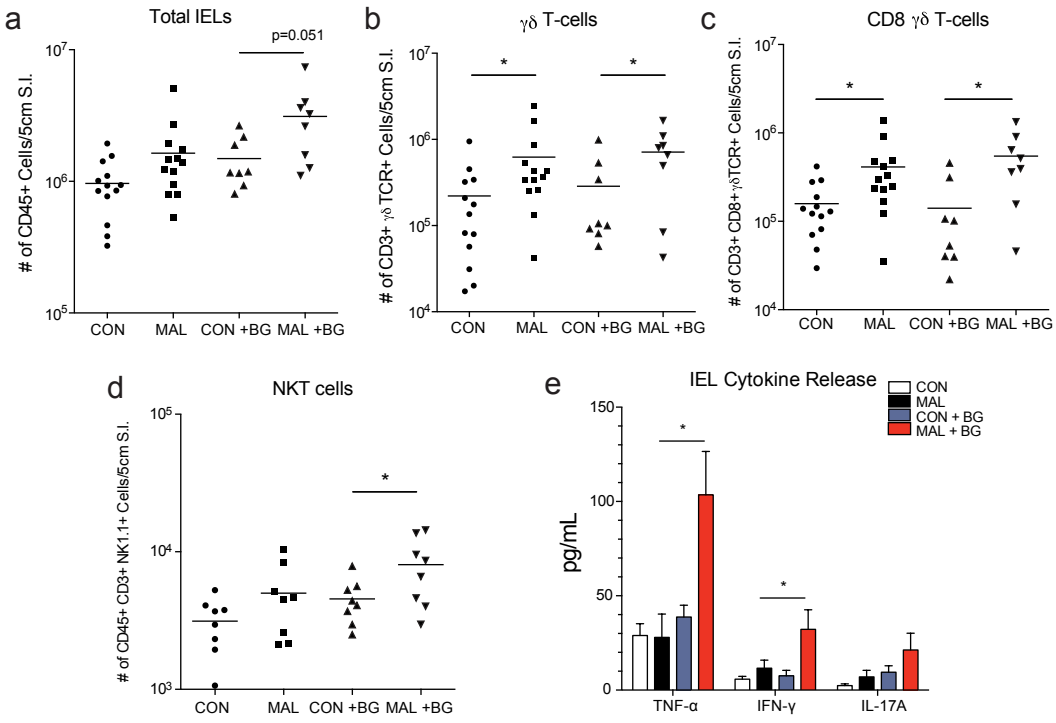

Figure 3.8 Flow cytometry and cytokine secretion analysis of small intestinal intraepithelial lymphocytes.

The total number of live (**a**) CD45+ cells, (**b**) CD45+CD3+γδTCR+ cells, (**c**) CD45+CD3+CD8+γδTCR+ cells and (**d**) CD45+CD3+NK1.1+ cells isolated from the upper 5 cm of the small intestine (duodenum) in BG-exposed and unexposed mice on each diet. Data from the unexposed malnourished and control mice are representative of 3 independent experiments pooled (n=13). Data from the BG-exposed malnourished and control mice are representative of 2 independent experiments (n=8). Bars indicate the mean values (*$p<0.05$, one-way ANOVA with post hoc Tukey's test). (**e**) Concentrations of TNF-α, IFN-γ, and IL-17A after stimulation of cultured IELs for 48 hours. Data are pooled from 2 independent experiments (n=8 per group). Bars indicate the mean values (*$p<0.05$, one-way ANOVA with post hoc Tukey's test).

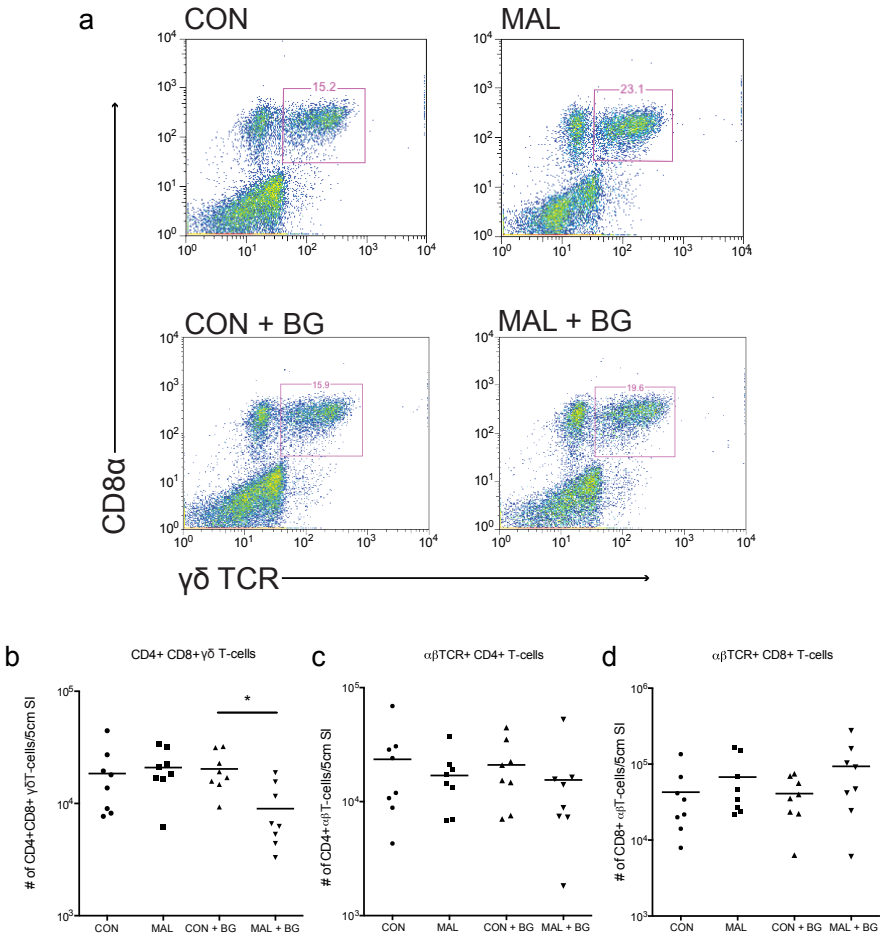

Figure 3.9 Flow cytometry of small intestinal intraepithelial lymphocytes.
(**a**) A graph generated by FlowJo showing the gating of CD8+γδTCR+ T-cells from CD45+ live lymphocytes isolated from the upper 5 cm of the small intestine (duodenum) in BG-exposed and unexposed mice on each diet. The total number of (**b**) CD45+CD3+CD8+CD4+γδTCR+ cells, (**c**) CD45+CD3+CD4+αβTCR+ cells and (**d**) CD45+CD3+CD8+αβTCR+ cells isolated from a 5 cm portion of the duodenum in BG-exposed and unexposed mice on each diet. All data are representative of 2 independent experiments (n=8). Bars indicate the mean values (*$p<0.05$, one-way ANOVA with post hoc Tukey's test).

Given that the BG cocktail contains Gram-negative bacteria, we sought to understand the role of TLR4 signaling in the induction of villous blunting and inflammation. Five of the seven *Bacteroidales* and *E. coli* strains used were able to sufficiently activate TLR4 (Fig. 3.10a). However, TLR4-deficient mice exposure to BG still resulted in significant blunting of the jejunal villi, along with upregulated IL-6 secretion, where MCP-1 secretion remained unchanged (Fig. 3.10b-e). Furthermore, the metabolic activity of the BG bacteria is required to induce any measurable level of villous blunting or small intestinal inflammation in malnourished mice as mice given a heat-inactivated BG did not develop these characteristic EE-features (Fig. 3.10c-e). The increased number of bacteria adhering to the epithelium (Fig. 3.5) is correlated with the increase in IELs observed. Of note, this increase in adherent bacteria coincides with an increased expression of antimicrobial peptides (AMPs) or defense molecules by the host epithelium in BG-exposed malnourished mice, as *matrix metalloproteinase 7* is significantly elevated, along with *resistin-like molecule β* and trends to higher expression of *REG3-γ* and *cryptidin* (Fig. 3.11). The induction of IEL proliferation, the inflammatory signature they produce, along with increased signaling of AMPs all have potential to either defend the host epithelium from damage or induce the damage to the intestinal villi. These three observations of our study represent potential immune mechanisms which correlate with EE-features in mice.

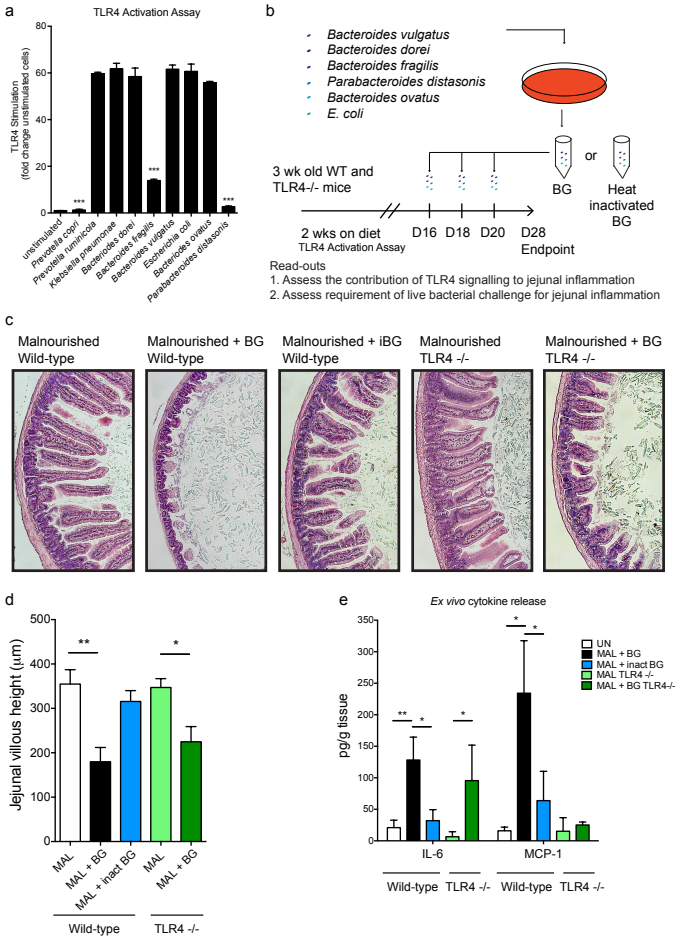

Figure 3.10 An assessment of the requirement of TLR4 signaling and metabolically active bacteria in the inflammatory potential of the Bacteroidales-E. coli gavage.
(**a**) A selection of Gram-negative LPS-containing microbes utilized in previous experiments (BG mix, *Prevotella* mix), along with a *Klebsiella* isolate were incubated with a TLR4 reporter cell line to assess the potential of each microbe to activate TLR4 signaling. Bars indicate the means, +/- S.E. of the fold change in activated compared to an unstimulated control. (**b**) A schematic of the experimental design for the following experiments in TLR4-deficient mice and wild-type mice given a heat-inactivated BG. (**c**) Representative images of the jejunal architecture from of H&E stained tissues in BG exposed and unexposed TLR4-deficient mice, wild type mice and wild-type mice given a heat-inactivated BG (iBG) mix. (**d**) Histological assessment of villous height in the malnourished and control mice exposed and unexposed to BG or heat-inactivated BG. Data from the images and graphs in wild-type mice are representative of 2 independent experiments, 8 mice per group. The TLR4-defecient mice data was based upon 6 mice per group. (**e**) Concentrations of IL-6 and MCP-1 released in the tissue culture media by jejunal sections of tissue from BG-exposed, inactivated BG exposed and unexposed malnourished mice as measured by a cytokine bead array. Bars indicate the means, +/- S.E. Statistical analysis was performed using a one-way ANOVA with post hoc Tukey's test (*p<0.05, **p,0.01).

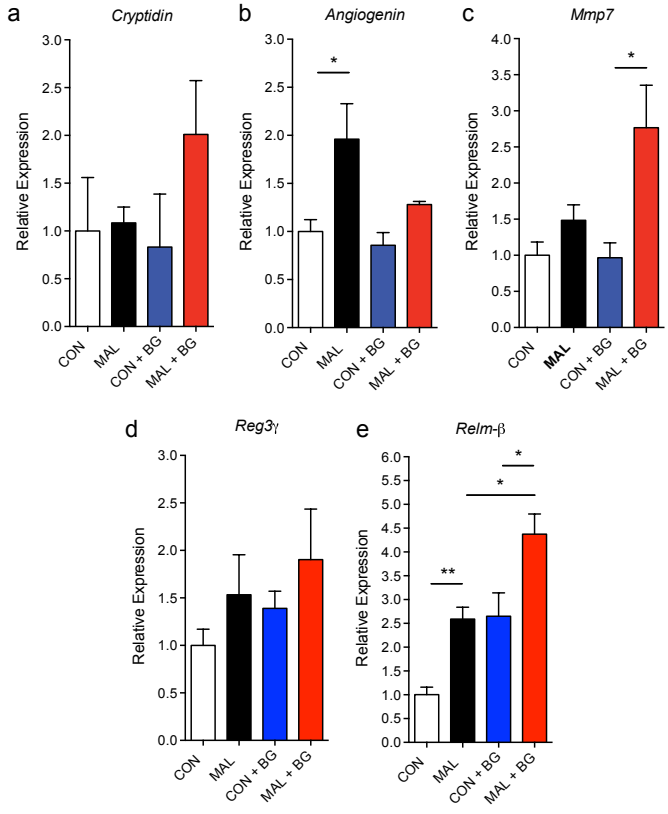

Figure 3.11 Assessing the jejunal gene expression of antimicrobial defense proteins by RT-qPCR.

The relative expression of **(a)** cryptidin, (**b**) angiogenin-4, (**c**) matrix metalloproteinase-7, (**d**) Reg3-γ and resistin-like molecule-β in the jejunum of BG exposed and unexposed mice on each diet was determined by real-time qPCR analysis. Graphs are representative of 2 independent experiments, 8 mice per group. Bars indicate the mean values +/- S.E. (*p<0.05, Student's *t*-test).

3.6 Discussion

These results indicate that a malnourished diet profoundly alters the small intestinal ecosystem, permitting a greater probability of colonization from environmentally acquired microbes. We have identified a set of commensal *Bacteroidales* and *E. coli* strains that, only in combination with a malnourished diet, are able to reproduce the features of human EE in young mice. To date, it has been unclear which species of bacteria, if any, contribute to EE phenotypes (Syer and Wallace, 2014). This observed impact of the *Bacteroidales*-*E. coli* challenge (BG) is consistent with our hypothesis and previous literature suggesting a microbial etiology for EE (Humphrey, 2009), where environmental ingestion of particular microbes can trigger EE and worsen the impact of childhood malnutrition.

A number of epidemiological and microbiological studies indicate increased oral bacterial exposure early in life (due to poor environmental sanitation) is behind the etiology of EE (Lin et al., 2013; Scharf et al., 2014), and in a number of these cases, children exhibit small intestinal bacterial overgrowth (SIBO) (dos Reis et al., 2007; Trehan et al., 2009). Notably, contamination of the household environment with *E. coli* and *Bacteroidales* species was common and correlated to increased intestinal permeability, as well as growth rate deficiencies in rural areas of Zimbabwe and Bangladesh (Ngure et al., 2014; Lin et al., 2013). However, this observation remains a correlative one and other microbes could be involved. In the limited studies assessing the small intestine of malnourished children with EE-features, breath test and culture-based analysis indicated the presence of SIBO (Mello et al., 2012) and Gram-negative bacteria colonizing in the duodenum (Ghoshal et al., 2003), consistent with our observations in malnourished mice. To date, no studies have performed high-throughput sequencing analysis on

the small intestine of children with EE, thus we don't have information on the prevalence of *Bacteroidales* and *E. coli* in these patients, or whether other Gram-negative bacteria may be involved. There are a number of strains of bacteria we did not expose to the mice which could also hypothetically result in EE-features, and future studies are warranted to characterize which bacteria correlate tightly with observations of growth stunting, intestinal permeability, villous blunting, and inflammation in humans. There are three large studies ongoing that aim to characterize the microbial signature correlated with growth stunting and inflammation in young children in Bangladesh (Ahmed et al., 2014a), and Zimbabwe (Ngure et al., 2014) and these results will be important to complement the experiments in mice performed from our study and others to gain a deeper insight into whether there is a microbial etiology for EE.

Utilizing FISH we were able to visualize an increased abundance of tissue-adherent bacteria triggered by the diet and exacerbated with exposure to *Bacteroidales-E. coli* mixture, this observation is also in agreement with other forms of chronic intestinal inflammation (Swidsinski et al., 2009), suggesting the microbiota drive the inflammation. More specifically the qPCR and FISH data indicate the *Enterobacteriaceae* abundance was substantially higher in the *Bacteroidales-E. coli* exposed malnourished mice. These data indicate that the BG exposure combined with a malnourished diet aids in the ability of *Enterobactericeae* species to associate or adhere to the mucosa. Also, the increased abundance of *Bacteroidales* and *Enterobacteriaceae* after BG exposure suggests the malnourished diet promotes the growth potential of these microbes in the small intestine. The inflammatory-driving properties of *Enterobactericeae* species have been well documented, and human commensal *E. coli* species are linked to the development of intestinal inflammation in susceptible hosts (Mukhopadhya et al., 2012; Carvalho

et al., 2012b). Unexpectedly, when administered separately, neither *Bacteroidales* species nor *E. coli* were sufficient to induce EE features, indicating that these species could work in synergy to alter the small intestinal ecosystem enough to promote the dysbiotic changes in function observed. This result was supported by recent data which demonstrated that IgA-linked microbiota from severely malnourished children were sufficient to transfer the Kwashiokor phenotype to germ-free mice (severe inflammation and villous blunting), and *Enterobacteriaceae* were essential however were not able to induce villous blunting alone without the other bacteria in the mixture (Kau et al., 2015). Interestingly, this mixture of bacteria included two of the same species of *Bacteroidales* strains to induce EE-features in the BG mix, and also an *E. coli* strain. Despite their symbiotic capabilities (Round et al., 2011), *Bacteroidales* species also possess the ability to be pathobionts and drive inflammation in the intestine of susceptible hosts (Bloom et al., 2011), however in our model they are not pathogenic unless combined with commensal *E. coli.* Species of the Bacteroidetes are adept at breaking down complex polysaccharides in the intestine which are otherwise indigestible by any host-associated enzyme, using a number of polysaccharide utilization loci to break down cellulose, xyloglucan, *ß*-glucan and many others (Wexler, 2007). Enterobacteriaceae, such as *E. coli* generally utilize simple sugars such as glucose and fructose for their growth, which are hard to come by in the competitive environment of the gut where millions of bacteria operate within their specific niche (Bolick et al., 2013). We hypothesize a reason for Bacteroidetes species being positively associated with *E. coli* blooms in the gut is because they breakdown the complex sugars into simple sugars which the exogenously-acquired *E. coli* could use to get a competitive advantage in the gut ecosystem.

The expansion of duodenal IELs observed in malnourished mice seems contradictory to the literature, since protein malnutrition is known to lead to depressed immune function (Calder, 2013). However, in the limited studies where biopsies of the small intestine were taken from children with EE features, there is evidence of a dramatic infiltrate of lymphocytes to the epithelium, notably γδ T-cells and activated CD8+ T-cells (Campbell et al., 2003), an observation consistent with our results in this model. While BG exposure did not alter total numbers of CD8+γδ T-cells in malnourished mice, IELs isolated from BG-exposed malnourished mice secreted more inflammatory cytokines after stimulation and this increase in inflammatory potential after stimulation may be driving the histopathology observed after BG-exposure. γδ T-cells also proliferate to high numbers in celiac disease, which shares similar histopathological characteristics in the small intestine as EE (Green and Cellier, 2007), as well as small intestinal microbiota dysbiosis (Schippa et al., 2010).

Sphingolipids can impact host immunity by signaling to immune cells through the MHC-like receptor Cd1d, and bacterial-derived sphingolipids can control levels of NKT cells (An et al., 2014), which we found were increased in the IELs of *Bacteroidales-E. coli* exposed malnourished mice. More specifically, the abundance of the Cd1d-restricted NKT-cells were increased upon exposure to the *Bacteroides-E. coli* gavage, hinting at the possibility sphingolipids in this context could result in an expansion of this cell type. Other mechanisms could explain the increase in IELs and T-cells. A role for the vitamin D receptor has been described as important for the ability of CD8+ IELs to home to the small intestine (Yu et al., 2008), interesting since vitamin D metabolites were over-represented in malnourished mice as viewed through both untargeted and vitamin-targeted metabolomics. The fact EE-features can be observed in mice in the absence of TLR4 and the strains must be viable to induce the phenotype,

suggests adaptive or more complex immune responses must be responsible for the inflammation observed in the mice and it's not a simple overexpression of the LPS-TLR4-MyD88 signaling pathway turning on NF-kB. Future studies should expose the *Bacteroides-E. coli* cocktail to Rag1 KO mice and other mice with defective immune systems to understand which immune cells are involved in triggering the inflammation and villous blunting observed in this study.

3.7 Summary

In summary, we show that an orally administered cocktail of specific bacteria are able to reproducibly replicate features of EE only in mice fed a malnourished diet. Utilizing this model, we were able achieve for the first time, an in-depth characterization of the impact of malnutrition on the microbiota, metabolism and immune system in the mammalian small intestine. Future studies will utilize this murine model to gain a deeper understanding of the pathophysiological nature of EE. Furthermore, this model will allow further studies testing the impact of early-life interventions to reverse EE induction.

Chapter 4: Interactions between diet, infection, metabolites and mucosal immunity: from pathogens to sphingolipids

4.1 Introduction

Enteric infections, such as those from *Salmonella,* pathogenic *E. coli* and parasites, such as hookworms, are one defining feature of populations living in regions of the world where malnutrition is widespread and there is poor sanitation with a lack of clean drinking water (Guerrant et al., 2012). While there is a burgeoning recognition of the problem of growth stunting caused by chronic enteric inflammation with no pathogenic signature or known cause, including environmental enteropathy (EE), there are still children who do not live to their teenage years due to the spread of endemic infections (DeBoer et al., 2012). A number of epidemiological studies (Ahmed et al., 2014a), clinical trials (Jones et al., 2014) and vaccine development research (Serazin et al., 2010) has been directed towards combating this issue. Yet, studying pathogens and disease in humans has its own limitations, in that we still don't fully understand how the effects of malnutrition could mechanistically alter pathogen susceptibility. For this, murine models can be useful, especially given the technological growth in the number and depth of assays available to understand complex interactions between, diet, immunity, the microbiome and metabolic changes. Here, the success or failure of infection can be studied at the molecular level, leveraging genetic manipulation of mice, progress in deep sequencing, metabolomics, and improved understanding of the mucosal immune system over the past 10 years. To understand how malnutrition impacts enteric infections, murine models give another advantage in that the colonization of the pathogen can be measured in every tissue if the study

calls for it, most importantly including the small intestine which we have previously shown to be drastically impacted during malnutrition. This enables the full effect of the dietary shift to be studying as it correlates with pathogen burden in a mammalian system.

Many previous studies have utilized murine models to explore how enteric infection is affected by a number of factors, including antibiotic treatment (Wlodarska et al., 2011), prebiotics (Gibson et al., 2005), probiotics (Amara and Shibl, 2015), gnotobiotic conditions (Stecher et al., 2005), temperature (Crepin et al., 2016), SCFAs (Rivera-Chávez et al., 2016), and a wide variety of immune knockouts (Perez-Lopez et al., 2016). How specific dietary components impact enteric infection has also been widely studied, yet mostly with respect to micronutrient deficiency and severe malnutrition. There remains a lack of studies which aim to understand how a moderately malnourished diet, modeling the diet of populations in regions of the world where enteric pathogens such as *Salmonella* and *E. coli* are still endemic, impacts the dynamics of infection. Also, we lack an understanding of how parasites and malnutrition interact. Greater than 700 million people are infected with hookworm, which can profoundly alter mucosal and systemic immune responses in their respective hosts, yet how diet-immune interactions could impact worm colonization also remains unexplored (Brooker et al., 2004). The use of murine models can help answer these questions and inform human intervention studies.

Murine model systems also enable research into specific mechanistic interactions between species of the gut microbiome, their metabolites, diet and immunity. Previous data generated by our study of malnutrition has uncovered a link between malnutrition and the

abundance of sphingolipid metabolites in the small intestine (Faith et al., 2011; Brown et al., 2015), surprising since the diet was low in fat (5% vs 15% fat by kcal). This also correlates with an increase in the number of Bacteroidetes species in the small intestine during malnutrition, known producers of sphingolipids with immunomodulatory effects (An et al., 2014; Wieland Brown et al., 2013; An et al., 2011). Specifically, a sphingolipid from *B. fragilis* called alpha-galactosylceramide, was isolated and shown to bind to CD1d on DCs and interact specifically with NKT-cells in mice (An et al., 2014; Wieland Brown et al., 2013). There was also an increase in IELs, and specifically CD1d-restricted gamma-delta and NKT-cells, after malnutrition, and this effect on NKT-cells was amplified after malnourished mice were gavaged with a cocktail which contained 5 species of Bacteroidetes (along with two *E. coli* strains). Altogether, we hypothesized that during malnutrition and after the *Bacteroides-E. coli* gavage to induce EE-features in mice, sphingolipids from the Bacteroidetes species could be triggering inflammatory and immunomodulatory effects, which potential relevance to chronic inflammation seen in EE. Sphingolipid metabolites from eukaryotic cells have well characterized impacts on metabolism, immunity, apoptosis, and cell membrane integrity (Maceyka and Spiegel, 2014). In chronic inflammatory diseases, such as IBD, sphingolipid signaling by sphingosine-1-phosphate regulate cell chemotaxis (Spiegel and Milstien, 2011) and ceramide-1-phosphate can modulate TLR responses as well as autophagy signaling during inflammation (Hla and Dannenberg, 2012). Sphingosine-1-phosphate receptor agonists specifically are being studied as drug targets to ameliorate inflammation during IBD (Abdel Hadi et al., 2016). We've only recently begun to appreciate there is a second source of sphingolipids in the intestine, from our resident microbiota. As a dominant phylum in the intestine of all mammals, the Bacteroidetes are ubiquitous and unique in their capability to synthesize complex sphingolipids and integrate them into their

membranes, and how these sphingolipid species interact with the host as yet to be fully determined. Aside from the previously characterized alpha-galactosylceramide in *B. fragilis, Bacteroides* species are known to produce three separate sphingolipids, sphingosine, ceramide and ceramide phosphoethanolamine (Olsen and Jantzen, 2001). How these two bacterial ceramides interact with the host immune system has not been studied.

In this study, we treated mice with a moderately malnourished diet (5% fat and 7% protein) compared to an isocaloric control diet with 15% fat and 20% protein and also utilized the novel EE mouse model developed from Chapter 2, where mice are given the Bacteroidales-*E. coli* gavage, and infected each moue with *S.* Typhimurium, *C. rodentium* and *H. polygyrus.* We discovered that malnutrition has a measurable effect on small intestinal colonization of *Salmonella* and liver histopathology. In *H. polygyrus* infected mice, malnutrition blunted the Th2 immune response in the MLN to worm infection, which correlated with higher worm burdens late in infection but no difference in systemic immunity, or vaccine efficacy to an *H. polygyrus* injectable vaccine. The secondary aim of this study was to not only understand how malnutrition impacts enteric infection but to further investigate in detail how metabolites produced by certain microbiota upregulated in malnutrition, sphingolipids, can interact with the host immune system and whether this interaction can mediate inflammation. We aimed to isolate pure fractions of ceramide-based sphingolipids from the species used in the *Bacteroides-E. coli* gavage that triggered EE-features, and understand how these sphingolipids can induce inflammation. To screen these lipids, we utilized a cutting-edge technique called transcription factor sequencing (TF-seq), coupled with RNA-seq, to assess the pathways these lipids are activating. These data were further followed up with proteomics and cytokine-assays from stimulated macrophages and

dendritic cells (DCs) to see the protein-level effects of these sphingolipids. We discovered for the first time that the sphingolipid ceramide phosphoethanolamine activates the innate immune responses and requires TLR-MyD88 interactions to secrete pro-inflammatory cytokines. Research into the pro-inflammatory potential of Bacteroidetes sphingolipids, combined with our data from our infection models, furthers our knowledge of the relevance of our previous work showing altered immunity during malnutrition and increased sphingolipid abundance. It also initiates novel angles of further investigation into specific mechanisms behind increased pathogen burdens and induction of inflammation in regions of the world with poor sanitation and nutrition.

4.2 Materials and methods

4.2.1 Bacterial and worm strains

The *Salmonella* Typhimurium strain SL1344 was used, and were grown on Luria-Bertani (LB) agar with 100 μM streptomycin. The *Citrobacter rodentium* strain that was used was DBS 100, grown in LB overnight. The *H. polygrus* bakeri strain of worm was used, generously provided by Dr. Georgia Perona-Wright. The Bacteroidetes strains used were *B. ovatus* ATCC 8482, *B. vulgatus* ATCC 8483, *B. dorei* 5/1/36 FAA, *B. thetaiotaomicron* Δtdk VPI-5482, *B. thetaiotaomicron* Δtdk SPT$^{-/-}$ VPI-5482, and *P. distasonis* 2/1/33B FAA. The *B. dorei* 5/1/36 FAA and *P. distasonis* 2/1/33B FAA strains were generously given to us by Dr. Emma Allen-Vercoe. The *B. thetaiotaomicron* Δtdk VPI-5482 was a generous donation to the lab from Dr. Harry Brumer.

4.2.2 Infection models of mice

A frozen stock of *Salmonella* Typhimurium (SL1344) was first plated on LB agar with 100 μM streptomycin and a single colony subsequently inoculated into LB broth and grown, with shaking, for 18 hours at 37°C. Using this culture, mice were infected by oral gavage with 100 μL of $5x10^6$ cells/mL. Mice were monitored daily throughout infection as per the animal care protocol, and euthanized 3 days post-infection. For *C. rodentium* infection, a frozen stock of *C. rodentium* DBS 100 was plated on MacConkey agar and a single colony was inoculated into LB broth and grown, with shaking, for 18 hours at 37°C. Mice were infected by oral gavage with 100 μL of $2.5x10^8$ cells/mL. *H. polygyrus* infection was carried out by inoculating mice with 200 L3 stage larvae in PBS no more than 6 months old, and volumes of the gavage varied depending on the initial concentration of the larvae.

4.2.3 *Salmonella* Typhimurium CFU and cytokine determination

At 3 days post-infection, tissues were collected from infected mice and placed into 1 mL of sterile PBS with complete EDTA-free protease inhibitor cocktail (Roche Diagnostics) at a final concentration as recommended by the manufacturer. All tissues were weighed, then homogenized with a MixerMill 301 bead miller (Reutsch) for 2 minutes at room temperature. Tissue homogenates were serially diluted in PBS, plated on LB agar with 100 μM streptomycin and incubated overnight at 37°C. Bacterial colonies were enumerated the following day to determine the CFU per gram of tissue. To determine the cytokine concentrations, tissue homogenates were centrifuged twice at 15,000 rpm for 20 min at 4°C to remove cell debris and the resulting supernatants were aliquoted and stored at -80°C. Cytokine levels in the

homogenates were measured using a Cytometric Bead Array Mouse Inflammation Kit (BD Biosciences), according the manufacturer's recommendations.

4.2.4 *Citrobacter rodentium* CFU determination

At either 3, 7 or 21 days post-infection, mice were sacrificed and tissues were collected from infected mice, where they were placed into 1 mL of sterile PBS. Colon tissues were washed with PBS vigorously to remove any residual fecal material. All tissues were weighed, then homogenized with a MixerMill 301 bead miller (Reutsch) for 2 minutes at room temperature. Tissue homogenates were serially diluted in PBS, plated on MacConkey agar and incubated overnight at 37°C. Bacterial colonies were enumerated the following day to determine the CFU per gram of tissue.

4.2.5 *H. polygyrus* infection measurement

H. polygyrus egg counts at day 14, 21 and 28 post-infection were performed on fecal pellets re-suspended in a concentrated saline solution, using a microscope at 40x magnification and a cell counter. At day 28 post-infection, the small intestine was collected in DMEM + 10% FBS and worms were enumerated by manual counting under a microscope at 40x magnification.

4.2.6 *H. polygyrus* vaccine administration

Vaccination was performed with inoculation of select *H. polygyrus* adult Excretory-Secretory (HES) antigen and which was produced from adult *H. polygyrus bakeri* (originally provided by Professor Rick M. Maizels, University of Edinburgh, UK) as described elsewhere (Hewitson et al., 2015). Mice were immunized essentially as before with 5 μg HES in alum adjuvant i.p., then

boosted with 1 μg in alum on days 28 and 35, before challenge with 200 *H. polygyrus* L3 generally 1–2 weeks later. Fecal egg counts were determined on days 14, 21 and 28 post-challenge, and intestinal adult worms counted as indicated.

4.2.7 MLN and spleen cell isolation and re-stimulation

MLN and spleen cell suspensions were prepared directly by passage through 70 μm nylon filters (BD Biosciences, Oxford, UK), RBCs were lysed and resulting cells were placed in complete RPMI 1640 medium (cRPMI) containing 10% FBS, 100 U/mL penicillin, 100 μg/mL streptomycin and 10 mM L-glutamine. Cells were enumerated and $1x10^6$ cells per well were re-stimulated in cRPMI with 1 μg/mL *H. polygyrus* adult Excretory-Secretory (HES) antigen, anti-CD3 or medium alone for 72 h at 37 °C, and cytokine production measured by CBA.

4.2.8 Flow cytometry

Purified lymphocytes were counted using an automatic cell counter (Countess, BD Biosciences). Cells were stained with fluorochrome-conjugated antibodies against CD45 (clone 30F-11), CD3ε (eBio500A2), CD4 (RM4-5), CD8 (53-6.7), IL-4 (11B11), IL-5 (TRFK5), IL-13 (eBio13A), and IL-17A (eBio17B7), (eBioscience), and their populations were analyzed by an LSR II flow cytometer (BD Biosciences) using software packages from CellQuest and FlowJo version 8.7.

4.2.9 Gastrointestinal motility

Carmine red, which cannot be absorbed from the lumen of the gut, was used to study total GI transit time (Yano et al., 2015). A 200 μl solution of 5% carmine red (Sigma-Aldrich) suspended

in 0.5% methylcellulose (Sigma-Aldrich) was administered by gavage. The time at which gavage took place was recorded as T_0. After gavage, fecal pellets were monitored at 10 min intervals for the presence of carmine red (bright red colour). Total GI transit time was considered as the interval between T_0 and the time of first observance of carmine red in stool.

4.2.10 ELISA titers

Serum was subsequently added in serial dilutions to ELISA plates coated with either 1 μg/mL HES, goat anti-mouse IgG (Southern Biotech) at 1 μg/mL or anti-IgE (clone R35-72, BD Biosciences) at 1.5 μg/mL in carbonate buffer. Antibody binding was detected using HRP-conjugated goat anti-mouse IgG1 or IgE (both Southern Biotech) and TMB substrate.

4.2.11 Isolation and purification of CerPE sphingolipids from bacterial cell culture

B. ovatus, B. dorei, B. thetaiotaomicron WT, *B. thetaiotaomicron* SPT-/-, *B. vulgatus* and *P. distasonis* were grown in 1 L batches of either BHI with vitamin K/hemin supplementation or FAA, and harvested cells were extracted with a 1:2:0.8 ratio of $CHCl_3$:MeOH:H_2O for 18 hrs (all reagents purchased from Sigma-Alderich). Subsequently, a 2:1 ratio of $CHCl_3$ and H_2O was added to the cell suspension, for a final solvent ratio of 1:1:0.9 of $CHCl_3$:MeOH:H_2O. This organic extract was bubbled off under a N_2 stream and subjected to alkaline hydrolysis (0.05M NaOH) for 1 hr at 37 ºC. The crude extract was purified by a 2 mm silica preparative TLC plate (Sigma-Alderich) with a running solvent of $CHCl_3$:MeOH:AcOH:H_2O at a 100:20:12:5 ratio, along with a CerPE migration standard C12 SPE. Bacterial CerPE was confirmed by migration Rf equal to C12 SPE (Avanti) standard and staining with ninhydrin (Sigma-Alderich). The resulting CerPE sphingolipid fraction was scraped and excised (Rf=0.3) and re-purified on a 0.2

mm TLC plate (Sigma-Alrich) using the same separation solvent as above and extraction technique. Eluted lipids were stored dried down in glass vials at -20 ºC. Each bacterial CerPE was isolated in 5-8 independent batches, and the *in vitro* and *in vivo* experiments were repeated with different batches of purified compound.

4.2.12 Mass spectrometry

Similar to as described previously for sphingolipid identification from TLC fractions (Wieland Brown et al., 2013). A Waters Acquity UPLC system coupled to a Thermo LTQ-Orbitrap Velos Pro mass spectrometer was used for sphingolipid analysis. The mass spectrometer was equipped with a heated ESI source and was operated in the Fourier transform (FT) MS scan mode with mass resolution of 60,000 FWHM at m/z 400. The m/z detection range was 80 to 1600. A Waters BEH C_{18} UPLC column (2.1 mm x 50 mm, 1.7 μm) was used for chromatographic separation with the mobile phases being 0.1% NH_4OH in water (solvent A) and 0.1% NH_4OH in methanol (solvent B). The binary solvent elution gradient was 65% B increasing to 100% B over 30 min., isocratic at 100% B for 1 min before returning to 65%B and re-equilibrating over 3 min. The capillary voltage was set to 3500 kV, and the fragmentor voltage at 125 V. The drying gas temperature was maintained at 320 °C with a flow rate of 12 L/min and a nebulizer pressure of 45 psi. MS runs per sample were performed in the negative ion detection mode. Lock mass calibration was applied to ensure mass accuracy throughout LC-MS runs.

4.2.13 Construction of a *B. thetaiotaomicron* sphingolipid knockout

The serine palmitoyl transferase (*SPT*) mutant was created in the *B. thetaiotaomicron* VPI-5482 Δ*tdk* background. The Δ*SPT* mutant was constructed using the counter-selectable allele exchange

method described by Koropatkin and coworkers (Koropatkin et al., 2008). Briefly, ~1-kb fragments upstream and downstream of the *BT SPT* gene were cloned and fused using primer pairs Δ*SPT* Xba1-UPF (5'AGTCACGACGTTGTAAAACGACGGCCAGT-3'), BamH1-UPR (5'-GGCGTAATCATGGTCATAGCTGTTTCCTG-3'), EcoR1-DNF (5'-GTTGTAAAACGACGGCCAGT-3') and HindIII-DNR (5'-GGCGTAATCATGGTCATAGC-3'), respectively, and ligated into the suicide vector pExchange-*tdk* (obtained from Dr. Harry Brumer, UBC). The resulting vector was electroporated into *Escherichia coli* S17-1 λ *pir* and then conjugated into *B. thetaiotaomicron.* Single recombinants were selected on BHI agar plates containing 200 μg/ml gentamicin and 25 μg/liter erythromycin. Single recombinants were cultured in TYG medium overnight and then plated onto BHI agar plates containing 200 μg/ml 5-fluoro-2-deoxyuridine (FUdR). Candidate *SPT* deletions were screened and confirmed by PCR using the diagnostic primers SPT-F (5'-AAAGCAGAAGTAATTTGTTTGCTGT-3') and SPT-R (5'-ATTTTGTTATCTTTGCCCCCTG-3').

4.2.14 Bone-marrow derived macrophage and dendritic cell culture, stimulation and TF-seq transduction

Mouse bones from 6-12 week old female C57BL/6 WT, *TLR2*$^{-/-}$, *TLR4*$^{-/-}$ and *MyD88*$^{-/-}$ knockout mice were used for all experiments. All knockout mouse strains were generously provided by Dr. Bruce Vallance (UBC). BMDCs and BMDMs were differentiated in penicillin/streptomycin containing DMEM, 10% FBS, 10mM L-glutamine and 20 ng/mL M-CSF or GM-CSF for 8 days, before being aliquoted into 96-well plates of $1.0x10^5$ cells/well. For stimulation experiments, 7 day old cells were stimulated with either 0.5% DMSO, 50 ng/mL LPS or 1/200 of a 1 mg/mL stock of CerPE sphingolipid, in two-fold dose curve starting at 5 ug/mL. For TF-seq

experiments, BMDMs were differentiated in penicillin/streptomycin containing DMEM + 10% FBS and 4% M-CSF-conditioned medium (TOPO) for 7 days. HEK293T lentiviral packaging cells (a gift from the Broad Institute's Genetic Perturbation Platform) were propagated in DMEM + 10% FBS. HEK293T cells were transfected with pCMV-dR8.91, VSV-G, and an equimolar pool of 58 pathway reporter vectors using Lipofectamine 2000. BMDMs were transduced in 90% concentrated lentiviral supernatant + 10% CMG on day 4. BMDMs were scraped off of petri dishes, counted on a hemocytometer, and plated overnight in DMEM + 10% FBS at $1.0x10^5$ cells/well in 96-well tissue culture-treated plates (Corning) before stimulation with DMSO, LPS and CerPE sphingolipids, and assay collection the next day.

4.2.15 TF-seq and 3' DGE RNA-seq

TF-seq was carried out using protocols as previously described (O'Connell et al., 2016). In short, cells were lysed in RLT lysis buffer (Qiagen) and stored at −80°C until the start of RNA-seq library preparation. RNA was purified using Agentcourt RNA Clean XP to precipitate the nucleic acids in 1.25 M NaCl and 10% PEG-8000. Maxima reverse transcriptase (Thermo Fisher Scientific) was run according to the manufacturer's instructions using a multiplexed primed reverse transcriptase reaction. The biotinylated 96-well sequence tagged TF-seq-specific reverse transcriptase primers, and the biotinylated 96-well degenerate sequence-tagged polydT reverse transcriptase primers were used at 750 and 250 nM final concentrations, respectively, with 50 units of Maxima. After sequencing-tagging all cDNA during reverse transcription, each 96-well plate was pooled and the unincorporated primers were washed away from the cDNA by precipitating with 10% PEG-8000 and 1.25 M NaCl. Amplification of the TF-seq gene reporter amplicon was performed on 50% of the cDNA using primers with full Illumina-compatible

sequencing adapters in a 600-µl PCR reaction for 28 cycles. The 422-bp amplicon was then gel extracted for sequencing. The remaining 50% of the first strand cDNA was converted to double-strand cDNA using NEB's Second Strand Synthesis Module. The pooled cDNA libraries for TF-seq are sequence tagged only on the 3′ end of the sense transcript; therefore, after full-length double-strand cDNA tagmentation, we performed enrichment PCR of only the sequence-tagged 3′ end of the mRNA transcript.

4.2.16 Normalization and statistical analysis for TF-seq and global RNA expression

Normalization was done as previously described (O'Connell et al., 2016). In short, the number of unique RNA molecules were enumerated for every well and reporter element, requiring a perfect match for the respective tags. The 3′ DGE sequencing is paired-end reads. Read 1 contains the well-tag and RNA UMI. Read 2 contains a fragment from the 3′ end of the transcript. Reads were mapped to RefSeq transcript sequences using Burrows-Wheeler Alignment (Li and Durbin, 2009) with default settings. Both TF-seq and 3′ DGE returned counts of unique RNA molecules corresponding to reporters or genes. Downstream processing for both matrices was identical. For statistical testing, we used generalized linear models from the edgeR package that assume negative binomial distribution and are optimized for analyzing count data (Robinson and Oshlack, 2010). When plotting the TF activity and gene expression patterns, we used the log-fold changes returned by edgeR tests. The p-values correspond to the ANOVA test for each time series, also with edgeR.

4.2.17 SILAC proteomics

For proteomic analyses, samples were reduced, alkylated and digested as described (Rappsilber et al., 2007). Digested peptides were purified and concentrated on C18 tips, eluted

in 80% acetonitrile, 0.5% acetic acid, and dried in a vacuum concentrator (Eppendorf). Dried peptides were re-suspended in 100 m mol/L triethylammonium bicarbonate and chemical dimethylation labelling was performed using light (CH_2O), medium (CD_2O), or heavy ($13CD_2O$) isotopologues of formaldehyde (Boersema et al. 2008). Labelled samples were combined together and re-purified on C18 prior to analysis on a Q-Exactive coupled to a EasyLC-1000 nanoHPLC, as described. Subsequent data was searched using MaxQuant 1.5.3.30 and analyzed using Perseus.

4.3 Colonization dynamics of enteric pathogens *Salmonella* and *Citrobacter* in malnourished and EE-mice

To understand the impact of malnutrition and BG exposure on enteric infection, we utilized the well-studied enteric pathogen *Salmonella enterica subsp. typhimurium* (*S.* Typhimurium) as its colonization dynamics in the small intestine are well known. Furthermore, its greatest burden is in regions of the world where children are also affected by EE. To set up the experiment, 3-week-old C57BL/6 mice were given two different diets for 2 weeks and subsequently two sub-groups were gavaged with the BG mix to induce EE-features (Fig. 4.1). Mice were infected with $3x10^6$ cells of *Salmonella* in LB and sacrificed 3 days post-infection, where caecum, small intestine, spleen and liver were harvested to assay for *S.* Typhimurium burden (Fig. 4.1). In mice fed a control diet and orally infected with *S.* Typhimurium, very few *S.* Typhimurium CFU were detected in the small intestine (Fig. 4.2a). In contrast, mice infected orally after being fed a malnourished diet for 3 weeks post-weaning had a 3-log fold increase in the burden of *S.* Typhimurium adherent to the jejunum 3 days post-infection in BG exposed and

unexposed mice (Fig. 4.2a). There was a trend towards increased *S.* Typhimurium colonization in the caecum of malnourished mice, but *S.* Typhimurium colonization significantly increased in the caecum of BG exposed malnourished mice compared to controls (Fig. 4.2b). Malnourishment led to increased systemic burdens of *S.* Typhimurium with significantly increased colonization in the liver and spleen (Fig. 4.2c,d). The liver of the infected malnourished mice exhibited striking gross and histological changes. Histological examination showed greater levels of cell necrosis and the presence of fatty lipid droplets (Fig. 4.2e). Higher levels of inflammatory cytokines, including IL-6, IFN-γ, TNF-α and MCP-1, were released in the livers of BG exposed and unexposed malnourished mice 3 days p.i. compared to control, infected mice (Fig. 4.2f). Overall, malnourished mice were more susceptible to *S.* Typhimurium infection, and this increased susceptibility was maintained upon exposure to BG, exhibiting higher bacterial burdens in the intestine, while also invading systemically to greater levels, and inducing a prominent pathological change in the liver.

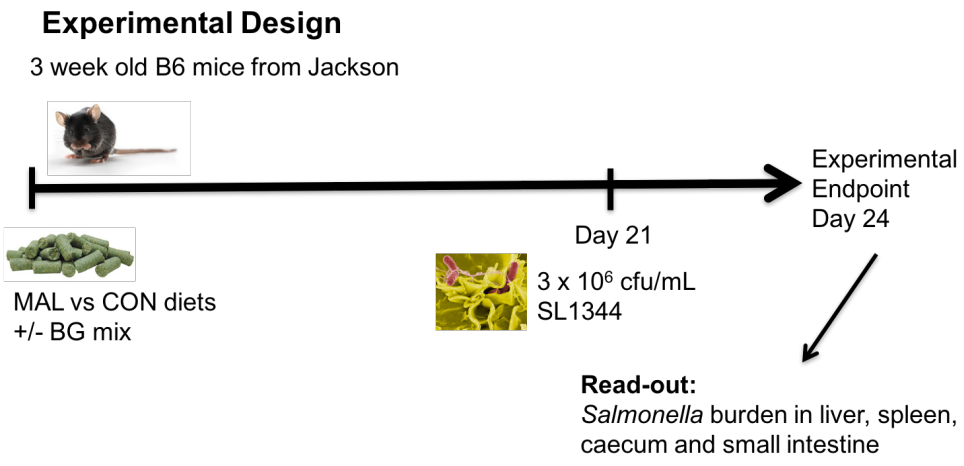

Figure 4.1 Experimental design for S. Typhimurium infection experiment.

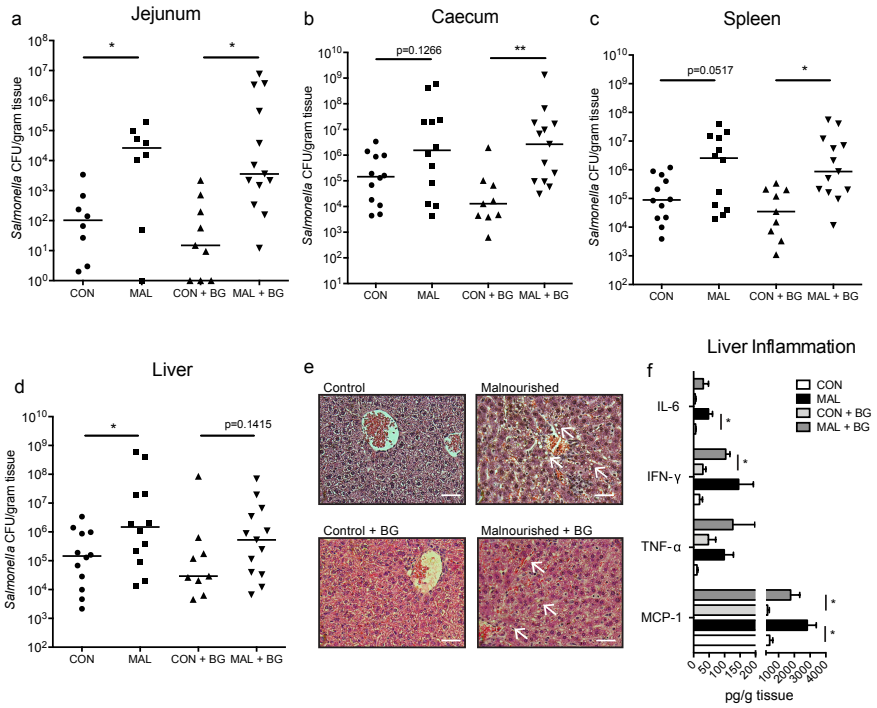

Figure 4.2 Systemic colonization and tissue burden of Salmonella Typhimurium in malnourished and control mice.
Total CFU of *Salmonella* per gram of tissue was assessed 3 days post-infection in the (a) jejunum, (b) caecum, (c) spleen and (d) liver in BG exposed and unexposed malnourished and control mice fed the diet for 3 weeks. Data are pooled from 2 independent experiments (n=8-13 per group), and bars indicate median values (*p<0.05, Mann-Whitney *U*-test). (e) H&E stained slices of the livers of BG exposed and unexposed malnourished and control mice 3 days post *Salmonella* infection. Scale bar represents 100 μm in length, and white arrows point towards pathological features. (f) Concentrations of IL-6, MCP-1, TNF-α, and IFN-γ per gram of liver tissue 3 days post *Salmonella* infection as measured by cytokine bead array. Data is pooled from 2 independent experiments (n=8-13 per group). Bars indicate the mean with S.E. (*p<0.05, Student's *t*-test).

To further investigate how malnutrition can impact the colonization dynamics of intestinal pathogens, we infected mice fed the malnourished and control diet with *Citrobacter rodentium* an attaching and effacing pathogen sharing similarity to EPEC (Crepin et al., 2016). *C. rodentium* is a natural mouse pathogen, and infection leads to gastroenteritis and diarrhea, and it mainly colonizes in the colon. Three-week-old C57BL/6 mice were fed the control and malnourished diet for three weeks before being inoculated with $5x10^8$ cells/mL of *Citrobacter* culture in LB (Fig. 4.3). Mice were sacrificed 3, 7 and 21 days post infection and the feces and colonic tissue were taken to assay for any differences in CFU of *Citrobacter* between the control and malnourished mice. When plates were analyzed, no differences in *Citrobacter* colonization in the feces was observed, with infection peaking at day 7 and beginning to be cleared by day 21 (Fig. 4.4). In the colon, which we referred to as the adherent bacteria, there was no significant change in *Citrobacter* burden at day 3 or day 7, however at day 21 there was ~1 log more bacteria on average in attached to the colon of malnourished mice compared to control mice (Fig. 4.4). This indicates that the mice on the malnourished diet take longer to clear *Citrobacter* from the gut compared to the control fed mice, however it is unclear how biologically significant these findings are since there was no difference in colon histopathology or inflammation. The colonization efficiency of *Citrobacter* was also very variable at the early time points of day 3 and 7, had a non-parametric spread and thus median values were analyzed.

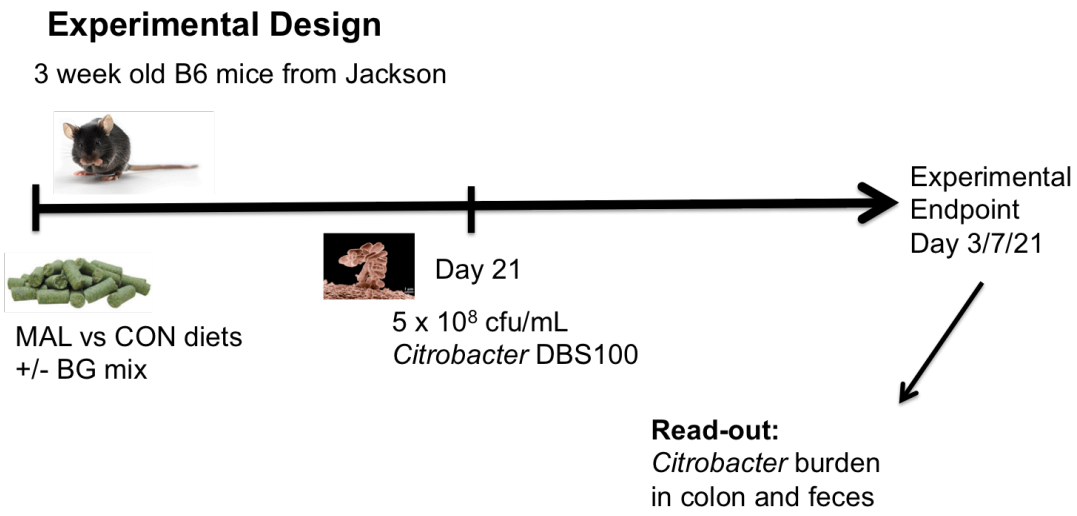

Figure 4.3 Experimental design for Citrobacter infection experiment.

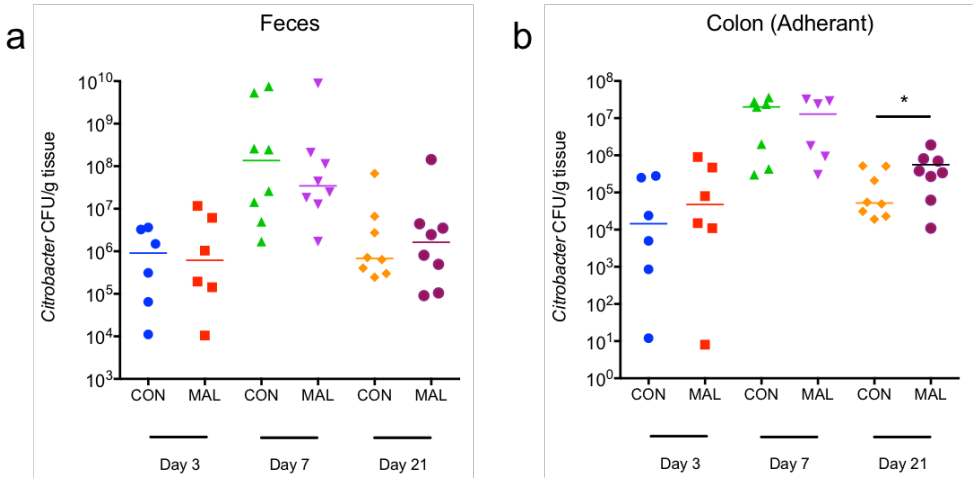

Figure 4.4 Fecal and colonic tissue burden of Citrobacter in the intestine of malnourished and control-fed mice.
Total CFU of *Citrobacter* per gram of feces and tissue was assessed 3 days, 7 days and 21 days post-infection in the (a) feces and (b) colonic tissue. Data are representative of 2 independent experiments and bars indicate median values (*p<0.05, Mann-Whitney *U*-test).

4.4 Effect of a malnourished diet on immune responses and colonization of *H. polygyrus* in mice

Previous experiments in our study has revealed a malnourished diet remodels the small intestinal environment to allow for pathogen expansion to a much greater extent than other regions of the intestine. For example, *Salmonella* colonized to similar levels in the caecum however to levels nearly 100 times greater in CFU in the small intestine (Fig. 4.2). *Citrobacter* normally colonizes the colon and no large changes were seen in pathogen burden with mice on the malnourished diet (Fig. 4.4). To explore further whether the small intestine in malnourished mice is more conducive to the establishment of an infection and colonization, malnourished and control mice were exposed to the intestinal hookworm *Heligmosomoides polygyrus*. *H. polygyrus* colonizes exclusively in the small intestine of mice, resulting in a strong T-helper-2 (Th2) response from the immune system, characterized by T-cell secretion of IL-4, IL-5 and IL-13, along with greater number of T-regulatory cells (Tregs) (Reynolds et al., 2012). To set up the experiment, 3-week-old mice were given either the malnourished or control diet for two weeks before each mouse was infected with 200 L3 larvae from *H. polygyrus* (Fig. 4.5). Feces were collected to analyze the number of eggs being shed at day 14 and 21 post-infection before mice were sacrificed 28 days post-infection (Fig. 4.5).

When the dynamics of the infection were analyzed using egg counts, there was no difference in the number of *H. polygyrus* eggs in the feces of control and malnourished mice at day 14 and 21 post-infection, however by day 28 there was a trend to greater numbers of eggs (Fig. 4.6a). At day 28 post-infection, the number of worms in the small intestine was counted and found to be significantly higher in malnourished mice compared to control mice, with an average

of ~40 remaining in the malnourished mice compared to ~8 in the control mice (Fig. 4.6b). The data suggested a deficiency in clearance of *H. polygyrus* in malnourished mice, and following up on literature describing gut transit time being a significant variable in worm clearance (Masure et al., 2013), we tested this hypothesis using the Carmine Red assay. Malnourished and control mice were gavaged with Carmine Red in 0.5% methylcellulose and feces were collected every 10 minutes to monitor the mice for the presence of red dye. We discovered no significant change in the intestinal transit time in control mice that were infected with *H. polygyrus,* or between uninfected malnourished and control mice (Fig. 4.6c).

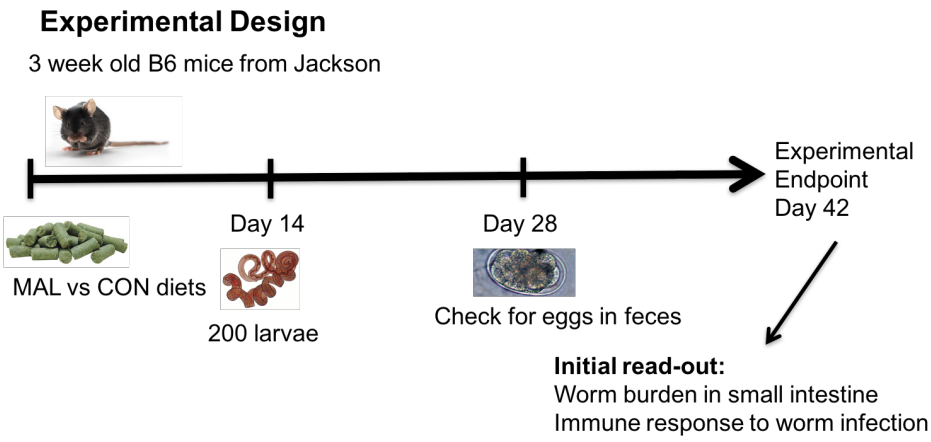

Figure 4.5 Experimental design for H. polygyrus infection experiment.

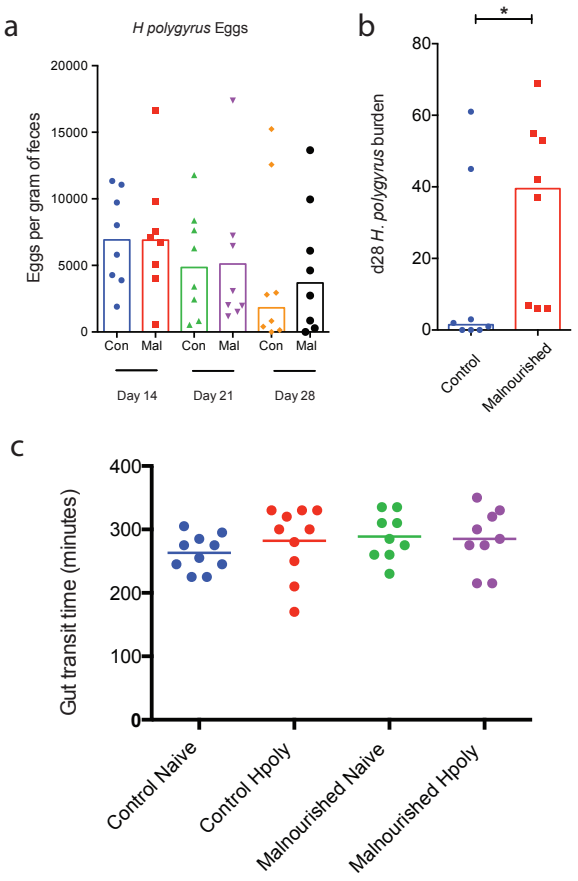

Figure 4.6 Worm colonization dynamics in malnourished and control fed mice.
(**a**) Fecal samples from control and malnourished mice were harvested at and analyzed for number of eggs produced by *H. polygyrus* per gram of feces at day 14, 21 and 28 post-infection. Each dot represents an egg count and bars represent the means. Data is representative of 3 independent experiments. (**b**) The number of *H. polygyrus* worms in the small intestine of each mouse was counted 28 days post-infection. The dots on the plot represent total worm counts found in each mouse and bars represent the mean. Data is representative of 3 independent experiments of 8 mice per group (*$p<0.05$, Mann-Whitney *U*-test). (**c**) A plot of intestinal transit time as assessed using Carmine Red. Each dot represents number of minutes required for gastric emptying in control and malnourished mice both infected and uninfected and bars represent the mean values. Data is representative of 2 independent experiments, 8 mice per group.

To explain the consistently higher burden of worms colonizing the small intestine in malnourished mice, we next analyzed the immunoglobulin response before and after infection, as antibodies linked with type 2 immunity, including IgG1and IgE, are secreted by the immune system to protect mice against worm infection (Reynolds et al., 2012). Surprisingly, there was no difference in the concentration of total or worm-specific IgG1 (Fig. 4.7 a, b) and IgE (Fig. 4.7c,d) between malnourished and control mice infected with *H. polygyrus*. The total circulating IgG in the serum in the worm infected mice was significantly higher in each group compared to the uninfected mice, each having ~250 times the concentration of antibodies, exhibiting the potent ability of *H. polygyrus* to induce adaptive immunoglobulin responses from its murine host (Fig. 4.7b). The IgE response was unchanged after infection however and was lower in concentration compared to IgG1, and no difference between malnourished and control mice was observed (Fig. 4.7d).

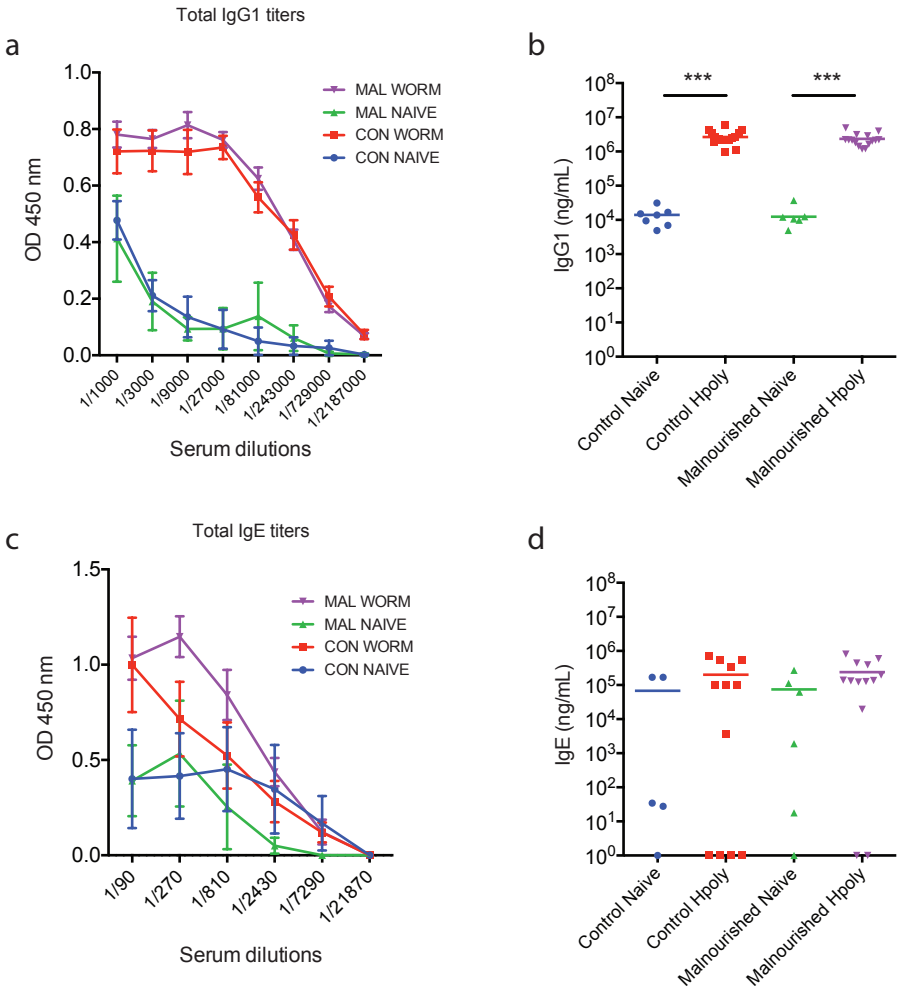

Figure 4.7 Analysis of circulating Immunoglobin levels in control and malnourished mice before and after infection with H. polygyrus.
IgG in serum of worm infected and uninfected mice fed each diet was (**a**) titred and (**b**) concentration was interpolated from a standard curve using an ELISA. Similarly, IgE was analyzed in each mouse and treatment group by (**c**) titre and (**d**) concentration based on a standard curve from an ELISA. All data is representative of 2 independent experiments, 8 mice per group. Bars represent the mean and statistical analysis was performed using a Mann-Whitney *U*-test (***p<0.001).

As intestinal transit time and B-cell antibody response to *H. polygyrus* had no defect in malnourished mice that could not explain the infection phenotype, we next sought to understand whether malnourished mice had an altered T-cell response to *H. polygyrus* compared to control mice. Much of the intestinal immune response to *H. polygyrus* takes place in the mesenteric lymph nodes (MLNs), and this is also where CD4+ T-helper cells secrete cytokine to prime type 2 immunity and regulatory responses that are characteristic of *H. polygyrus* infection (Reynolds et al., 2012). To analyze the Th2 responses in malnourished and control mice, we isolated immune cells from the MLN and stimulated the T-cells with anti-CD3, *H. polygyrus* secretory proteins (HEX) or a mock stimulation, cultured the cells for 48 hours and analyzed their supernatants for presence of T-cell associated cytokines. We first observed the MLNs of *H. polygyrus* infected mice were much larger on average and contained more total cells compared to the uninfected mice (Fig. 4.8f). Cells isolated from uninfected mice had no significant boost in cytokine secretion after being exposed to the HEX or mock stimulation, and cells stimulated with anti-CD3 showed no change in Th2 cytokines IL-4, IL-5, IL-13 and the anti-inflammatory cytokine IL-10 (Fig. 4.8a,b,d,e). However, IL-17A was higher upon stimulation with anti-CD3 compared to the mock controls and there was more IL-17A secreted from malnourished cells from uninfected mice compared to the control mice, though this was not statistically significant (Fig. 4.8c). Once infected, there was no change in IL-17A secretion between the malnourished and control mice, and in each group there was a significant increase in IL-4, IL-5, IL-10 and IL-13 secretion after anti-CD3 treatment of the infected mouse T-cells only (Fig 4.8). T-cells from malnourished mice infected with *H. polygyrus* had a trend to lower secretion of Th2 cytokines IL-5, IL-13 and anti-inflammatory IL-10 in comparison to the control mice stimulated with anti-

CD3 (Fig. 4.8b,d,e). These data signify the possibility of a T-cell mediated defect in the malnourished mice which could result in their delayed clearance of worms. To follow this up further, we isolated cells from the spleen and repeated the same procedure as was done on the MLN cells. The increase in IL-17A secretion persisted in the spleen cells from malnourished, uninfected mice, however there was no change between IL-4, IL-5, IL-10, or IL-13 in the anti-CD3 stimulated infected cells from each group (Fig. 4.9a,b,d-f). We tested for IFN-γ secretion as well, a classical Th1 cytokine and found no difference in naïve or infected mice from each diet (Fig. 4.9c). In total spleen cells, there was an increased amount recovered from the spleen of malnourished infected mice, however this trend was not significant or repeatable through subsequent experiments (Fig. 4.9g). These data could infer a localized effect of the worm infection on the immune system rather than a systemic effect on T-cell responses in each diet group.

These changes in T-cell secretion of cytokines were observed 28 days post-infection, thus to understand if there was an observable change earlier in infection and to confirm the cellular source of each cytokine, cells from the MLN were stained and sorted using flow cytometry at day 14 post infection. Our data confirms the source of the IL-4, IL-5, IL-13 and IL-17A was from CD45+CD3+ cells (Fig. 4.10). In worm infected mice, there was a significant increase in the percentage of cells which secreted IL-4, IL-5, IL-13 and IL-17A, yet no observable change in the percentage staining of the cells from the malnourished and control groups was seen. On average 1% of T-cells secreted IL-4, 0.2% secreted IL-5, 1.5% secreted IL-13 and 0.05% secreted IL-17A in worm infected mice (Fig 4.10a-d).

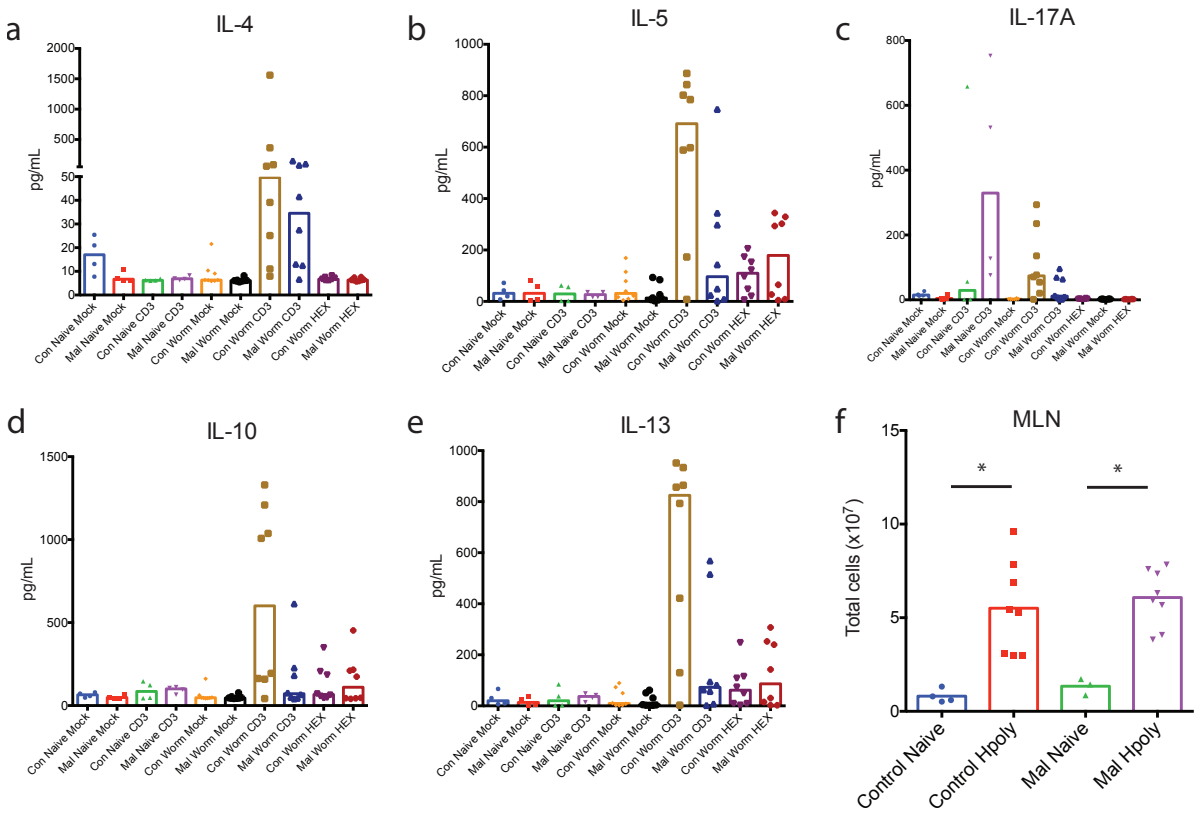

Figure 4.8 Re-stimulation of T-cells from the MLN of malnourished and control mice infected with H. polygyrus.
Supernatants from MLN cells re-stimulated with anti-CD3, *H. polygyrus* secretory proteins (HEX), and a mock stimulation were analyzed for concentrations of (**a**) IL-4, (**b**) IL-5, (**c**) IL-17A, (**d**) IL-10, and (**e**) IL-13. (**f**) Total live cells in the MLN were enumerated and plotted on a log scale. Bars represent the mean and each dot is the value of the concentration of the cytokine for each mouse or the lymphoid cell number. All data is representative of 3 independent experiments, 8 mice per group.

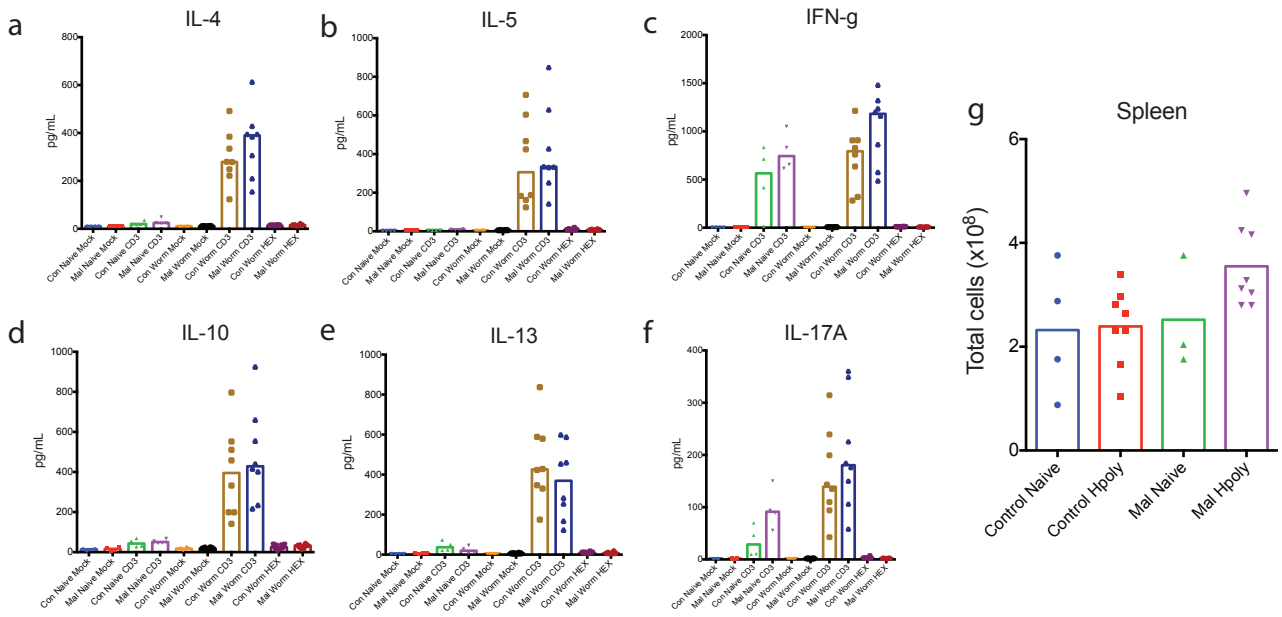

Figure 4.9 Re-stimulation of T-cells from the Spleen of malnourished and control mice infected with H. polygyrus.
Supernatants from spleen cells re-stimulated with anti-CD3, *H. polygyrus* secretory proteins (HEX), and a mock stimulation were analyzed for concentrations of (**a**) IL-4, (**b**) IL-5, (**c**) IFN-γ, (**d**) IL-10, (**e**) IL-13 and (**f**) IL-17A. (**g**) Total live cells in the spleen were enumerated and plotted on a log scale. All data is representative of 3 independent experiments, 8 mice per group.

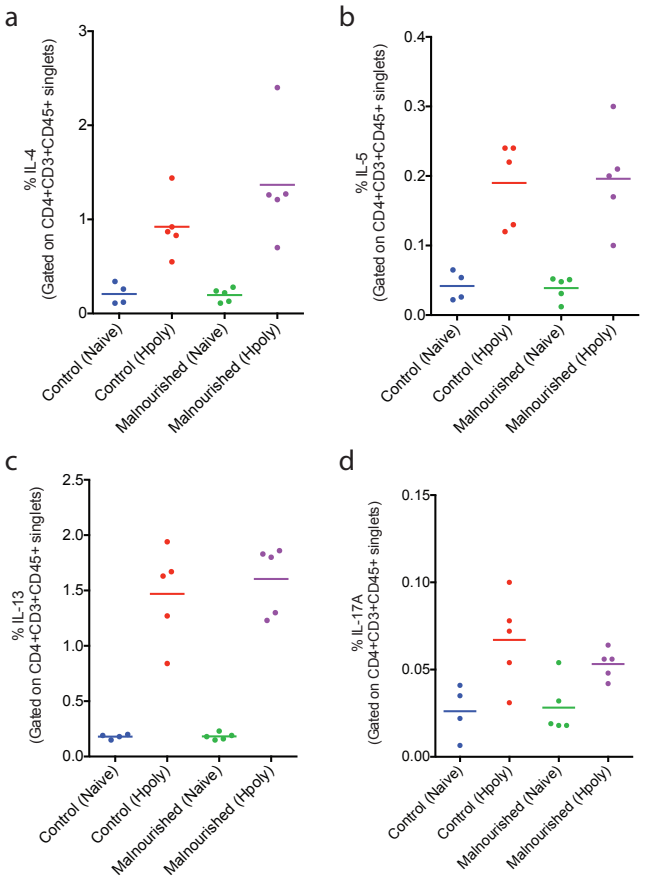

Figure 4.10 Flow cytometry analysis of re-stimulated T-cells from the MLN of malnourished and control mice infected with H. polygyrus.
Live CD45+CD3+ cells from the MLN were analyzed for intracellular expression of (**a**) IL-4, (**b**) IL-5, (**c**) IL-13, and (**d**) IL-17A. Values are expressed as a percentage of total cells secreting each cytokine. Bars represent the mean and each dot is the value of the concentration of the cytokine for cell. Data is representative of 2 independent experiments, 5 mice per group.

Evidence of an altered Th2 immune response to worm infection in malnourished mice, and higher worm burden in malnourished humans from epidemiological data, then led us to investigate the potential effects of a published *H. polygyrus* vaccine in prevention of worm infection in control and malnourished mice, as well as malnourished mice given the *Bacteroides-E. coli* gavage (EE-mice). To set up the experiment, we gave 3 week old mice either control or a malnourished diet and in a subset of the malnourished mice, we gavaged them with the *Bacteroides-E. coli* mix. Mice were subsequently vaccinated intra-perinatally at day 28, 56 and 63 of the experiment with either HES proteins or PBS mock with aluminum hydroxide (alum) (Fig. 4.11). One week after the final vaccination, all mice were infected with 200 L3 *H. polygyrus* larvae and eggs were monitored every week for 4 weeks until the experimental endpoint at day 28 post-infection (Fig. 4.11). Upon analysis, the HES vaccine began to show efficacy at day 14 post-infection in all groups based on the egg counts (Fig. 4.12a) and this observation persisted into day 21 and day 28, where less than 5 eggs were observed in every single mouse given the HES vaccine (Fig. 4.12a-c). When the worms in the small intestine were counted at day 28 post-infection, it confirmed the results seen via analysis of eggs, and every mouse had either a very significantly reduced worm burden or no worms at all in the small intestine (Fig. 4.12d). These data suggest the HES vaccine contains a high level of efficacy in both control, malnourished and EE-mice. Also, the phenotype of greater numbers of *H. polygyrus* at day 28 post-infection in malnourished mice repeated in the mock-vaccinated mice that were malnourished, however the EE-mice had slightly lower worm burdens (Fig. 4.12d).

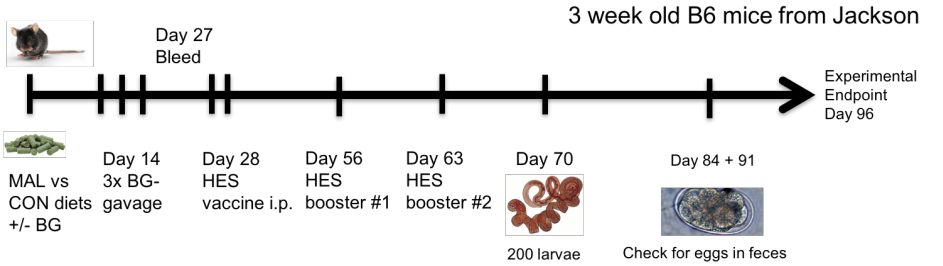

Figure 4.11 Experimental design for H. polygyrus HES vaccine experiment.

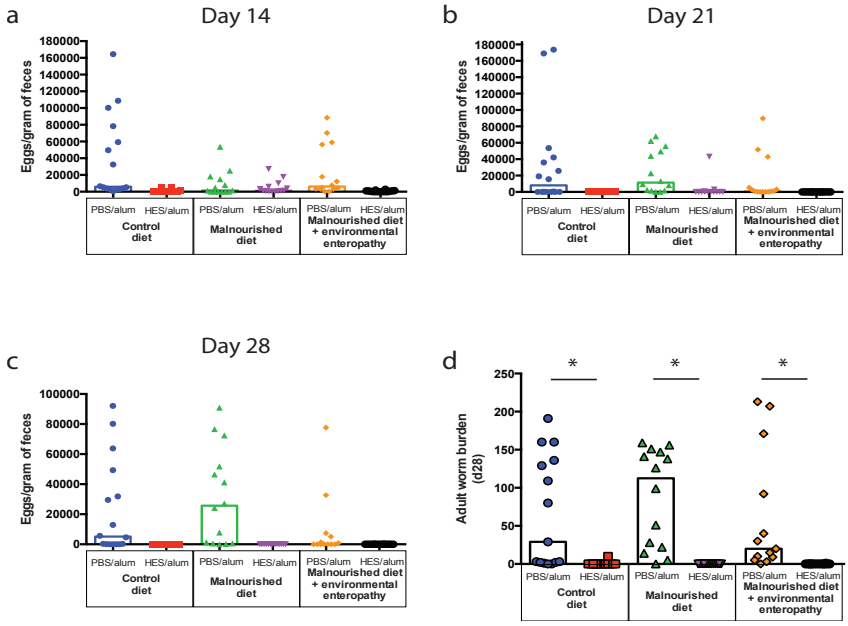

Figure 4.12 H. polygyrus burden after vaccination of control, malnourished and malnourished mice with EE-features with HES proteins.
After vaccination and infection with *H. polygyrus,* feces of mice were analyzed for presence of eggs at (**a**) day14, (**b**) day 21 and (**c**) day 28 post-infection and compared with the PBS-alum controls. Bars represent the median values and graphs are representative of 2 independent experiments, 8 mice per group. (**d**) Number of worms counted in the small intestine 28 days post infection. Bars represent the median values and graph is representative of 2 independent experiments, 8 mice per group. (*p<0.05 Mann-Whitney *U*-test).

4.5 Impact of bacterial sphingolipids on innate immunity in mice

During malnutrition in mice there is a significantly higher representation of sphingolipids in the intestinal tract as described by our metabolomic analysis of mice (Fig. 2.7) and in a human cohort of malnourished children from Madagascar (data not shown). There is also a greater abundance of Bacteroidetes in the small intestine of mice (Fig. 2.4). Members of the Bacteroidetes phyla are unique intestinal inhabitants in the that their membranes contain sphingolipids, which have recently been shown to interact with the mammalian adaptive immune system and counteract gut inflammation (An et al., 2014). In our study, we aim to further parse the role of sphingolipids in innate immunity, and assess the biological relevance of our findings of increased sphingolipids during malnutrition.

We first sought to isolate sphingolipids from 4 different strains of Bacteroidetes; *B. ovatus, B. dorei, B. vulgatus,* and *P. distasonis,* all of which were part of the BG mix of bacteria able to induce EE-features in malnourished mice. Sphingolipids were isolated from Bacteroidetes strains using a modified Bligh-Dyer technique, which resulted in approximately 50-200 mg of crude lipid. Lipids were treated with 0.5M NaOH to enrich for sphingolipids which are resistant to alkaline treatment, where phospholipids and many triglycerides are not. After separation by polarity on a TLC solvent with a 100:20:12:5 ratio of chloroform, methanol, acetic acid and water, respectively, the bands on the TLC were stained with iodine to reveal different lipid species (Fig. 4.13). Four prominent bands representing different lipids were scraped and eluted from the TLC plate, and labelled as fractions #1-4. We hypothesized at least one of these bands would contain a sphingolipid and these sphingolipids could interact with immune cells. To test their bioactivity, we cultured bone-marrow derived macrophages (BMDMs) from wild-type C57BL/6 mice and stimulated them with each lipid fraction from *B. ovatus* in DMSO, as well as

a mock DMSO control and found only fraction #1 was able to induce inflammatory signaling pathways resulting in IL-6 secretion (Fig. 4.13). The concentration that resulted in the greatest induction of IL-6 was 5 µg/mL in fraction #1 and this induced approximately the same amount of IL-6 secretion compared to the total crude lipid extract (Fig. 4.13). These observations held true for *P. distasonis, B. vulgatus* and *B. dorei*.

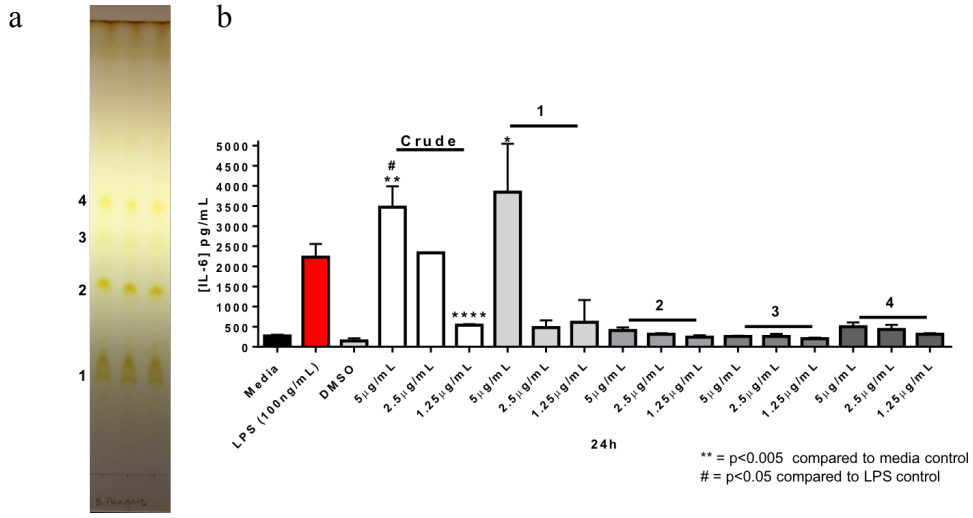

Figure 4.13 IL-6 production after stimulation of BMDMs with isolated lipid fractions from B. ovatus.
(**a**) TLC plate with 4 major lipid bands as visualized by iodine staining (yellow). (**b**) IL-6 secretion by BMDMs stimulated for 24 hrs with media and DMSO controls, LPS (red), crude lipid (white) and lipid fractions (grey) in different concentrations. Data is representative of 3 biological replicates, and two independent experiments. Statistical analysis performed using a one-way ANOVA (**p<0.005).

We next sought to test whether the lipid species in fraction #1 was a sphingolipid. *B. ovatus* cultures were treated with 5 µM of the serine palmitoyl transferase (SPT) inhibitor

myriocin, which has previously been shown to inhibit sphingolipid production in bacteria. Lipids were extracted from each culture, separated using TLC and stained to reveal decreased abundance of the band correlating to fraction #1 in the myriocin treated cultures (Fig. 4.14). When sent for mass spectrometry, this fraction was identified to be similar to the previously identified sphingolipid ceramide phosphoethanolamine (CerPE), with a m/z at [M-H] of ~678.54 (Fig. 4.14). The abundance of this lipid at 679.54 mz was decreased in myriocin-treated cells (Fig. 4.14).

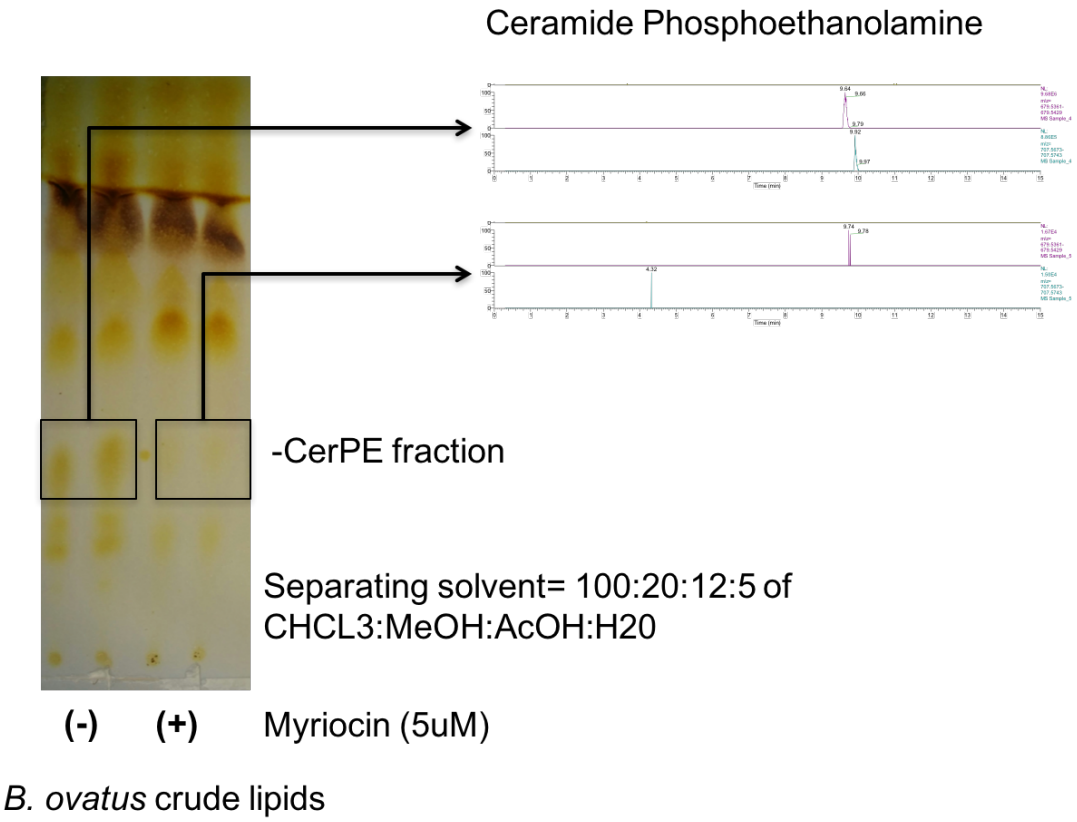

Figure 4.14 TLC separation of B. ovatus lipids and MALDI analysis of the predicted CerPE fraction.
TLC-based separation and identification of bacterial CerPE using iodine to stain lipids (yellow), and myriocin to identify bands decreased in abundance. Arrows indicate the spectra of each band that was excised from the TLC silica. The top spectra represents CerPE band without myriocin treatment and bottom is with myriocin treatment. The top part of the spectral plot (pink) are elutions of lipids on a C18 column at masses of ~679.5 (pink) and ~707.5 (blue).

In order to confirm this lipid was CerPE, we ordered a pure CerPE analogue standard called C12 Sphingosyl Phosphoethanolamine (C12 SPE) which has a C17 backbone analogous to the predicted bacterial lipids and a very similar structure to the predicted CerPE structure. We also created a *B. thetaiotaomicron* strain that was deficient in sphingolipid production by deleting the putative SPT gene as previously described for *B. fragilis* (Wieland Brown et al., 2013). When crude lipids from our *Bacteroides* strains were separated on the TLC, we stained the plate with ninhydrin which reacts with the amine group of the CerPE, producing a bright pink colour (Fig. 4.15a). The C12 SPE lipid ran at the same Rf value as the predicted CerPE in *B. thetaiotaomicron* and this lipid was not detectable in the *B. thetaiotaomicron* $SPT^{-/-}$ or myriocin treated cultures (Fig. 4.15b). Myriocin treated *B. ovatus* showed no detectable CerPE band, similar to *A. colihominus,* a gram-positive bacterium with no membrane sphingolipids (Fig. 4.15a). The CerPE also ran at the same Rf value as previously purified *B. ovatus* CerPE and C12 SPE (Fig. 4.15a). When eluted, this band was sent for mass spectrometry and compared to the band from the $SPT^{-/-}$ strain (Fig. 4.15c). The spectra showed three prominent lipid species relating to CerPE at ~701 m/z, 715 m/z and 723 m/z, and the predicted structure from these mass spectrometry peaks can be deduced (Fig. 4.15c). The peak at 701 had a sodium attached, thus the base structure has a peak ~678, similar to what was predicted for the C17 base CerPE previously in our study (Fig. 4.14) and others (An et al., 2014). We identified similar peaks for *B. dorei* and *B. ovatus* CerPE fractions (Fig. 4.15d,e) as to the ones identified in *B. thetaiotaomicron,* indicating the base CerPE lipid in these strains was similar. No spectra for *P. distasonis* or *B. fragilis* has been collected to date, this is in progress.

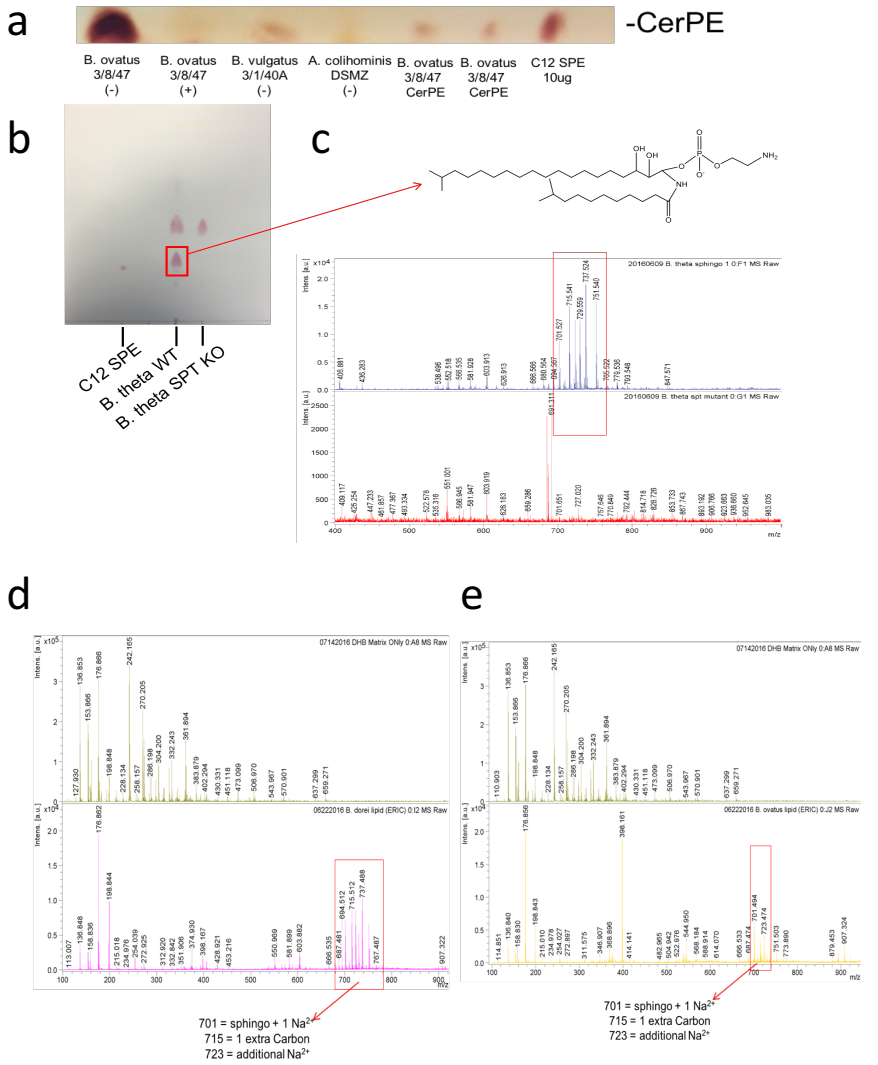

Figure 4.15 Purification and identification of the bacterial sphingolipid CerPE by mass spectrometry.

(**a**) TLC separation of bacterial CerPE bands stained by ninhydrin (pink) +/- myriocin treatment in *B. ovatus* and from *B. vulgatus, A. colihominus,* previously isolated *B. ovatus* CerPE and the sphingolipid standard C12 SPE. (**b**) TLC separation *B. thetaiotaomicron* WT and SPT$^{-/-}$ CerPE and PE bands stained by ninhydrin (pink), along with the C12 SPE standard. No detectable staining in CerPE in the SPT$^{-/-}$. (**c**) The predicated structure of bacterial CerPE based upon peaks present in MALDI results from *B. thetaiotaomicron* WT CerPE fraction and not present in the SPT$^{-/-}$ CerPE fractions. There is a C17 sphingosyl backbone with a phosphoethanolamine head group. MALDI spectra from (**d**) *B. dorei* and (**e**) *B. ovatus* CerPE fractions, yielding peaks identical to those observed in the *B. thetaiotaomicron* WT MALDI analysis. The matrix background spectra is above (green) and the *B. dorei* CerPE peaks (pink) and *B. ovatus* peaks (yellow) are in the panel below.

To identify which immune and metabolic pathways bacterial CerPE was able to activate in macrophages, we stimulated BMDMs transfected with unique lentiviral DNA barcodes used to assay the activity of transcription factors (TFs), with bacterial CerPE +/- LPS for 4 hours, using a previously described TF-seq method (O'Connell et al., 2016). The CerPE fractions were from *B. ovatus, B. dorei, B. vulgatus, P. distasonis,* and C12 SPE, along with α-galactosylceramide (α-GC) analogues, were used as controls as a previously purified sphingolipid from *Sphingomonas*. Once the data were analyzed, we found that treatment with CerPE sphingolipids alone, without LPS, can significantly activate a number of TFs after 4 hours in BMDMs. The most significantly upregulated TF (FDR<0.1) in all bacterial CerPE treatments was NF-kB, which was upregulated between 2-4 fold at the highest dose at the 1/200 dilution (5 μg/mL) and went up in a dose dependent manner (Fig. 4.16a). The type-1 interferon TF ISGF3G (also known as IRF9) was increased almost 4-fold only in the *P. distasonis* CerPE fractions and not in *B. dorei* or *B. ovatus* CerPE treated BMDMs (Fig. 4.16b). IFNB was also only upregulated in *P. distasonis* CerPE (Fig. 4.16c). Each bacterial CerPE induced RORC and downregulated the activity of the TFs TFEB and AP-1 in a dose dependent manner (Fig. 4.16d-f). Aside from the robust activation of NF-kB, the *P. distasonis* CerPE was unique from the other bacterial CerPE lipids, as at its highest concentration, it turned on type-1 interferon systems in the macrophages, while simultaneously downregulating NFE2L2, CEBPB, and CREB1 (Fig. 4.16g,h). C12 SPE also upregulated NF-kB, and RORC in a dose-dependent manner (Fig. 4.16a,d). Some TFs were significantly upregulated (FDR<0.1), however only at the highest concentration. In *P. distasonis* CerPE stimulations, the TFs ELK1, CREB1, STAT1 and IRF1 were all higher at a concentration of 5 μg/mL (Fig. 4.16h). For *B. dorei* CerPE, ATF4 was induced at 5 μg/mL, while NFE2L2 and IRF3 were decreased (Fig. 4.17a). *B. ovatus* CerPE treatment at 5 μg/mL induced RARA and

decreased PPARg (Fig. 4.17b) and C12 SPE also increased RARA while decreasing IRF3 and NFE2L2 (Fig. 4.17c). Of note, α-GC also induced NF-kB only at the highest dose, and decreased IRF3, however it consistently increased NFE2L2 (Fig. 4.17d).

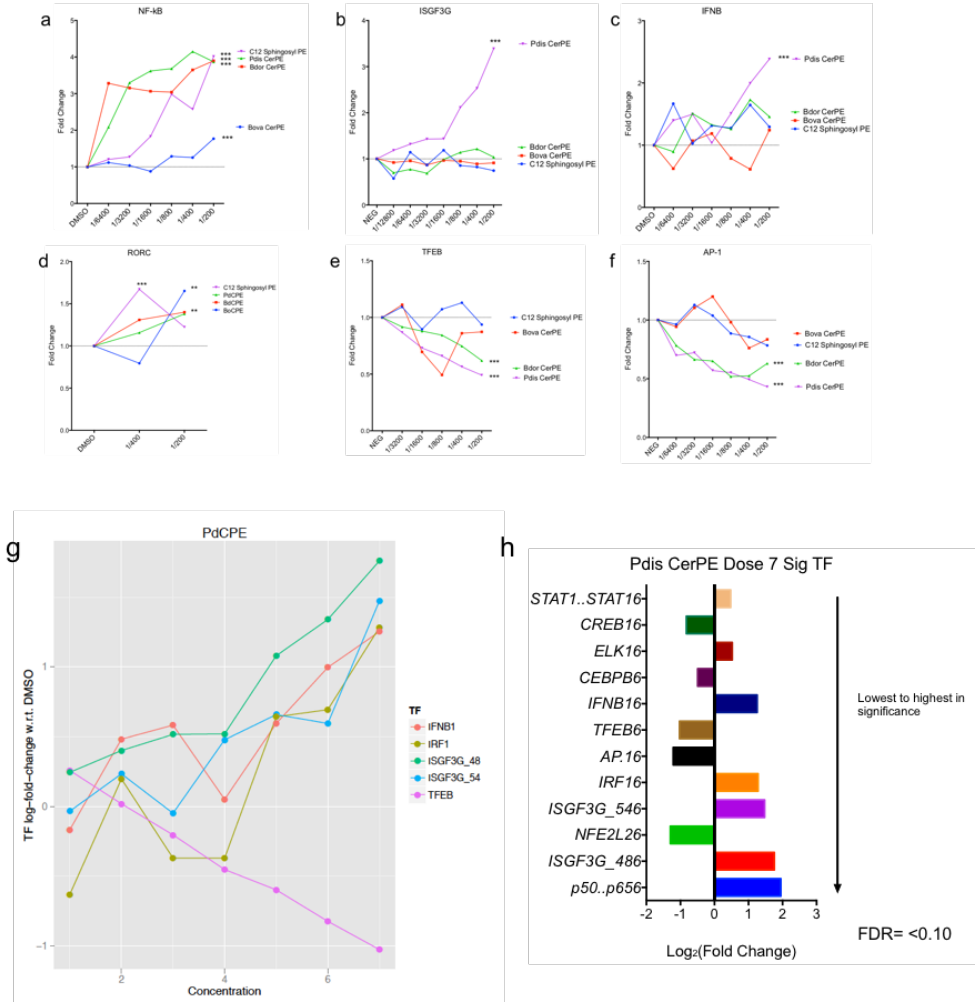

Figure 4.16 Dose-dependent induction of TFs from bacterial CerPE sphingolipids. The fold induction of (**a**) NF-kB, (**b**) ISGF3G, (**c**) IFNB, (**d**) RORC, (**e**) TFEB and (**f**) AP-1 after stimulation of *B. ovatus, B. dorei,* and *P. distasonis* CerPE, as well as a C12 SPE standard. Doses increase two-fold along the x-axis, representing dilution from a 1 mg/mL stock solution of CerPE in DMSO. Dilutions peak at 5 µg/mL (1/200) and decrease from there (**FDR<0.05; ***FDR<0.01). (g) A plot of the fold-change of the TFs IFNB (orange), IRF1 (yellow), ISGF3G_48 (green), ISGF3G_54 (blue), and TFEB (pink). Concentrations increase on the x-axis from left to right, from 0 (DMSO control) to 7 (5 µg/mL). (**f**) A plot of the fold change, up or down, of each TF in *P. distasonis* treated BMDMs less than 10% FDR, listed in order of significance based on FDR. Fold changes are expressed in Log_2.

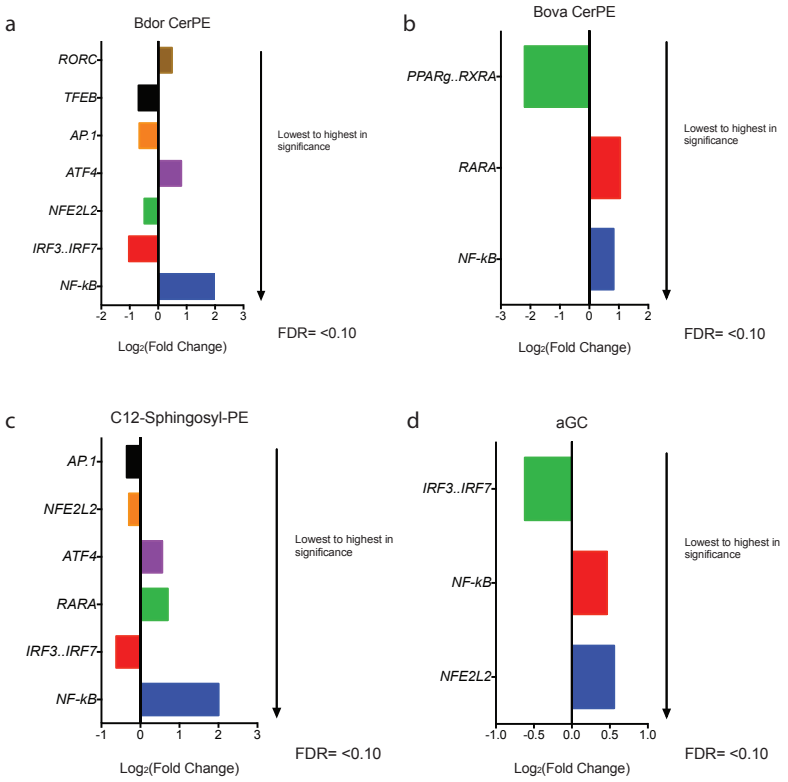

Figure 4.17 Most significant TFs changed in each CerPE sphingolipid treatment.
A plot of the fold change, up or down, of each TF in (**a**) *B. dorei,* (**b**) *B. ovatus,* (**c**) C12 SPE and (**d**) α-GC treated BMDMs less than 10% FDR, listed in order of significance based on FDR. Fold changes are expressed in Log_2.

RNA was also extracted from the TF-seq screen of CerPE sphingolipid stimulation of BMDMs, and sent for RNA-seq. Of the genes analyzed, ~200 were significantly upregulated in each bacterial CerPE treatment of BMDMs (FDR <0.05). Collating all the data together, we identified 19 genes that were significantly upregulated (FDR <0.01) and had a fold change greater than 10-fold in every bacterial CerPE treatment after 4 hours of stimulation at 5 μg/mL (Fig. 4.18a, Table 4.1). To understand which pathways are impacted based on our RNA-seq results, we submitted our list for analysis on DAVID and discovered 13 KEGG pathways enriched in the bacterial CerPE stimulated BMDMs (Fig. 4.18b). These pathways included TNF signaling, Toll-like receptor signaling and NF-kB signaling pathways (Fig. 4.18b). Also, GPCR ligand binding was enriched, MAPK signaling and NOD-receptor signaling pathways indicating these sphingolipids could be activating multiple pathways simultaneously (Fig. 4.18b). When assessing the function of the genes most significantly and consistently upregulated in each bacterial CerPE treatment, we observed that most genes were involved in the immune response, specifically chemotaxis and chemo-attractants for immune cells (*CCL2, CCL4, CCL5, CXCL10*), anti-viral interferon responses (*RSAD2, GBP2, IFIT1*), pro-inflammatory cytokines (*IL1A, IL1B*), factors involved in fibrosis (*MMP13, SERPINE1*) and itaconic acid production induced antimicrobial responses (*IRG1*) (Table 4.1). Of note, the RNA-seq data supports the two main observations of the TF-seq data, which was bacterial CerPE turning on NF-kB, since it also came up in RNA-seq, and induction of type-1 interferon anti-viral responses (Table 4.1).

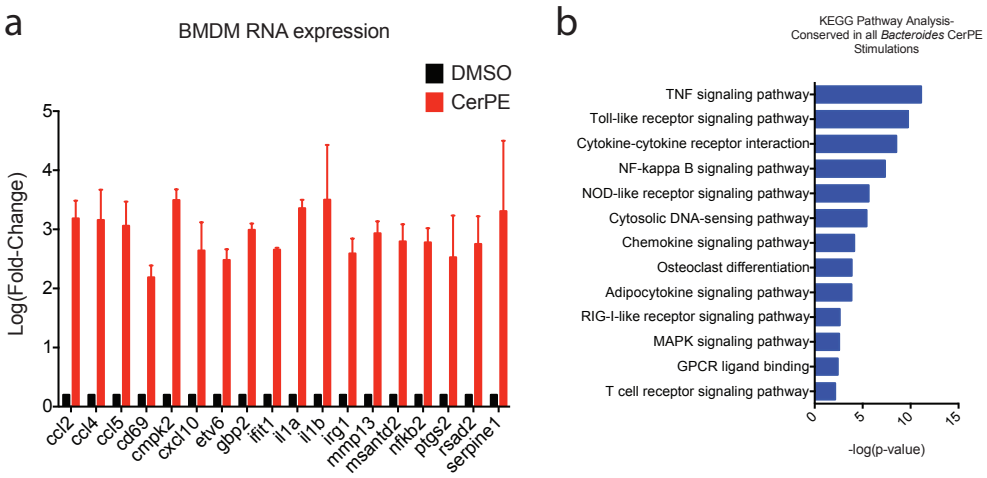

Figure 4.18 Genes and pathways significantly upregulated in BMDMs consistently in all bacterial CerPE treatments.
(**a**) The genes which were consistently and significantly upregulated by *B. ovatus, B. vulgatus, B. dorei* and *P. distasonis* CerPE treatment of BMDMs for 4 hours. Fold change is expressed in Log and statistical significance was determined by using a FDR cutoff of 0.01. (**b**) The KEGG pathways which were consistently and significantly upregulated by *B. ovatus, B. vulgatus, B. dorei* and *P. distasonis* CerPE treatment of BMDMs for 4 hours. P-values are expressed in –log and reflective of the enrichment of the pathway over DMSO control for each pathway. Statistical analysis performed using DAVID software. All data is representative of 4 technical replicates and 3 biological replicates.

Table 4.1 Alphabetical list of genes upregulated in BMDMs stimulated with bacterial CerPE as seen by RNA-seq, FDR <0.01. Each of these genes was significantly upregulated in all CerPE treatments from *B. ovatus, B. vulgatus, B. dorei* and *P. distasonis.*

Gene	LogFC	LogCPM	p-value	FDR	Function
CCL2	3.28	6.74	1.71E-22	4.10E-20	Chemotactic factor that attracts monocytes and basophils.
CCL4	3.74	8.82	5.64E-163	9.79E-160	Monokine with inflammatory and chemokinetic properties, binds to CCR5.
CCL5	3.32	6.92	2.02E-26	5.98E-24	Chemoattractant for blood monocytes, memory T-helper cells and eosinophils.
CD69	2.42	6.14	2.71E-05	0.001677097	Involved in lymphocyte proliferation and functions as a signal transmitting receptor in lymphocytes
CMPK2	3.29	6.59	2.09E-19	4.21E-17	dUTP and dCTP synthesis in mitochondria.
CXCL10	2.10	8.47	1.51E-33	6.18E-31	Chemotactic for monocytes and T-lymphocytes, binds to CXCR3.
ETV6	2.69	6.13	3.85E-08	2.38E-06	TF that plays a role in hematopoiesis and malignant transformation
GBP2	2.90	6.26	1.25E-10	1.16E-08	Makes GDP, exhibits antiviral activity and promotes oxidative killing and deliver antimicrobial peptide production
GPR160	4.01	5.71	4.96E-08	6.81E-06	Orphan G-protein coupled receptor, rhodopsin-like
IFIT1	2.68	8.13	8.61E-49	5.69E-46	Interferon-induced antiviral RNA-binding protein that specifically binds single-stranded RNA bearing a 5'-triphosphate group from ssRNA viruses.
IL1A	3.44	6.07	1.22E-10	1.15E-08	Produced by activated macrophages, IL-1 stimulates thymocyte proliferation by inducing IL-2 release, B-cell maturation and proliferation, and fibroblast growth factor activity.
IL1B	4.57	8.68	5.76E-212	1.33E-208	Potent pro-inflammatory cytokine, induces prostaglandin synthesis, neutrophil influx and activation, T-cell activation and cytokine production, B-cell activation and antibody production.
IRG1	2.78	7.05	5.36E-22	1.24E-19	Involved in antimicrobial response of innate immune cells, specifically itaconic acid production which contributes to the antimicrobial activity of macrophages.
MMP13	2.97	6.61	3.92E-16	6.41E-14	Collagenase, plays a role in the degradation of extracellular matrix proteins including fibrillar collagen, fibronectin.

Gene	LogFC	LogCPM	p-value	FDR	Function
MSANTD2	3.13	5.83	4.07E-06	0.000153884	Unknown function.
NFKB2	2.95	6.02	3.36E-08	2.10E-06	A pleiotropic transcription factor present in almost all cell types and is the endpoint of a series of signal transduction events that are initiated by a vast array of stimuli related to many biological processes such as inflammation, immunity, differentiation, cell growth, tumorigenesis and apoptosis.
PTGS2	2.24	7.50	1.87E-17	1.99E-14	Responsible for production of inflammatory prostaglandins.
RSAD2	2.21	8.98	9.12E-59	7.91E-56	Interferon-inducible iron-sulfur cluster-binding antiviral protein which plays a major role in the cell antiviral state and can inhibit a wide range of DNA and RNA viruses
SERPINE1	3.30	5.94	1.15E-06	0.000152166	Serine protease inhibitor, major control point in the regulation of fibrinolysis.

To further validate the RNA-seq data, we performed a proteomic analysis using SILAC, in order to understand which genes could be detected at the protein level from our RNA-seq analysis. BMDCs were treated with either DMSO mock control, 50 ng/mL LPS, or 5 μg/mL of *P. distasonis* CerPE for 8 hours. Cells were pelleted, lysed, trypsinized and resulting peptides were labelled with either a light formaldehyde (DMSO), medium formaldehyde (LPS) or heavy formaldehyde (CerPE), and subsequently run on a QTOF mass spectrometer (Fig. 4.19a). We isolated and labelled peptides from 2 different biological replicates of BMDCs and found an approximately 81% overlap in proteins identified between the groups (Fig. 4.19b). Data was analyzed by analyzing the ratio of medium/light labelled peptides (LPS/DMSO) or heavy/light labelled peptides (CerPE/DMSO). When heavy/light labelled peptides were analyzed (CerPE induced proteins), there were 24 peptides which had a z-score >2 (2 standard deviations above the mean) and were also present in the analysis all technical and biological replicates (Table 4.2). On average, there was a positive correlation between which proteins were upregulated by LPS

and also by CerPE, indicating they could be activating similar pathways (Fig. 4.19c). When examining the list of the most upregulated proteins, we discovered that 4 of the 25 proteins were also significantly upregulated in the RNA-seq analysis; RSAD2, GBP2, SERPINE and IRG1 (Table 4.2). Other proteins that were significantly upregulated include many calcium response elements, including the calcium response regulator and inflammasome activator P2X purinoceptor 4 (P2RX4), calmodulin (CALM2), myosin light polypeptide 6 (MYL6) and the calmodulin binding and signalling protein striatin-4 (STRN4).

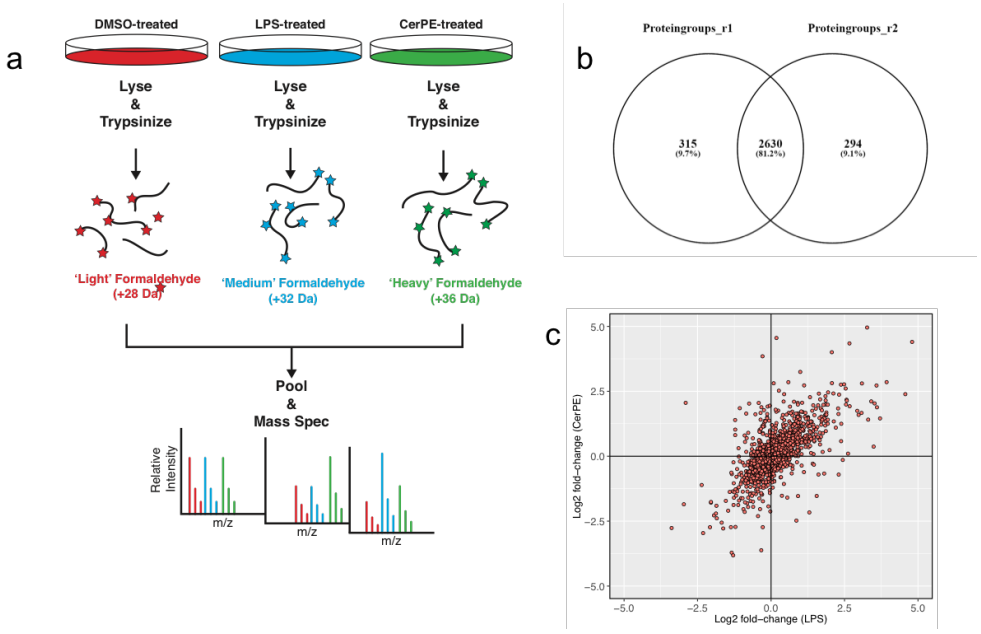

Figure 4.19 Proteomic analysis of BMDCs treated with LPS and P. distasonis CerPE
(**a**) Flow chart of the SILAC process, and how peptides were isolated, labelled and identified from BMDCs. (**b**) Venn-diagram of each biological replicate from the BMDC treatments, each circle indicating which proteins were identified in each and the central number indicating how many were identified in both analysis (2630 or 81.2%). (**c**) A dot plot with fold-change of CerPE (y-axis) and fold-change of LPS (x-axis) induced proteins plotted to show a positive correlation between the two stimulations (r>0).

Table 4.2 Most significantly upregulated proteins (z-score >2) in BMDCs treated with *P. distasonis* CerPE for 8 hours. Proteins in bold were identified in RNA-seq analysis as well.

CerPE only	FC	Protein	Symbol	Pathway
yes	80.98	Cathepsin S	CTSS	antigen processing and presentation of exogenous peptide antigen
	77.41	**Radical S-adenosyl methionine domain-containing protein 2**	**RSAD2**	**cellular response to type I interferon**
	52.26	Protein S100-A6	S100A6	regulation of cell cycle progression and proliferation
yes	42.04	Glycogenin-1	GYG1	glycogen biosynthesis
yes	32.30	Histone H2B	HIST1H2BL	chromatin modelling protein
	31.03	Alpha-endosulfine	ENSA	KATP-channel function and insulin
yes	23.47	Myotrophin	MTPN	positive regulator of NF-kB binding
	21.12	Glucose-6-phosphate isomerase	GPI	too many functions to name
yes	20.31	Superoxide dismutase [Cu-Zn]	SOD1	redox response regulator
yes	16.04	P2X purinoceptor 4	P2RX4	calcium response regulator and inflammasome activator
yes	14.39	Calmodulin	CALM2	calcium binding protein, regulates inflammation
yes	9.48	Ubiquilin-2	UBQLN2	proteosome and ubiquitination
	7.22	**Interferon-induced guanylate-binding protein 2**	**GBP2**	**anti-viral activity**
yes	7.21	Sulfhydryl oxidase 1	QSOX1	redox and growth regulation
	7.03	Complement C3	C3	complement system and innate immunity
yes	7.00	Myosin light polypeptide 6	MYL6	calcium binding and motor activity
	6.97	**Plasminogen activator inhibitor 2**	**SERPINB2**	**thrombosis and coagulation factor; adaptive immunity**
	6.80	Acyl-coenzyme A thioesterase 1	ACOT1	hydrolysis of CoenzymeA
	6.76	Stathmin	STMN2	microtubule structure and function
yes	6.62	Protein canopy homolog 2	CNPY2	not well characterized
	6.60	**Cis-aconitate decarboxylase**	**IRG1**	**regulation of TLR-signaling- itacanoate production**
	6.09	Cullin-2	CUL2	E3 ubiquitin ligase; IBD SNP
yes	5.74	Hematopoietic system regulatory peptide	TMSB4X	actin cytoskeleton organization
	5.49	Striatin-4	STRN4	calcium signalling; binds calmodulin

TF-seq, RNA-seq and the proteomics data all suggested bacterial CerPE was targeting inflammatory responses in macrophages, specifically NF-kB, to activate cytokine and other immune responses. However, which receptor the sphingolipid was binding too was still unknown. We hypothesized that it could be signaling through the TLR-MyD88 receptor pathway similar to LPS. To test this, we isolated BMDMs and BMDCs from wild-type (WT), TLR2$^{-/-}$, TLR4$^{-/-}$, and MyD88$^{-/-}$ mice and stimulated them with different bacterial CerPE (5 µg/mL), C12 SPE (10 µg/mL), LPS (50 ng/mL) and the DMSO or ethanol mock control. After 24 hours of stimulation, supernatants were removed and assayed for IL-6 as the main pro-inflammatory cytokine. Subsequently, we also assayed for the presence of IL-10, MCP-1 and TNF-α in the supernatants. In WT BMDMs stimulated with CerPE from *B. ovatus, P. distasonis,* and *B. dorei* there was a significant induction of IL-6 secretion compared to mock-treated BMDMs as seen previously (Fig. 4.20a). However, when the MyD88$^{-/-}$ BMDMs were stimulated with bacterial CerPE, each showed a significant reduction in IL-6 secretion and it was not significantly more than what was observed in the mock-treated WT BMDMs. This ablation of IL-6 secretion in the MyD88-/- BMDMs was also observed in the TLR2$^{-/-}$ BMDMs from *B. ovatus, P. distasonis,* and *B. dorei* CerPE stimulated cells, but not in TLR4$^{-/-}$ BMDMs stimulated with CerPE (Fig. 4.20a). C12 SPE stimulated WT BMDMs to produce IL-6 also, and this signaling was also downregulated in MyD88$^{-/-}$ BMDMs (Fig. 4.20a). However, C12 SPE still could signal BMDMs to produce IL-6 in the TLR2$^{-/-}$ cells and this time TLR4$^{-/-}$ cells showed the ablation of IL-6 signaling (Fig. 4.20a). The CerPE sphingolipids could also induce stimulation of TNF-α and MCP-1 in both WT BMDMs (Fig. 4.20b-d) and WT BMDCs (Fig. 4.20e-g). IL-10 was induced in the BMDMs but not in BMDCs by bacterial CerPE (Fig. 4.20d, g). For signaling of NF-kB-

associated cytokines TNF-α and MCP-1, the bacterial CerPE and C12 SPE signaling for these cytokines was also ablated in the MyD88-/- BMDMs (Fig. 4.20b,c) and BMDCs (Fig. 4.19e,f).

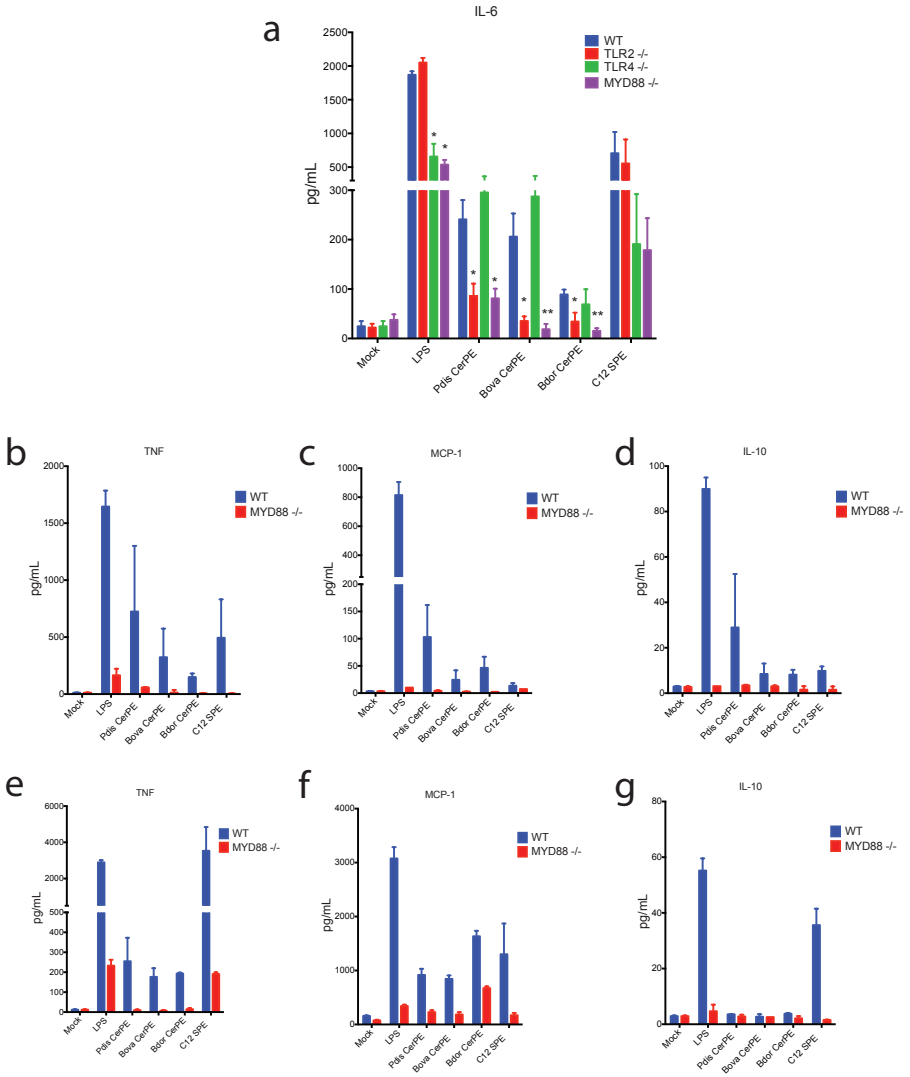

Figure 4.20 Cytokine secretion of wild-type, TLR2-/-, TLR4-/- and MyD88-/- BMDMs and BMDCs after stimulation with CerPE sphingolipids.
(**a**) IL-6 secretion by WT and KO BMDMs stimulated for 24 hrs with *B. ovatus, P. distasonis* and *B. dorei* CerPE with C12 SPE standard, ethanol negative control (mock) and LPS positive control. Wild-type and MyD88$^{-/-}$ BMDM secretion of (**b**) TNF-α, (**c**) MCP-1 and (**d**) IL-10 after stimulation with *B. ovatus, P. distasonis* and *B. dorei* CerPE with C12 SPE standard, ethanol negative control (mock) and LPS positive control. Wild-type and MyD88$^{-/-}$ BMDC secretion of (**e**) TNF-α, (**f**) MCP-1 and (**g**) IL-10 after stimulation with *B. ovatus, P. distasonis* and *B. dorei* CerPE with C12 SPE standard, ethanol negative control (mock) and LPS positive control. Data is representative of 3 biological replicates, and two independent experiments. Statistical analysis performed using a one-way ANOVA (*p<0.05; **p<0.005).

4.6 Discussion

In this study, we aimed to investigate the role of the malnutrition-induced intestinal changes observed in Chapter 2 and 3 on different infection models of mice; *Salmonella, Citrobacter* and *H. polygrus* colonization of the GI tract. Further, we followed up on the metabolomics and microbiome data collected in the previous chapters to understand a potential mechanism for the induction of inflammation by the Bacteroidetes strains in the BG mix and the increase in IEL recruitment to the epithelium of malnourished mice.

The burden of enteric infections is significantly higher in regions where early-life protein malnutrition is common, and we sought to test directly whether moderate protein and fat deficiency early in life could mimic these clinical and epidemiological observations in humans. The metabolomic analysis of the small intestine from Chapter 2 revealed for the first time that malnutrition leads to drastic shifts in small intestinal bile acid pool, which we hypothesized could be the mechanism that permits for the increased colonization of commensal *Bacteroidales* and *E. coli* strains in the small intestine. In line with previous research from our lab and others (Semba et al., 2016), it may also be behind the ability of *S.* Typhimurium to proliferate in the malnourished small intestine to higher abundance, as this area of the intestine was the most significantly changed in the malnourished mice compared to the caecum, liver or spleen. The infection with *S.* Typhimurium highlighted the observations from the BG exposure, that malnutrition induces an increased proliferative capacity and colonization potential of Gram-negative bacteria in the small intestine. The moderately increased ability for *S.* Typhimurium to invade systemically also gives biological relevance to the increase in intestinal permeability observed pre-infection in malnourished mice. In the liver, *Salmonella* was able to proliferate to

higher abundance and the gross histopathological changes suggest malnourished mice responded differently to *Salmonella* as clear fatty droplets were only observed in malnourished mice. These observations from *Salmonella* infection supports other studies showing greater burden of enteric infections being correlated to nutritional defects in humans and fatty liver changes affecting bile acid secretion during severe malnutrition (Semba et al., 2016).

To date, no studies had assessed *C. rodentium* infection dynamics during early-life protein malnutrition in mice. We had evidence from previous work in our lab and others that a thinner mucus layer, decreased fecal microbiota diversity, altered microbiota composition and decrease in secondary bile acids all result in higher burdens of *C. rodentium* (Wlodarska et al., 2011; Collins et al., 2014). Each of these phenotypes were observed in the malnourished mice, to different degrees of severity. Yet, the colonization of *C. rodentium* in the colon of malnourished mice at day 3 and 7 post-infection was largely unaffected by these features of malnutrition, namely the bile acid, microbiome or mucus layer changes. By day 21 post-infection, there was a ~1 log increase in adherence to the colon in malnourished mice but no change in the feces (luminal content), hinting that *C. rodentium* may persist for longer in malnourished mice and have a greater ability to penetrate to the mucus layer. The biological relevance of this is unclear, since *C. rodentium* did not induce any changes to histopathology or inflammation in the colon of malnourished mice (data not shown). With respect to the stochasticity of *C. rodentium* infection and high standard deviations of colonization in our infection model, it is hard to conclude malnourished mice are more susceptible to *C. rodentium* and more studies are needed to make any concrete conclusions. Future studies should assess the impact of malnutrition on *Citrobacter* colonization in different strains of mice more susceptible to the infection than C57BL/6 mice,

such as C3H/HeJ mice, or take the infection out to a longer time-point in the C57BL/6 mice such as 28 days.

Rampant diarrhea and chronic enteric infections in countries with poor nutrition and sanitation are not limited to bacterial infections, as the prevalence of intestinal worm burden is also higher in these regions (Schmidt, 2014; Brooker et al., 2004). The relationship between malnutrition, immunity, microbiome and worm infection had not been extensively studied, and little is known on which factors of a malnourished diet could potentially alter susceptibility to worm colonization. The *H. polygyrus* infection model we used to study this is widely used in the field as it is a natural worm parasite, and classically can induce a potent Th2 and Treg response in the intestine; both required for clearance of the worm (Reynolds et al., 2012). In contrast to *C. rodentium* and *S.* Typhimurium infection, *H. polygyrus* colonizes exclusively in the small intestine, which we also observed in our mice. Worm burden was assayed at day 28, since this is when the combination of an IgG response and Th2-immunity begins to clear the worm infection, and the greater worm burden seen at this time-point suggests malnutrition-induced immune or metabolic changes needed to clear *H. polygyrus* could be impaired. Tracking the egg production of worms in malnourished and control mice, a surrogate marker for worm burden, showed no change until past 21 which suggests that any impaired response to worm viability happens later in infection and initially upon gavage of the larvae.

Our first hypothesis was that, given the delayed phenotype in counting eggs, it was a defect in adaptive immunity that resulted in greater *H. polygyrus* colonization. These antibodies are crucial for *H. polygyrus* clearance (Harris et al., 2014) and some studies have found

decreased antibody production during protein malnutrition (Maier et al., 2013). However, no change in the Th2-induced antibodies IgG1 and IgE during malnutrition nullified this. We also looked at Th2 immunity in the mesenteric lymph node (MLN) since local, mucosal immune responses in the GI tract also play a key role in clearing *H. polygyrus* (Pelly et al., 2016). Re-stimulation of T-cells from the MLN but not the spleen, with anti-CD3 showed a decreased secretion of Th2 cytokines IL-4, IL-5 and IL-13 from malnourished, worm infected mice and we concluded that the phenotype is a local immune effect since the spleen T-cell response was normal. MLNs harbor distinct T-cell populations compared to the spleen, which react more to small intestinal microbial signals sampled by APCs and acts as a firewall to invading pathogens (Buettner and Bode, 2012). It is still unclear how less type-2 cytokine production after re-stimulation of T-cells in the MLN could mechanistically alter *H. polygyrus* clearance in this model. GI motility is induced by IL-4 and increases in motility have been linked to worm clearance (Maizels and Holland, 1998), but we demonstrated no difference in any group in GI motility. Pre-infection levels of IL-17 secreted by the MLN was higher in the malnourished mice compared to control fed mice which could impact the percentage of T-cells able to differentiate into IL-4, IL-5 or IL-13 producing CD4+ helper cells, however again when cells were tested for percentage of type-2 cytokine secretion in the MLN of malnourished and control mice there were no differences.

The existence of a *H. polygyrus* vaccine that is effective for mice (Hewitson et al., 2015) led us to test whether this defect in Th2 immunity in the MLN of malnourished mice was relevant for developing protective responses worm infection after vaccination. After administration of the HES protective proteins to control, malnourished and EE-mice, the vaccine

was effective in inducing sterile immunity in mice from every treatment group. In this scenario, the injectable nature of the vaccine, bypassing the mucosal immune system, may have rendered it more effective during malnutrition. There is more evidence that oral vaccines needing a boost from the mucosal immune are less efficacious in regions of the world where malnutrition and EE is common (Serazin et al., 2010). Future studies should give these mice an orally administered vaccine to further pry into the mechanisms of protections against parasites and worms during malnutrition.

We finally aimed to follow a lead from the metabolomics, immune and microbiome data we collected previously, and investigate the impact of bacterial sphingolipids on host immunity. This study was set up to, for the first time, test the impact of bacterial sphingolipids on TF and RNA expression in macrophages and DCs to understand the impact of these sphingolipids on the host. The first screen of lipids from the TLC separation yielded a lipid, that closely resembled ceramide phosphoethanolamine (CerPE), which activated BMDMs to produce IL-6. Inhibition of sphingolipid biosynthesis using myriocin and knocking-down the committed enzyme in sphingolipid biosynthesis (SPT), coupled with mass spectrometry, confirmed this in *B. ovatus, B. dorei, B. vulgatus* and *B. thetaiotaomicron.* Yet, we are unable get a consistent reading from the MALDI technique to determine the structure of *P. distasonis* CerPE, and there is a chance it is a different structure from the other *Bacteroides.* The predicted structure of bacterial CerPE has been communicated (Wieland Brown et al., 2013), however it's function was unknown and we postulated a combination of TF-seq and RNA-seq on macrophages would be the appropriate screen to identify pathways it activated. In the screen, we included the only characterized sphingolipid from intestinal Bacteroidetes is α-galactosylceramide (α-GC), which was found to

bind to CD1d on DCs and interact with NKT-cells (An et al., 2014). LPS was used as a positive control, and also in combination with the CerPE sphingolipids. When analyzing the data from the TF-seq, we were surprised to see so many changes upon sphingolipid treatment alone since we had hypothesized these lipids would only change pathways upon LPS stimulation based on previous research (Köberlin et al., 2015). We discovered that bacterial CerPE from *B. ovatus, B. dorei* and *B. vulgatus* all turned on similar pathways, including the TF NF-kB, and this was also demonstrated by the purified eukaryotic CerPE analogue, C12 SPE. *P. distasonis* CerPE was unique in the TF-seq data as it was the only sphingolipid to activate type-1 interferon TFs ISGF3G (also known as IRF9). In the RNA-seq data, this was not as clear as all the other CerPE isolates from *Bacteroides* also turned on genes on the transcript level related to type-1 interferon signaling, such as *RSAD2, GBP2, IFIT1* and *IRG1*. Proteomics data also confirmed type-1 interferon signaling was induced by CerPE treatment and 3 of these 4 aforementioned genes also showed up as significantly upregulated at the protein level. Reasoning why bacterial membrane components, such as LPS and now sphingolipids, can activate anti-viral responses, we propose that viral entry into cells at mucosal surfaces and viral membrane stabilization in the gut could involve bacterial by-products, something which has already been described for LPS (Robinson et al., 2014). Further, the CerPE sphingolipids could just broadly be activating the macrophages to induce type-1interferon responses, which represent an M1 phenotype, backed up by the high levels of *CCL2, CCL4,* and *CCL5* detected at the RNA-level and IL-6, TNF-α detected.

Combining the TF-seq, RNA-seq and proteomics data, the most obvious theme which arose from the data analysis, was that bacterial CerPE activates NF-kB signaling. By using TLR2, TLR4 and MyD88 knockout BMDMs and BMDCs, we discovered NF-kB is turned on, at

least partially, through a TLR2-MyD88 dependent pathway, adding to the long list of molecules that can bind to TLR2 (Botos et al., 2011). C12 SPE, which has a very similar structure to the bacterial CerPE, also signals in a MyD88 dependent manner but through TLR4. Of note, it's structure does not have the branched acyl-chains or extra hydroxyl group on the acyl chain typical of bacterial sphingolipids (Olsen and Jantzen, 2001), which could alter its signaling pathway. The purity of each CerPE lipid fraction isolated was confirmed by TLC separation and staining showing a single lipid band at the expected region of the gel. C12 SPE was purchased 99.9% pure by HPLC, and also checked for purity on TLC. When the CerPE lipids were sent for MALDI, no other bands of significance appeared that represented lipids that were not CerPE. All CerPE fractions were tested using the LAL assay and came up negative, adding confidence there is no endotoxin contamination in any CerPE fraction. Further, LPS, peptidoglycan or any polar molecule, will not migrate on the silica using the TLC separation solvent used in this study and was also likely degraded during the sodium hydroxide, sphingolipid enriching treatment of the crude lipid extract. We cannot discount that each CerPE fraction contained multiple CerPE class lipids with different acyl chain lengths. Some evidence in LPS shows the number and variety of acyl chains can augment or inhabit its signaling properties and it is possible each bacterial species has CerPE sphingolipids of differing acyl chain lengths, however this was not evident in our data with the Bacteroidetes species tested. There is a chance the fractions include a previously unknown lipid in very low abundance which could account for some of the signal. However, it is clear the fractions contained a high-abundance of CerPE sphingolipid and only those fractions from Bacteroidetes were able to stimulate and activate BMDMs and BMDCs to produce cytokine.

The CerPE sphingolipids could also be signaling through another pathway independent from TLR2-MyD88, to impart other effects on the cell such as increase cell proliferation, calcium signaling, redox signaling or other inflammatory pathways such as prostaglandin synthesis. The upregulation of the orphan G-protein coupled receptor *GPR160* seen in the RNA-seq data of CerPE treated BMDMs, coupled with the abundance of calcium-associated proteins in the proteomics, makes it tempting to speculate CerPE could alternatively activate GPCR pathways, given these have known endpoints of activation of calcium signaling and other cell proliferation and cytokine secretion events downstream (Kiselyov et al., 2003). Further, breakdown of CerPE by internalization or enzymatic reaction of the cells, into a sphinosine-1-phosphate or other sphingolipid could result in some difference in signaling events. Exogenous lipids at high concentration are known to form micelles, and when cells are stimulated with them could be internalized by the cell and exert intracellular effects (Futerman and Hannun, 2004). We have no evidence which form CerPE is in when given to the cells. Of note, calcium release and signaling has been documented as present during cells treated with sphingosine-1-phosphate, a mammalian sphingolipid, but no known intracellular receptor or signaling mechanism for this has been identified (Spiegel and Milstien, 2011).

Overall, bacterial CerPE is a potent inflammatory activator of macrophages and dendritic cells, which at least in part signals through TLR-MyD88 to activate cells and induce type-1 interferon responses. CerPE is conserved and present on all Bacteroidetes membranes tested in this study and could have an altered structure in species such as *P. distasonis.* The impact of these lipids in *in vivo* is still unknown and their potential as mediators during chronic inflammatory diseases such as IBD or EE remains unresolved. It is evident however that we have

identified a new class molecule from the Bacteroidetes which can interact with the host immune system. Future studies should utilize mono-colonized germ-free mice with either WT or sphingolipid KO *Bacteroides* strains to understand its role on initiating inflammation or activating immune cells. Further, these CerPE sphingolipids could act as a "danger signal" that induces a unique inflammatory activation pattern that should be explored further. Also, their role in mediating viral immunity in the intestine could be a role of these sphingolipids that may yield some novel insights into the interaction between our gut microbes, their metabolites, immunity and invading pathogens. During malnutrition, we have identified a greater abundance of sphingolipids in the intestine compared to control fed mice and humans, and whether these metabolites are markers for epithelial damage, or just potentially reflect the greater number of *Bacteroides* species during malnutrition is something that should be assessed and followed up. Clearly, *Bacteroides* species contribute to many inflammatory and metabolic pathways in the host immune system and our studies of CerPE add to the number of molecules which mediate these effects.

4.7 Summary

Taken together, these studies indicate early life malnutrition affects the colonization potential of *S.* Typhimurium in the small intestine and exerts a more exacerbated impact on liver pathology and inflammation compared to control-fed mice. Infection of malnourished and control mice with *C. rodentium,* which primarily colonizes the colon, revealed no significant changes at day 3 or 7 post-infection and a small change in bacterial burden of adherent bacteria at day 21 post-infection. Malnourished mice are also more susceptible to greater small intestinal

colonization of *H. polygyrus* and this increased colonization is correlated with decreased MLN production of IL-4, IL-5 and IL-13 but not systemic Th2 responses in the spleen. The malnourished diet exerts a local effect on the immune response to *H. polygyrus* and the only changes observed were found in the MLN. Overall, pathogens targeting the small intestine were able to gain a greater competitive advantage to colonize to higher burdens in the malnourished mice, indicated the small intestinal microenvironment is more sensitive to diet-induced changes to immunity and microbiota.

Further, when following up our data from metabolomics and microbiota analysis of the small intestine of malnourished, we discovered that each Bacteroidetes strain in the BG mix contains CerPE, a sphingolipid with previously unknown interactions with the immune system. We determined the structure of CerPE from each bacterial strain, and screened for its function in macrophages and dendritic cells using a novel TF-seq method, coupled with RNA-seq. These data revealed CerPE activates a number of immune pathways, namely NF-kB and type-1 interferon signaling. Proteomic data confirmed some hits and showed differences in calcium signaling as well as redox regulation in the cell, something that was also shown to be downregulated through NFE2L2 in the TF-seq. Using *TLR2*, *TLR4* and *MyD88* knockdown BMDM and BMDCs, we found that bacterial CerPE is only able to induce IL-6, TNF-α, MCP-1 or IL-10 secretion in wild-type cells and not in *TLR2*$^{-/-}$ or *MyD88*$^{-/-}$ BMDMs or BMDCs. Therefore, our data suggests that CerPE signals through TLR2-MyD88-dependent mechanisms to induce pro-inflammatory responses and macrophage/dendritic cell activation. We have discovered a novel interaction for bacterial sphingolipids and the host immune system which

could have importance for triggering or fueling chronic inflammation in the gut in disease like IBD or EE.

Chapter 5: Conclusion

Five years ago, when this work began, the broad impact on worldwide malnutrition and mortality and the pathogenic mechanisms of EE had received little attention and the underlying etiology was unknown. The lack of an animal model was a major limitation in understanding the basic mechanisms leading to EE and development of a model would be fundamental for generating therapeutic interventions in the clinic. At present, there still remains a plethora of unanswered questions regarding the pathophysiology, prevalence, impact and mechanisms of EE; we still know very little and it will likely take years of research from multiple models, institutions, and fields of research to start to answer some of the big questions. Given how much research there is in IBD, and the lack of a cure or full understanding of the disease demonstrates how far there is to go for EE research and a full grasp of malnutrition-immune-microbe interactions. However, in the past 5 years, there has been much more attention paid to EE and malnutrition and numerous findings and studies have begun to do just this; fill in the gaps with our understanding of EE and how to reverse malnutrition using our knowledge of immunity, the microbiota and metabolism. These studies include MAL-ED, formed in 2013 as a large consortium of researchers aiming to understand how the immune and microbiota sequelae of early-life infections with enteric pathogens impact EE and malnutrition in 7 different countries (Kosek et al., 2014). A study in Zimbabwe led by Jean Humphrey called WASH, aims to study how early-life maternal health, nutrition and sanitation of the environment (e.g. presence of toilets) correlates with growth velocity and EE-features (Ngure et al., 2014). There is also a study we are playing a small role in called Afribiota, which aims to assess the impact of immunity, the microbiota and pathogen infection on EE-features in Madagascar and the Central African

Republic (www.Afribiota.org). As funding begins to reflect the enormity of the problem, the field is beginning to think about how interventions for reversing malnutrition should take into account the presence of gut dysfunction in many of these populations, and intervene with not just diet but interventions to reverse these gut features leading to malabsorption (Petri et al., 2014). This study also represents a step-forward in our understanding of the interplay between the microbiota, metabolism and immunity during malnutrition and provides the first working murine model to aid in the understanding of EE. This may lead to the development of new and much needed diagnostic and therapeutic tools for the study of EE in humans.

At the outset of this study, our hypothesis was that malnutrition alters the small intestinal microbiota, metabolism and immune system which, in combination the with specific microbial exposure, could be the trigger for EE-features and these features can be reproduced in a murine model system. Our aims were to determine: (1) the microbiota, immune and metabolic changes in the small intestine after early-life malnutrition; (2) whether we can utilize these data to reproduce the defining features of human EE reproducibly in mice; (3) how early-life malnutrition impacts enteric infection and discover novel mechanisms which could potentially trigger EE-features. By the end of this study, we were able to generate data which was able to, at least partially, answer these questions and provide a framework for future research.

In conclusion, our study demonstrated that moderate, early-life malnutrition results in reduced expression of tight-junction proteins and increased intestinal permeability as viewed by leakage of fluorescently-labelled dextran into the bloodstream. The localization, abundance and composition of the small and large intestinal microbiota is also shifted, with more microbes able to colonize closer to the epithelial barrier and a bloom of Bacteroidetes and Proteobacteria in the

small intestine, followed by a decrease in *Lactobacillus* abundance during malnutrition. Malnutrition also led to a decrease in the abundance of *A. muciniphila* colonization of the mucus layer and also resulted in a thinning of the mucus layer. When analyzing the resulting metabolic changes correlating with the microbiota shifts, we discovered that bile acids were the most affected by malnutrition depending on where in the intestinal tract they were sampled as well. Decreased concentration of conjugated bile acids was seen in the small intestine, and this trend reversed in the colon where there were more conjugated bile acids malabsrobed and decreased levels of microbially-produced secondary bile acids such as lithocholic acid and hyodeoxycholic acid. The small intestine also had increased abundance of sphingolipid and steroid metabolism in malnourished mice, along with altered bioavailability of a number of vitamins in the intestine.

In aim 2, we sought to develop a novel model of EE and this was done by first screening cocktails of specific microbial species in malnourished and control mice and finding that a *Bacteoriodes* and *E. coli* species exacerbated growth stunting seen in malnourished mice early in life. While the malnourished diet alone led to growth stunting and increased intestinal permeability, the mixture of a malnourished diet with a cocktail of *Bacteroides* and *E. coli* species induced small intestinal villous blunting and inflammation similar to that of EE in humans. These features were not seen in the malnourished mice treated with diet alone or any other microbial mixture, leading us to conclude that in our system, a combination of a malnourished diet and specific microbial exposure results in EE-features in mice (Table 5.1). The presence of EE-features was also correlated with CD8+ T-cells from the IELs producing inflammatory cytokines TNF-α, IFN-γ and IL-17A.

Table 5.1: An outline of the four main features of environmental enteropathy and which can be replicated by the malnourished diet alone and which need malnutrition and the *Bacteroides-E. coli* cocktail to induce features.

Feature	Read-out	Diet-induced	Microbes + Diet
Growth stunting	Weight gain/tail-length	+	++
Intestinal permeability	TJP expression and serum FitC dextran	+	++
Chronic inflammation	Cytokine release and histopathology	-	+
Villous blunting	Villous height/crypt depth	-	+

In this study, we also further characterized the impact of malnutrition on enteric infections with *Salmonella, Citrobacter* and *H. polygyrus,* finding that in the case of *Salmonella* and *H. polygyrus* there was an increased burden of infection in the small intestine of malnourished mice compared to control-fed mice. Following up on our microbiome and metabolomics data, we further uncovered a potential role for a bacterial sphingolipid triggering inflammation in a TLR-MyD88-dependent manner in dendritic cells and macrophages. This sphingolipid was found to be ceramide phosphoethanolamine and we also characterized its structure and its cell signaling properties by RNA-seq, TF-seq and proteomics.

5.1 Limitations of animal models of human disease

Mice are the most commonly used animal model for intestinal studies, and preclinical studies of potential therapeutics for inflammatory diseases, such as IBD (Jiminez et al., 2015). Any clinical study on humans requires preclinical data and the mouse system is the most advantageous one to generate this data in a timely and relevant manner. Mice share many

specific intestinal genes with people, and mapping of the mouse genome and comparative genomic studies concluded that over 90% of human and mouse genes are shared among the two species, and approximately 80% of the mouse genes have a human orthologue (Mouse Genome Sequencing Consortium et al., 2002). Furthermore, human and murine intestinal communities exhibit a similar diversity of species within the Firmicutes, Bacteroidetes, and Proteobacteria phyla (Dethlefsen et al., 2007). The mouse gastrointestinal tract is also anatomically and functionally similar to human beings, and importantly, mice have many features analogous to the adaptive immune response such as the presence of similar populations of B-cells, T-cells, and isotype antibodies (Mestas and Hughes, 2004). Other relevant advantages of mice as an animal model includes the ability to create genetic knockdowns, ease of husbandry, their relatively short gestation period, and their large litter sizes (Jiminez et al., 2015).

Despite these many similarities between mice and human beings, there are some significant disadvantages to employing mice and other rodent models to study aspects of human intestinal inflammation (Jiminez et al., 2015). In preclinical studies of many inflammatory diseases, a large majority of findings (>90%) in mouse models fail to replicate in human studies (Justice and Dhillon, 2016). A study comparing the genomic responses of mice and humans to common inflammatory triggers found that among genes changed significantly in humans, the murine orthologues are close to random in matching their human counterparts (Seok et al., 2013). For example, there are differences between the murine and human expression of many innate immune genes such as TLR2, TLR3, TLR4, and TLR9. Behavioral patterns in mice also impact intestinal disease and can potentially confound the study of diet on the induction and progression of intestinal inflammation. For example, the fact mice can eat their own feces

(referred to as coprophagy) is one that is important to point out given the nature of our study. Coprophagy is common nocturnal behavior in mice and leads to the re-ingestion of nutrients which can affect dietary balance, microbial populations, and potentially affect intestinal health. In contrast, coprophagy is not considered a normal behavior in people, and fecal ingestion is linked to diseases such as EE. These confounders can affect the interpretations of our results in this study. Although there are drawbacks to using mice, the multitude of advantages over any other model make mice an excellent choice to investigate processes involved in intestinal inflammation of mammals and in some cases the only strategy to develop therapies for inflammatory disorders such as EE. Even given the clear limitations of this study, our development of the first mouse model for EE will hopefully aid in the potential to screen therapeutics and develop preclinical data which can be used to inform future humans intervention trials.

5.2 Research applications and future directions

This study uncovered novel findings into how malnutrition impacts the intestinal microbiota, immune system and metabolism, while also resulting in the development of the first animal model to study EE. Future directions for this research includes the use of the EE-model as a preclinical model to screen potential therapies for EE to break this "vicious cycle of malnutrition" (Fig. 5.1). The Gates Foundation is funding a large clinical consortium, of which we are members, which aims to use our model and others to develop the first approved drug to reverse EE. The potential therapies for EE include a butyrate-producing *E. coli Nissle* probiotic, a prebiotic galacto-oligosaccharide molecule, and small doses of antibiotics before dietary

interventions. The microbiome data generated here is also being further investigated, using a novel technique called IgA-seq to understand how IgA-microbe interactions impact malnutrition and EE-features. The behavior and brain function of the malnourished and EE-mice are also being tested in future studies currently to understand what, if any, cognitive defects in malnutrition could be microbially-driven. Further on, future research in this area should focus on understanding the trigger and physiological mechanisms of EE, potentially leveraging new technology and understanding of gut-immune-microbe interactions from IBD.

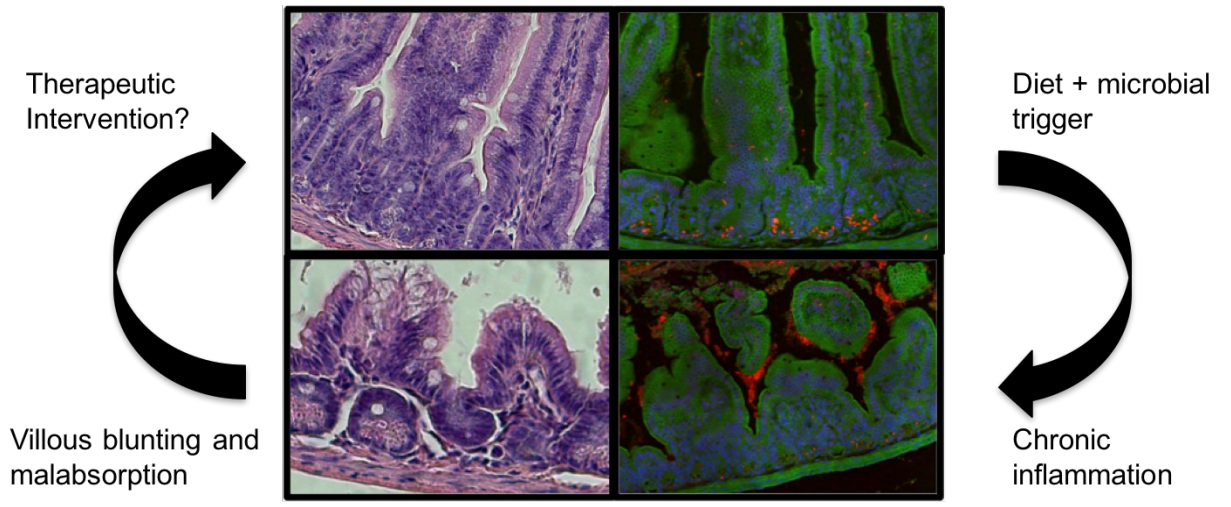

Figure 5.1: The vicious cycle of malnutrition as viewed from data using our mouse model

We also need to perform research to yield a greater understanding of EE in humans, which will require new techniques to sample the small intestine and a multidisciplinary effort given the complex nature of this condition. We do not yet know if there is a genetic component to EE, or whether features of EE present in changed prevalence, different symptoms or have diverse triggers in particular regions of the world. Future studies looking to reverse growth

stunting should pay attention to subclinical inflammation and permeability issues when designing future interventions to potentially increase the efficacy of dietary intervention for malnutrition and reverse these symptoms in the millions of children it effects worldwide.

Bibliography

Abdel Hadi, L., Di Vito, C., and Riboni, L. (2016). Fostering Inflammatory Bowel Disease: Sphingolipid Strategies to Join Forces. Mediators Inflamm. *2016*, 1–13.

Abreu, M. (2010). Toll-like receptor signalling in the intestinal epithelium: how bacterial recognition shapes intestinal function. Nat. Rev. Immunol. *10*, 131–144.

de Aguiar Vallim, T.Q., Tarling, E.J., and Edwards, P.A. (2013). Pleiotropic roles of bile acids in metabolism. Cell Metab. *17*, 657–669.

Ahern, P.P., Schiering, C., Buonocore, S., McGeachy, M.J., Cua, D.J., Maloy, K.J., and Powrie, F. (2010). Interleukin-23 drives intestinal inflammation through direct activity on T cells. Immunity *33*, 279–288.

Ahmed, T., Mahfuz, M., Islam, M.M., Mondal, D., Hossain, M.I., Ahmed, A.S., Tofail, F., Gaffar, S.A., Haque, R., Guerrant, R.L., et al. (2014a). The MAL-ED Cohort Study in Mirpur, Bangladesh. Clin. Infect. Dis. *59*, S280–S286.

Ahmed, T., Auble, D., Berkley, J.A., Black, R., Ahern, P.P., Hossain, M., Hsieh, A., Ireen, S., Arabi, M., and Gordon, J.I. (2014b). An evolving perspective about the origins of childhood undernutrition and nutritional interventions that includes the gut microbiome: Origins of childhood undernutrition and nutritional interventions. Ann. N. Y. Acad. Sci. *1332*, 22–38.

Amara, A.A., and Shibl, A. (2015). Role of Probiotics in health improvement, infection control and disease treatment and management. Saudi Pharm. J. *23*, 107–114.

An, D., Na, C., Bielawski, J., Hannun, Y.A., and Kasper, D.L. (2011). Membrane sphingolipids as essential molecular signals for Bacteroides survival in the intestine. Proc. Natl. Acad. Sci. *108*, 4666–4671.

An, D., Oh, S.F., Olszak, T., Neves, J.F., Avci, F.Y., Erturk-Hasdemir, D., Lu, X., Zeissig, S., Blumberg, R.S., and Kasper, D.L. (2014). Sphingolipids from a Symbiotic Microbe Regulate Homeostasis of Host Intestinal Natural Killer T Cells. Cell *156*, 123–133.

Assa, A., Vong, L., Pinnell, L.J., Avitzur, N., Johnson-Henry, K.C., and Sherman, P.M. (2014). Vitamin D deficiency promotes epithelial barrier dysfunction and intestinal inflammation. J. Infect. Dis. *210*, 1296–1305.

Basu, R., O'Quinn, D., Silberger, D., Schoeb, T., Fouser, L., Ouyang, W., Hatton, R., and Weaver, C. (2012). Th22 Cells Are an Important Source of IL-22 for Host Protection against Enteropathogenic Bacteria. Immunity.

Bemark, M., Boysen, P., and Lycke, N. (2012). Induction of gut IgA production through T cell-dependent and T cell-independent pathways. Ann. N. Y. Acad. Sci. *1247*, 97–116.

den Besten, G., van Eunen, K., Groen, A.K., Venema, K., Reijngoud, D.-J., and Bakker, B.M. (2013). The role of short-chain fatty acids in the interplay between diet, gut microbiota, and host energy metabolism. J. Lipid Res. *54*, 2325–2340.

Bhutta, Z.A., Ahmed, T., Black, R.E., Cousens, S., Dewey, K., Giugliani, E., Haider, B.A., Kirkwood, B., Morris, S.S., Sachdev, H.P.S., et al. (2008). What works? Interventions for maternal and child undernutrition and survival. The Lancet *371*, 417–440.

Bickler, S. (2006). Tropical enteropathy protects against Western diseases in environments of poor sanitation. Med. Hypotheses *67*, 146–150.

Biswas, S., and Lopez-Collazo, E. (2009). Endotoxin tolerance: new mechanisms, molecules and clinical significance. Trends Immunol. *30*, 475–487.

Blackwell, T.S., Blackwell, T.R., and Christman, J.W. (1997). Impaired activation of nuclear factor-kappaB in endotoxin-tolerant rats is associated with down-regulation of chemokine gene expression and inhibition of neutrophilic lung inflammation. J. Immunol. *158*, 5934–5940.

Blanton, L.V., Charbonneau, M.R., Salih, T., Barratt, M.J., Venkatesh, S., Ilkaveya, O., Subramanian, S., Manary, M.J., Trehan, I., Jorgensen, J.M., et al. (2016). Gut bacteria that prevent growth impairments transmitted by microbiota from malnourished children. Science *351*.

Bloom, S., Bijanki, V., Nava, G., Sun, L., Malvin, N., Donermeyer, D., Dunne, W., Allen, P., and Stappenbeck, T. (2011). Commensal Bacteroides species induce colitis in host-genotype-specific fashion in a mouse model of inflammatory bowel disease. Cell Host Microbe *9*, 390–403.

Bolick, D., Roche, J., Hontecillas, R., Bassaganya-Riera, J., Nataro, J., and Guerrant, R. (2013). Enteroaggregative Escherichia coli strain in a novel weaned mouse model: exacerbation by malnutrition, biofilm as a virulence factor and treatment by nitazoxanide. J. Med. Microbiol. *62*, 896–905.

Borsutzky, S., Cazac, B., Roes, J., and GuzmÃ¡n, C. (2004). TGF-beta receptor signaling is critical for mucosal IgA responses. J. Immunol. Baltim. Md 1950 *173*, 3305–3309.

Botos, I., Segal, D.M., and Davies, D.R. (2011). The Structural Biology of Toll-Like Receptors. Struct. Lond. Engl. 1993 *19*, 447–459.

Bourke, C.D., Berkley, J.A., and Prendergast, A.J. (2016). Immune Dysfunction as a Cause and Consequence of Malnutrition. Trends Immunol. *37*, 386–398.

Brooker, S., Bethony, J., and Hotez, P.J. (2004). Human Hookworm Infection in the 21st Century. Adv. Parasitol. *58*, 197–288.

Brown, E.M., Sadarangani, M., and Finlay, B.B. (2013). The role of the immune system in governing host-microbe interactions in the intestine. Nat. Immunol. *14*, 660–667.

Brown, E.M., Wlodarska, M., Willing, B.P., Vonaesch, P., Han, J., Reynolds, L.A., Arrieta, M.-C., Uhrig, M., Scholz, R., Partida, O., et al. (2015). Diet and specific microbial exposure trigger features of environmental enteropathy in a novel murine model. Nat. Commun. *6*, 7806.

Buettner, M., and Bode, U. (2012). Lymph node dissection – understanding the immunological function of lymph nodes. Clin. Exp. Immunol. *169*, 205–212.

Calder, P. (2013). Feeding the immune system. Proc. Nutr. Soc. *72*, 299–309.

Campbell, D., Murch, S., Elia, M., Sullivan, P., Sanyang, M., Jobarteh, B., and Lunn, P. (2003). Chronic T cell-mediated enteropathy in rural west African children: relationship with nutritional status and small bowel function. Pediatr. Res. *54*, 306–311.

Campbell, J.M., Fahey, G.C., and Wolf, B.W. (1997). Selected indigestible oligosaccharides affect large bowel mass, cecal and fecal short-chain fatty acids, pH and microflora in rats. J. Nutr. *127*, 130–136.

Cani, P., Possemiers, S., Van de Wiele, T., Guiot, Y., Everard, A., Rottier, O., Geurts, L., Naslain, D., Neyrinck, A., Lambert, D., et al. (2009). Changes in gut microbiota control inflammation in obese mice through a mechanism involving GLP-2-driven improvement of gut permeability. Gut *58*, 1091–1103.

Cani, P.D., Amar, J., Iglesias, M.A., Poggi, M., Knauf, C., Bastelica, D., Neyrinck, A.M., Fava, F., Tuohy, K.M., Chabo, C., et al. (2007). Metabolic Endotoxemia Initiates Obesity and Insulin Resistance. Diabetes *56*, 1761–1772.

Carvalho, F., Aitken, J., Vijay-Kumar, M., and Gewirtz, A. (2012a). Toll-like receptor-gut microbiota interactions: perturb at your own risk! Annu. Rev. Physiol. *74*, 177–198.

Carvalho, F.A., Koren, O., Goodrich, J.K., Johansson, M.E.V., Nalbantoglu, I., Aitken, J.D., Su, Y., Chassaing, B., Walters, W.A., González, A., et al. (2012b). Transient inability to manage proteobacteria promotes chronic gut inflammation in TLR5-deficient mice. Cell Host Microbe *12*, 139–152.

Cebra, J.J. (1999). Influences of microbiota on intestinal immune system development. Am. J. Clin. Nutr. *69*, 1046S–1051S.

Charbonneau, M.R., O'Donnell, D., Blanton, L.V., Totten, S.M., Davis, J.C.C., Barratt, M.J., Cheng, J., Guruge, J., Talcott, M., Bain, J.R., et al. (2016a). Sialylated Milk Oligosaccharides Promote Microbiota-Dependent Growth in Models of Infant Undernutrition. Cell *164*, 859–871.

Charbonneau, M.R., Blanton, L.V., DiGiulio, D.B., Relman, D.A., Lebrilla, C.B., Mills, D.A., and Gordon, J.I. (2016b). A microbial perspective of human developmental biology. Nature *535*, 48–55.

Cho, I., Yamanishi, S., Cox, L., MethÃ©, B., Zavadil, J., Li, K., Gao, Z., Mahana, D., Raju, K., Teitler, I., et al. (2012). Antibiotics in early life alter the murine colonic microbiome and adiposity. Nature *488*, 621–626.

Collins, S. (2007). Treating severe acute malnutrition seriously. Arch. Dis. Child. *92*, 453–461.

Collins, J.W., Keeney, K.M., Crepin, V.F., Rathinam, V.A.K., Fitzgerald, K.A., Finlay, B.B., and Frankel, G. (2014). Citrobacter rodentium: infection, inflammation and the microbiota. Nat. Rev. Microbiol. *12*, 612–623.

Collins, S., Dent, N., Binns, P., Bahwere, P., Sadler, K., and Hallam, A. (2006). Management of severe acute malnutrition in children. Lancet Lond. Engl. *368*, 1992–2000.

Cong, Y., Feng, T., Fujihashi, K., Schoeb, T., and Elson, C. (2009). A dominant, coordinated T regulatory cell-IgA response to the intestinal microbiota. Proc. Natl. Acad. Sci. U. S. A. *106*, 19256–19261.

Coombes, J., and Powrie, F. (2008). Dendritic cells in intestinal immune regulation. Nat. Rev. Immunol. *8*, 435–446.

Crepin, V.F., Collins, J.W., Habibzay, M., and Frankel, G. (2016). Citrobacter rodentium mouse model of bacterial infection. Nat. Protoc. *11*, 1851–1876.

David, L.A., Maurice, C.F., Carmody, R.N., Gootenberg, D.B., Button, J.E., Wolfe, B.E., Ling, A.V., Devlin, A.S., Varma, Y., Fischbach, M.A., et al. (2014). Diet rapidly and reproducibly alters the human gut microbiome. Nature *505*, 559–563.

DeBoer, M.D., Lima, A.A., Oría, R.B., Scharf, R.J., Moore, S.R., Luna, M.A., and Guerrant, R.L. (2012). Early childhood growth failure and the developmental origins of adult disease: do enteric infections and malnutrition increase risk for the metabolic syndrome? Nutr. Rev. *70*, 642–653.

Deshpande, G., Rao, S., and Patole, S. (2011). Progress in the field of probiotics: year 2011. Curr. Opin. Gastroenterol. *27*, 13–18.

Dethlefsen, L., McFall-Ngai, M., and Relman, D.A. (2007). An ecological and evolutionary perspective on human-microbe mutualism and disease. Nature *449*, 811–818.

Dewey, K.G., and Begum, K. (2011). Long-term consequences of stunting in early life. Matern. Child. Nutr. *7 Suppl 3*, 5–18.

DiBaise, J., and Islam, R. (2012). Bile Acids: An Underrecognized and Underappreciated Cause of Chronic Diarrhea. Pract. Gastroenterol.

Dominguez-Salas, P., Moore, S.E., Baker, M.S., Bergen, A.W., Cox, S.E., Dyer, R.A., Fulford, A.J., Guan, Y., Laritsky, E., Silver, M.J., et al. (2014). Maternal nutrition at conception modulates DNA methylation of human metastable epialleles. Nat. Commun. *5*, 3746.

Donia, M.S., and Fischbach, M.A. (2015). HUMAN MICROBIOTA. Small molecules from the human microbiota. Science *349*, 1254766.

Duboc, H., Rajca, S., Rainteau, D., Benarous, D., Maubert, M.-A., Quervain, E., Thomas, G., Barbu, V., Humbert, L., Despras, G., et al. (2013). Connecting dysbiosis, bile-acid dysmetabolism and gut inflammation in inflammatory bowel diseases. Gut *62*, 531–539.

El Aidy, S., van den Bogert, B., and Kleerebezem, M. (2015). The small intestine microbiota, nutritional modulation and relevance for health. Curr. Opin. Biotechnol. *32*, 14–20.

Elinav, E., Strowig, T., Kau, A., Henao-Mejia, J., Thaiss, C., Booth, C., Peaper, D., Bertin, J., Eisenbarth, S., Gordon, J., et al. (2011). NLRP6 inflammasome regulates colonic microbial ecology and risk for colitis. Cell *145*, 745–757.

Everard, A., Belzer, C., Geurts, L., Ouwerkerk, J.P., Druart, C., Bindels, L.B., Guiot, Y., Derrien, M., Muccioli, G.G., Delzenne, N.M., et al. (2013). Cross-talk between Akkermansia muciniphila and intestinal epithelium controls diet-induced obesity. Proc. Natl. Acad. Sci. *110*, 9066–9071.

Faith, J., McNulty, N., Rey, F., and Gordon, J. (2011). Predicting a human gut microbiota's response to diet in gnotobiotic mice. Science *333*, 101–104.

Farache, J., Koren, I., Milo, I., Gurevich, I., Kim, K.-W., Zigmond, E., Furtado, G.C., Lira, S.A., and Shakhar, G. (2013). Luminal bacteria recruit CD103+ dendritic cells into the intestinal epithelium to sample bacterial antigens for presentation. Immunity *38*, 581–595.

Fasano, A. (2011). Zonulin and its regulation of intestinal barrier function: the biological door to inflammation, autoimmunity, and cancer. Physiol. Rev. *91*, 151–175.

Fonseca, D.M. da, Hand, T.W., Han, S.-J., Gerner, M.Y., Glatman Zaretsky, A., Byrd, A.L., Harrison, O.J., Ortiz, A.M., Quinones, M., Trinchieri, G., et al. (2015). Microbiota-Dependent Sequelae of Acute Infection Compromise Tissue-Specific Immunity. Cell *163*, 354–366.

Foussat, A., Cottrez, F., Brun, V., Fournier, N., Breittmayer, J.-P., and Groux, H. (2003). A comparative study between T regulatory type 1 and CD4+CD25+ T cells in the control of inflammation. J. Immunol. Baltim. Md 1950 *171*, 5018–5026.

Futerman, A.H., and Hannun, Y.A. (2004). The complex life of simple sphingolipids. EMBO Rep. *5*, 777–782.

Galpin, L., Manary, M., Fleming, K., Ou, C.-N., Ashorn, P., and Shulman, R. (2005). Effect of Lactobacillus GG on intestinal integrity in Malawian children at risk of tropical enteropathy. Am. J. Clin. Nutr. *82*, 1040–1045.

Ghoshal, U., Ghoshal, U., Ayyagari, A., Ranjan, P., Krishnani, N., Misra, A., Aggarwal, R., Naik, S., and Naik, S. (2003). Tropical sprue is associated with contamination of small bowel

with aerobic bacteria and reversible prolongation of orocecal transit time. J. Gastroenterol. Hepatol. *18*, 540–547.

Gibbs, B.G., and Forste, R. (2014). Socioeconomic status, infant feeding practices and early childhood obesity. Pediatr. Obes. *9*, 135–146.

Gibson, G.R., McCartney, A.L., and Rastall, R.A. (2005). Prebiotics and resistance to gastrointestinal infections. Br. J. Nutr. *93 Suppl 1*, S31-34.

Gordon, J., Dewey, K., Mills, D., and Medzhitov, R. (2012a). The human gut microbiota and undernutrition. Sci. Transl. Med. *4*.

Gordon, J.I., Dewey, K.G., Mills, D.A., and Medzhitov, R.M. (2012b). The human gut microbiota and undernutrition. Sci. Transl. Med. *4*, 137ps12–137ps12.

Green, P.H.R., and Cellier, C. (2007). Celiac disease. N. Engl. J. Med. *357*, 1731–1743.

Gregor, M.F., and Hotamisligil, G.S. (2011). Inflammatory mechanisms in obesity. Annu. Rev. Immunol. *29*, 415–445.

Griffin, N.W., Ahern, P.P., Cheng, J., Heath, A.C., Ilkayeva, O., Newgard, C.B., Fontana, L., and Gordon, J.I. (2017). Prior Dietary Practices and Connections to a Human Gut Microbial Metacommunity Alter Responses to Diet Interventions. Cell Host Microbe *21*, 84–96.

Gu, S., Chen, D., Zhang, J.-N., Lv, X., Wang, K., Duan, L.-P., Nie, Y., and Wu, X.-L. (2013). Bacterial community mapping of the mouse gastrointestinal tract. PloS One *8*, e74957.

Guerrant, R., OriÃ¡, R., Moore, S., OriÃ¡, M., and Lima, A. (2008a). Malnutrition as an enteric infectious disease with long-term effects on child development. Nutr. Rev. *66*, 487–505.

Guerrant, R., DeBoer, M., Moore, S., Scharf, R., and Lima, A. (2013). The impoverished gut--a triple burden of diarrhoea, stunting and chronic disease. Nat. Rev. Gastroenterol. Hepatol. *10*, 220–229.

Guerrant, R.L., Oriá, R.B., Moore, S.R., Oriá, M.O., and Lima, A.A. (2008b). Malnutrition as an enteric infectious disease with long-term effects on child development: Nutrition Reviews©, Vol. 66, No. 9. Nutr. Rev. *66*, 487–505.

Guerrant, R.L., DeBoer, M.D., Moore, S.R., Scharf, R.J., and Lima, A.A.M. (2012). The impoverished gut—a triple burden of diarrhoea, stunting and chronic disease. Nat. Rev. Gastroenterol. Hepatol. *10*, 220–229.

Guerrant, R.L., Leite, A.M., Pinkerton, R., Medeiros, P.H.Q.S., Cavalcante, P.A., DeBoer, M., Kosek, M., Duggan, C., Gewirtz, A., Kagan, J.C., et al. (2016). Biomarkers of Environmental Enteropathy, Inflammation, Stunting, and Impaired Growth in Children in Northeast Brazil. PloS One *11*, e0158772.

Han, J., Liu, Y., Wang, R., Yang, J., Ling, V., and Borchers, C.H. (2015). Metabolic profiling of bile acids in human and mouse blood by LC-MS/MS in combination with phospholipid-depletion solid-phase extraction. Anal. Chem. *87*, 1127–1136.

Hand, T., Dos Santos, L., Bouladoux, N., Molloy, M., PagÃ¡n, A., Pepper, M., Maynard, C., Elson, C., and Belkaid, Y. (2012). Acute gastrointestinal infection induces long-lived microbiota-specific T cell responses. Science *337*, 1553–1556.

Hapfelmeier, S., Lawson, M., Slack, E., Kirundi, J., Stoel, M., Heikenwalder, M., Cahenzli, J., Velykoredko, Y., Balmer, M., Endt, K., et al. (2010). Reversible microbial colonization of germ-free mice reveals the dynamics of IgA immune responses. Science *328*, 1705–1709.

Harris, N.L., Pleass, R., and Behnke, J.M. (2014). Understanding the role of antibodies in murine infections with Heligmosomoides (polygyrus) bakeri: 35 years ago, now and 35 years ahead. Parasite Immunol. *36*, 115–124.

Hashimoto, T., Perlot, T., Rehman, A., Trichereau, J., Ishiguro, H., Paolino, M., Sigl, V., Hanada, T., Hanada, R., Lipinski, S., et al. (2012). ACE2 links amino acid malnutrition to microbial ecology and intestinal inflammation. Nature *487*, 477–481.

Hewitson, J.P., Filbey, K.J., Bieren, J.E., Camberis, M., Schwartz, C., Murray, J., Reynolds, L.A., Blair, N., Robertson, E., Harcus, Y., et al. (2015). Concerted Activity of IgG1 Antibodies and IL-4/IL-25-Dependent Effector Cells Trap Helminth Larvae in the Tissues following Vaccination with Defined Secreted Antigens, Providing Sterile Immunity to Challenge Infection. PLOS Pathog. *11*, e1004676.

Hla, T., and Dannenberg, A.J. (2012). Sphingolipid Signaling in Metabolic Disorders. Cell Metab. *16*, 420–434.

Hofmann, A., and Eckmann, L. (2006). How bile acids confer gut mucosal protection against bacteria. Proc. Natl. Acad. Sci. U. S. A. *103*, 4333–4334.

Hooper, L.V., Littman, D.R., and Macpherson, A.J. (2012). Interactions Between the Microbiota and the Immune System. Science *336*, 1268–1273.

Humphrey, J. (2009). Child undernutrition, tropical enteropathy, toilets, and handwashing. Lancet *374*, 1032–1035.

Ibs, K.-H., and Rink, L. (2003). Zinc-altered immune function. J. Nutr. *133*, 1452S–6S.

Jiminez, J.A., Uwiera, T.C., Douglas Inglis, G., and Uwiera, R.R.E. (2015). Animal models to study acute and chronic intestinal inflammation in mammals. Gut Pathog. *7*.

Johansson, M., Larsson, J., and Hansson, G. (2011). The two mucus layers of colon are organized by the MUC2 mucin, whereas the outer layer is a legislator of host-microbial interactions. Proc. Natl. Acad. Sci. U. S. A. *108 Suppl 1*, 4659–4665.

Jones, K., HÃ¼nten-Kirsch, B., Laving, A., Munyi, C., Ngari, M., Mikusa, J., Mulongo, M., Odera, D., Nassir, H., Timbwa, M., et al. (2014). Mesalazine in the initial management of severely acutely malnourished children with environmental enteric dysfunction: a pilot randomized controlled trial. BMC Med. *12*, 133.

Justice, M.J., and Dhillon, P. (2016). Using the mouse to model human disease: increasing validity and reproducibility. Dis. Model. Mech. *9*, 101–103.

Kane, A.V., Dinh, D.M., and Ward, H.D. (2015). Childhood malnutrition and the intestinal microbiome. Pediatr. Res. *77*, 256–262.

Katona, P., and Katona-Apte, J. (2008). The Interaction between Nutrition and Infection. Clin. Infect. Dis. *46*, 1582–1588.

Kau, A., Ahern, P., Griffin, N., Goodman, A., and Gordon, J. (2011). Human nutrition, the gut microbiome and the immune system. Nature *474*, 327–336.

Kau, A.L., Planer, J.D., Liu, J., Rao, S., Yatsunenko, T., Trehan, I., Manary, M.J., Liu, T.-C., Stappenbeck, T.S., Maleta, K.M., et al. (2015). Functional characterization of IgA-targeted bacterial taxa from undernourished Malawian children that produce diet-dependent enteropathy. Sci. Transl. Med. *7*, 276ra24–276ra24.

Kaufman, D., De Calisto, J., Simmons, N., Cruz, A., Villablanca, E., Mora, J., and Barouch, D. (2011). Vitamin A deficiency impairs vaccine-elicited gastrointestinal immunity. J. Immunol. Baltim. Md 1950 *187*, 1877–1883.

Kelly, P., Menzies, I., Crane, R., Zulu, I., Nickols, C., Feakins, R., Mwansa, J., Mudenda, V., Katubulushi, M., Greenwald, S., et al. (2004). Responses of small intestinal architecture and function over time to environmental factors in a tropical population. Am. J. Trop. Med. Hyg. *70*, 412–419.

Kerac, M., and Seal, A. (2014). Preventing acute malnutrition in young children: improving the evidence for current and future practice. PLoS Med. *11*.

Keusch, G.T., Denno, D.M., Black, R.E., Duggan, C., Guerrant, R.L., Lavery, J.V., Nataro, J.P., Rosenberg, I.H., Ryan, E.T., Tarr, P.I., et al. (2014). Environmental Enteric Dysfunction: Pathogenesis, Diagnosis, and Clinical Consequences. Clin. Infect. Dis. *59*, S207–S212.

Kiselyov, K., Shin, D.M., and Muallem, S. (2003). Signalling specificity in GPCR-dependent Ca2+ signalling. Cell. Signal. *15*, 243–253.

Knoop, K.A., Miller, M.J., and Newberry, R.D. (2013). Transepithelial antigen delivery in the small intestine: different paths, different outcomes. Curr. Opin. Gastroenterol. *29*, 112–118.

Köberlin, M.S., Snijder, B., Heinz, L.X., Baumann, C.L., Fauster, A., Vladimer, G.I., Gavin, A.-C., and Superti-Furga, G. (2015). A Conserved Circular Network of Coregulated Lipids Modulates Innate Immune Responses. Cell *162*, 170–183.

Konikoff, M.R., and Denson, L.A. (2006). Role of fecal calprotectin as a biomarker of intestinal inflammation in inflammatory bowel disease. Inflamm. Bowel Dis. *12*, 524–534.

Koropatkin, N.M., Martens, E.C., Gordon, J.I., and Smith, T.J. (2008). Starch catabolism by a prominent human gut symbiont is directed by the recognition of amylose helices. Struct. Lond. Engl. 1993 *16*, 1105–1115.

Korpe, P., and Petri, W. (2012). Environmental enteropathy: critical implications of a poorly understood condition. Trends Mol. Med. *18*, 328–336.

Kosek, M., Guerrant, R.L., Kang, G., Bhutta, Z., Yori, P.P., Gratz, J., Gottlieb, M., Lang, D., Lee, G., Haque, R., et al. (2014). Assessment of Environmental Enteropathy in the MAL-ED Cohort Study: Theoretical and Analytic Framework. Clin. Infect. Dis. *59*, S239–S247.

Krajmalnik-Brown, R., Ilhan, Z.-E., Kang, D.-W., and DiBaise, J.K. (2012). Effects of Gut Microbes on Nutrient Absorption and Energy Regulation. Nutr. Clin. Pract. *27*, 201–214.

Lagos, R., Fasano, A., Wasserman, S., Prado, V., San Martin, O., Abrego, P., Losonsky, G., Alegria, S., and Levine, M. (1999). Effect of small bowel bacterial overgrowth on the immunogenicity of single-dose live oral cholera vaccine CVD 103-HgR. J. Infect. Dis. *180*, 1709–1712.

Lee, G.O., Kosek, P., Lima, A.A.M., Singh, R., Yori, P.P., Olortegui, M.P., Lamsam, J.L., Oliveira, D.B., Guerrant, R.L., and Kosek, M. (2014). Lactulose:Mannitol Diagnostic Test by HPLC and LC-MSMS Platforms: Considerations for Field Studies of Intestinal Barrier Function and Environmental Enteropathy. J. Pediatr. Gastroenterol. Nutr. *59*, 544–550.

Levine, M. (2010). Immunogenicity and efficacy of oral vaccines in developing countries: lessons from a live cholera vaccine. BMC Biol. *8*, 129.

Lewis, Z.T., Totten, S.M., Smilowitz, J.T., Popovic, M., Parker, E., Lemay, D.G., Van Tassell, M.L., Miller, M.J., Jin, Y.-S., German, J.B., et al. (2015). Maternal fucosyltransferase 2 status affects the gut bifidobacterial communities of breastfed infants. Microbiome *3*, 13.

Li, H., and Durbin, R. (2009). Fast and accurate short read alignment with Burrows-Wheeler transform. Bioinforma. Oxf. Engl. *25*, 1754–1760.

Li, M.O., Wan, Y.Y., and Flavell, R.A. (2007). T cell-produced transforming growth factor-beta1 controls T cell tolerance and regulates Th1- and Th17-cell differentiation. Immunity *26*, 579–591.

Lin, A., Arnold, B.F., Afreen, S., Goto, R., Huda, T.M.N., Haque, R., Raqib, R., Unicomb, L., Ahmed, T., Colford, J.M., et al. (2013). Household Environmental Conditions Are Associated with Enteropathy and Impaired Growth in Rural Bangladesh. Am. J. Trop. Med. Hyg. *89*, 130–137.

Littman, D.R., and Rudensky, A.Y. (2010). Th17 and regulatory T cells in mediating and restraining inflammation. Cell *140*, 845–858.

Loy, A., Maixner, F., Wagner, M., and Horn, M. (2007). probeBase--an online resource for rRNA-targeted oligonucleotide probes: new features 2007. Nucleic Acids Res. *35*, D800-804.

Lutter, C.K., Daelmans, B.M.E.G., Onis, M. de, Kothari, M.T., Ruel, M.T., Arimond, M., Deitchler, M., Dewey, K.G., Blössner, M., and Borghi, E. (2011). Undernutrition, Poor Feeding Practices, and Low Coverage of Key Nutrition Interventions. Pediatrics *128*, e1418–e1427.

Maceyka, M., and Spiegel, S. (2014). Sphingolipid metabolites in inflammatory disease. Nature *510*, 58–67.

Macpherson, A., and Uhr, T. (2004). Induction of protective IgA by intestinal dendritic cells carrying commensal bacteria. Science *303*, 1662–1665.

Macpherson, A., Gatto, D., Sainsbury, E., Harriman, G., Hengartner, H., and Zinkernagel, R. (2000). A primitive T cell-independent mechanism of intestinal mucosal IgA responses to commensal bacteria. Science *288*, 2222–2226.

Maier, E., Weage, K., Guedes, M., Denson, L., McNeal, M., Bernstein, D., and Moore, S. (2013). Protein-energy malnutrition alters IgA responses to rotavirus vaccination and infection but does not impair vaccine efficacy in mice. Vaccine *32*, 48–53.

Maizels, R.M., and Holland, M.J. (1998). Parasite immunity: Pathways for expelling intestinal helminths. Curr. Biol. *8*, R711–R714.

Maloy, K.J., Salaun, L., Cahill, R., Dougan, G., Saunders, N.J., and Powrie, F. (2003). CD4+CD25+ T(R) cells suppress innate immune pathology through cytokine-dependent mechanisms. J. Exp. Med. *197*, 111–119.

Masure, D., Wang, T., Vlaminck, J., Claerhoudt, S., Chiers, K., Van den Broeck, W., Saunders, J., Vercruysse, J., and Geldhof, P. (2013). The Intestinal Expulsion of the Roundworm Ascaris suum Is Associated with Eosinophils, Intra-Epithelial T Cells and Decreased Intestinal Transit Time. PLoS Negl. Trop. Dis. *7*.

Mayneris-Perxachs, J., Lima, A.A.M., Guerrant, R.L., Leite, Á.M., Moura, A.F., Lima, N.L., Soares, A.M., Havt, A., Moore, S.R., Pinkerton, R., et al. (2016). Urinary N-methylnicotinamide and β-aminoisobutyric acid predict catch-up growth in undernourished Brazilian children. Sci. Rep. *6*, 19780.

McDole, J., Wheeler, L., McDonald, K., Wang, B., Konjufca, V., Knoop, K., Newberry, R., and Miller, M. (2012). Goblet cells deliver luminal antigen to CD103+ dendritic cells in the small intestine. Nature *483*, 345–349.

Mello, C., Tahan, S., Melli, L., Rodrigues, M., de Mello, R., Scaletsky, I., and de Morais, M. (2012). Methane production and small intestinal bacterial overgrowth in children living in a slum. World J. Gastroenterol. WJG *18*, 5932–5939.

Mengesha, M.M., Deyessa, N., Tegegne, B.S., and Dessie, Y. (2016). Treatment outcome and factors affecting time to recovery in children with severe acute malnutrition treated at outpatient therapeutic care program. Glob. Health Action *9*.

Mesquita, D.N., Barbieri, M.A., Goldani, H.A.S., Cardoso, V.C., Goldani, M.Z., Kac, G., Silva, A.A.M., and Bettiol, H. (2013). Cesarean Section Is Associated with Increased Peripheral and Central Adiposity in Young Adulthood: Cohort Study. PLOS ONE *8*, e66827.

Mestas, J., and Hughes, C.C.W. (2004). Of mice and not men: differences between mouse and human immunology. J. Immunol. Baltim. Md 1950 *172*, 2731–2738.

Mestecky, J., and Russell, M.W. (2009). Specific antibody activity, glycan heterogeneity and polyreactivity contribute to the protective activity of S-IgA at mucosal surfaces. Immunol. Lett. *124*, 57–62.

Monte, M.-J. (2009). Bile acids: Chemistry, physiology, and pathophysiology. World J. Gastroenterol. *15*, 804.

Mouse Genome Sequencing Consortium, Waterston, R.H., Lindblad-Toh, K., Birney, E., Rogers, J., Abril, J.F., Agarwal, P., Agarwala, R., Ainscough, R., Alexandersson, M., et al. (2002). Initial sequencing and comparative analysis of the mouse genome. Nature *420*, 520–562.

Mukhopadhya, I., Hansen, R., El-Omar, E.M., and Hold, G.L. (2012). IBD—what role do Proteobacteria play? Nat. Rev. Gastroenterol. Hepatol. *9*, 219–230.

Muñoz, C., Rios, E., Olivos, J., Brunser, O., and Olivares, M. (2007). Iron, copper and immunocompetence. Br. J. Nutr. *98 Suppl 1*, S24-28.

Ngure, F.M., Reid, B.M., Humphrey, J.H., Mbuya, M.N., Pelto, G., and Stoltzfus, R.J. (2014). Water, sanitation, and hygiene (WASH), environmental enteropathy, nutrition, and early child development: making the links: WASH and ECD: making the links. Ann. N. Y. Acad. Sci. *1308*, 118–128.

O'Connell, D.J., Kolde, R., Sooknah, M., Graham, D.B., Sundberg, T.B., Latorre, I.J., Mikkelsen, T.S., and Xavier, R.J. (2016). Simultaneous Pathway Activity Inference and Gene Expression Analysis Using RNA Sequencing. Cell Syst. *2*, 323–334.

Olsen, I., and Jantzen, E. (2001). Sphingolipids in Bacteria and Fungi. Anaerobe *7*, 103–112.

Owino, V., Ahmed, T., Freemark, M., Kelly, P., Loy, A., Manary, M., and Loechl, C. (2016). Environmental Enteric Dysfunction and Growth Failure/Stunting in Global Child Health. PEDIATRICS *138*, e20160641–e20160641.

Palm, N.W., de Zoete, M.R., Cullen, T.W., Barry, N.A., Stefanowski, J., Hao, L., Degnan, P.H., Hu, J., Peter, I., Zhang, W., et al. (2014). Immunoglobulin A Coating Identifies Colitogenic Bacteria in Inflammatory Bowel Disease. Cell *158*, 1000–1010.

Pelly, V.S., Kannan, Y., Coomes, S.M., Entwistle, L.J., Rückerl, D., Seddon, B., MacDonald, A.S., McKenzie, A., and Wilson, M.S. (2016). IL-4-producing ILC2s are required for the differentiation of TH2 cells following Heligmosomoides polygyrus infection. Mucosal Immunol. *9*, 1407–1417.

Perez-Lopez, A., Behnsen, J., Nuccio, S.-P., and Raffatellu, M. (2016). Mucosal immunity to pathogenic intestinal bacteria. Nat. Rev. Immunol. *16*, 135–148.

Peterson, D.A., McNulty, N.P., Guruge, J.L., and Gordon, J.I. (2007). IgA response to symbiotic bacteria as a mediator of gut homeostasis. Cell Host Microbe *2*, 328–339.

Petri, W.A., Naylor, C., and Haque, R. (2014). Environmental enteropathy and malnutrition: do we know enough to intervene? BMC Med. *12*, 187.

Prendergast, A., and Kelly, P. (2012). Enteropathies in the developing world: neglected effects on global health. Am. J. Trop. Med. Hyg. *86*, 756–763.

Prendergast, A.J., and Humphrey, J.H. (2014). The stunting syndrome in developing countries. Paediatr. Int. Child Health *34*, 250–265.

Prendergast, A.J., Humphrey, J.H., Mutasa, K., Majo, F.D., Rukobo, S., Govha, M., Mbuya, M.N.N., Moulton, L.H., and Stoltzfus, R.J. (2015). Assessment of Environmental Enteric Dysfunction in the SHINE Trial: Methods and Challenges. Clin. Infect. Dis. *61*, S726–S732.

Rappsilber, J., Mann, M., and Ishihama, Y. (2007). Protocol for micro-purification, enrichment, pre-fractionation and storage of peptides for proteomics using StageTips. Nat. Protoc. *2*, 1896–1906.

Read, S., Malmström, V., and Powrie, F. (2000). Cytotoxic T lymphocyte-associated antigen 4 plays an essential role in the function of CD25(+)CD4(+) regulatory cells that control intestinal inflammation. J. Exp. Med. *192*, 295–302.

dos Reis, J., de Morais, M., Oliva, C., and Fagundes-Neto, U. (2007). Breath hydrogen test in the diagnosis of environmental enteropathy in children living in an urban slum. Dig. Dis. Sci. *52*, 1253–1258.

Relman, D. (2013). Microbiology. Undernutrition--looking within for answers. Science *339*, 530–532.

Reynolds, L.A., Filbey, K.J., and Maizels, R.M. (2012). Immunity to the model intestinal helminth parasite Heligmosomoides polygyrus. Semin. Immunopathol. *34*, 829–846.

Ridaura, V.K., Faith, J.J., Rey, F.E., Cheng, J., Duncan, A.E., Kau, A.L., Griffin, N.W., Lombard, V., Henrissat, B., Bain, J.R., et al. (2013). Gut microbiota from twins discordant for obesity modulate metabolism in mice. Science *341*, 1241214.

Riley, L.W., Raphael, E., and Faerstein, E. (2013). Obesity in the United States – Dysbiosis from Exposure to Low-Dose Antibiotics? Front. Public Health *1*.

Rivera-Chávez, F., Zhang, L.F., Faber, F., Lopez, C.A., Byndloss, M.X., Olsan, E.E., Xu, G., Velazquez, E.M., Lebrilla, C.B., Winter, S.E., et al. (2016). Depletion of Butyrate-Producing Clostridia from the Gut Microbiota Drives an Aerobic Luminal Expansion of Salmonella. Cell Host Microbe *19*, 443–454.

Robinson, M.D., and Oshlack, A. (2010). A scaling normalization method for differential expression analysis of RNA-seq data. Genome Biol. *11*, R25.

Robinson, C.M., Jesudhasan, P.R., and Pfeiffer, J.K. (2014). Bacterial lipopolysaccharide binding enhances virion stability and promotes environmental fitness of an enteric virus. Cell Host Microbe *15*, 36–46.

Round, J., Lee, S., Li, J., Tran, G., Jabri, B., Chatila, T., and Mazmanian, S. (2011). The Toll-like receptor 2 pathway establishes colonization by a commensal of the human microbiota. Science *332*, 974–977.

Salcedo, R., Worschech, A., Cardone, M., Jones, Y., Gyulai, Z., Dai, R.-M., Wang, E., Ma, W., Haines, D., O'hUigin, C., et al. (2010). MyD88-mediated signaling prevents development of adenocarcinomas of the colon: role of interleukin 18. J. Exp. Med. *207*, 1625–1636.

Santaolalla, R., and Abreu, M. (2012). Innate immunity in the small intestine. Curr. Opin. Gastroenterol. *28*, 124–129.

Savy, M., Edmond, K., Fine, P.E.M., Hall, A., Hennig, B.J., Moore, S.E., Mulholland, K., Schaible, U., and Prentice, A.M. (2009). Landscape analysis of interactions between nutrition and vaccine responses in children. J. Nutr. *139*, 2154S–218S.

Sayin, S., Wahlstram, A., Felin, J., Jantti, S., Marschall, H.-U., Bamberg, K., Angelin, B., *et. al.,* (2013). Gut Microbiota Regulates Bile Acid Metabolism by Reducing the Levels of Tauro-beta-muricholic Acid, a Naturally Occurring FXR Antagonist. Cell Metab. *17*, 225–235.

Schaible, U., and Kaufmann, S. (2007). Malnutrition and infection: complex mechanisms and global impacts. PLoS Med. *4*.

Scharf, R., Deboer, M., and Guerrant, R. (2014). Recent advances in understanding the long-term sequelae of childhood infectious diarrhea. Curr. Infect. Dis. Rep. *16*, 408.

Schippa, S., Iebba, V., Barbato, M., Di Nardo, G., Totino, V., Checchi, M., Longhi, C., Maiella, G., Cucchiara, S., and Conte, M. (2010). A distinctive "microbial signature" in celiac pediatric patients. BMC Microbiol. *10*, 175.

Schloss, P.D., Westcott, S.L., Ryabin, T., Hall, J.R., Hartmann, M., Hollister, E.B., Lesniewski, R.A., Oakley, B.B., Parks, D.H., Robinson, C.J., et al. (2009). Introducing mothur: Open-Source, Platform-Independent, Community-Supported Software for Describing and Comparing Microbial Communities. Appl. Environ. Microbiol. *75*, 7537–7541.

Schmidt, C.W. (2014). Beyond Malnutrition: The Role of Sanitation in Stunted Growth. Environ. Health Perspect. *122*, A298–A303.

Schmidt, D.R., Holmstrom, S.R., Fon Tacer, K., Bookout, A.L., Kliewer, S.A., and Mangelsdorf, D.J. (2010). Regulation of Bile Acid Synthesis by Fat-soluble Vitamins A and D. J. Biol. Chem. *285*, 14486–14494.

Schwarzer, M., Makki, K., Storelli, G., Machuca-Gayet, I., Srutkova, D., Hermanova, P., Martino, M.E., Balmand, S., Hudcovic, T., Heddi, A., et al. (2016). Lactobacillus plantarum strain maintains growth of infant mice during chronic undernutrition. Science *351*, 854–857.

Semba, R.D., Gonzalez-Freire, M., Moaddel, R., Trehan, I., Maleta, K.M., Khadeer, M., Ordiz, M.I., Ferrucci, L., and Manary, M.J. (2016). Environmental Enteric Dysfunction is Associated with Altered Bile Acid Metabolism: J. Pediatr. Gastroenterol. Nutr. 1.

Seok, J., Warren, H.S., Cuenca, A.G., Mindrinos, M.N., Baker, H.V., Xu, W., Richards, D.R., McDonald-Smith, G.P., Gao, H., Hennessy, L., et al. (2013). Genomic responses in mouse models poorly mimic human inflammatory diseases. Proc. Natl. Acad. Sci. *110*, 3507–3512.

Sequeira, I.R., Lentle, R.G., Kruger, M.C., and Hurst, R.D. (2014). Standardising the Lactulose Mannitol Test of Gut Permeability to Minimise Error and Promote Comparability. PLoS ONE *9*.

Serazin, A., Shackelton, L., Wilson, C., and Bhan, M. (2010). Improving the performance of enteric vaccines in the developing world. Nat. Immunol. *11*, 769–773.

Setchell, K.D.R., Heubi, J.E., Shah, S., Lavine, J.E., Suskind, D., Al–Edreesi, M., Potter, C., Russell, D.W., O'Connell, N.C., Wolfe, B., et al. (2013). Genetic Defects in Bile Acid Conjugation Cause Fat-Soluble Vitamin Deficiency. Gastroenterology *144*, 945–955.e6.

Shin, N.-R., Lee, J.-C., Lee, H.-Y., Kim, M.-S., Whon, T., Lee, M.-S., and Bae, J.-W. (2014). An increase in the Akkermansia spp. population induced by metformin treatment improves glucose homeostasis in diet-induced obese mice. Gut *63*, 727–735.

Simrén, M., Barbara, G., Flint, H.J., Spiegel, B.M.R., Spiller, R.C., Vanner, S., Verdu, E.F., Whorwell, P.J., and Zoetendal, E.G. (2013). Intestinal microbiota in functional bowel disorders: a Rome foundation report. Gut *62*, 159–176.

Slack, E., Hapfelmeier, S., Stecher, B., Velykoredko, Y., Stoel, M., Lawson, M., Geuking, M., Beutler, B., Tedder, T., Hardt, W.-D., et al. (2009). Innate and adaptive immunity cooperate flexibly to maintain host-microbiota mutualism. Science *325*, 617–620.

Slack, E., Balmer, M.L., Fritz, J.H., and Hapfelmeier, S. (2012). Functional Flexibility of Intestinal IgA – Broadening the Fine Line. Front. Immunol. *3*.

Smith, M., Yatsunenko, T., Manary, M., Trehan, I., Mkakosya, R., Cheng, J., Kau, A., Rich, S., Concannon, P., Mychaleckyj, J., et al. (2013). Gut microbiomes of Malawian twin pairs discordant for kwashiorkor. Science *339*, 548–554.

Smolen, K.K., Ruck, C.E., Fortuno, E.S., Ho, K., Dimitriu, P., Mohn, W.W., Speert, D.P., Cooper, P.J., Esser, M., Goetghebuer, T., et al. (2014). Pattern recognition receptor-mediated cytokine response in infants across 4 continents⋆. J. Allergy Clin. Immunol. *133*, 818–826.e4.

Sommer, F., and BÃ¤ckhed, F. (2013). The gut microbiota--masters of host development and physiology. Nat. Rev. Microbiol. *11*, 227–238.

Spencer, S., Wilhelm, C., Yang, Q., Hall, J., Bouladoux, N., Boyd, A., Nutman, T., Urban, J., Wang, J., Ramalingam, T., et al. (2014). Adaptation of Innate Lymphoid Cells to a Micronutrient Deficiency Promotes Type 2 Barrier Immunity. Science *343*, 432–437.

Spiegel, S., and Milstien, S. (2011). The outs and the ins of sphingosine-1-phosphate in immunity. Nat. Rev. Immunol. *11*, 403–415.

Stecher, B., Macpherson, A.J., Hapfelmeier, S., Kremer, M., Stallmach, T., and Hardt, W.-D. (2005). Comparison of Salmonella enterica Serovar Typhimurium Colitis in Germfree Mice and Mice Pretreated with Streptomycin. Infect. Immun. *73*, 3228–3241.

Subramanian, S., Huq, S., Yatsunenko, T., Haque, R., Mahfuz, M., Alam, M., Benezra, A., DeStefano, J., Meier, M., Muegge, B., et al. (2014). Persistent gut microbiota immaturity in malnourished Bangladeshi children. Nature *510*, 417–421.

Suzuki, K., Meek, B., Doi, Y., Muramatsu, M., Chiba, T., Honjo, T., and Fagarasan, S. (2004). Aberrant expansion of segmented filamentous bacteria in IgA-deficient gut. Proc. Natl. Acad. Sci. U. S. A. *101*, 1981–1986.

Swidsinski, A., Ung, V., Sydora, B., Loening-Baucke, V., Doerffel, Y., Verstraelen, H., and Fedorak, R. (2009). Bacterial overgrowth and inflammation of small intestine after carboxymethylcellulose ingestion in genetically susceptible mice. Inflamm. Bowel Dis. *15*, 359–364.

Syer, S., and Wallace, J. (2014). Environmental and NSAID-enteropathy: dysbiosis as a common factor. Curr. Gastroenterol. Rep. *16*, 377.

Takeuchi, O., and Akira, S. (2010). Pattern recognition receptors and inflammation. Cell *140*, 805–820.

Tautenhahn, R., Böttcher, C., and Neumann, S. (2008). Highly sensitive feature detection for high resolution LC/MS. BMC Bioinformatics *9*, 504.

Teodósio, N.R., Lago, E.S., Romani, S.A., and Guedes, R.C. (1990). A regional basic diet from northeast Brazil as a dietary model of experimental malnutrition. Arch. Latinoam. Nutr. *40*, 533–547.

Tilg, H., and Moschen, A.R. (2013). Gut microbiota: Malnutrition and microbiota—a new relationship? Nat. Rev. Gastroenterol. Hepatol. *10*, 261–262.

Trehan, I., Shulman, R., Ou, C.-N., Maleta, K., and Manary, M. (2009). A randomized, double-blind, placebo-controlled trial of rifaximin, a nonabsorbable antibiotic, in the treatment of tropical enteropathy. Am. J. Gastroenterol. *104*, 2326–2333.

Trehan, I., Goldbach, H., LaGrone, L., Meuli, G., Wang, R., Maleta, K., and Manary, M. (2013). Antibiotics as part of the management of severe acute malnutrition. N. Engl. J. Med. *368*, 425–435.

Turnbaugh, P., Ridaura, V., Faith, J., Rey, F., Knight, R., and Gordon, J. (2009). The effect of diet on the human gut microbiome: a metagenomic analysis in humanized gnotobiotic mice. Sci. Transl. Med. *1*.

Ubeda, C., Lipuma, L., Gobourne, A., Viale, A., Leiner, I., Equinda, M., Khanin, R., and Pamer, E. (2012). Familial transmission rather than defective innate immunity shapes the distinct intestinal microbiota of TLR-deficient mice. J. Exp. Med. *209*, 1445–1456.

Ueno, P.M., Oriá, R.B., Maier, E.A., Guedes, M., de Azevedo, O.G., Wu, D., Willson, T., Hogan, S.P., Lima, A.A.M., Guerrant, R.L., et al. (2011). Alanyl-glutamine promotes intestinal epithelial cell homeostasis in vitro and in a murine model of weanling undernutrition. Am. J. Physiol. Gastrointest. Liver Physiol. *301*, G612-622.

Ulluwishewa, D., Anderson, R., McNabb, W., Moughan, P., Wells, J., and Roy, N. (2011). Regulation of tight junction permeability by intestinal bacteria and dietary components. J. Nutr. *141*, 769–776.

Uysal, K.T., Wiesbrock, S.M., Marino, M.W., and Hotamisligil, G.S. (1997). Protection from obesity-induced insulin resistance in mice lacking TNF-alpha function. Nature *389*, 610–614.

Vaishnava, S., Behrendt, C.L., Ismail, A.S., Eckmann, L., and Hooper, L.V. (2008). Paneth cells directly sense gut commensals and maintain homeostasis at the intestinal host-microbial interface. Proc. Natl. Acad. Sci. U. S. A. *105*, 20858–20863.

Veitch, A.M., Kelly, P., Zulu, I.S., Segal, I., and Farthing, M.J. (2001). Tropical enteropathy: a T-cell-mediated crypt hyperplastic enteropathy. Eur. J. Gastroenterol. Hepatol. *13*, 1175–1181.

Victora, C.G., Adair, L., Fall, C., Hallal, P.C., Martorell, R., Richter, L., and Sachdev, H.S. (2008). Maternal and child undernutrition: consequences for adult health and human capital. The Lancet *371*, 340–357.

Vijay-Kumar, M., Sanders, C.J., Taylor, R.T., Kumar, A., Aitken, J.D., Sitaraman, S.V., Neish, A.S., Uematsu, S., Akira, S., Williams, I.R., et al. (2007). Deletion of TLR5 results in spontaneous colitis in mice. J. Clin. Invest. *117*, 3909–3921.

Vijay-Kumar, M., Aitken, J., Carvalho, F., Cullender, T., Mwangi, S., Srinivasan, S., Sitaraman, S., Knight, R., Ley, R., and Gewirtz, A. (2010). Metabolic syndrome and altered gut microbiota in mice lacking Toll-like receptor 5. Science *328*, 228–231.

Wada, M., Tamura, A., Takahashi, N., and Tsukita, S. (2013). Loss of claudins 2 and 15 from mice causes defects in paracellular Na+ flow and nutrient transport in gut and leads to death from malnutrition. Gastroenterology *144*, 369–380.

Wahlström, A., Sayin, S.I., Marschall, H.-U., and Bäckhed, F. (2016). Intestinal Crosstalk between Bile Acids and Microbiota and Its Impact on Host Metabolism. Cell Metab. *24*, 41–50.

Walker, W.A., and Iyengar, R.S. (2015). Breast milk, microbiota, and intestinal immune homeostasis. Pediatr. Res. *77*, 220–228.

Wei, M., Shinkura, R., Doi, Y., Maruya, M., Fagarasan, S., and Honjo, T. (2011). Mice carrying a knock-in mutation of Aicda resulting in a defect in somatic hypermutation have impaired gut homeostasis and compromised mucosal defense. Nat. Immunol. *12*, 264–270.

Wexler, H. (2007). Bacteroides: the good, the bad, and the nitty-gritty. Clin. Microbiol. Rev. *20*, 593–621.

Wieland Brown, L.C., Penaranda, C., Kashyap, P.C., Williams, B.B., Clardy, J., Kronenberg, M., Sonnenburg, J.L., Comstock, L.E., Bluestone, J.A., and Fischbach, M.A. (2013). Production of α-Galactosylceramide by a Prominent Member of the Human Gut Microbiota. PLoS Biol. *11*, e1001610.

Wlodarska, M., Willing, B., Keeney, K.M., Menendez, A., Bergstrom, K.S., Gill, N., Russell, S.L., Vallance, B.A., and Finlay, B.B. (2011). Antibiotic treatment alters the colonic mucus layer and predisposes the host to exacerbated Citrobacter rodentium-induced colitis. Infect. Immun. *79*, 1536–1545.

Wlodarska, M., Thaiss, C.A., Nowarski, R., Henao-Mejia, J., Zhang, J.-P., Brown, E.M., Frankel, G., Levy, M., Katz, M.N., Philbrick, W.M., et al. (2014). NLRP6 inflammasome orchestrates the colonic host-microbial interface by regulating goblet cell mucus secretion. Cell *156*, 1045–1059.

Wlodarska, M., Kostic, A.D., and Xavier, R.J. (2015). An integrative view of microbiome-host interactions in inflammatory bowel diseases. Cell Host Microbe *17*, 577–591.

World Health Organization, and Nutrition for Health and Development (2013). Guideline.

Xia, J., Mandal, R., Sinelnikov, I.V., Broadhurst, D., and Wishart, D.S. (2012). MetaboAnalyst 2.0--a comprehensive server for metabolomic data analysis. Nucleic Acids Res. *40*, W127-133.

Yano, J.M., Yu, K., Donaldson, G.P., Shastri, G.G., Ann, P., Ma, L., Nagler, C.R., Ismagilov, R.F., Mazmanian, S.K., and Hsiao, E.Y. (2015). Indigenous bacteria from the gut microbiota regulate host serotonin biosynthesis. Cell *161*, 264–276.

Yatsunenko, T., Rey, F., Manary, M., Trehan, I., Dominguez-Bello, M., Contreras, M., Magris, M., Hidalgo, G., Baldassano, R., Anokhin, A., et al. (2012). Human gut microbiome viewed across age and geography. Nature *486*, 222–227.

Yu, S., Bruce, D., Froicu, M., Weaver, V., and Cantorna, M.T. (2008). Failure of T cell homing, reduced CD4/CD8alphaalpha intraepithelial lymphocytes, and inflammation in the gut of vitamin D receptor KO mice. Proc. Natl. Acad. Sci. U. S. A. *105*, 20834–20839.

Zivkovic, A.M., German, J.B., Lebrilla, C.B., and Mills, D.A. (2011). Human milk glycobiome and its impact on the infant gastrointestinal microbiota. Proc. Natl. Acad. Sci. *108*, 4653–4658.